The MDMX (MDM4) oncoprotein as a therapeutic target and determinant of response to MDM2-p53 binding antagonists in human cancer

Laura Gamble
YI-HSUAN HO

(SHIRLEY)

Doctor of Philosophy

Northern Institute for Cancer Research

Faculty of Medical Sciences

Newcastle University

June 2017

Abstract

The tumour suppressor p53 is activated by cellular stress to induce cell cycle arrest and/or apoptosis. Despite being frequently mutated, the *TP53* gene is wild-type and functional in approximately 50% of human cancers. Targeting the p53 tumour suppressor pathway by inhibition of its negative factors MDM2 and MDMX is central to many cancer therapies. Small molecule antagonists have been developed to inhibit p53-MDM2 binding to release p53 and reactivate p53 function. However, previous studies have indicated that MDMX amplification or expression may be associated with resistance to MDM2-p53 binding inhibitors. MDMX could also play a significant role in the response to other therapeutic agents that act by a p53-dependent mechanism.

The effects of MDM2-p53 binding antagonists (Nutlin-3 and RG7388) and the MDM2/X–p53 binding co-inhibitor (RO5963) were compared in a panel of cell lines of different *TP53* and MDMX(*MDM4*) status. The endpoints tested included expression of p53 and its downstream transcriptional targets, growth inhibition, cell cycle distribution changes and caspase 3/7 apoptotic activity. Moreover, the effect of suppression of MDMX expression by lentiviral shRNA and siRNA systems on the response to MDM2 inhibitors and co-inhibitors was tested in a panel of cell lines. Affymetrix Human Transcriptome Array 2.0 was used to detect differences in the expression of full-length genes and alternatively spliced forms after suppression of MDMX expression in *MDM4*-amplified MRK-nu-1 cells.

The results showed that cells with wild-type p53 respond to both MDM2-p53 and MDM2/X-p53 antagonists by growth inhibition. *TP53* mutational status is the main factor governing resistance to MDM2-p53 binding antagonists. In *TP53* wild-type cells, MDMX expression is associated with sensitivity to the RO5963 MDM2/X con-inhibitor and has only minor impact on resistance to MDM2-p53 binding antagonists. Knockdown of MDMX reduced cell growth by induction of cell cycle arrest in both p53 dependent and independent ways, while the effect of MDMX suppression had a modest effect on the efficacy of MDM2-p53 binding antagonists which was cell line dependent. Reduction of MDMX expression slightly increased *TP53*-dependent downstream transcriptional activity measured by Affymetrix Human transcriptome

array 2.0. The gene showing the greatest increase in response to MDMX knockdown was *VGLL1*, which is an oncogene associated with the Hippo pathway that regulates organ size. Suppression of MDMX may activate VGLL1-TEAD dependent transcriptional activity, thereby regulating cell proliferation via an increase of VGLL1 expression, linking to the Hippo signalling pathway.

In summary, *TP53* status has a much greater impact on the response to pure MDM2-p53 binding antagonists compared with MDMX expression. In wild-type *TP53* cell lines, MDMX amplification and high expression was modestly associated with resistance to MDM2-p53 binding antagonists.

Declaration

I hereby declare that the work presented in this thesis is original and has not been previously submitted to any other academic institution.

Signed: _____

Date: 23rd September 2016

Acknowledgements

Table of Contents

List of Tables

List of Figures

Abbreviations

Ac	acetylation
ADP	ribosylation
AKT	Protein kinase B (PKB)
Amp	amplified; amplification
ANOVA	Analysis of variance
Arg	Arginine, R
ASN	antisense
AT	annealing temperature
ATM	ataxia telangiectasia
ATR	ataxia telangiectasia and Rad3-related kinase
Av.	Average
BAX	BCL2 associated X protein
BCA	bicinchoninic Acid
bp	base pair
BRAF	v-Raf murine sarcoma viral oncogene homolog B
BSA	bovine serum albumin
BTG2	BTG family, member 2
CCNG2	cyclin G2, Cyclin G
CDKN1A	cyclin-dependent kinase inhibitor 1A (p21, Cip1)
CEACAM1	carcinoembryonic antigen-related cell adhesion molecule 1 (biliary glycoprotein)
Chk1	checkpoint kinase 1
Chk2	checkpoint kinase 2
CLCA2	chloride channel accessory 2
c-myc	Cellular proto-oncogene myc
CO2	carbon dioxide
COP-1	constitutively photomorphogenic 1
CRD	C-terminal regulatory (CRD) domains
CRISPR	Clustered regularly interspaced short palindromic repeats
DAPI	4',6-diamidino-2-phenylindole
DBD	DNA binding domain
del	deleted
dH2O	distilled water
DMEM	Dulbecco's modified Eagle's medium
DMSO	dimethyl sulfoxide
DNA	deoxyribonucleic acid
DNA-PK	DNA protein kinase
dNTP	deoxyribonucleoside triphosphate
Dox	Doxycycline
ECL	enhanced chemiluminescence
EDA2R	ectodysplasin A2 receptor

EDTA	ethylenediamine tetra acetic acid
EMEM	Eagle's Minimum Essential Medium
EMP1	epithelial membrane protein 1
FACs	fluorescence activated cell sorting/flow cytometry
FAS	Fas cell surface death receptor; Fas (TNF receptor superfamily, member 6)
FBS	fetal bovine serum
FBXO32	F-box protein 32
FL2-A	fluorescent detector 2-area
FL2-W	fluorescent detector 2-width
FU	fluorescence unit
G1	Gap 1
G2	Gap 2
GAPDH	Glyceraldehyde 3-phosphate dehydrogenase
GHR	growth hormone receptor
GI	Growth inhibition
GI50	the concentration at which a compound reduces the growth of the cell population by 50%
HCl	hydrochloric acid
HE	High expression
HMGCS2	3-hydroxy-3-methylglutaryl-CoA synthase 2 (mitochondrial)
HRP	horeseraddish peroxidase
HSD17B13	hydroxysteroid (17-beta) dehydrogenase 13
HTA 2.0	Affymetrix Human Transcriptome Array 2.0
IC50	Concentration of an inhibitor at which 50% inhibition of the response is seen
IGF-1	Insulin-like growth factor 1
K-Ras	V-Ki-Ras2 Kirsten Rat Sarcoma 2 Viral Oncogene Homolog
KRT4	keratin 4
L1	lentiviral shRNA clone 1
LATS	Large Tumor Suppressor Kinase
LC50	the concentration at which a compound reduced the re-formed colonies of the cells population by 50%
LE	low expression
Len	lentivirus; lentiviral
Leu	Leucine, L
MDM2	murine double minute 2, HDM2
MDMX (*MDM4*)	murine double minute X, murine double minute 4, HDM4, HDMX, gene name *MDM4*
MDMX-FL	MDMX full-length
Me	methylation
MgCl2	magnesium chloride
MTBP	MDM2 binding protein
MUC15	mucin 15, cell surface associated

MYCN	V-Myc Avian Myelocytomatosis Viral Oncogene Neuroblastoma Derived Homolog
N (n)	number of repeats
N20R1	NGP daughter resistant cell line with mutant p53
N8	neddylation
NA	not amplified
NES	nuclear export signal
NLS	nucleolar localisation signal
NPM	nucleophosmin
Nut-3	Nutlin-3, Nut
O-Glc	glycosylation
OR2J2	olfactory receptor, family 2, subfamily J, member 2
P	phosphorylation
p21WAF1	p21 wildtype activated fragment 1
PBS	Dulbecco's A phosphate buffered saline
PCA	Principal Component Analysis
PCR	polymerase chain reaction
Pen/Strep	Penicillin / Streptomycin
Phe	Phenylalanine, F
Pirh2	RINGH2 domain-containing protein
pp53ser	p53 phosphorylation at serine 15
PRD	proline rich domain
Pro	Proline, F
PSR	probe selection region
PUMA	p53-upregulated modulator of apoptosis
Puro	puromycin
RFP	red fluorescence protein
RIN	RNA integrity number
RING	really interesting new gene
RNA	Ribonucleic acid
RPMI	Roswell Park Memorial Institute
RRM2B (p53R2)	ribonucleotide reductase M2 B (*TP53* inducible)
S	sumoylation
SCR	Scramble siRNA negative control
SDS	sodium dodecyl sulphate
SDS-PAGE	sodium dodecyl sulphate-polyacrylamide gel electrophoresis
Ser	serine
shRNA	A short hairpin RNA or small hairpin RNA
SI	splicing index
siControl	siRNA negative control, siCon
siMDMX	siRNA mediated kncokdown of MDMX
siRNA	Small interfering RNA

S-M6R1	SJSA-1 resistant MI-63 cell line
SN	sense
S-N40R2	SJSA-1 resistant nutlin-3 cell line
SNP	single nucleotide polymorphism
SRB	Sulforhodamine B
STR	short tandem repeat DNA profiling
TAC	Transcriptome Analysis Console 3.0 software
TAD	transcriptional activation domain
TBE	Tris/Borate/EDTA
TBP	TATA-binding protein
TBS	Tris Buffered Saline
TD	tetramerization domain
TFIID	transcription initiation factor D
TNFRSF10C	tumor necrosis factor receptor superfamily, member 10c, decoy without an intracellular domain
TNFSF10	tumor necrosis factor (ligand) superfamily, member 10
Trp53	Transformation related protein 53 (Murine protein)
Tyr	Tyrosine, Y
Ub	ubiquitin, ubiquitination
UCR	Universal siRNA negative control
Un	untreated
VGLL1	vestigial-like family member 1; vestigial like 1 (Drosophila)
WT	wild-type
XTT	Tetrazolium salt
YAP	Yes Associated Protein
ZMAT3 (PAG608)	zinc finger, matrin-type 3; zinc finger, matrin type 3

Chapter 1 Introduction

1.1   Cancer

Cancer is a collection of related genetic diseases involving growth and division of abnormal cells that invade adjoining parts of the body and spread to surrounding organs. Metastasis is the latter process and the major cause of death from cancer. Tumour cells are abnormal dividing cells, which are caused by genomic change such as mutation leading to out-of-control cell growth and proliferation. Oncogenes (from Greek onkos, a tumour) are activated versions of normal genes that generally share the ability to accelerate cell division and growth, but often also variously contribute to less of differentiation, increased cell motility, and avoidance of apoptosis and invasion (Pelengaris and Khan, 2013). By contrast, Tumour suppressor are the cell's guardians against DNA damage induced. Tumour suppressors also monitor critical cellular checkpoints that govern the mitotic cycle, DNA repair transcription, apoptosis, and differentiation (Pelengaris and Khan, 2013). Normal cell growth is controlled in a balance between cell proliferation and death by tumour suppressors and oncogenes. The multiple alternative sequential alterations in tumour suppressor genes and oncogenes result in heterogeneity in cancer. The hallmarks of cancer, as diagrammatically and elegantly summarised by Hanahan and Weinberg, are shown in figure 1.1, including the capabilities of tumour growth, progression and metastatic dissemination, to provide a framework to consider the biology of cancer (Hanahan and Weinberg, 2011). Figure 1.2 illustrates different classes of therapeutic agents and examples of their capabilities of targeting the different features of cancer, including tumour growth and progression (Hanahan and Weinberg, 2011).
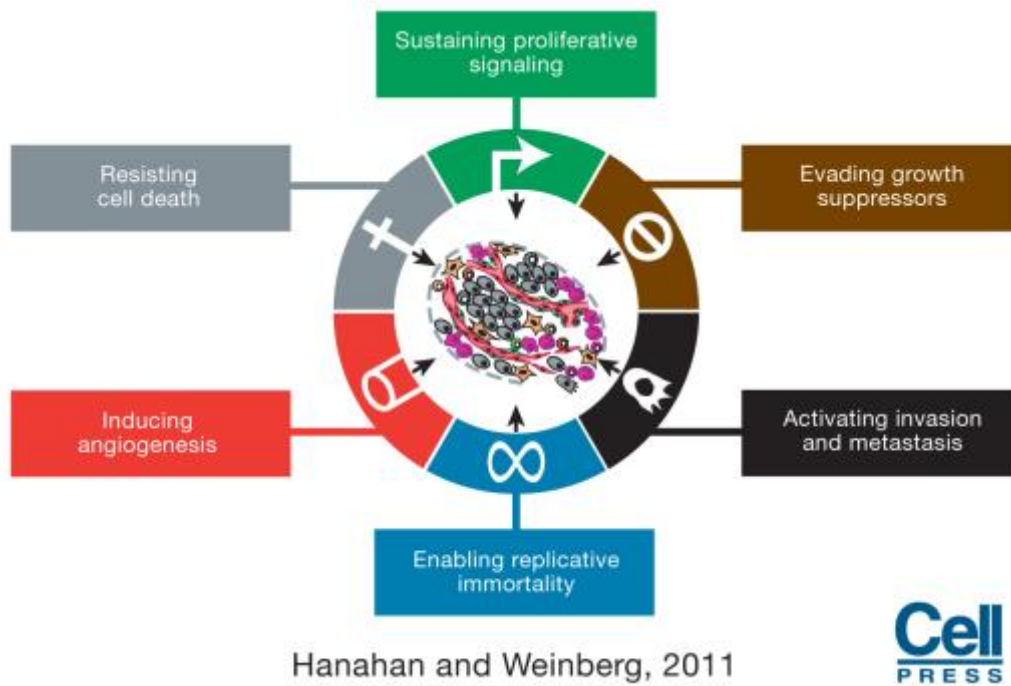
Figure 1.1. The Hallmarks of Cancer (Hanahan and Weinberg, 2011)
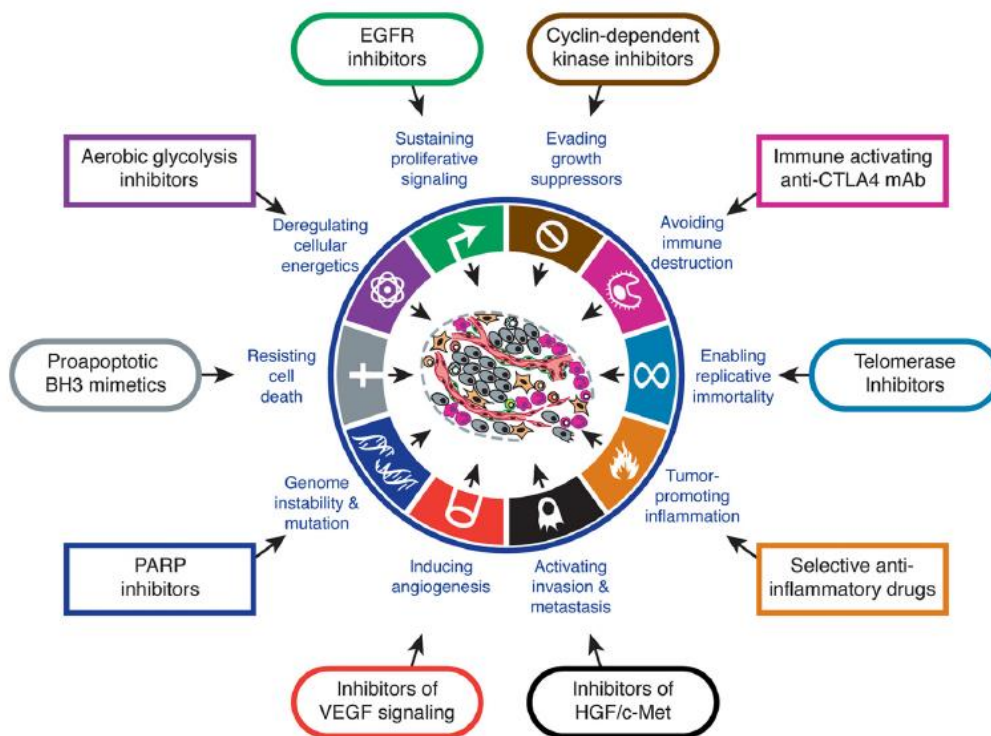
Figure 1.2. Therapeutic Targeting of the Hallmarks of Cancer (Hanahan and Weinberg, 2011).

1.2 Tumour suppressors and Oncogenes

Oncogenes (from Greek onkos, a tumour) are activated versions of normal genes that generally share the ability to accelerate cell division and growth, but often also variously contribute to less differentiation, increased cell motility, and avoidance of apoptosis and invasion.

An oncogene, sometimes referred to in its normal form as a proto-oncogene, is a gene that has the potential to cause cancer. Mutation and amplification (high copy numbers) of proto-oncogenes result in the activation of the oncogenes. This can lead to out-of-control cell growth in human tumour cells. For example, *B-RAF* and *K-RAS* mutation in melanoma leads to continuous activation of the mitogen-activated protein kinase (MAPK) growth regulatory pathway in tumour division (Fecher *et al.*, 2008). The products of oncogenes can be classified into six broad groups: transcription factors, chromatin remodelers, growth factors, growth factor receptors, signal transducers, and apoptosis regulators (Croce, 2008).

Nowadays, a number of oncogene products can be targeted for cancer therapy. For example, MDM2 and MDMX are two oncoproteins which inhibit p53 activation by binding to p53 as a heterodimer (Hu *et al.*, 2007). Drug development researchers have produced small molecular weight compounds or peptides targeted at MDM2 and MDMX to release and reactivate the p53 tumour suppressor to inhibit tumour growth.

Tumour suppressor are the cell's guardians against induced DNA damage. Tumour suppressors also monitor critical cellular checkpoints that govern the mitotic cycle, DNA repair transcription, apoptosis, and differentiation. Mutation, deletion or suppression of the activity of tumour suppressor genes causes loss or reduction of their function, allowing abnormal cell division which can lead to tumour progression. For example, the *TP53* tumour suppressor gene is found mutated in half of all human cancers (Hollstein *et al.*, 1991).

Epigenetic modifications such as DNA methylation and histone modifications are crucial to regulate the activation of tumour suppressor genes by changing chromatin architecture in mammals. It is commonly known that inactivation of certain tumour

suppressor genes occurs as a consequence of hypermethylation within the promoter regions. The CpG sites in CpG islands of promoter regions of DNA where cytosines can be methylated. The multiple methylated CpG sites in CpG islands of promoters causes stable silencing of genes such as tumour suppressor genes. Loss of expression of tumour suppressor genes in cancers occurs more frequently by hypermethylation of promoter CpG islands than by mutations (Clark and Melki, 2002; Baylin, 2005; Kulis and Esteller, 2010). A previous study listed 147 genes which were found with high frequency of hypermethylated promoters are associated with colon cancers (Schnekenburger and Diederich, 2012). DNA repair genes are also frequently repressed in cancers due to hypermethylation of CpG islands within their promoters (Jin and Robertson, 2013; Rieke *et al.*, 2016).

1.3   RB and Cell cycle

The Rb (retinoblastoma) protein is a tumour suppressor, which is located at position chromosome 13q14. Most inactivating Rb mutations lead to retinoblastoma. Rb plays a crucial role in the negative control of the cell cycle and cell proliferation in tumour progression (Weinberg, 1995).

Rb protein (pRb) is responsible for a major G1 checkpoint (restriction point) blocking S-phase entry and cell growth, promoting terminal differentiation by inducing both cell cycle exit and tissue-specific gene expression (figure 1.3A) (Weinberg, 1995). Rb is physically associated with E2F factors and blocks their transactivation domain in G0 and early-G1 phase. In late G1 phase, phosphorylated form of Rb releases E2Fs, allowing the expression of genes that encode products necessary for S-phase progression (figure 1.3A). The pRb is hypophosphorylated in resting G0 cells (Sherr and McCormick, 2002; Giacinti and Giordano, 2006). Loss of pRb functions may induce cell cycle deregulation. The interaction between the pRb family of proteins and the E2F family of transcription factors plays a central role in governing cell cycle progression and DNA replication by controlling the expression of cell cycle E2Fs-dependent genes (Macaluso *et al.*, 2005). The other two members of Rb family are p107 (20q11.2) and p130 (16q13). The Rb family are referred to as pocket proteins. The term pocket proteins derives from the conserved binding pocket region through which Rb, p107 and p130 bind viral oncoproteins and cellular factors such as the E2F family of transcription factors (Weinberg, 1995). In G0 and early-G1 phase, p107 and p130 also bind to the E2F family and inhibit E2Fs' responsive gene expression (figure 1.3B). In G1 phase, cyclin D-Cdk4/6 and cyclin E-Cdk2 holoenzymes phosphorylate pRb proteins, allowing E2Fs to induce the transcription of genes required for S-phase entry (figure 1.3B) (Pelengaris and Khan, 2013).
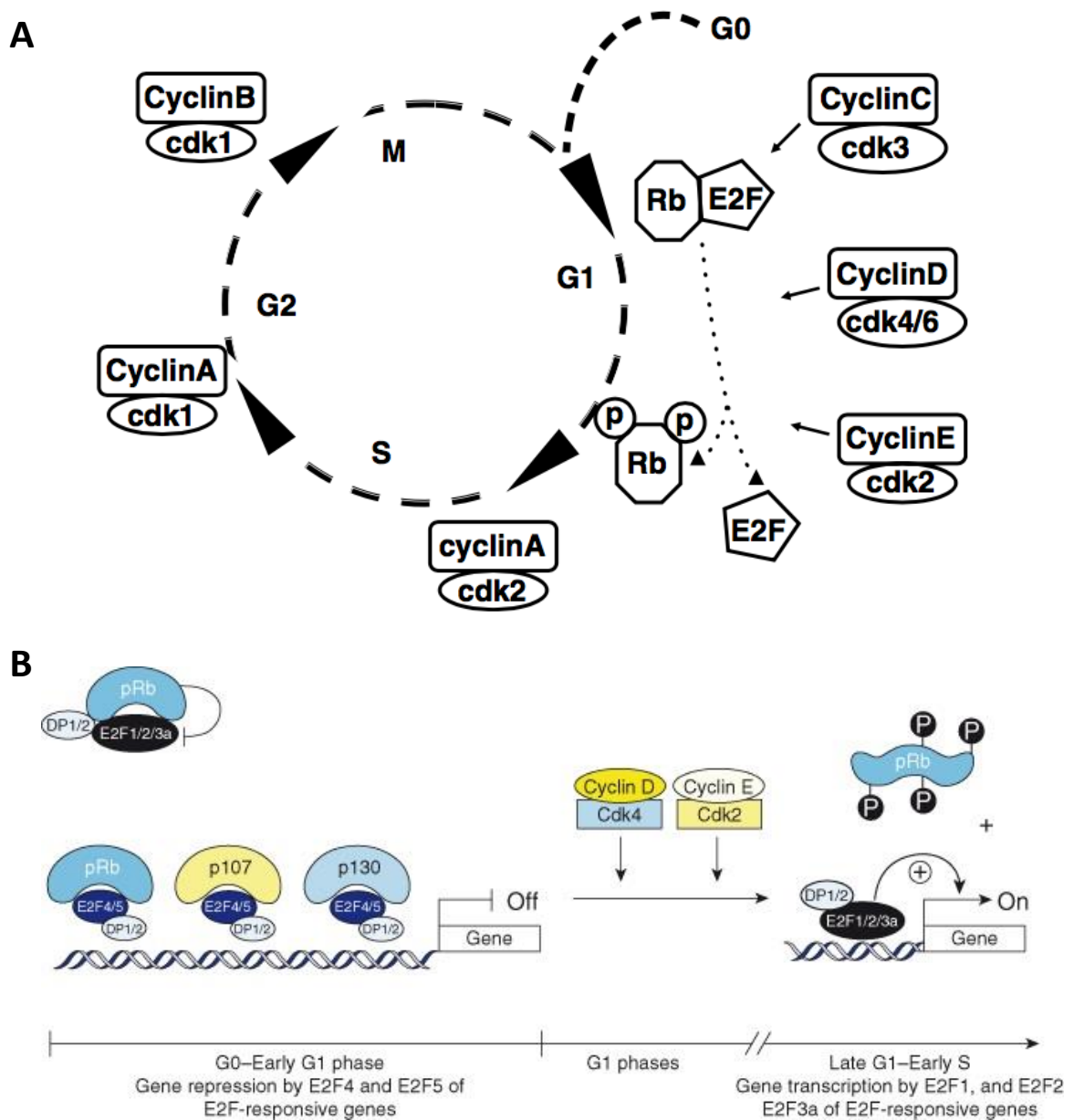
Figure 1.3. Rb controls the cell cycle. (A) Rb and pRB (phosphorylated forms of RB) control E2F transactivation in G0, G1 and S (Giacinti and Giordano, 2006). (B) The Rb family of proteins regulate E2F4/5 in G0 and early G1 phase (Pelengaris and Khan, 2013).

1.4   Tumour suppressor – p53

A tumour suppressor is anti-oncogene which is a factor preventing the development of tumours. Mutation or deletion of tumour suppressor genes causes loss or reduction of their function, allowing abnormal cell division which can lead to tumour progression. For example, the *TP53* tumour suppressor gene is found mutated in half of all human cancers (Hollstein *et al.*, 1991).

1.4.1   Regulation of p53

Activation of transcriptional factor p53 function includes three steps, which are p53 stabilization, DNA binding and transcriptional activation (figure 1.4). Cellular stress, including DNA damage, oncogenic activity, ribosomal stress and metabolic stress, stabilizes and activates p53 to induce down-stream cellular effects such as apoptosis, cell cycle arrest and senescence (Harris and Levine, 2005; Rufini *et al.*, 2013). The genes involved in these cellular effects are transactivated by p53 via interaction with DNA through its DNA binding domain (Shadfan *et al.*, 2012). ATM, ATR and other DNA damage and stress-dependent kinases phosphorylate and stabilize p53. DNA-bound p53 then recruits the transcriptional machinery to activate the transcription of p53 target genes that inhibit growth and promote apoptosis (Kruse and Gu, 2009). P53 is degraded via MDM2-mediated ubiquitination (Haupt *et al.*, 1997; Honda *et al.*, 1997; Kubbutat *et al.*, 1997; Brooks and Gu, 2011).

The *TP53* tumour suppressor gene plays a crucial role in protecting cells from genomic instability by regulating apoptosis and cell cycle arrest in response to cellular stress. Amplification or overexpression of negative regulators such as MDM2 and MDMX can be alternative mechanisms by which p53 function is compromised in cancer, even though tumour cells are often more sensitive to apoptosis signals than normal cells. The *TP53* gene is nevertheless wild-type in approximately half of human cancers, therefore where it is suppressed by other mechanisms, re-activation of p53 has been of major interest in the development of tumour-specific therapies in different types of cancers (Kim and An, 2016).
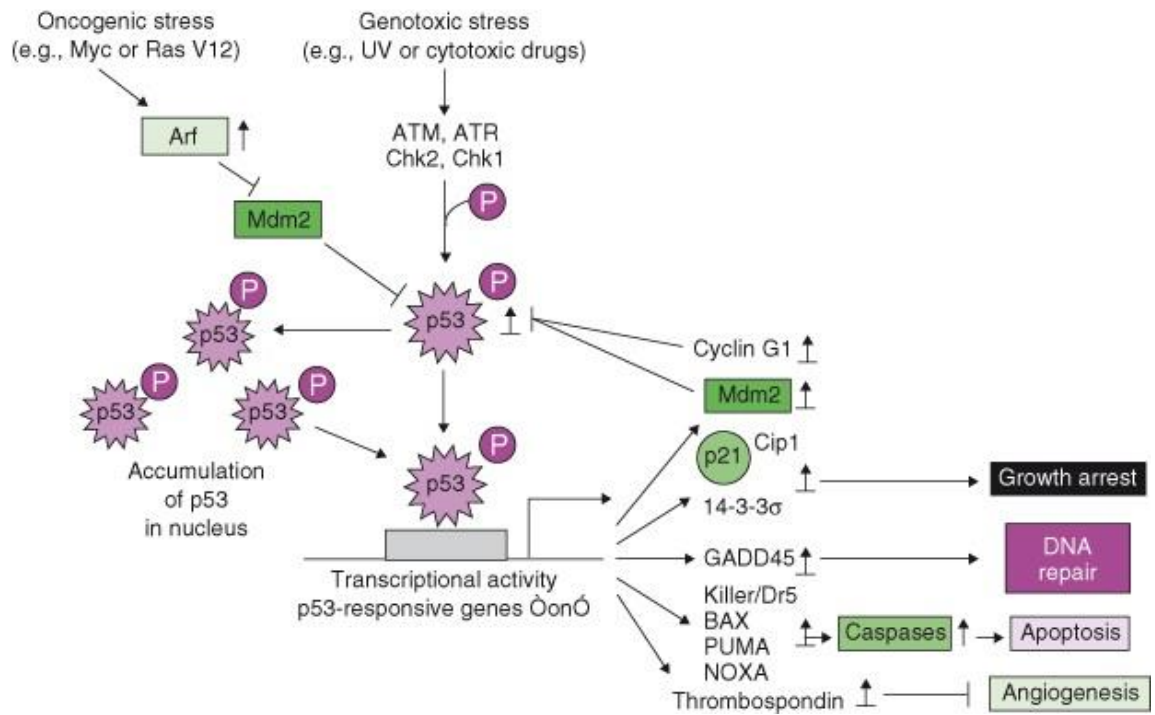
Figure 1.4. The transcription factor p53 is activated by phosphorylation in response to oncogenic and cellular stress (Pelengaris and Khan, 2013).

1.4.2 TP53 mutation

Mutant p53 is found in around 50% of human cancer. *TP53* has several mutational hot spots shown in figure 1.5. The majority (75%) of *TP53* mutations are missense substitutions in its central DNA-binding domain (Olivier *et al.*, 2002; Petitjean *et al.*, 2007; Goh *et al.*, 2011). Other alterations include frameshift insertions and deletions (9%), nonsense mutations (7%), silent mutations (5%) and other infrequent alterations (Olivier *et al.*, 2002). About 30% of *TP53* missense mutations found in cancer correspond to nucleotide substitutions at highly mutable CpG dinucleotides, at codons encoding residues that play essential structural and chemical roles in the contact between the p53 protein and specific DNA sequences that constitute the p53 response elements (Hainaut and Hollstein, 2000). Most tumour somatic mutations are accompanied by deletion of the remaining wild-type *TP53* allele. High expression of mutant p53 can also contribute to transformation, metastasis and drug resistance in part by inhibiting wild-type p53 and p53 family members in many cancers (Goh *et al.*, 2011).

Mutations in *TP53* confer susceptibility to cancer and may be somatic or inherited. Li–Fraumeni syndrome (LFS) is a cancer predisposition syndrome caused by germline mutations in *TP53* (Petitjean *et al.*, 2007). The family with LFS are predisposed to diverse types of cancer including breast cancer, bone, soft tissue, brain, adrenal, colorectal carcinoma and melanoma. The p53 mutation is transmitted from one generation to the next. The position of *TP53* mutation at R337H was initially found in young Brazilian patients with LFS (Pelengaris and Khan, 2013).

Some forms of mutant p53 can have a dominant negative effect on wild-type p53 (figure 1.6). Mutant p53 also inhibits p63 and p73 (Goh *et al.*, 2011). In normal cells on figure 1.6A, wild-type p53 is synthesised in the cytoplasm and forms dimers. After being transported to nucleus, tetramers of p53 bind to p53-binding sites in the DNA. At low mutant p53 protein levels (figure 1.6B), mutant p53 dimers do not block wild-type p53 tetramers and activation. At high levels of mutant p53 (figure 1.6C), inactive heterotetramers are formed and inhibit the formation and function of wild-type p53 tetramers (Goh *et al.*, 2011). Mutant p53 can have oncogenic gain-of-function

properties (Bossi *et al.*, 2006). Mutant p53 results in chromosomal instability accelerating tumour progression in cells (Bossi *et al.*, 2006).
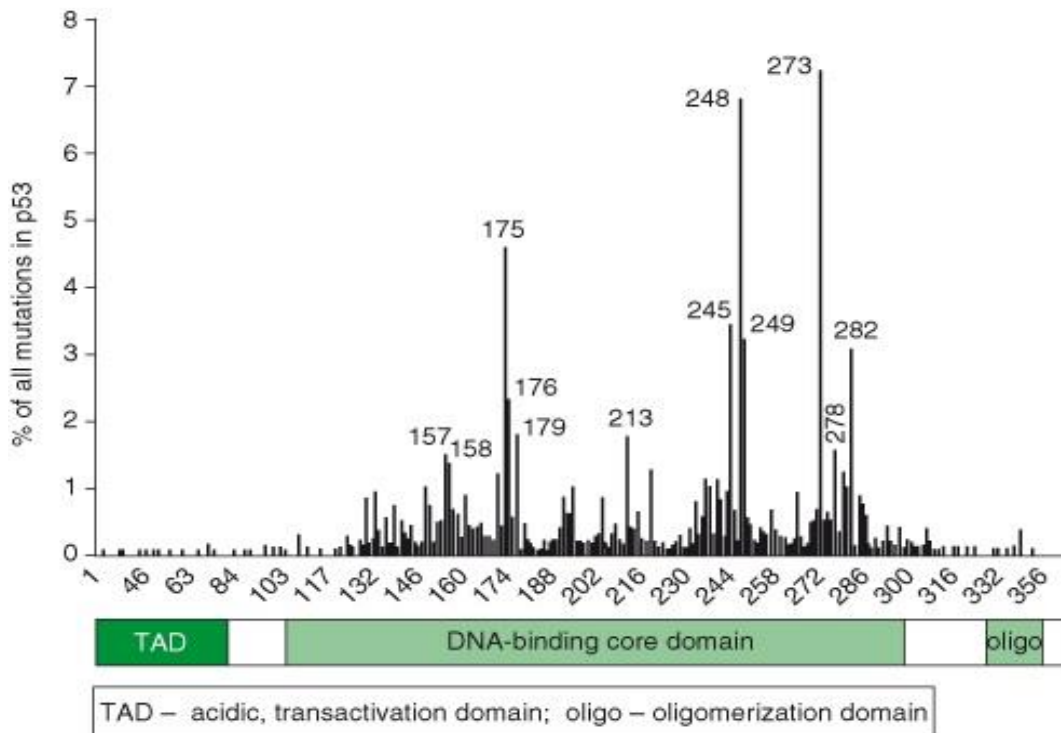
Figure 1.5. The hot spots of *TP53* mutation in human cancer. The majority of mutations are located in DNA-binding domain (Pelengaris and Khan, 2013).
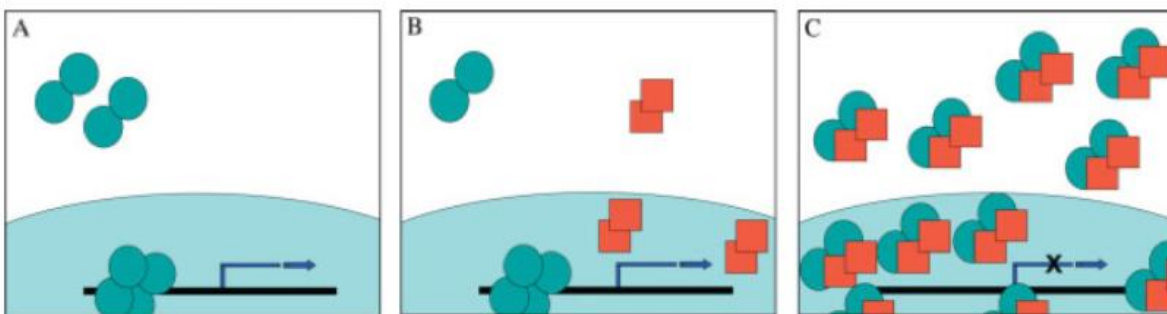
Figure 1.6. Models to explain dominant mutant p53 effect to wild-type p53 (Goh *et al.*, 2011). Wild-type p53 dimers and tetramers are green circles. Mutant p53 dimers are orange squares.

1.4.3 Modification of p53

Phosphorylation of p53 mediates its activation by DNA damage ATM (Ataxia Telangiectasia Mutated), which is a serine/threonine protein, is a key up-stream activator of p53 responsible for activation by DNA double-stand break (Banin *et al.*, 1998; Chun and Gatti, 2004) or DNA-PK (Shieh *et al.*, 1997). Ser20 of p53 is phosphorylated by Chk2, which is activated by ATM. Ser20 is also a part of the MDM2-binding site on p53, and phosphorylation of this residue prevents p53 binding to MDM2 (Chehab *et al.*, 2000; Shieh *et al.*, 2000). However, individual phosphorylation site mutation does not block p53 stabilization. It was demonstrated in a mouse model that Ser18 (equivalent of Ser15 in human p53) single-site mutation does not affect p53 stabilization or tumour suppression significantly. After DNA damage, it only causes poor activation of certain p53 target genes (Chen *et al.*, 2012).

Ubiquitin (Ub) conjugation is a general targeting modification and poly-ubiquitin chains constituting lysine 48 (K48) linkages specifically target proteins to the proteasome for degradation. The lysines on C-terminal basic domains of p53 are targets for ubiquitination by MDM2 leading to proteasomal degradation (figure 1.7). MDM2 functions as an E3 ligase to add ubiquitin chains to p53, leading to p53 degradation in co-operation with MDMX (Wade *et al.*, 2013). Ubiquitins on p53 are deubiquitinated by the enzyme HAUSP for activation of p53 (Li *et al.*, 2002b). MDM2-mediated monoubiquitylation of p53 greatly promotes its mitochondrial translocation and apoptosis (Marchenko *et al.*, 2007). On the other hand, p53 undergoes rapid deubiquitylation by mitochondrial HAUSP via a stress-induced mitochondrial p53–HAUSP complex (Marchenko *et al.*, 2007).

Histone acetyltransferases (HATs) provide an important role of p53 regulation and transcription (Brooks and Gu, 2003). The p53 protein was the first nonhistone substrate found to be acetylated by the histone acetyltransferase CBP/p300. Also CBP/p300 mutations are found in several types of human tumours (Goodman and Smolik, 2000; Iyer *et al.*, 2004). Acetylation of p53 lysine residues is critically important both for the efficient recruitment of cofactors and for the activation of p53 target genes in vivo. The acetyltransferases Tip60 and hMof can acetylate p53 as

well as histones (Tang *et al.*, 2006). The acetyltransferase activity of Tip60 is implicated in both DNA repair and apoptosis (Tang *et al.*, 2006; Kruse and Gu, 2009).

Methylation, sumoylation, and neddylation may contribute to p53 promoter specificity (Kruse and Gu, 2009) as indicated in Figure 1.7A. Three different methyltransferases have been shown to be able to methylate C-terminal lysine residues of p53. Set7/9-mediated monomethylation of p53 at lysine K372 promotes p53 activation of p21 (Chuikov *et al.*, 2004). Monomethylation of p53 at K370 and K382 by Smyd2 and SET8, respectively, represses p53 activity (Huang *et al.*, 2006; Shi *et al.*, 2007). Regulated dimethylation of K370 and K382 provides a binding site for the DNA repair factor 53BP1, and DNA damage increases p53 dimethylation and therefore promotes the interaction of p53 and 53BP1 (Kruse and Gu, 2009). Modification of p53 by the ubiquitin-like modifications SUMO and Nedd8 further add to the competition for the C-terminal lysines. Some studies report that sumoylation promotes p53 transcriptional activity (Melchior and Hengst, 2002) but others demonstrate that sumoylation promotes the localization of p53 to the cytoplasm (Carter *et al.*, 2007). MDM2-mediated neddylation of K370, K372, and K373 (Xirodimas *et al.*, 2004) and FBXO11-mediated neddylation of K320 and K321 (Abida *et al.*, 2007) appear to inhibit p53-mediated transcriptional activation.
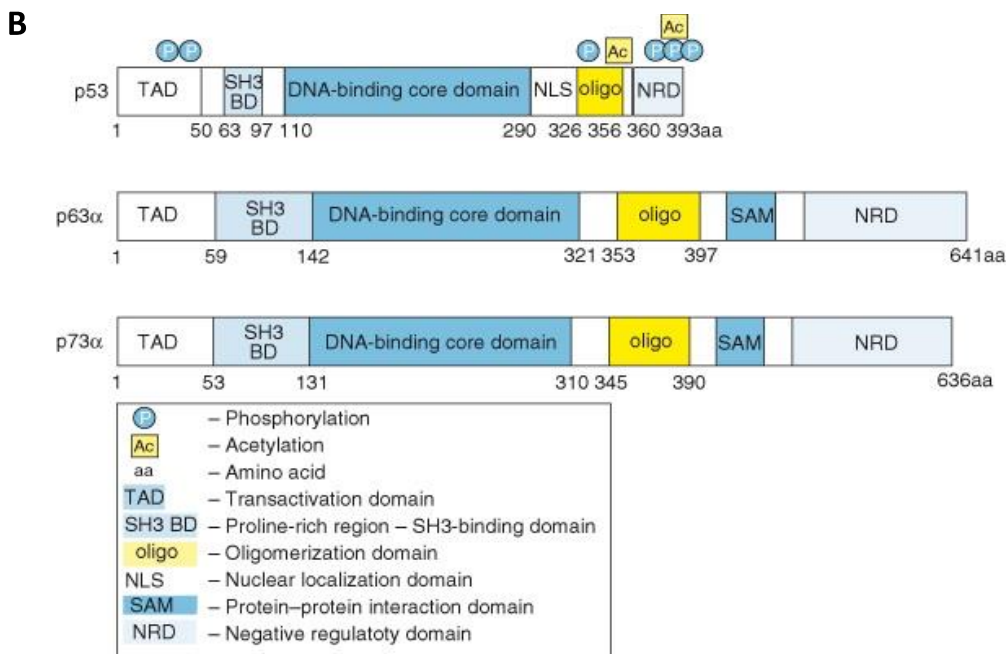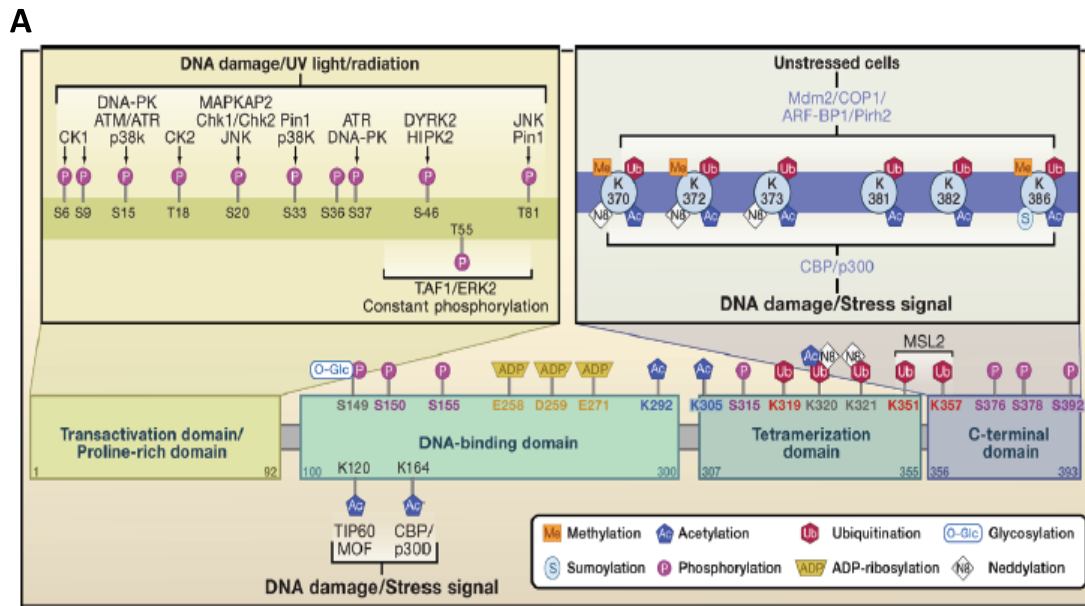
Figure 1.7. Structure and modification of the p53 family. (A)Structure and posttranslational modification of p53 (Kruse and Gu, 2009) . Phosphorylation (P), ubiquitination (Ub), acetylation (Ac), methylation (Me), sumoylation (S), neddylation (N8), glycosylation (O-Glc), and ribosylation (ADP) are indicated. (B) Structural domains of p53, p63 and p73 proteins. All three proteins share common domains but contain different lengths of negative regulatory domains (NRD) (Pelengaris and Khan, 2013).

1.4.4 Mouse models of TP53

TP53 family members have been deleted by homologous recombination in the mouse, leading to tumorigenesis and developmental effects summarised in table 1.1. Knockout mice with one or two copies of p53 deleted develop cancers with high frequency, including lymphomas, sarcomas, lung and brain tumours (Pelengaris and Khan, 2013). TP53-null mice have been used to test potential new therapies. A single amino acid substitution at 172 (R172H) in the mouse p53 allele induces an increase in the number of carcinoma and metastases in TP53+/- mice (Pelengaris and Khan, 2013). However, knockout of p63 and p73 does not make mice tumour prone, but is associated with developmental defects.

Genotype	Phenotype
$p53^{-/-}$	Highly tumor prone; mostly lymphomas and sarcomas with other tumors with less penetrance
$p53^{+/-}$	Tumor prone with LOH
$p53$ $R172H$	Higher penetrance of carcinomas and metastases
"Super $p53$"	No tumors
$p63^{-/-}$	No tumors. Limb defects, craniofacial and epithelial development defects; no skin
$p73^{-/-}$	No spontaneous tumors; hydrocephaly and chronic infections

Table 1.1 Mouse model of *TP53* family (Pelengaris and Khan, 2013)

1.5   Oncogene MDM2

MDM2 (murine double minute 2) is one of two members of the MDM family and a major inhibitory regulator of p53 by binding to the N-terminal domain of p53. The *MDM2* gene is located on chromosome 12 at q15 9. MDMX (also known as *MDM4 gene*) is a structural MDM2 paralogue. The percentage of domain amino acid similarity between MDM2 and MDMX is around 50% shown in figure 1.8.

1.5.1   MDM2 structure and function

The structure of both MDM2 and MDMX includes three main domains (figure 1.5 & figure 1.6): a hydrophobic pocket N-terminal p53 binding domain, a zinc-finger domain and a C-terminal RING-finger domain (Toledo and Wahl, 2007). The C-terminal RING domains are responsible for homodimerisation or heterodimer formation by interaction between MDM2 and MDMX RING domains (Sharp *et al.*, 1999; Tanimura *et al.*, 1999).

The first difference between MDM2 and MDMX is that MDM2 has nuclear localization signal (NLS) and nuclear export signal (NES) domains, which MDMX does not. MDM2 is localized in the nucleus of the cell in non-stressed conditions by the NLS, whereas the NES allows MDM2 to shuttle between the cytoplasm and the nucleus (Tao and Levine, 1999; Boyd *et al.*, 2011). The NES facilitates the ability to export p53 from the nucleus to inhibit the transactivation of genes by keeping p53 in the cytoplasm and blocking its interaction with DNA. Although p53 cannot induce transcription outside of the nucleus, some research has shown that p53 also performs different activities in the cytoplasm (Chipuk *et al.*, 2005; Tasdemir *et al.*, 2008).

The other difference is that the RING domain in the C-terminal region of MDM2 carries an E3 ligase activity, which MDMX does not have (figure 1.8). As an E3 ubiquitin ligase, MDM2 has several substrates including itself, p53, and MDMX. MDMX and p53 can be ubiquitinated for proteasomal degradation by MDM2 (Kawai *et al.*, 2003; Pan and Chen, 2003). The RING domain of MDM2 has been shown to be required for MDM2 to transport p53 out of the nucleus (Boyd *et al.*, 2000c; Geyer *et al.*, 2000). MDM2-mediated mono-ubiquitination of p53 localises it in the cytoplasm

and greatly promotes its mitochondrial translocation and thus its direction of mitochondrial-mediated apoptosis (Marchenko *et al.*, 2007).

1.5.2 Modification and regulation of MDM2

The kinases related to DNA damage activate the p53 pathway and stop the cell cycle in order to repair the damage or, if the damage is irreparable, put the cell into a state of permanent cell cycle arrest (senescence) or programmed cell death (apoptosis).

ATM has been reported to indirectly cause phosphorylation of MDM2 via the c-Abl kinase at Y394, which also inhibits the E3 ligase activity to stabilize p53 for activation of apoptosis (Sionov *et al.*, 2001; Goldberg *et al.*, 2002) (figure 1.9). The AKT kinases regulate cell growth and survival, and they are activated in human cancers; among their targets are MDM2 and MDMX. Phosphorylation of MDM2 at Ser166 and Ser186 (Mayo and Donner, 2001) leads to MDM2 stabilization, and is associated with p53 inhibition.

DNA-PK (DNA-activated Protein Kinase) has been shown to phosphorylate the p53-binding domain of MDM2 at S17 to decrease the affinity of MDM2 for p53 (Mayo *et al.*, 1997). DNA damage-mediated modification of MDM2 not only stops ubiquitination of p53, but it also actively changes the affinity of MDM2 for p53 and instead MDM2 tags MDMX with ubiquitin for degradation. Activation of p53 also causes the transcriptional induction of MDM2 and increases the level of MDM2 protein generating a negative feedback loop (Stommel and Wahl, 2004; Shadfan *et al.*, 2012) (figure 1.9).

A cellular protein MTBP (MDM2 binding protein), which is located on human chromosome 8q24 (Boyd *et al.*, 2000b), has been reported to bind to MDM2 resulting in the induction of G1 arrest (Boyd *et al.*, 2000a). A subsequent study found that MTBP contributes to MDM2-mediated ubiquitination and degradation of p53 (Brady *et al.*, 2005).

The inhibition of p53 by MDM2 and MDMX cooperation can be involved in both the proliferation and altered differentiation status of cancer cells (Marine *et al.*, 2007). Both MDM2 and MDMX have been implicated in regulation of the stability and/or

activity of several other proteins that control cell proliferation, such as the retinoblastoma protein Rb, the heterodimer E2F1-DP1, Numb and Smad (Ganguli and Wasylyk, 2003; Marine and Jochemsen, 2005). Mice lacking both *MDM2* and *MDM4* in the CNS exhibited a phenotype that is more severe and appears earlier than that of *MDM2*-null mice embryos (Xiong *et al.*, 2006). Similarly, p53-mediated apoptosis was increased in the neuroepithelium and in post-mitotic cells in mice lacking both *MDM2* and *MDM4* compared with mice lacking *MDM2* alone (Francoz *et al.*, 2006).
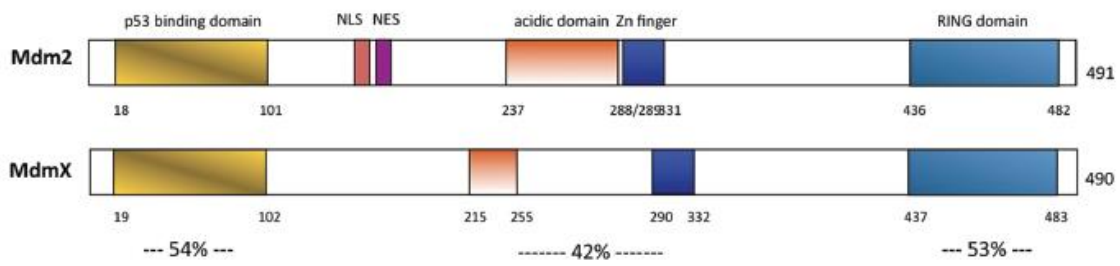
Figure 1.8. Functional domains and similarity of the MDM2 and MDMX oncoproteins. The percentages indicate the degree of amino acid sequence similarity between the individual domains shared by MDM2 and MDMX. NLS = nuclear localization signal; NES = nuclear export signal; Zn finger = Zinc finger (Gannon and Jones, 2012).
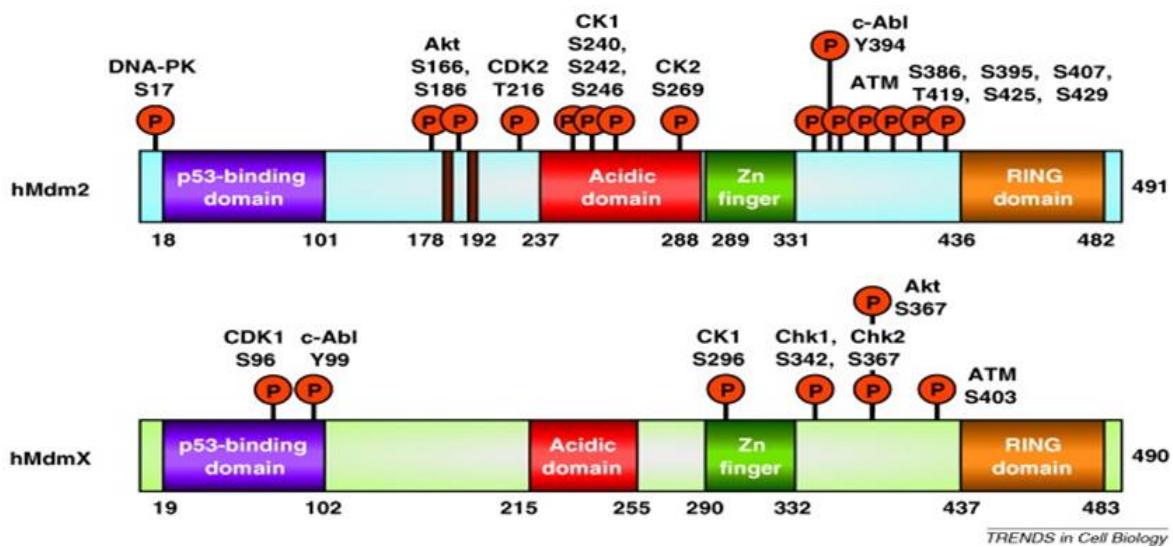
Figure 1.9. Post-translational modification of the MDM2 and MDMX oncoproteins (Wade *et al.*, 2010)

1.5.3 MDM2 and p53 interaction

MDM2 has been demonstrated to negatively regulate p53 in three ways. Firstly, MDM2 binds to the N-terminal transactivation domain (TAD) of p53 and blocks its transcriptional activity. Secondly, MDM2 exports p53 from the nucleus to the cytoplasm. Monoubiquitination can directly promote further modifications of p53 with ubiquitin-like proteins and MDM2 promotes the interaction of the SUMO E3 ligase PIASy with p53, enhancing both sumoylation and nuclear export (Carter *et al.*, 2007). Finally, MDM2 has E3 ligase function leading to poly-ubiquitination of and then proteasomal degradation of p53 and MDMX (Zhang and Xiong, 2001; Vousden and Lu, 2002; Pei *et al.*, 2012; Wade *et al.*, 2013). MDM2 is also a p53 transcriptional target regulated by p53 activation in a negative feedback loop (figure 1.10). Superimposed crystal structures of MDM2 and MDMX docked with p53 illustrating the structural similarity of 54% between MDM2 and MDMX in the p53 binding domain are shown in figure 1.11. MDM2 binds to p53 using three amino acid residues of the p53 peptide, Phe19, Trp23 and Leu26, in the hydrophobic p53 binding pocket (Kussie *et al.*, 1996).

1.5.4 MDM2 mutation and overexpression in cancer

MDM2 is commonly found to be over-expressed in some cancers, including around 20% of sarcoma, and around 10% of stomach, bladder and lung adenocarcinoma as seen in the cBioPortal data shown in figure 1.12A. MDM2 mutations are rare and the distribution of those few *MDM2* mutations that have been reported is shown in figure 1.12B. The mutations of *MDM2* can increase MDM2 protein expression leading to p53 inhibition.
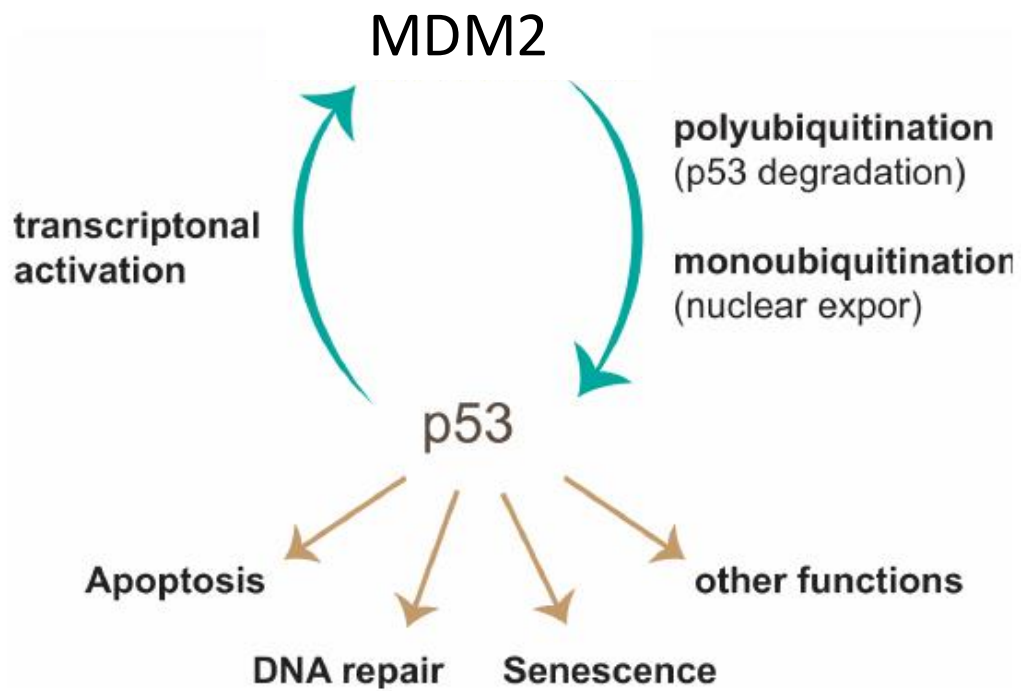
Figure 1.10. MDM2-p53 negative feedback loop (Landre *et al.*, 2014).
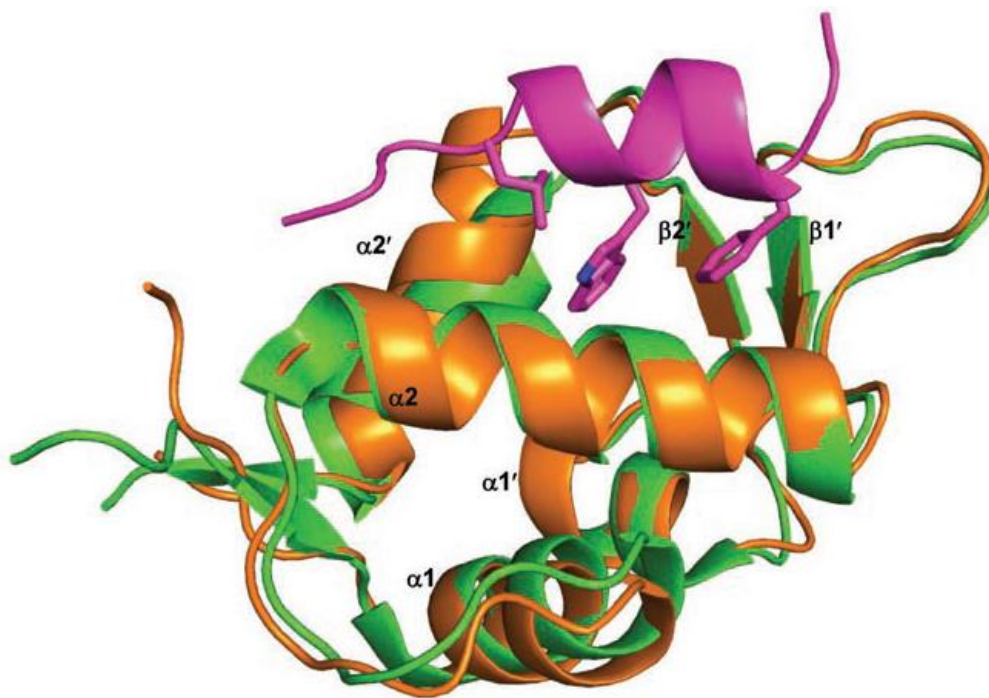
Figure 1.11. Crystal structures of p53 (pink) complexed to MDM2 (orange) and MDMX (green) shown as superimposed ribbon diagrams, with the three key interacting residues of p53 shown as stick structures (Joseph *et al.*, 2010).
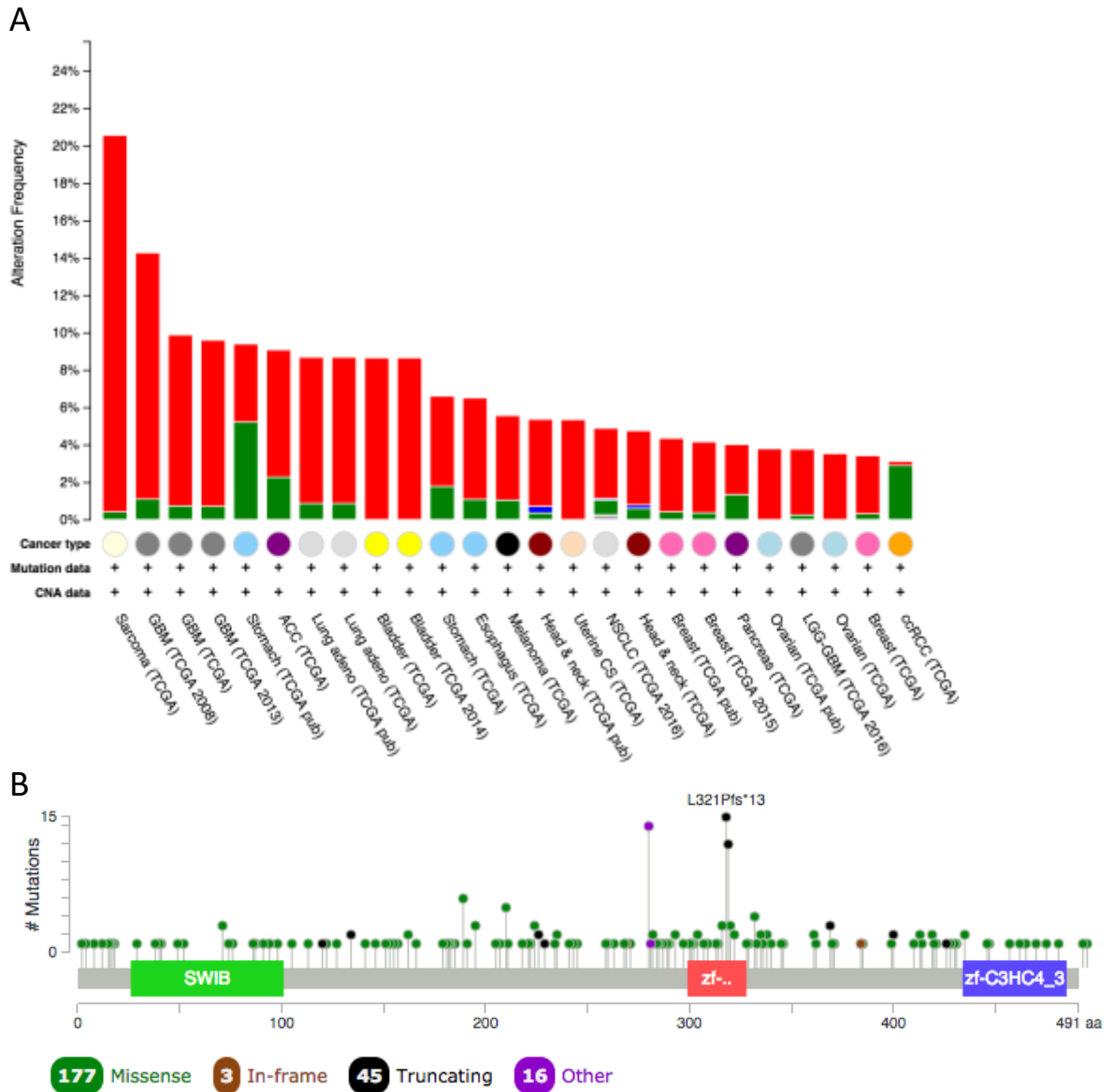
Figure 1.12. (A) The *MDM2* genes data from cBioPortal website (Cerami *et al.*, 2012; Gao *et al.*, 2013). The data was gated to show cancers with over 3% amplification (red) and mutation (green). (B) The position of *MDM2* mutations in human cancer. (http://www.cbioportal.org/) (Cerami *et al.*, 2012; Gao *et al.*, 2013)

1.6   Oncoprotein MDMX

MDMX (gene name *MDM4*) is one of the set of murine double minute (MDM) genes originally discovered as amplified genes carried on double minute chromosomes in a spontaneously transformed mouse NIH3T3 cell line, from which their name is derived. The human *MDM4* gene is located on chromosome 1 at q32-33 and codes for a protein of 490 amino acids (Shvarts *et al.*, 1997; Mancini *et al.*, 2009).

1.6.1   MDMX structure and function

MDMX and MDM2 can form heterodimers by C-terminal RING-RING domain interactions between both proteins. MDMX is closely related to MDM2 in amino acid sequence and overall structure (figure 1.8). N-terminals of both MDM2 and MDMX have p53 binding domains but the similarity of p53 binding domains between MDM2 and MDMX is lower than 50% (figure 1.8) (Gannon and Jones, 2012). MDMX does not have E3 ligase function like MDM2 to ubiquinate p53, although it can still inhibit p53 by direct binding (Jackson *et al.*, 2001).

1.6.2   Modification of MDMX

The overall domain structure and posttranslational modification of MDMX is shown in figure 1.9. C-terminal serine residues of MDMX are phosphorylated through the induction of DNA damage by ATM, Chk1 and Chk2, which stimulates MDMX degradation by MDM2 contributing to p53 activation (Chen *et al.*, 2005a; Chen *et al.*, 2005c; Okamoto *et al.*, 2005; LeBron *et al.*, 2006). AKT was found to directly phosphorylate MDMX at S367, enhancing 14-3-3 binding, which stabilized MDMX and downregulated p53 (figure 1.13) (Lopez-Pajares *et al.*, 2008).Casein kinase 1α (CK1α)-mediated phosphorylation of MDMX increases its affinity for p53 and may reduce p53 activity (Chen *et al.*, 2005b), and c-Abl (also known as ABL1) phosphorylates Tyr99 of MDMX (Zuckerman *et al.*, 2009) leading to the dissociation of p53 from its negative regulators. Chk2 and 14-3-3 cooperatively stimulate MDMX ubiquitination and overcome the inhibition of p53 by MDMX response to DNA damage (LeBron et al., 2006). Oncogenes such as c-Myc can engage damage-independent pathways such as the p14^{ARF} tumour suppressor in order to inhibit

MDM2 and activate p53, or may induce DNA damage kinases and other kinases, which then phosphorylate either MDM2 or MDMX (Wade *et al.*, 2010).

Following resolution of a DNA damage response, Wip1 (wild-type p53-inducible phosphatase-1) can dephosphorylate MDM2 and MDMX, leading to their stabilization. Wip1 directly dephosphorylates MDMX at the ATM-targeted Ser403 and indirectly suppresses phosphorylation of MDMX at Ser342 and Ser367. Wip1 inhibits the DNA damage-induced ubiquitination and degradation of MDMX, leading to the stabilization of MDMX and reduction of p53 activities (Zhang *et al.*, 2009)..

1.6.3 Regulation of MDMX

In contrast to MDM2, MDMX is not regulated by p53. MDMX expression is regulated by mitogenic signals and growth factors (Gilkes *et al.*, 2008). Mitogenic survival signals have also been shown to modulate MDMX. One previous study showed that K-Ras and insulin-like growth factor-1 (IGF1) can increase levels of MDMX mRNA and subsequently increase MDMX protein levels (Gilkes *et al.*, 2008). Some mitogenic signals can also enhance MDM2-MDMX stabilization, thereby further suppressing p53 in order to transform a cell.

The levels of MDM2 and MDMX ubiquitination are in part controlled by the deubiquitinase HAUSP (Meulmeester *et al.*, 2005), which removes ubiquitin from each protein, leading to their stabilization (figure 1.13). However, there is a lack of studies linking HAUSP levels with response to MDM2 inhibitors.

MDMX has been reported to exert oncogenic activity via suppression of retinoblastoma protein (RB), suggesting that both MDM2 and MDMX could be chemotherapeutic targets, although this would have to undergo specific target validation (Zhang *et al.*, 2015). MDMX binds to and promotes RB degradation in an MDM2-dependent manner. Specifically, the MDMX C-terminal RING domain binds to the RB C-pocket and enhances MDM2–RB interaction (Hu *et al.*, 2016).

Ribosomal stress proceeds via the release of ribosomal proteins that inhibit MDM2 ubiquitin ligase activity and stabilize p53. Overexpression of MDMX increases the resistance of cells to low dose 5-Fu, which causes ribosomal stress (Gilkes and

Chen, 2007). Ribosomal proteins bound to MDM2 have also been found to induce degradation of MDMX as a potential step in p53 activation (Gilkes *et al.*, 2006). Ribosomal subunit S7 was found to inhibit MDM2, but this effect, and the subsequent stabilization of p53, were dependent on the presence of MDMX (Zhu *et al.*, 2009). It has been demonstrated by researchers that ribosomal noncoding 5S rRNA can also stabilize MDMX, possibly playing a role in the stable level of MDMX under non-stress conditions (Li and Gu, 2011).
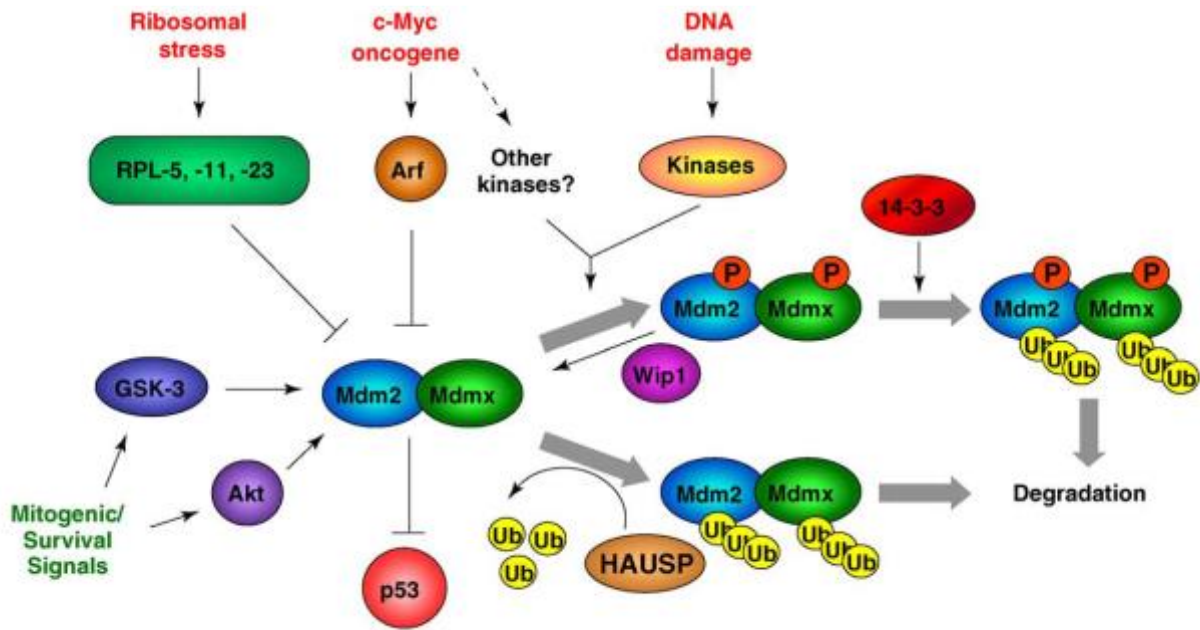
Figure 1.13. Multiple cell signalling cascades converge on MDM2 and MDMX. p53 activating stresses (red print) can signal through damage-dependent and independent pathways to activate p53. Ribosomal stress proceeds via the release of ribosomal proteins that inhibit MDM2 ubiquitin ligase activity and stabilise p53. Kinases associated with proliferation and survival (green print) can also phosphorylate MDM2 and enhance its p53 inhibitory function (Wade *et al.*, 2010).

1.6.4 Isoforms of MDMX

The presence of different isoforms of MDMX have been reported. Immunoblot (Western Blot) analysis detected at least 5 shorter MDMX forms in a panel of 31 human tumour cell lines (Ramos *et al.*, 2001). Seven different shorter isoforms of MDMX have been characterized and shown to be derived from alternative splicing. The transcript variants and different predicted isoforms of MDMX in relation to the functional domains are shown in figure 1.14. These transcript variants, shown in figure 1.15, are designated MDM4-S, MDM4-A and MDM4-G, MDM4-211, MDM4-XALT1 and MDM4–XALT2 (Mancini *et al.*, 2009; Lenos and Jochemsen, 2011).

1.6.4.1 MDMX-S

MDMX-S has been reported to suppress p53-mediated transcription from a p53 target promoter better than full-length MDMX. The DNA damage inducibility of these p53 responsive promoters was suppressed better by MDMX-S than by MDMX. Analysis of the MDMX-S protein indicated that the 13 novel amino acids at its carboxy terminus were responsible for high affinity binding to p53 *in vitro* and for high level expression of the protein in cells. Deletion of this 13 amino acid sequence resulted in a protein that was not able to bind p53 and was not expressed well in cells (Rallapalli *et al.*, 2003).

The MDMX-S splice variant also leads to a decrease in MDMX-FL (MDMX full-length) expression. The mutant allele MDMXΔE6 (MDMX exon 6 deleted) prevented the expression of MDMX-FL, but also led to increased *MDMX-S* mRNA levels (figure 1.15). Mice homozygous for this allele died during embryonic development, but were rescued by a concomitant p53 deficiency. The main effect of a skipping of *MDMX* exon 6 that has been demonstrated is not the synthesis of the Mdm4-S protein, but rather a decrease in *MDMX*-FL expression (Bartel *et al.*, 2005; Bardot *et al.*, 2015). Both the overexpression of the MDMX-S transcript and *MDMX* gene amplification are important prognostic markers for soft-tissue sarcomas (Bartel *et al.*, 2005). The increase in MDMX-S isoform, which results from skipping of *MDMX* exon 6, correlates with more aggressive cancers (Rallapalli *et al.*, 2003).
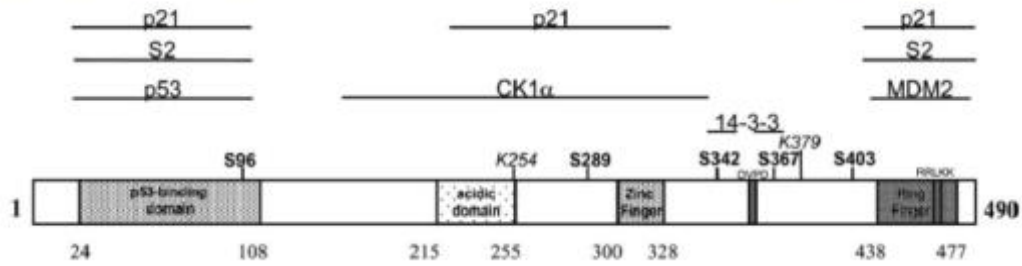
Figure 1.14. MDMX domains and the regions involved in protein-protein interaction (Mancini *et al.*, 2009).
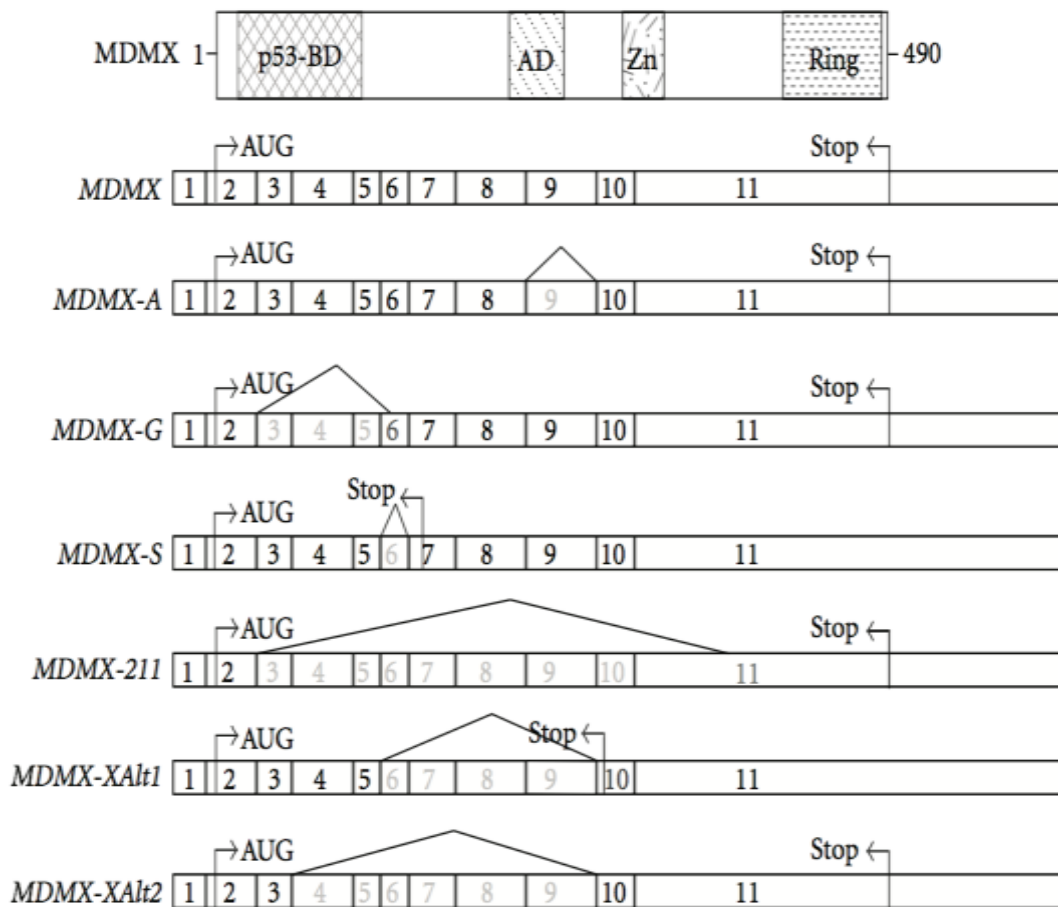
Figure 1.15. Schematic representation of the MDMX protein and scheme of the MDMX mRNA and the reported MDMX splicing variants (Lenos and Jochemsen, 2011)

1.6.4.2 MDMXp60

Cap-independent translation of an N-terminal truncated isoform of human MDMX, MDMXp60 (figure 1.16), is initiated at the 7th AUG codon downstream of the initiation site for full length MDMX-FL at position C384. MDMXp60 lacks the p53 binding motif but retains the RING domain and interacts with MDM2 and MDMX-FL. MDMXp60 shows higher affinity for MDM2. Low levels of MDMXp60 promote degradation of MDM2 whereas higher levels stabilize hMDM2 and prevent MDM2-mediated degradation of MDMX-FL. These results describe a novel alternatively translated MDMX isoform that exhibits unique regulatory activity toward MDM2 autoubiquitination. The data illustrate how the N-terminus of MDMX regulates its C-terminal RING domain and hMDM2 activity (Tournillon *et al.*, 2015).
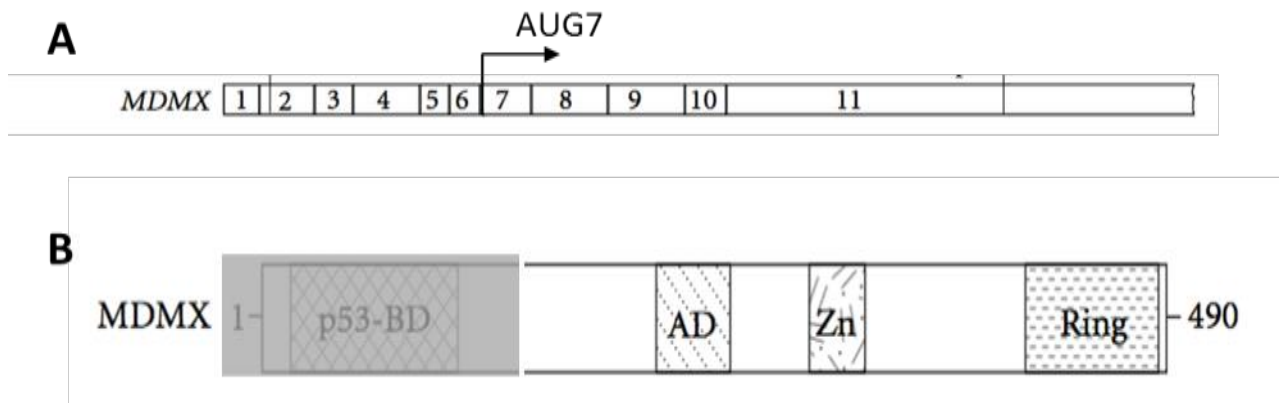
Figure 1.16. The MDMXp60 isoform is initiated at the 7th in frame AUG codon. (A) MDMX mRNA constructs and the mutated AUG sites. (B) The MDMXp60 lacks the first 127 amino acids (grey part), including the p53 binding domain (Lenos and Jochemsen, 2011).

1.6.4.3 WWW element

MDMX has recently been found to contain an autoinhibitory sequence element called the WWW element (figure 1.17A) (Bista *et al.*, 2013). Full-length MDMX has an approximately ~100-fold weaker affinity for the N-terminal domain of p53 than its isolated N-terminal domain. Previous research using NMR spectroscopy and binding studies observed that MDMX (but not MDM2) contains a self-inhibitory element that competes intramolecularly for binding with the N-terminal domain of p53 (figure 1.17B). Deletion or mutation of this element increased binding affinity of MDMX to the level of the isolated N-terminal domain. An alternative splicing variant of MDMX that does not contain the WWW element is found in some aggressive cancers (Bista *et al.*, 2013).

1.6.4.4 MDMX-ALT2

MDMX-ALT2 (MDM4-XAL2 in figure 1.15) is able to dimerize with both full-length MDMX and MDM2, and the expression of MDM2-ALT1 and MDMX-ALT2 leads to the upregulation of p53 protein, and of its downstream transcriptional target, p21. Moreover, the stress-inducible alternative splice forms MDM2-ALT1 and MDMX-ALT2 are important modifiers of the p53 pathway and present a potential mechanism to tailor the p53-mediated cellular stress response (Jacob *et al.*, 2014). The occurrence of cancer-associated splice variants, MDMX-S (that possesses high affinity for p53) and MDMX-ALT2 (that lacks the p53-binding domain), has been reported upon cisplatin treatment (Chandler *et al.*, 2006; Markey and Berberich, 2008; Jacob *et al.*, 2013).
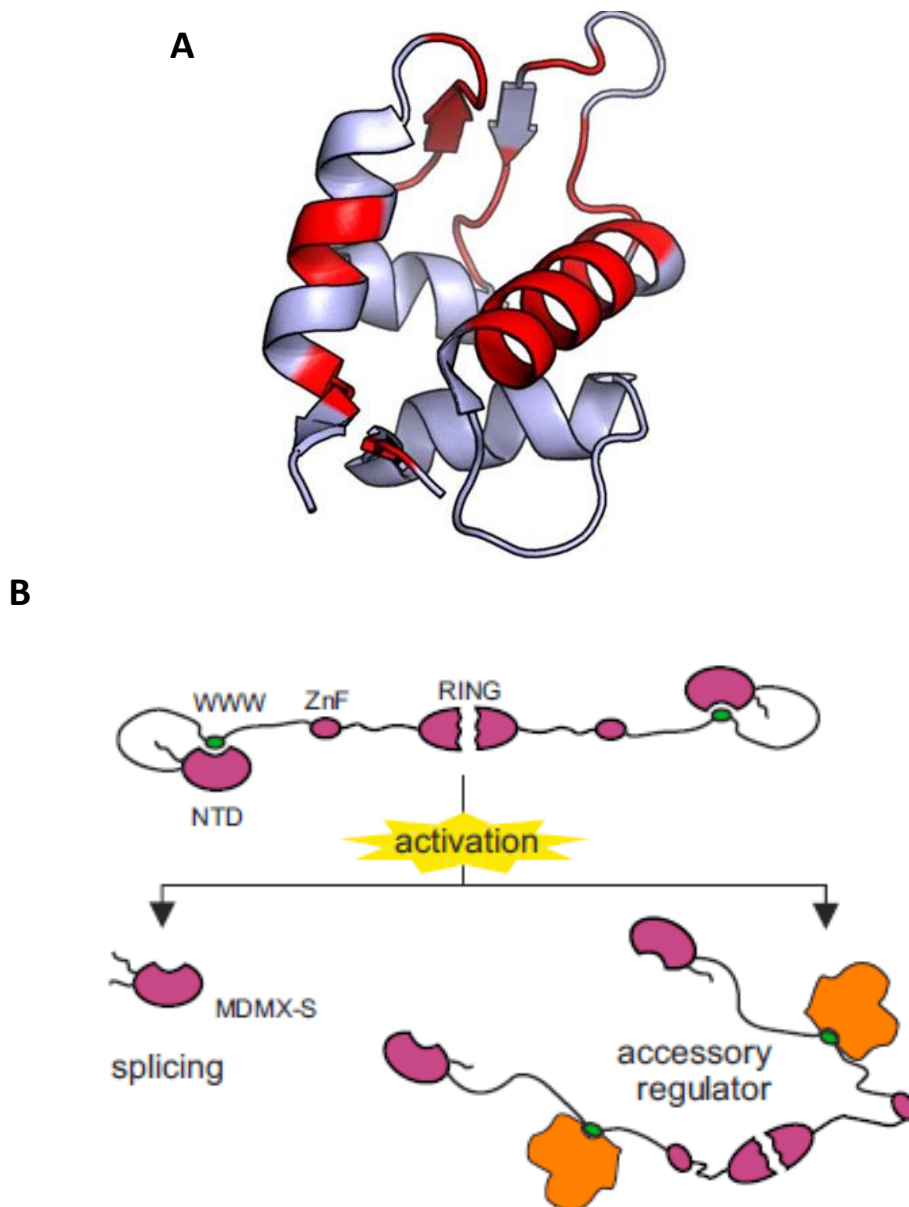
Figure 1.17. (A) Structure of MDMX and WWW binding site (red) mapping. (B) Regulation of MDMX activity by autoinhibition. Full-length MDMX rests in a latent state in which its binding activity with p53TAD is masked. Activation of MDMX can achieved either by alternative splicing, yielding a truncated MDMX variant (MDMX-S), or by binding of the inhibitory module by an accessory factor (Bista *et al.*, 2013).

1.6.5 MDMX in cancer

MDMX as an MDM2 structural homolog and p53 negative regulator has been reported with high expression in 40% of tumour cell lines (Ramos *et al.*, 2001; Danovi *et al.*, 2004). MDMX is also overexpressed in several types of cancers that retain wild-type p53 including gliomas (Riemenschneider *et al.*, 1999), a number of pre-B acute lymphoblastic leukemias (Han *et al.*, 2007) and some primary tumours including breast tumours (Yu *et al.*, 2014; Haupt *et al.*, 2015), head and neck squamous cell carcinomas (Valentin-Vega *et al.*, 2007), retinoblastomas (Laurie *et al.*, 2006), and cutaneous melanoma (Gembarska *et al.*, 2012).

Figure 1.18A shows the frequency of amplification and mutation of *MDM4(MDMX)* in a panel of primary tumour types from the cBioportal database website (Cerami *et al.*, 2012; Gao *et al.*, 2013). *MDM4* amplification can be found in primary data of 13 % of breast, 10% of glioblastoma (GBM), 10% of cholangiocarcinoma, nearly 10% of liver and nearly 10% of lung adenocarcinoma (Burgess *et al.*, 2016). *MDM4* with gain and amplification has been reported in 10% of sarcoma. (Ohnstad *et al.*, 2013). The hot spot of mutations in *MDM4* was shown in figure 1.18B. The higher frequency of mutations locates on V371I (colorectal and stomach adenocarcinoma) and E141K (invasive breast carcinoma and non-small cell lung cancer) and both sites of mutations are not in the domains of MDMX. However, these two mutant sites did not located at the MDMX-S isoform (chapter 1.6.4.1) and WWW autoinhibitory element (chapter 1.6.4.3)
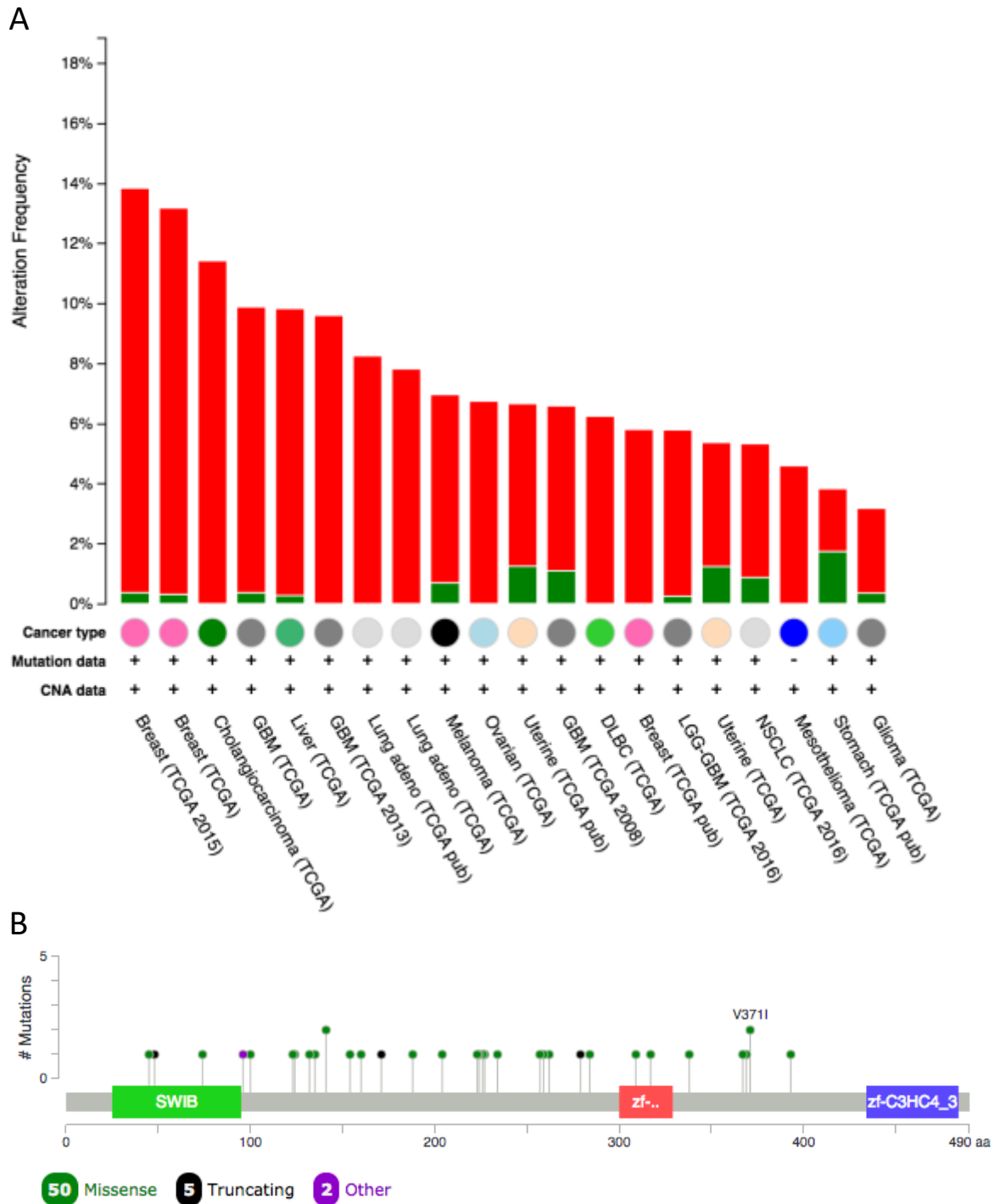
Figure 1.18. The *MDM4 (MDMX)* genes data from cBioPortal website (Cerami *et al.*, 2012; Gao *et al.*, 2013). (A)The data was gated to show over 3% amplification (red) and mutation (green). (B) The distribution of *MDM4* mutations in human cancer. (http://www.cbioportal.org/)(Cerami *et al.*, 2012; Gao *et al.*, 2013).

1.7   MDM2-p53 antagonists

MDM2 blocks the p53 transactivation domain by interacting with three key p53 amino acids which are Phe19 (F19), Tyr23 (W23) and Leu26 (L26) (figure 1.18B) (Bottger *et al.*, 1997). Small molecular compounds are designed to disrupt p53-MDM2 interaction and bind into the N-terminal hydrophobic pocket of MDM2 (Kussie *et al.*, 1996). In wild-type p53 cells these compounds prevent p53 from binding to MDM2 and release the p53 to carry out its transcriptional activation and cell cycle arrest and pro-apoptotic functions (Vassilev, 2004; Vassilev *et al.*, 2004).

A number of small molecule inhibitors of the MDM2-p53 binding interaction have been developed (Hardcastle *et al.*, 2006). Targeting of MDM2 by small molecule antagonists to reactivate p53 function has been developed for cancer therapy. The MDM2-p53 binding inhibitor Nutlin-3, shown in figure 1.19A, is a cis-imidazoline analogue (MDM2 IC_{50} ~36nM; MDMX IC_{50} ~18 µM) (Vassilev *et al.*, 2004). Nutlin-3 has been demonstrated to activate the p53 pathway and inhibit the growth of tumour cells with wild-type p53 both *in vitro* and *in vivo*. Reactivation of p53 by Nutlin-3 causes cell cycle arrest in G1 and G2 phases of the cell cycle and apoptosis. Nutlin-3 binding to MDM2 leads to reactivation of p53, but in the same dose range does not affect cells with transcriptionally inactive mutant p53 (Vassilev *et al.*, 2004). MI-63 (figure 1.20) is a spiro-oxindole compound used as another first generation small-molecule inhibitor of MDM2, which is a more potent MDM2-binding inhibitor than Nutlin-3 (Canner *et al.*, 2009).

RG7112 (figure 1.20) was subsequently the first of cis-imidazoline class to enter clinical trials. The results from several Phase I trials indicated RG7112-induced thrombocytopenia and insight into the role of the p53-MDM2 auto-regulatory loop in normal megakaryocytopoiesis (Iancu-Rubin *et al.*, 2014). Limiting toxicity RG7388 (figure 1.20) is high-affinity spiroindoline-3,3′-pyrrolidine MDM2 inhibitor which have been tested as second-generation clinical antagonists with more potency and selectivity than the earlier nutlin series by Hoffmann-La Roche (Ding *et al.*, 2013). RG7112 and RG7388 have been subject to early phase clinical trials in acute myeloid leukemia (Andreeff *et al.*, 2016; Reis *et al.*, 2016). RG7112 has been shown

to activate the p53 pathway and decrease cell proliferation in patients with MDM2 amplification and wild-type p53 Liposarcoma (Ray-Coquard *et al.*, 2012).
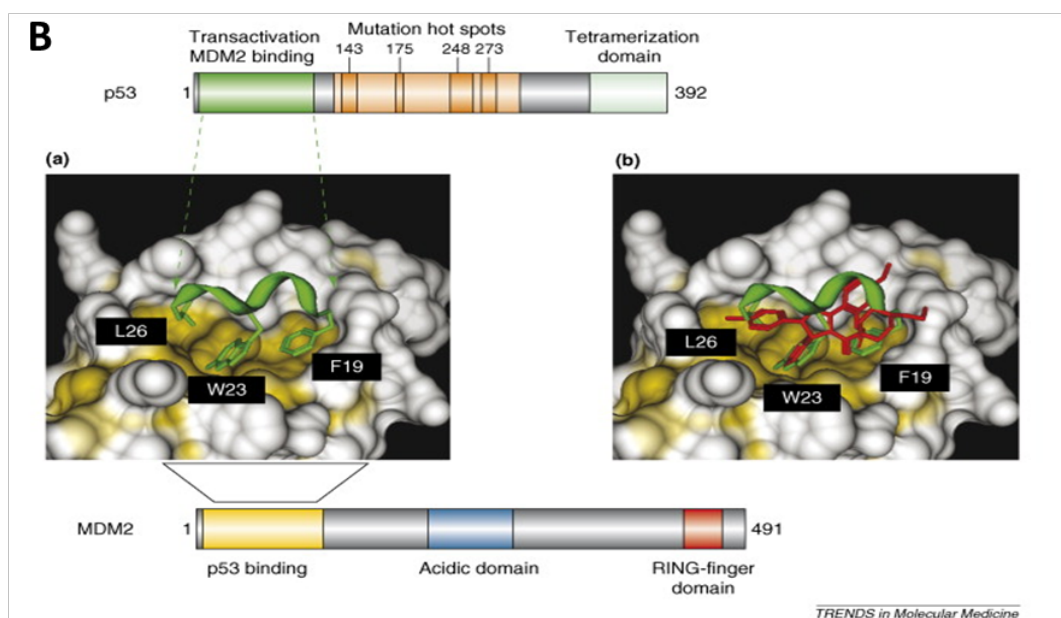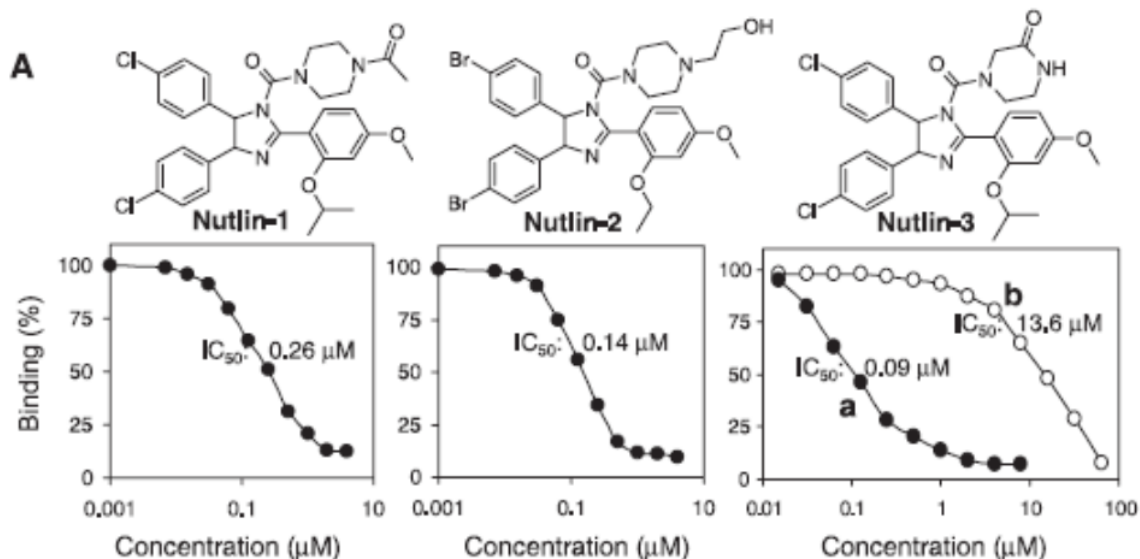
Figure 1.19. (A) Chemical structures and binding ability of Nutlin-1, Nutlin-2 and Nutlin-3 (a and b) (Vassilev *et al.*, 2004). (B) Structure of the p53–MDM2 interaction and nutlin-2 binding. (a) MDM2 (yellow) and p53 (green) interact with each other at their N-terminal domains through a well-defined p53 binding pocket. MDM2 binds to p53 though three amino acid residues of the p53 peptide. (b) Nutlin-2 (red) binds to the p53 pocket of MDM2 by mimicking the interaction of the three crucial amino acid residues from the p53 peptide (green) (Janz *et al.*, 2007).
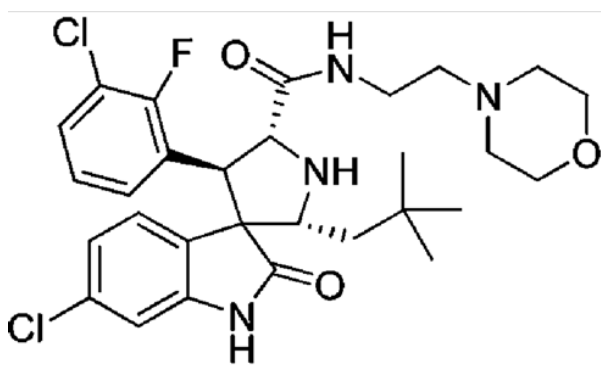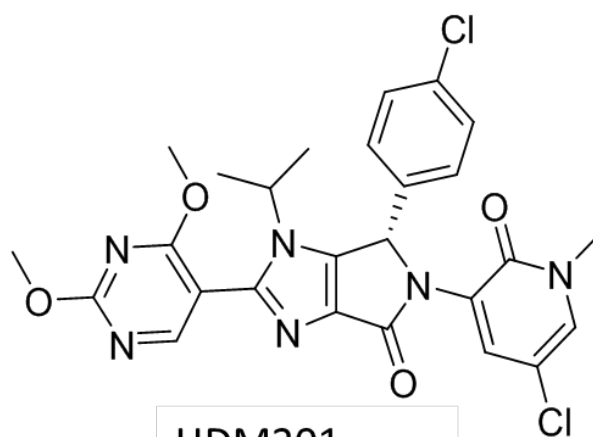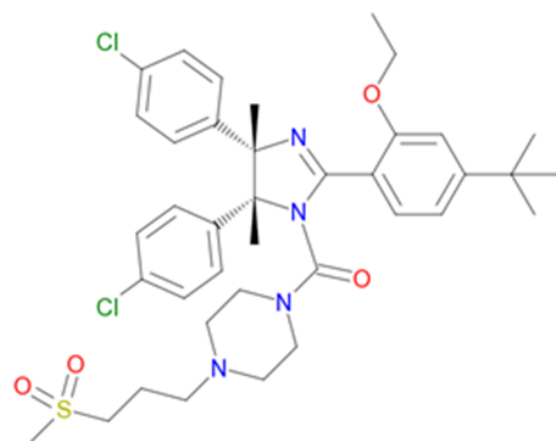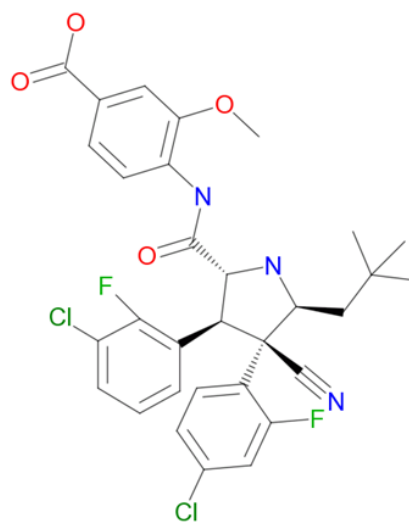
Figure 1.20. Chemical structures of MI-63, HDM201, RG7112 and RG7388 (Canner *et al.*, 2009; Yu *et al.*, 2009; Ding *et al.*, 2013; Furet *et al.*, 2016).

1.7.1 MDM2 inhibitors in cancer treatment

Figure 1.21 shows the type of drugs targeted at the MDM2/X-p53 network. The alteration frequency of *TP53, MDM2* and *MDM4(MDMX)* in different types of cancers showed in figure 1.21A. There are plenty of pre-clinical studies and a limited number of clinical trials that have tested MDM2 inhibitors in a wide range of cancers. Cancers such as chronic lymphocytic leukaemia (CLL) (Secchiero *et al.*, 2006), acute lymphoblastic leukaemia (ALL) (Long *et al.*, 2010), acute myeloid leukaemia (AML) (Long *et al.*, 2010), renal cell myeloma (Saha *et al.*, 2010), carcinoma (RCC) (Polanski et al., 2014), laryngeal carcinoma (Arya et al., 2010), neuroblastoma (Van Maerken *et al.*, 2009), melanoma (Lu *et al.*, 2013), and mantle cell lymphoma (Tabe *et al.*, 2009) often contain wild-type p53, which allows the targeting of interactions between MDM2 and p53 in order to activate p53 (Khoo *et al.*, 2014). Insert in figure 1.21A shows the mutual exclusivity observed between MDM2 expression and p53 deletion in sarcomas.

HDM201 (MDM2 IC$_{50}$ ~ 0.13 nM) is an imidazolopyrrolidinone analogue developed by Novaris (figure 1.20). HDM201 as a second generation p53-MDM2 inhibitor is recently entered phase I clinical trials in advanced solid tumour with wild-type *TP53.* (Furet *et al.*, 2016).
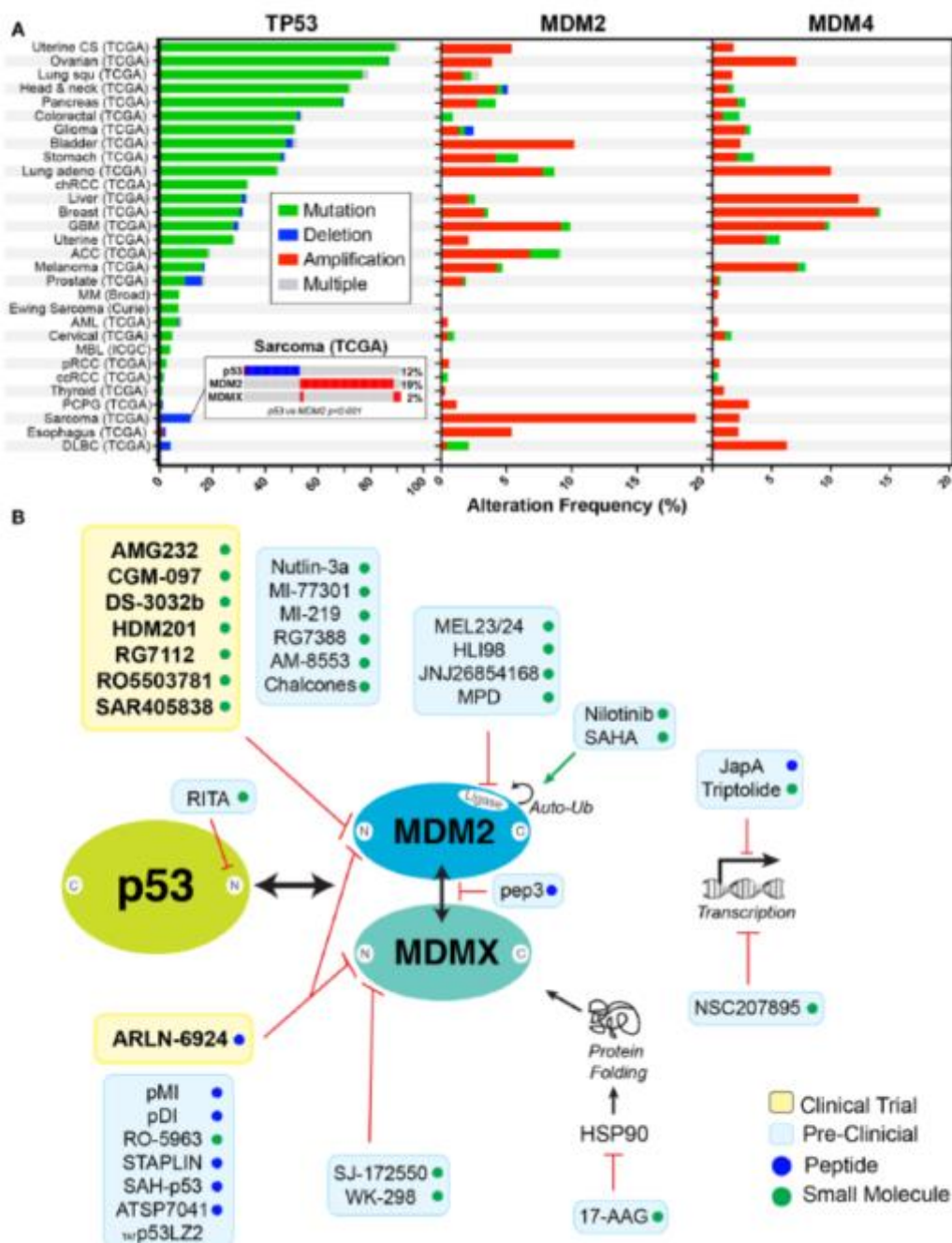
Figure 1.21. Targeting of p53 in cancer. (A). Frequency of alterations are shown with mutation (green), deletion (blue), amplification (red), and combination of alterations (grey) in *TP53, MDM2*, and *MDM4* in cancers. Data derived from cBioPortal (http://www.cbioportal.org)**) (Cerami *et al.*, 2012; Gao *et al.*, 2013). (B) Schematic representation of inhibitors in clinical trials (yellow box) or in preclinical studies (blue box) targeting the p53–MDM2/X axis. Compounds are either small molecules (green circle) or peptides (blue circle) (Burgess *et al.*, 2016).**

1.7.2   Combination therapy with MDM2 antagonists

A number of researchers have reported on combination treatment of Nutlin MDM2 antagonists with traditional treatment or different drugs in cancer therapy (table 1.2) (Khoo *et al.*, 2014). Previous research has reported that combinations of RG7388 with cisplatin, doxorubicin, topotecan, temozolomide and busulfan were synergistic in growth inhibitions. Furthermore, combination treatments led to increased apoptosis, as evident by higher caspase-3/7 activity, compared to either agent alone. The data of increasing caspase-3/7 activity showed that RG7388 is highly potent against wild-type p53 neuroblastoma cells (Chen *et al.*, 2015). It has been documented that combination treatment with MDM2 inhibitors (Nutlin-3 & RG7388) and cisplatin has synergistic potential for the treatment of ovarian cancer, dependent on cell genotype (Zanjirband *et al.*, 2016).

Recent evidence reported potentiation of MDM2 inhibitors (Nultin-3 and RG7388) by combination with WIP1 (wild-type p53-inducible phosphatase-1) inhibitor (Esfandiari *et al.*, 2016; Pechackova *et al.*, 2016; Sriraman *et al.*, 2016). The potentiation correlated with significant increase in MDM2 inhibitor–induced cell death. The WIP1 inhibitor (GSK2830371) promotes the degradation of WIP1 protein as well as directly blocking WIP1 phosphatase enzymatic activity and suppressing WIP1 dephosphorylation of $p53^{ser15}$ to enhance p53 transcriptional activity by MDM2 antagonists. The combination treatment provided an increase of gene expression in the subset of early RG7388-induced p53 transcriptional target genes. These findings demonstrate that potent and selective WIP1 inhibition potentiates the response to MDM2 inhibitors in *TP53* wild-type cells (Esfandiari *et al.*, 2016).

List of drug combinations	Tumour types (xenograft models)
Nutlin with doxorubicin; nutlin with cytarabine	AML and B-CLL
Nutlin with vincristine	Neuroblastoma, rhabdomyosarcoma and melanoma
Nutlin with roscovitine	Various cancers
Nutlin with valproic acid	AML
Nutlin with Aurora kinase inhibitors	Various cancers
Nutlin with 1,2,5-dihydroxyvitamin D_3	AML
Nutlin with XIAP inhibitor	AML
Nutlin with cisplatin	Ovarian cancer
Nutlin with androgen-depleting agent	Prostate cancer
Nutlin with CDK1 inhibitor; JNJ-7706621	Melanoma
Nutlin with TRAIL	Haematological malignancies
Nutlin with sorafenib	Renal cell carcinoma
Nutlin with ABT-737	Various cancers
Nutlin with selumetinib (AZD6244)	AML
Nutlin with KPT-185	AML
Nutlin with sorafenib (independent of p53 status)	AML
Nutlin with dasatinib (independent of p53 status)	B-CLL
Nutlin with radiation	Lung and prostate cancer

Table 1.2. Summary of published experimental drug combinations with Nutlin. AML, acute myeloid leukaemia; B-CLL, B cell chronic lymphocytic leukaemia; CDK1, cyclin-dependent kinase 1; p53, tumour suppressor p53; TRAIL, TNF-related apoptosis-inducing ligand; XIAP, X-linked inhibitor of apoptosis protein (Khoo *et al.*, 2014) (Secchiero *et al.*, 2004; Cao *et al.*, 2006; Ribas *et al.*, 2006; Kojima *et al.*, 2008; Wade *et al.*, 2008; Michaelis *et al.*, 2009; Van Maerken *et al.*, 2009; Carter *et al.*, 2010; Thompson *et al.*, 2010; Zhang *et al.*, 2010; Tovar *et al.*, 2011; Zauli *et al.*, 2011; McCormack *et al.*, 2012; Zauli *et al.*, 2012; Dagnell *et al.*, 2013; Kojima *et al.*, 2013; Mir *et al.*, 2013; Vatsyayan *et al.*, 2013).

1.8 MDMX-p53 antagonists & MDM2/X- p53 co-antagonists

MDMX has poor binding ability to MDM2 inhibitors (Vassilev, 2004; Vassilev *et al.*, 2004; Patton *et al.*, 2006; Wade *et al.*, 2006; Shangary and Wang, 2009). Some studies suggested that cells with overexpression or amplification of MDMX might not be sensitive to MDM2 antagonists because of poor binding ability to MDMX. Overexpression or amplification of MDMX might reduce the efficiency of MDM2 inhibitors to activate p53-dependent pathways (Hu *et al.*, 2006; Koblish *et al.*, 2006; Wade *et al.*, 2006). The N-terminal hydrophobic p53 binding pockets of MDM2 and MDMX show structural differences resulting in poor binding ability of MDMX and MDM2 antagonists (Popowicz *et al.*, 2007; Popowicz *et al.*, 2008; Riedinger and McDonnell, 2009). Inhibition of both MDM2 and MDMX has been suggested in order to achieve complete activation of p53 in MDM2 and/or MDMX high expression and amplified tumour cells.

Several small molecule compounds have been developed in an attempt to target MDMX, although this has proved more difficult than specifically targeting MDM2 (figure 1.22). A benzofuroxan derivative (NSC207895) has been identified to target MDMX protein expression. It seems to suppress the *MDM4* promoter leading to downregulation of MDMX protein levels, and causes p53-independent transactivation of pro-apoptosis genes (Wang *et al.*, 2012). WK298, targeting the MDMX-p53 protein-protein interaction, was the first reported crystal structure of a small molecule inhibitor-MDMX complex, and WK298 has been shown to disrupt the p53-MDMX interaction to reactivate p53 function. However, WK298 does not have specific cellular activity (Popowicz *et al.*, 2010).

The research to date has tended to focus on MDM2 rather than MDMX. Although for small molecule inhibitors of the MDM2-p53 interaction, development is progressing fast, with multiple compounds available for the inhibition of MDM2-p53 binding, the development of MDMX-p53 binding antagonists is still in the early stages and proving to be less readily tractable.

Dual antagonists for MDM2-p53 and MDMX-p53 binding may reactivate p53 more effectively than only MDM2 or MDMX antagonists. RO-2443 is a small molecule dual

inhibitor in the early stage of drug development for targeting MDM2-p53 and MDMX-p53. It was reported to bind to MDMX by dimer formation, but has poor water solubility (Graves *et al.*, 2012). RO-5963, which is an Indolyl hydantoin close analogue of RO-2443, has improved water solubility. The MDM2/X co-inhibitor RO-5963 has a similar inhibitory activity to Nutlin-3a, as shown in figure 1.22 (MDM2 IC_{50} ~17.3 nM; MDMX IC_{50} ~24.7nM). This co-inhibitor also binds to the p53 binding pocket of MDMX and results in protein dimerization (Graves *et al.*, 2012). Although Nutlin-3a activates p53 potently in cell culture models, it is inactive against MDMX, whereas RO-5963 is reported to inhibit high levels of both MDM2 and MDMX in cells (Graves *et al.*, 2012; Wade *et al.*, 2013). In this project, RO5963 was used to test the response to MDM2/X-p53 binding inhibitors in a panel of cell line models.

Previous studies have also described peptide compounds which disrupt MDM2-p53 and MDMX-p53 complexes such as SAH-p53-8 (Bernal *et al.*, 2010), PDI (peptide dual inhibitor) (Madden *et al.*, 2011) and PMI (Pazgier *et al.*, 2009). SAH-p53-8, which is based on the p53 transactivation domain alpha-helix, has a higher binding affinity for MDMX than MDM2, and is a poor antagonist of MDM2-p53 in the presence of high level MDM2 expression (Bernal *et al.*, 2010; Verdine and Hilinski, 2012). Recent studies also show that stapled α−helical peptide MDM2/X inhibitors have the ability to disrupt the p53 interaction with both MDMX and MDM2 (Chang *et al.*, 2013). A stapled peptide MDM2/X inhibitor has also been tested in a phase I clinical trial in advanced solid tumour or lymphomas with wild-type *TP53*.

This study has focused more on the MDMX oncoprotein as a therapeutic target and determinant of the response to MDM2-p53 binding antagonists and MDM2/X-p53 binding dual antagonists in human cancer.
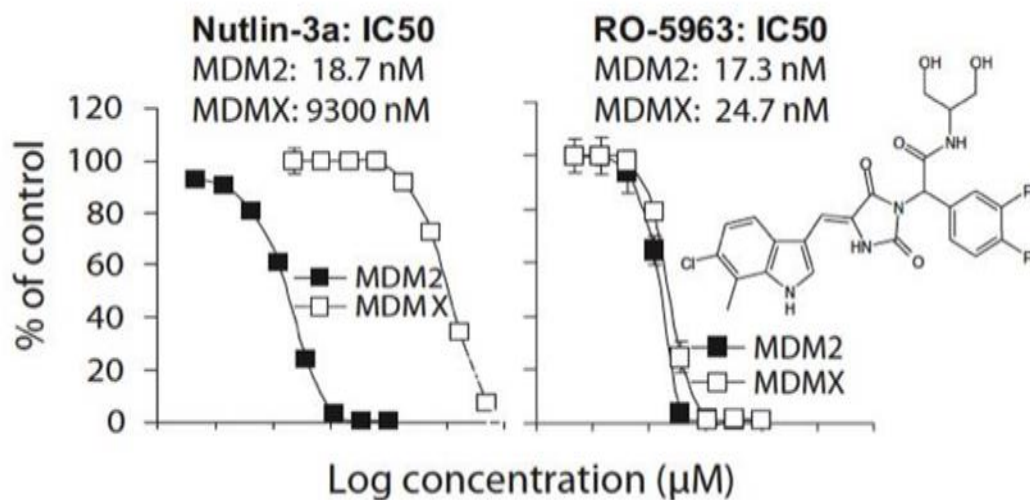
Figure 1.22 The structure and of potency of RO-5963 compared with Nutlin-3a in cell free assays. RO-5963 is an inhibitor of both MDM2-p53 and MDMX-p53 interactions, in contrast to Nutlin-3a, which is a potent inhibitor of MDM2, but shows much less activity against MDMX (Graves *et al.*, 2012).

1.9 Hypotheses

MDMX(*MDM4*) amplification and over-expression is associated with altered response to MDM2-p53 binding antagonists in a wide range of human cancers.

1.10 Aims

1) To study the response of cell line models to small molecule MDM2-p53 binding antagonists Nutlin-3 & RG7388 and the MDM2/X- p53 co-antagonist RO5963.

2) To confirm the wild-type p53 status of MDMX amplified JEG3 and MRK-nu-1 cells by DNA sequence analysis.

3) To investigate the p53 functional response in JEG3, MRK-nu-1 cells exposed to Nutlin-3, RG7388 and RO5963 by the induction of p53 responsive genes, including p21, MDM2 and BAX.

4) To test the ability of MDM2-p53 binding inhibitors Nutlin-3, RG7388 and RO5963 to activate p53 in the presence and relative reduction of MDMX expression achieved by a regulated lentiviral shRNA and siRNA knockdown system.

5) To develop and characterise *TP53* mutant sub-clones of JEG-3 and MRK-nu-1 *MDM4(MDMX)* amplified cell lines. This will provide matched *TP53* wild-type and mutant cell line pairs for testing the specificity of agents targeted against the MDMX-p53 binding interaction.

6) To better understand the cellular function and therapeutic potential of targeting MDMX by investigating the downstream expression transcriptomic consequences of knocking down MDMX.

Chapter 2 Materials and Methods

2.1 Cell culture

Cell culture work was carried out in sterile conditions in class II biological safety containment hoods (Biomat, Medair Technologies, MA, USA). All cell lines used in this study are displayed in table 2.1, alongside their MDMX, MDM2 and p53 status. All cell lines were authenticated using short tandem repeat (STR) DNA profiling (LGC Standards) and early post-authentication passages were cryogenically preserved in liquid nitrogen until the working stock reached post-authentication passage 30, after which a lower passage number reserve batch was revived and used in subsequent experiments. STR DNA sequences are 1-6bp long variable repeated DNA motifs providing unique molecular fingerprints which can be used to identify each individual cell line or host (Reid *et al.*, 2004). Cell lines were tested every 3-6 months for mycoplasma infection (Work carried out by Elizabeth C. Matheson).

The *MDM4*-amplified tumour cell line JEG-3 (placental choriocarcinoma) was maintained in EMEM medium (Sigma-Aldrich, UK) with 10% heat-inactivated FBS (Gibco, Scotland), 2 mM L-glutamine (Sigma-Aldrich, UK) and 1% Pen/Strep (Sigma-Aldrich, UK). MRK-nu-1 (breast carcinoma) was cultured in Dulbecco's modified Eagle's medium (DMEM/F12, Gibco, Scotland) with 10% FBS. These two *MDM4*-amplified cell lines are both reported to be wild-type for p53. The tumour cell lines SJSA-1, S-M6R1 (SJSA-1, MI63 resistant), SN40R2 (SJSA-1, Nutlin resistant), NGP, SKNSH, MCF-7, HCT116 +/+ & HCT116 -/- were maintained in RPMI-160 medium supplemented with 2 mM L-glutamine 10% FBS and 1% Penicillin / Streptomycin.

Cell line	Type	*MDMX*	*MDM2*	*TP53*
JEG-3	Placental choriocarcinoma	Amp	WT	WT
MRK-nu-1	Breast carcinoma	Amp	WT	WT
SJSA-1	Osteosarcoma	WT	Amp	WT
S-N40R2	SJSA-1 daughter cell line	WT	Amp	MUT
S-M6R1	SJSA-1 daughter cell line	WT	Amp	MUT
NGP	Neuroblastoma	HE	Amp	WT
N-20R1	NGP daughter cell line	HE	WT	MUT
SKNSH	Neuroblastoma	HE	WT	WT
MCF-7	Breast adenocarcinoma	HE	WT	WT
HCT116 +/+	Colorectal carcinoma	HE	Amp	WT
HCT116 -/-	Colorectal carcinoma	HE	Amp	Null

WT: Wild-type; Amp: amplified; MUT: mutant; Null: p53 null; HE: High expression.

Table 2.1. Gene status information on cell lines

2.1.1 Passage of cells

Cell lines were cultured as adherent monolayers in medium and grown in humidified incubators (MCO-20AIC, SANYO, UK) at 37°C and 5% CO_2. Cells were passaged at over 80 % confluency in 25 cm^2, 75 cm^2 and 175 cm^2 flasks (Nunc, Denmark). Cells were washed in 10ml PBS (Gibco, Paisley, Scotland) and then 1 ml 1x trypsin-EDTA (Sigma-Aldrich, UK) was added. Approximately 5 minutes incubation is required to detach cells from the surface of the flask or plate bottom. Cell suspension was diluted using fresh medium and was transferred into new flasks to continue growing. Otherwise, the cells were proceeded to experiments such as drug treatment.

2.1.2 Estimating cell densities

Cell densities for suspension cell cultures or harvested attached monolayer cultures were determined by cell counting. A haemocytometer (AC1000 Improved Neubauer, Hawksley, UK) was used to determine the cell density of a cell suspension. A small volume (10µl) of cell suspension was transferred from a growing cell culture flask to each side of the haemocytometer. Cells lying within a 1 mm^2 area in each chamber were counted by microscope examination. The average number observed in two chambers times 10^4 provided an estimate of the cell density in the sampled cell suspension (cell density=Av.x10^4).

2.1.3 Culture from cell stock and storage of cells

Cell stocks were defrosted in a waterbath at 37°C in order to resurrect cells. Then the stock vial was transferred to a sterile universal tube and centrifuged at 1200 rpm for 5 minutes (Mistral 3000, MSE, UK) to remove media containing Dimethyl Sulfoxide (DMSO, Sigma-Aldrich, UK.). The cell pellet was resuspended in fresh medium and transferred to a 25 cm^2 flask to be incubated at 37°C, 5% CO_2 in an incubator.

For cryogenic storage, cells were harvested by trypsinisation, resuspended in medium and the suspension was centrifuged at 200 g for 5 minutes at room temperature. The cell pellet was resuspended in freezing medium (culture medium, 20% FBS and 10% DMSO) to achieve a cell density of 1-2 x10^6 cells/ml. One millilitre aliquots of cell suspension were placed into a cryogenic vial (NUNC$_{TM}$, Rochester, NY, USA) labelled

with the name of the cell line and passage number. Vials were frozen at -80°C overnight and transferred into liquid nitrogen storage (Biosystem, Cryostor) for long-term maintenance.

2.1.4   MDM2 inhibitor resistant TP53 mutant sub-clones

MDM2 inhibitor resistant *TP53* mutant sub-clones were developed from parental cell lines by culturing the parental cells with MDM2 inhibitors. MDM2 inhibitor resistant *TP53* mutant daughter clones S-N40R2 and S-M6R1 (table 2.1) were SJSA-1 daughter cell lines from culturing in MI-63 and Nutlin-3 respectively. Nutlin-3 resistant *TP53* mutant daughter clones N_N20R1 (table 2.1) were NGP daughter cell lines from culturing in Nutlin-3. *TP53* mutant sub-clone cell lines were developed for comparison with *TP53* wild-type cells of their response to MDM2 antagonist-mediated p53-dependent cellular effect. Sanger sequencing later determined that these cell lines harbour *TP53* mutations and show loss of p53 transcriptional function. All MDM2 inhibitor resistant *TP53* mutant sub-clones work was carried out by Dr Junfeng Liu, Dr Xiaohong Lu and Dr Catherine Drummond (Drummond *et al.*, 2016) . STR profiling was not able to differentiate parental *TP53* wild-types from their MDM2 inhibitor resistant daughter cell lines because the daughter cell lines are isogenic or very closely related to their parental cell lines, but nevertheless provided confirmation that the resistant cell lines were otherwise isogenic with the parental cell lines.

2.2   Polymerase chain reaction (PCR)
2.2.1   DNA sample preparation and DNA extraction

Total DNA was extracted from JEG-3 and MRK-nu-1 cell lysates using a DNA extraction kit (QIAamp DNA mini kit, QIAGEN, USA). DNA samples were quantified and qualified by a Nano Drop (ND-1000, NanoDrop, Delaware USA) spectrophotometer with light absorbance at 260 nm and 280 nm wavelengths.

2.2.2   PCR and PCR product purification

Table 2.2 shows the sequences of all sense and antisense primers used to amplify the *TP53* exons, with their annealing temperatures. Sample DNA and primers were

added to PCR master mix (PCR gold buffer (Promega, Southampton, UK), 2.5 mM MgCl$_2$ (Roche, USA), dNTP's (Promega, Southampton, UK) and dH$_2$O) as shown in table 2.3. The *TP53* gene DNA in JEG-3 and MRK-nu-1 cells was amplified by PCR using p53 exon 2-11 primers (table 2.2) and running touchdown55, touchdown58 and touchdown60 PCR programmes for annealing temperatures 55°C, 58°C and 60°C, respectively, on the thermal cycler (GeneAmp PCR System 9700, Applied Biosystems) (table 2.3).

The PCR products were analysed using a 2% agarose gel to check for a clean product of the expected size, which was then extracted using a PCR product purification kit (Invitrogen by Thermo Fisher Scientific, USA). The PCR products were sent to DBS genomics for Sanger dideoxy sequencing. The p53 exon sequencing results were analysed by visual inspection of the chromatograms and alignment with a normal reference sequence using the SeqMan software package (DNAStar).

Exon	Sense	Antisense	AT*
Exon 2	CGA GCT GTC TCA GAC ACT GG	CCT TGT CCT TAC CAG AAC GTT G	58 °C
Exon 3	CAT GGG ACT GAC TTT CAG CTC TTG	CGG GGA CAG CAT CAA ATC ATC	55 °C
Exon 4	GTT CTG GTA AGG ACA AGG GT	ATA CGG CCA GGC ATT GAA GT	55 °C
Exon 5	ATC TGT TCA CTT GTG CCC TG	CAA CCA GCC CTG TCG TCT CTC	55 °C
Exon 6	GCC TCT GAT TCC TCA CTG AT	GGA GGG CCA CTG ACA ACC A	55 °C
Exon 7	AAG GCG CAC TGG CCT CAT CTT	ACAG GGG TCA GCG GCA AGC AGA	60 °C
Exon 8	GAG CCT GGT TTT TTA AAT GG	TTT GGC TGG GGA GAG GAG CT	60 °C
Exon 9	AGC GAG GTA AGC AAG CAG G	GCC CCA ATT GCA GGT AAA ACA G	55 °C
Exon 10	CTT CTC CCC CTC CTC TGT TGC	GAA GGC AGG ATG AGA ATG GA	60 °C
Exon 11	TGG TCA GGG AAA AGG GGC AC	GAG AGA TGG GGG AGG GAG GC	58 °C

*AT: Annealing temperature

Table 2.2. Primer sequences and annealing temperatures of *TP53* exons

Reagent	Amount
PCR Gold Buffer	2.5 µl
MgCl$_2$ (50 mM)	2.5 µl
dNTP's (2.5 mM)	2.5 µl
Primer SN (10µM)	1 µl
Primer ASN (10µM)	1 µl
dH$_2$O	10.25 µl
Ampliq Gold	0.25 µl
DNA	5 µl

Touchdown programme	Temperature	Time
Hot start	94 °C	10 min
14 cycles	94 °C	20 sec
	AT* + 7 °C	1** min
	72 °C	1 min
26 cycles	94 °C	20 sec
	AT*	1 min
	72 °C	1 min
End	72 °C	5 min

Total 25 µl   *AT: Annealing temperature show on Table 2.2

Table 2.3. PCR reagents and Touchdown running programme.

2.3 Quantitative real-time PCR

2.3.1 Total RNA extraction

MRK-nu-1 cells were seeded into a 6-well plate with 2x10^5 cell/well. Total RNA was extracted for gene expression profiling by Affymetrix HTA 2.0 microarray and for following qRT-PCR validation. After cells were harvested and lysed, RNA was extracted from MRK-nu-1 cell lysates using an RNeasy mini kit (QIAGEN, Germany).

2.3.2 Estimation of nucleic acid concentration

Extracted MRK-nu-1 total RNA samples were quantified and the quality checked using a Nano Drop (ND-1000) spectrophotometer to measure light absorbance at 260 & 280 nm wavelengths. A 260:280 ratio of ~2.0 was considered as pure RNA. The concentrations were used to calculate the volumes required for qRT-PCR reactions.

The Nanodrop sample loading platform has a receiving fibre optic and was washed with distilled water before and after use. One microlitre of the sample was loaded and detected by the fibre optic. The solvent containing the sample (e.g. elution buffer or

distilled water) was used as blank control. The Nanodrop covers a spectrum of 220nm-750nm which is used for measurement of the concentration of samples containing molecules that show absorbance in this spectral range. Sample type DNA-50 software option was used for DNA quantification and RNA-40 for RNA quantification. Nucleic acids absorb at 260nm and protein or phenol contaminants absorb at 280. Therefore this ratio can be used to evaluate the purity of samples. A 260:280 ratio of ~1.8 was considered as pure DNA and ~2.0 as pure RNA. 260:230 ratio is another measure of nucleic acid purity which is normally higher than the 260:280 ratio for a given sample (normally 1.8-2.2). Considerably lower 260:230 ratio suggests carbohydrate or solvent contamination as they both absorb strongly at 230.

2.3.3 *Quantitative real-time PCR*

Quantitative real-time PCR (qRT-PCR) is used for quantification of nucleic acids. Total messenger RNA was reverse-transcribed to cDNA using the Promega Reverse Transcription System (A3500, Promega, Southampton, UK). In order to assess the quantity of transcripts of interest, specific primers were designed to flank regions of a given gene's mRNA, including all known splice variants for that gene (table 2.4). SYBR® green RT- PCR master mix (Life technologies) was used for qRT-PCR reactions. SYBR green is a double stranded DNA (dsDNA) binding (fluorescent dye with an excitation wavelength of ~485nm and an emission wavelength of ~524nm. Fluorescent signal from SYBR green directly correlates with dsDNA quantity and therefore the amount of PCR dsDNA sample can be measured after every elongation step in real time. The final reaction volume used was 10µl (with 50ng/µl of the cDNA samples) per well to run qRT-PCR using the standard cycling parameters (Stage 1: 50℃ for 2 minutes, Stage 2: 95℃ for 10 minutes then 40 cycles of 95℃ for 15 sec and 60℃ for 1 minute), which were set and carried out on an ABI 7900HT sequence detection system. Data were presented as the mean ± standard error of mean (SEM) relative quantities (RQ) of three independent repeats where GAPDH was used as endogenous reference control. Analysis was carried out using SDS 2.2 software (Applied Biosystems) and GraphPad Prism 6.0 (GraphPad Software, Inc.).

	Sequence (5' -> 3')
MDM4 (MDMX)	
Forward Primer	TGATTGTCGAAGAACCATTTCGG
Reverse Primer	TGCAGGGATCAAAAAGTTTGGAG
BTG	
Forward Primer	CCTGTGGGTGGACCCCTAT
Reverse Primer	GGCCTCCTCGTACAAGACG
CDKN1A (p21)	
Forward Primer	TGTCCGTCAGAACCCATGC
Reverse Primer	AAAGTCGAAGTTCCATCGCTC
VGLL1	
Forward Primer	TCAGAGTGAAGGTGTGATGCT
Reverse Primer	GCACGGTTTGTGACAGGTACT
CCNG2	
Forward Primer	TCTCGGGTTGTTGAACGTCTA
Reverse Primer	GTAGCCTCAATCAAACTCAGCC
RRM2B	
Forward Primer	ATTGGGCCTTGCGATGGATAG
Reverse Primer	GAGTCCTGGCATAAGACCTCT
FAS	
Forward Primer	AGATTGTGTGATGAAGGACATGG
Reverse Primer	TGTTGCTGGTGAGTGTGCATT
TNFRSF10C	
Forward Primer	TCCCCAAGACCCTAAAGTTCG
Reverse Primer	CAGTGGTGGCAGAGTAAGC
GHR	
Forward Primer	CCATTGCCCTCAACTGGACTT
Reverse Primer	AATATCTGCATTGCGTGGTGC
GAPDH	
Forward Primer	CAATGACCCCTTCATTGACC
Reverse Primer	GATCTCGCTCCTGGAAGAT

Table 2.4. Primer sequences for qRT-PCR

2.4 Growth curves and cell characteristics

Growth curves were generated to establish the pattern of cell growth for different seeding densities and to measure the doubling time. The conditions of the cell density and incubation time required for growth inhibition studies can be decided from the growth curves and doubling time.

2.4.1 SRB assay for adherent cells

SRB (sulforhodamine-B) which is a water-soluble dye can be measured at 564nm absorbance. SRB can be used to bind with the basic amino acids of cellular proteins and to assess population growth (Skehan et al., 1990)(Papazisis *et al.*, 1997). The SRB dissolved by 10mM Tris buffer was quantified by absorbance readings at 570nm as a measure of protein content and hence number of cells in a well.

Cells were fixed in Carnoy's fixative (100ml of concentrated acetic acid to 300ml of methanol) on the plates and stored at 4°C for at least 1 hour. Then the plates were washed with tap water five times and were subsequently dried on the bench. The dried and fixed cells on the plates were stained with 0.4 % SRB in 1% acetic acid solution using 100 µl/well for 30 minutes, followed by washing with 1% acetic acid five times and drying the plates. Then the residual bound stain on the cells was dissolved by incubation with 10mM Tris pH10.5 for 20 minutes. After reading the absorbance at 570nm on a 96-well spectrophotometer with FLUOstar Omega plate reader (BMG Labtech, Germany), the relative cell number could be quantified.

2.4.2 XTT assay for suspension cells

Tetrazolium salt (XTT), a soluble formazan orange dye, was used to measure cell viability via mitochondria activity in metabolically active cells. Cells were seeded and incubated with XTT reagent (Roche, USA) mixture (labelling reagent: electron-coupling reagent ratio of 50:1) at 37°C for a period of time depending on the cell density and cell lines. Figure 2.1 shows the different cell density of MRK-nu-1 cells with different incubation times using the XTT assay. After incubation, the colour change was quantified spectrophotometrically by absorbance measurements at 450nm wavelength (Kondo *et al.*, 1991; Roehm *et al.*, 1991).

58
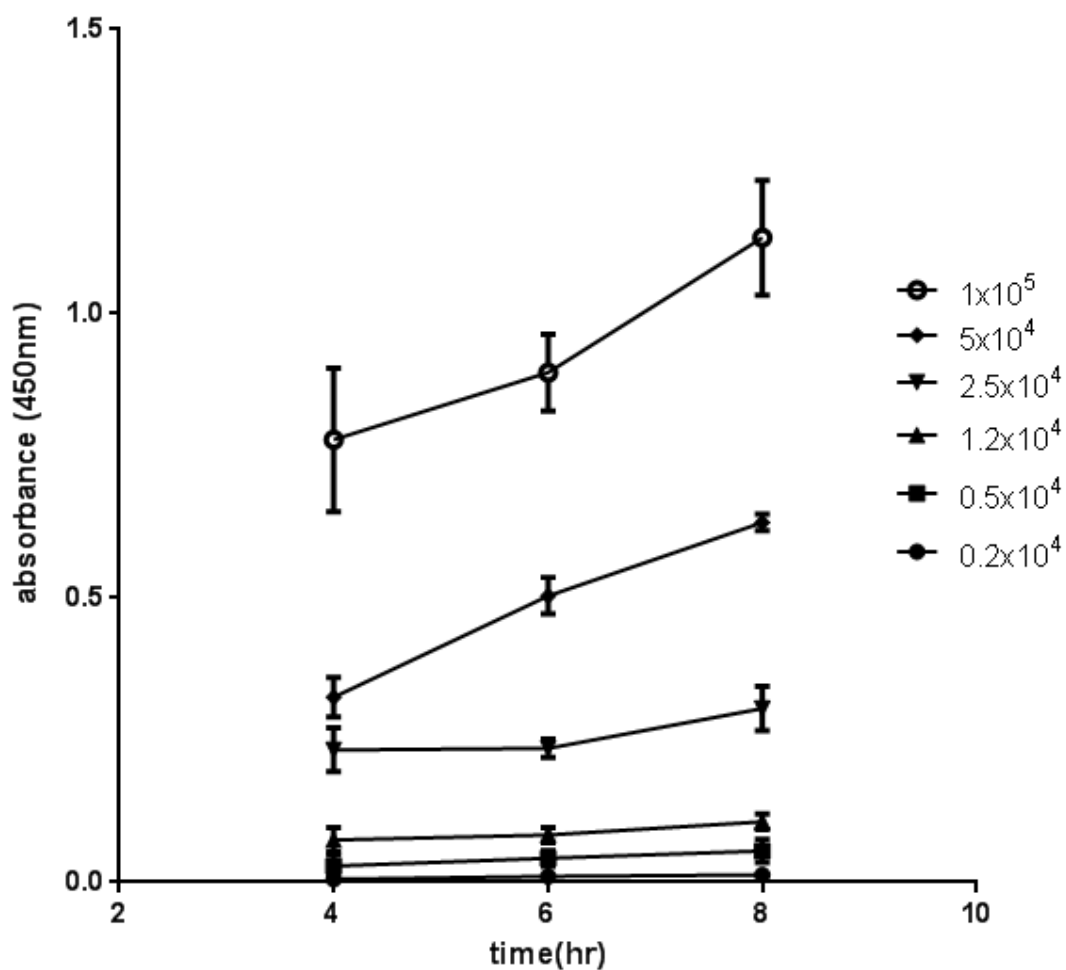
Figure 2.1. Proliferation of MRK-nu-1 cells measured by XTT assay for different starting cell densities. The different cell densities of MRK-nul1 cells were used for testing the absorbance values of XTT reagents mixture after incubating for 4, 6 and 8 hours. The best incubating time for XTT reagents mixture was chosen to 4 hour for the following growth curve and growth inhibition experiments.

2.5   Cell counting

Cell counting was used to set up an experiment with suitable cell density in different sized plates or dishes. Seeding density was cell line-dependent as shown in table 2.5.

2.5.1   Haemocytometer

Haemocytometer (Improved Neubauer haemocytometer, AC1000, Hawksley, UK). was used for cell counts with both adherent and suspension cells to set up equal cell numbers for drug treatment. Cell suspension was added in both chambers of the haemocytometer after detachment by trypsin-EDTA. The cells in the square of both chambers were counted by visualization down a microscope. The average of both chambers was taken and multiplied by 10^4. The number provided the cell density per ml of medium. (cell density=Av.x10^4).

2.5.2   Cell counter

An automatic cell counter was used for the early stages of cell density calculation and growth curve estimations for the suspension cell line MRK-nu-1. A 0.5ml cell suspension was fixed in 0.5ml Carnoy's fixative and then 9 ml fluid was added (BD FACSFlowTM Sheath Fluid #342003). The diluted cell suspension was passed through a particle Coulter counter ((Beckman Coulter) in which the cells or particles flow through a small hole to be detected electronically by a transient resistance change between electrodes and their number calculated. Cell clumps and cell debris could affect detection, so measures were taken to ensure single cell suspensions and optimal threshold settings. The coulter counter counts the number of events per 0.5ml. The average of three repeats was multiplied by 40 to obtain the original cell density of cells/ml.

Cell line	In 96-well plate (cell/well)	In 60mm dish (cell/dish)	In 6-well plate (cell/well)
MRK-nu-1	5000	3×10^5	2×10^5
JEG-3	4000	3×10^5	1×10^5
HCT116 +/+ & -/-	5000	5×10^5	2×10^5
SJSA-1 & S-M6R2 & S-N40R1	5000	2×10^5	2×10^5
MCF-7	4000	4×10^5	1×10^5
NGP & N20R1	5000	5×10^5	2×10^5

Table 2.5. Seeding density for cell lines

2.6 Drug information and preparation

2.6.1 Drug information

Nutlin-3 (Enzo Life Sciences & Newchem Tech., UK) is a mixture of active enantiomer Nutlin-3a and inactive enantiomer Nutlin-3b. RG7388 and RO5963 were synthesised in-house by Newcastle University's medicinal chemistry group and prepared as a 10 mM stock in DMSO. These compounds were all dissolved in 100% DMSO to produce 10mM stock solutions stored at -20°C.

2.6.2 Drug preparation

Working stocks were diluted into media before treatment, and the concentrations of the drug were prepared 100-fold from the final treating concentrations in media with final 1 % DMSO drug solvent (table 2.6). The final doses for treating cells were from 0 (1% DMSO only) to 50 μM drug dissolved to give a final concentration in 1% DMSO when the working stocks were diluted into the medium. Cell viability was maintained over 80% while testing with 1% of DMSO or 0.5 % of DMSO solvent controls. Thus, DMSO as solvent did not affect cell viability.

2.7 Growth inhibition

Growth inhibition assays determine the concentration at which a compound reduces the growth of the cell population compared to the solvent-only DMSO control. DMSO sensitivity testing was performed to confirm that the drug solvent did not affect cell growth and solvent control growth rate was maintained at over 80%, especially in some sensitive cell lines.

GI_{50} values were calculated using GraphPad Prism Version 6.0 software (GraphPad Software, Inc.). The percentage cell number relative to control (DMSO control cells) was determined for each concentration of Nutlin-3 or RG7388 or RO5963, and data were plotted using Prism statistical software. GI_{50} values were determined by transforming X values (concentrations) using X=log(X), and performing a nonlinear regression (curve fit) analysis to generate a GI_{50} value.

2.7.1 Growth inhibition for adherent cells

Cells were seeded at 5×10^3 cells/well density in two 96-well plates and incubated at 37^0C, 5% CO_2 for 24 hours. The medium in the wells of one plate was aspirated and replaced with 100 µl/well of fresh medium containing test agent. Different test agents were made up according to table 2.6, with 0%, 0.5%, 1.0%, 1.5% and 2% DMSO for testing the DMSO sensitivity of JEG-3 cells. The medium in the wells of the other plate was aspirated and replaced with 100 µl/well fresh media with final concentrations of 0 - 50 µM Nutlin-3 in 1 % DMSO (table 2.7). Both of the plates were incubated at 37^0C, 5% CO_2 in a humidified incubator for 72 hours. The 72 hour treating time was chosen based on cell growth curve and doubling time shown in Figure 3.4. The SRB assay was used to measure JEG-3 cell line growth inhibition compared to solvent DMSO control.

2.7.2 Growth inhibition for suspension cells

Cells were seeded 5×10^3 cells/well in 50 µl/well of medium in two 96-well plates, to which was added the other half of the medium containing the drug. The cells were incubated at 37^0C, 5% CO2 for 24 hours. The effect of DMSO alone was tested at a final concentration of 0%, 0.5%, 1.0%, 1.5% and 2%. The Nutlin-3 concentrations

tested were 0 - 50 µM Nutlin-3 in 1 % DMSO (table 2.7). Both of the plates were incubated at 37^{0}C, 5% CO2 for 72 hours. The XTT assay was used to measure cell growth inhibition compared to solvent DMSO control.

Adherent cells

100% DMSO	Add medium	Conc. Of DMSO	Add 100µl/well → Final conc. of DMSO
0	1000 µl	0%	0%
6 µl	1194 µl	0.5%	0.5%
12 µl	1188µl	1.0%	1.0%
18 µl	1182 µl	1.5%	1.5%
24 µl	1176 µl	2.0%	2.0%

Suspension cell

100% DMSO	Add medium	Conc. Of DMSO	Add 50 µl/well → Final conc. of DMSO
0	1000 µl	0%	0%
10 µl	990 µl	1%	0.5%
20 µl	980 µl	2%	1.0%
30 µl	970 µl	3%	1.5%
40 µl	960 µl	4%	2%

Table 2.6. DMSO dilution for DMSO sensitivity in adherent and suspension cell lines. The values of 100% DMSO were calculated and added into media for testing the toxicity of 0 – 2% of DMSO in different type of cell lines.

Adherent cells		
Working stock mM (µM) in 100% DMSO	Nutlin-3 conc. (µM) & 1% DMSO with media	Final conc. (µM) & 1% DMSO in wells
0.01 (10)	0.1	0.1
0.05 (50)	0.5	0.5
0.1 (100)	1	1
0.2 (200)	2	2
0.4 (400)	4	4
0.6 (600)	6	6
0.8 (800)	8	8
1.0 (1000)	10	10
3.0 (3000)	30	30
5.0 (5000)	50	50
Use 10 µl working stock + 990 µl media, then add 100 µl/well		

Suspension cells		
Working stock mM (µM) in 100% DMSO	Nutlin-3 conc. (µM) & 2% DMSO with media	Final conc. (µM) & 1% DMSO in plates
0.01 (10)	0.2	0.1
0.05 (50)	1.0	0.5
0.1 (100)	2	1
0.2 (200)	4	2
0.4 (400)	8	4
0.6 (600)	12	6
0.8 (800)	16	8
1.0 (1000)	20	10
3.0 (3000)	60	30
5.0 (5000)	100	50
Use 10µl working stock + 490µl media, then add 50 µl/well		

Table 2.7. Drug dilution with DMSO for growth inhibition with adherent cells and suspension cells. Drug was solved in 100% DMSO. The working stocks of drug was calculated and added into media to provide final concentrations of 0 to 50 µM in 1% DMSO in the treatment of different types of cell lines.

2.8   Lentiviral shRNA expression knockdown systems

A Lentiviral shRNA system was used to produce long-term and inducible knockdown of gene expression. Once the cell lines have been transduced with the MDMX shRNA plasmid (pTRIPZ plasmid, Thermo Fisher Scientific, figure 2.2) using lentiviral particles, the fragment which carries target shRNA will ingrate into the host DNA. Puromycin (Invitrogen by thermos Scientific, USA) was used to select the cells carrying shRNA fragment along with the puromycin resistance gene. Doxycycline (Sigma-Aldrich, UK) is used to induce the promoter of the targeted shRNA and turbo red fluorescent protein (tRFP) gene so that the knockdown can be switched on and off by adding doxycycline. The red fluorescence protein allows monitoring of the successful uptake of the viral vector and regulation of expression by doxycycline using fluorescence microscopy of live cells. The cells which have integrated more copies of lentivirus can be selected by an increase of the puromycin dose. The knockdown efficiency of the cells is potentially increased after doxycycline induction (Manjunath *et al.*, 2009).

2.8.1   pTRIPZ with shRNA lentiviral transfection (work of Claire Hutton)

The pTRIPZ plasmid containing the shRNA for MDMX was prepared from a glycerol stock using Qiagen Midi-prep kit (QIAGEN, Germany). The shRNA for MDMX was designed by Thermo Fisher Scientific. The concentration of plasmid DNA was calculated by NanoDrop and stored at -20°C. The plasmid carrying shRNA DNA was transfected into HEK293T host cells to produce lentiviral particles by using Trans-Lentiviral Packaging Mix (including reagents and HEK293T cells, Thermo Fisher Scientific, USA). The viral particle was collected from the cell supernatant and extraneous cell debris was removed by centrifuging at 1600g at 4°C. The lentiviral particles were then passed through a 0.22 - 0.45 µm PVDF filter (Millipore, USA). and stored at -80°C. The lentiviral particles were tested by Lenti-X GoStix test (Clontech, USA). This test detected lentiviral p24 to determine sufficient lentivirus titre.

Multiplicity of infection (MOI) was established by serial dilution to optimise the number of transducing units per cell before transduction of the target mammalian cell line. HEK293T cells were seeded to a range of seeding densities and then

transduced by the same volume of lentiviral particles to determine optimal MOI for the target mammalian cell line. The target cell line was seeded overnight and transduced by the lentiviral particles using different MOI (a range is recommended initially. Eg. 0, 0.5, 1, 2, 5, 10).

The puromycin kill curve in figure 2.3 was used to find the minimum antibiotic puromycin concentration required to kill non-transduced cells. Successfully transduced cells would be selected through this process. The lowest concentration was chosen which eliminated 100% of the cells in 1-4 days.

2.8.2 Doxycycline induction system

The transduced cell lines could be induced by 1 µg/ml doxycycline. The presence of a doxycycline inducible red fluorescent protein (RFP) gene on the plasmid also allowed successful uptake of the plasmid and doxycycline response to be monitored by FACS (fluorescence activated cell sorting) in figure 2.4 and fluorescence microscopy in figure 2.5.

Vector Element	Utility
TRE-minCMV promoter	Tetracycline responsive RNA Polymerase II promoter
UBC promoter	Drives expression of rtTA3 and IRES-puro
rtTA3	Reverse tetracycline transactivator
cPPT	Central Polypurine tract helps translocation into the nucleus of non-dividing cells
WRE	Enhances the stability and translation of transcripts
TurboRFP	Marker to track shRNAmir expression
IRES-Puro resistance	Mammalian selectable marker
Amp resistance	Ampicillin (carbenicillin) bacterial selectable marker.
5'LTR	5' long terminal repeat
pUC ori	High copy replication and maintenance of plasmid in *E.coli*
SIN-LTR	Self inactivating long terminal repeat (Shimada, et al. 1995)
RRE	Rev response element
Zeo resistance	Bacterial selectable marker

Figure 2.2. Map of lentivirus plasmid pTRIPZ (TRIPZ Technical Manual, Thermo Fisher Scientific, UK). Features of the pTRIPZ vector (TRIPZ Technical Manual, Thermo Fisher Scientific, UK).
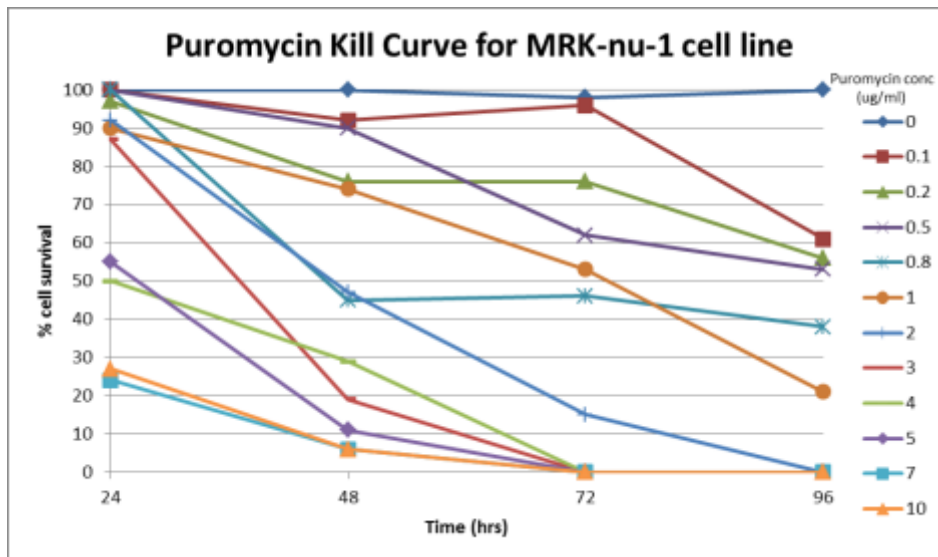
Figure 2.3. Puromycin (0-10µg/ml) kill curve in MRK-nu-1 (Data kindly provided by Claire Hutton). The cells were seeded with 5x10^4 cells per well into a 24 well plate. The media containing a dose range of 0-10 µg/ml of puromycin was tested. The cell growth inhibition curve from day 1 to day 4 was plotted for the different doses of puromycin. The final dose for puromycin used in MRK-nu-1 cells was 3 µg/ml.
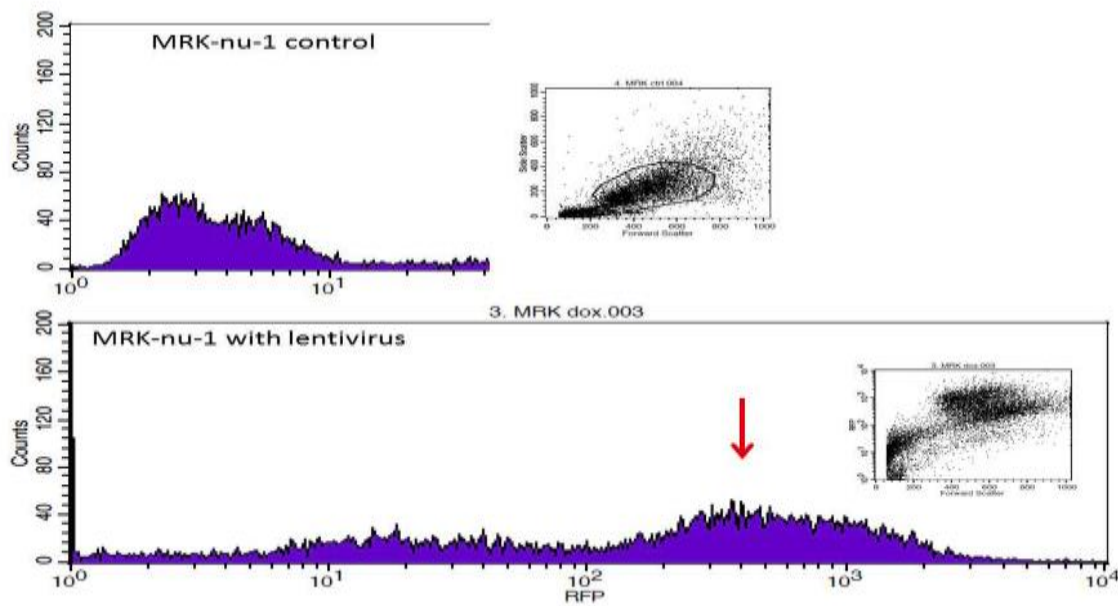
Figure 2.4. FACS results showing the increased population of MRK-nu-1 cells with high red fluorescence signal after 1 µg/ml doxycycline induction.
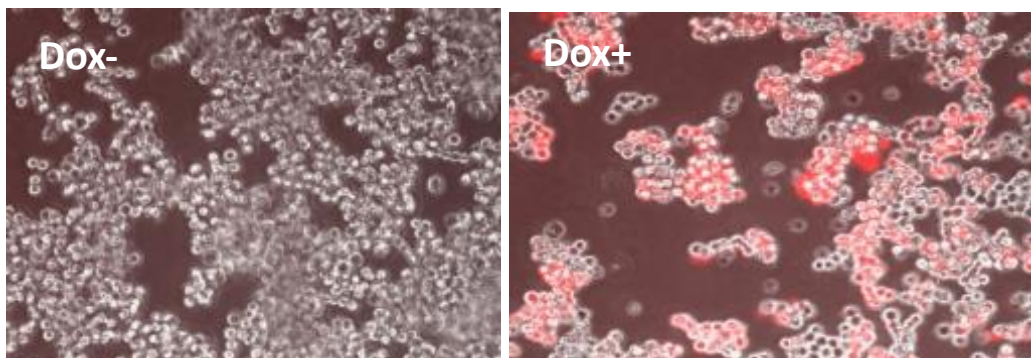
Figure 2.5. The negative control (Dox-) was MRK-nu-1 cells with lentiviral shRNA without doxycycline induction. The MRK-nu-1 cells with lentiviral shRNA were induced for 48 hours by 1 µg/ml doxycycline (Dox+). Fluorescence and phase contrast images were merged, showing red fluorescence only in the presence of doxycycline, confirming successful transduction and induction of expression.

2.9 SiRNA expression knockdown systems

RNA interference is a method of silencing post-transcriptionally regulated gene expression (Figure 2.6). Double stranded RNA is targeted specifically for degradation and is triggered by small interfering RNAs (siRNAs). A dicer nuclease cuts the larger initially formed siRNAs into 20-25 nucleotide siRNAs. The siRNAs then assemble on to the RNA-induced silencing complexes (RISCs), where they unwind, and subsequently guide the RISCs to complementary RNA molecules where they cleave and destroy the cognate RNA.

2.9.1 siRNA sequence

Small interfering RNA sequences for knockdown of MDMX expression were established by a previous PhD student Dr Laura Gamble. She designed and tested three MDMX siRNA sequences. One of them showed highly efficient knockdown of MDMX protein expression in neuroblastoma cell lines. The sequence is 5'GCAGUUAGGUGUUGGAAUAtt3' (Gamble, 2011). In the present study, the siRNA sequence was also confirmed to show a high efficiency of knockdown in *MDMX*-amplified cell lines, shown in figure 2.7. The sequence of the universal negative control is 5'GCGCGCUUUGUAGGAUUCGtt3'.

2.9.2 siRNA transfection

Cells were seeded into 6-well plates with the seeding densities shown in table 2.8 for 24 hours before siRNA work. Lipofectamine (Invitrogen Lipofactamine 2000, Thermo Fisher Scientific) reagent was used to transfect siRNA duplexes with final 20 – 60 nM into target cells to suppress MDMX expression. SiRNAs were stored at stock concentrations of 20μM. The ratio of siRNA: lipofectamine is 1:1.25. Table 2.9 shows the volume of siRNA, lipofectamine and optimem per well with different final siRNA concentrations (Fiszer-Kierzkowska *et al.*, 2011).

The siRNA was added into optimem (Gibco) with the volumes shown in table 2.9 and vortexed for 10 seconds then left at room temperature for 10 minutes. The lipofectamine was added into optimem separately from the siRNA. The siRNA-optimem mixture and lipofectamine-optimem mixture were mixed and vortexed for 10

seconds and then left at room temperature for 30 minutes to 1 hour to wait for lipofectamine to react with siRNA. The media were aspirated and replaced by 1.6 ml fresh serum-free optimem in the well with the cells to be treated. The mixture of siRNA and lipotectamine in optimem was added as an 800 μl volume per well and the cells were placed in an incubator. After incubation overnight or for 24 hours, 10 % FBS was added to each well. The optimum medium also could be change to normal growing media contained 10 % FBS. Cell lysate was collected after siRNA treatment for 24, 48 and 72 hours to confirm the reduction of MDMX protein level.
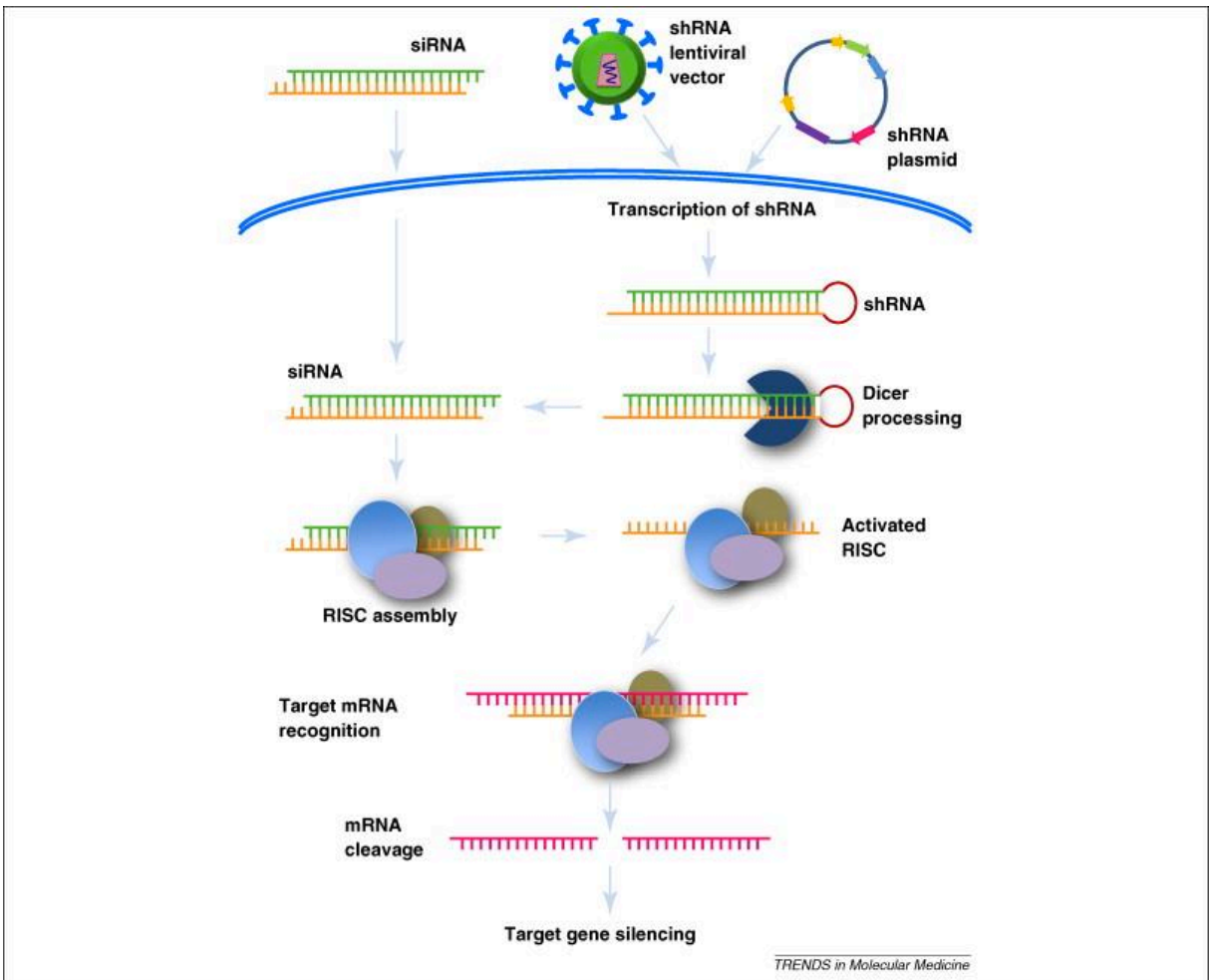
Figure 2.6. A diagram of siRNA and shRNA targeting mRNA and inhibition of target protein expression (Kim *et al.*, 2009).

Cell line	In 6-well plate (cell/well)
MRK-nu-1	4×10^5
JEG-3	2×10^5
HCT116 & HCT116-/-	4×10^5
MCF-7	2×10^5
NGP & N20R1	4×10^5

Table 2.8. Seeding density for siRNA work

Final siRNA conc.	20µM siRNA + Optimem	Lipofectamine + Optimem
20 nM	2.4µl + 400 µl	3µl + 400 µl
40 nM	4.8µl + 400 µl	6µl + 400 µl
60 nM	7.2µl + 400 µl	9µl + 400 µl

Table 2.9. Volume of siRNA and lipofactamine for one well of a 6-well plate
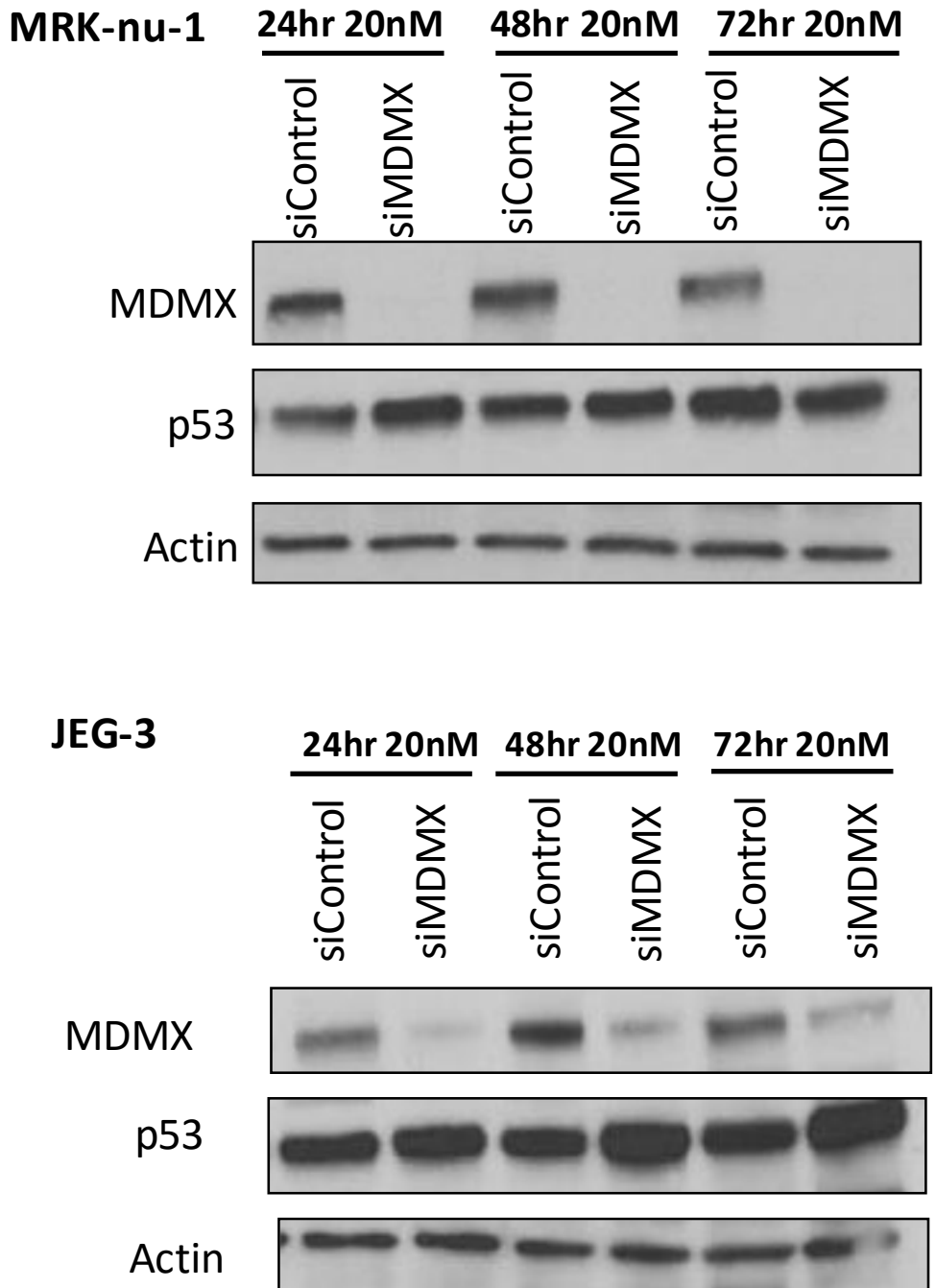
Figure 2.7. MDMX protein expression after knockdown of MDMX in two MDMX amplified cell lines detected by Western blots. MRK-nu-1 and JEG-3 cells were treated with final 20 nM of siMDMX and universal siRNA negative control for 24, 48 and 72 hours. The final 20 nM siRNA for 48 hours was chosen as the best condition of MDMX suppression for the following experiments such as drug treatment.

2.10 Western blot

Western blotting is a technique used to assess the protein expression levels of specific proteins by antibody-protein interaction in a mixture protein sample such as a cell lysate after separation by electrophoresis (van Kooten *et al.*, 2001). In the current study, whole protein lysate was quantified and 25-40 μg was used per well for the electrophoretic separation. All buffers used for western blot are shown in table 2.10.

2.10.1 Lysate collection

Media were aspired from the cell culture plates, and PBS was used to rinse the cells, then the PBS was removed and 30-40 μl Lysis buffer was added to the dish. The cells were then detached using a cell scraper. Cell lysate was transferred into a labelled 1.5 ml microfuge tube and the cell lysate was boiled at 100°C for 10 minutes, then stored at -20°C.

2.10.2 Lysate sonication

The cell lysate was sonicated with a 5-6 grade probe for 10 seconds 3 times. (Sonicator probe, Soniprep 150, MSE, UK). The probe must be cleaned with 70% ethanol before and after using with each sample to avoid cross-contamination.

2.10.3 Protein estimation

A Pierce BCA Protein Estimation Assay was performed to calculate protein concentration. A sample was diluted 1 in 10 into water before measuring the concentration. A standard curve was generated using: 0.2, 0.4, 0.6, 0.8, 1.0, 1.2 mg/ml standard protein concentrations which were diluted from BSA standard 2 mg/ml stock. 10 μl of the samples or standard were added into each well of a 96-well plate. Reagent A and Reagent B were mixed with 50:1 Pierce® BCA Protein Assay kit (Pierce, Rockford, IL, USA) and 190 μl of the mixture was added to the sample in each well. The plates were incubated at 37°C for 30 minutes. Absorbance values were detected at 562 nm using a 96-well spectrophotometer which was set up with an automatic standard curve to calculate the concentrations of the samples. The values were multiplied by 10 to give the original concentration of the samples. A 25-

35 µg aliquot of lysate from cell lines was loaded onto each well of an SDS-polyacrylamide electrophoresis gel.

2.10.4 SDS-PAGE (sodium dodecyl sulphate polyacrylamide gel electrophoresis) and transfer

Protein lysates were boiled with SDS loading buffer for 10min. Reducing agent β-mercaptoethanol was added into each sample to break disulphide bonds within the protein and coat the proteins uniformly with the negatively charged SDS. Equal quantities of protein were loaded onto SDS-polyacrylamide gels (4 - 20% gradient gel, Biorad, USA). The protein gel electrophoretic separation was performed at 180V for approximately 45 min. The gel was then moved to a transfer electrophoresis tank and the protein from the gel was transferred (100 V, 30 min) and immobilized onto a nitrocellulose membrane (Hybond C membranes Amersham & GE, USA). SeeBlue pre-stained protein molecular weight markers (Thermo Fisher Scientific, USA) were loaded into tracks on both ends of the gel for estimation of protein sizes. The buffers used for western blots are shown in table 2.10.

2.10.5 Primary and Secondary antibodies

To prevent non-specific binding of the antibody probes, the membranes were blocked by incubation with 5% skimmed milk in 1x TBS/Tween for 45 minutes at room temperature on the shaker (Belly Dancer, Strovall, USA). The membranes were probed for specific proteins by incubation with primary antibodies in a 50ml tube on a tube roller mixer (SRT6, Stuart, UK). Details of the antibodies used are shown in table 2.11. The detection of actin was used to check and control for sample loading differences. After washing off unbound primary antibody, the specifically bound primary antibodies were detected by secondary antibodies conjugated to horseradish peroxidise (HRP).

Chemiluminescence was used to detect and visualise the location of the HRP-conjugated secondary antibodies, which included polyclonal goat anti-mouse immunoglobulins (1:1000, Dako, Denmark) for MDM2, p53, p21 and actin; polyclonal goat anti-rabbit immunoglobulins (1:1000, Dako, Denmark) conjugated with HRP for BAX. After incubating at room temperature for 45 minutes with the antibodies, the

membranes were washed with TBS/Tween on the Belly Dancer shaker (Strovall, USA) for 4 minutes and this was repeated 7 times.

2.10.6 Protein detection by enhanced chemiluminescence

Chemiluminescence (ECL) reagent (GE Healthcare), which produces a light signal that can be captured on photographic film or digital camera system, was used to visualize protein bands. ECL 1 reagent and ECL 2 reagent (GE Healthcare) were mixed 1:1 in a universal tube. The mixture was pipetted onto the membrane and incubated at room temperature for 1 minute. The membranes were exposed to photographic films (Super RX, FUJI medical X-ray film, Thermo Fisher Scientific, UK) in a light-tight X-ray cassette in the darkroom for 30 seconds to 10 minutes, depending on the protein levels and signal intensity. The resultant signals on the X-ray film were developed using an automated film processor (Mediphot 937).

	volume	conc.
SDS loading buffer		
0.5 M Tris-HCL pH 6.8	2.5 ml	0.0625 M
SDS (Sigma-Aldrich, UK)	0.4 g	2%
β-mercaptoethanol (Sigma-Aldrich, UK)	1 ml	5%
Glycerol (Sigma-Aldrich, UK)	2 ml	10%
0.1% bromophenol blue (Biorad, UK)	1 ml	0.003%
distilled water	13.5 ml	
SDS Lysis buffer		
0.5 M Tris-HCL pH 6.8	12.5 ml	0.0625 M
SDS (Sigma-Aldrich, UK)	2 g	2%
Glycerol (Sigma-Aldrich, UK)	10 ml	10%
distilled water	to 100 ml	
10 x Running/Electrode Buffer		
Glycine (Sigma-Aldrich, UK)	144 g	
Tris base (Fisher Scientific, UK)	30 g	
SDS (Sigma-Aldrich, UK)	10 g	
distilled water	To 1 L	
Transfer buffer		
Tris base	3 g	
Glycine (Sigma-Aldrich, UK)	14.14 g	
Methanol (Fisher Scientific, HPLC grade)	200 ml	
distilled water	To 1 L	

10 x TBS	volume
Tris base (Sigma-Aldrich, UK)	24.2 g
NaCl (Sigma-Aldrich, UK)	80 g
distilled water	800 ml
Adjust pH to 7.6 with HCl	
distilled water	To 1 L

1 x TBS/Tween	
10 x TBS	100 ml
distilled water	900 ml
Tween 20 (Sigma-Aldrich, UK)	1 ml

Blocking buffer	
Milk powder	2.5 g
1 x TBS/Tween	50 ml
Tween 20 (Sigma-Aldrich, UK)	1 ml

Table 2.10. Western Blotting buffers

Protein	Size (kDa)	Dilution	Buffer	incubating	2nd Ab	Company and detail
MDM2	~ 90	1/300	milk	1 hour, RT	Mouse	CALBIOCHEM, OP46
MDMX	~ 80	1/1000	milk	1 hour, RT	Mouse	Millpore, 8C6
p53	53	1/500	milk	1 hour, RT	Mouse	Vector Lab. Inc., DO7
Actin	~ 42	1/2000	milk	1 hour, RT	Mouse	Sigma, AC4700
BAX	20	1/1000	BSA	O/N, 4℃	Rabbit	Cell Signaling, 2772
p21	21	1/100	milk	1 hour, RT	Mouse	CALBIOCHEM, OP64
PPM1D (Wip1)	~ 64	1/300	milk	O/N, 4℃	Rabbit	Santa Cruz, H-300

Table 2.11. Primary antibodies used in this study).

RT: Room temperature; O/N: Overnight; 2nd Ab: secondary antibody

2.11 Flow cytometry

Flow cytometry was used to analyze cell cycle distribution via fluorescence activated cell sorting (FACS) by FACSCalibur (Becton Dickinson, BD Biosciences, UK). Propidium iodide (PI) is induced by UV or blue light to emit a red fluorescence (Ormerod, 2000). PI binds to DNA and provides a quantitative measure of cellular DNA content, from which the stage of the cell cycle can be determined. A single flow of cells passes through the flow cell where light from the argon laser beam excites the fluorescent PI dye bound to DNA. Cells harbor one copy of the genome (n=2) in G1/G0 phases and a double copy (n=4) in G2/M phases. Cells in S phase have a DNA content between G1/G0 and G2/M (2<n<4). The change in population of cells in each phase of the cell cycle distribution can be estimated by quantifying the number of copies of DNA content. The cell cycle distribution changes in response to the treatment can therefore be measured and related to changes in cell proliferation.

2.11.1 Preparation of samples

Cell samples were seeded in a 6-well plate and living cells were prepared for analysis by flow cytometry. Following siRNA or drug treatments, both adherent and non-adherent cells were washed twice with PBS (spun at 1200rpm for 5 minutes) to remove media and drugs. Then 500µl of PBS was added to cell pellets and the cells suspended by a micro pipette (Gilson, WI, USA). 500µl of the PI solution shown in table 2.12 was added to the re-suspended cell samples before analysis by FACSCalibur flow cytometry.

2.11.2 FACSCalibur

Before running samples through the flow cytometer, cells were passed through a syringe and needle to remove cell clumps. CellQuest software (BD Biosciences, UK) was able to modify instrument settings and simultaneously acquire data from the FACSCalibur machine. FL2-A (fluorescent detector 2-area) vs FL2-W (fluorescent detector 2-width) plots were used to identify and gate-out a range of the cell events (figure 2.7). Scatter plots of FL2-A vs. FL2- W were set up to optimise instrument settings using an untreated control (figure 2.7), as well as a 2D histogram of counts

vs. FL2-A where the G1 peak was set to 200 on a linear scale, and the G2 peak at 400. 10,000 events were acquired per sample and data was saved as FCS files.

2.11.3 Analysis

FCS files were generated by CellQuest software. Flow cytometry data was analysed using Cyflogic v1.2.1 software. FL2-W versus FL2-A scatter plots were generated and cells were gated to the main population, either including sub-G1 or excluding sub-G1, as shown in the example in figure 2.7.

The sub-G1 cells were excluded in cell cycle analysis, to avoid inclusion of dead and fragmented cells. For a measure of apoptosis, the sub-G1 signals could be analysed separately. The gated data was used to generate FL2-A histograms, and the proportion of cells in G1/G0, S and G2/M phases was determined by marking the various phases of the cell cycle (shown in figure 2.7), and generating a table of statistics. An increase in the G1/S and G2/S ratio indicates G1 and G2 arrest, respectively.

	volume	Final concentration
PI solution		
Propidium iodide (Sigma-Aldrich, UK)	50 mg	100 µg/ml
DNase free RNase A (Sigma-Aldrich, UK)	50 ml	200 µg/ml
Triton-X-100 (Sigma-Aldrich, UK)	1.5 ml	0.3 %
Sodium Citrate (Sigma-Aldrich, UK)	500mg	1 mg/ml
PBS (Gibco, Paisley, Scotland)	500 ml	

Table 2.12. PI solution
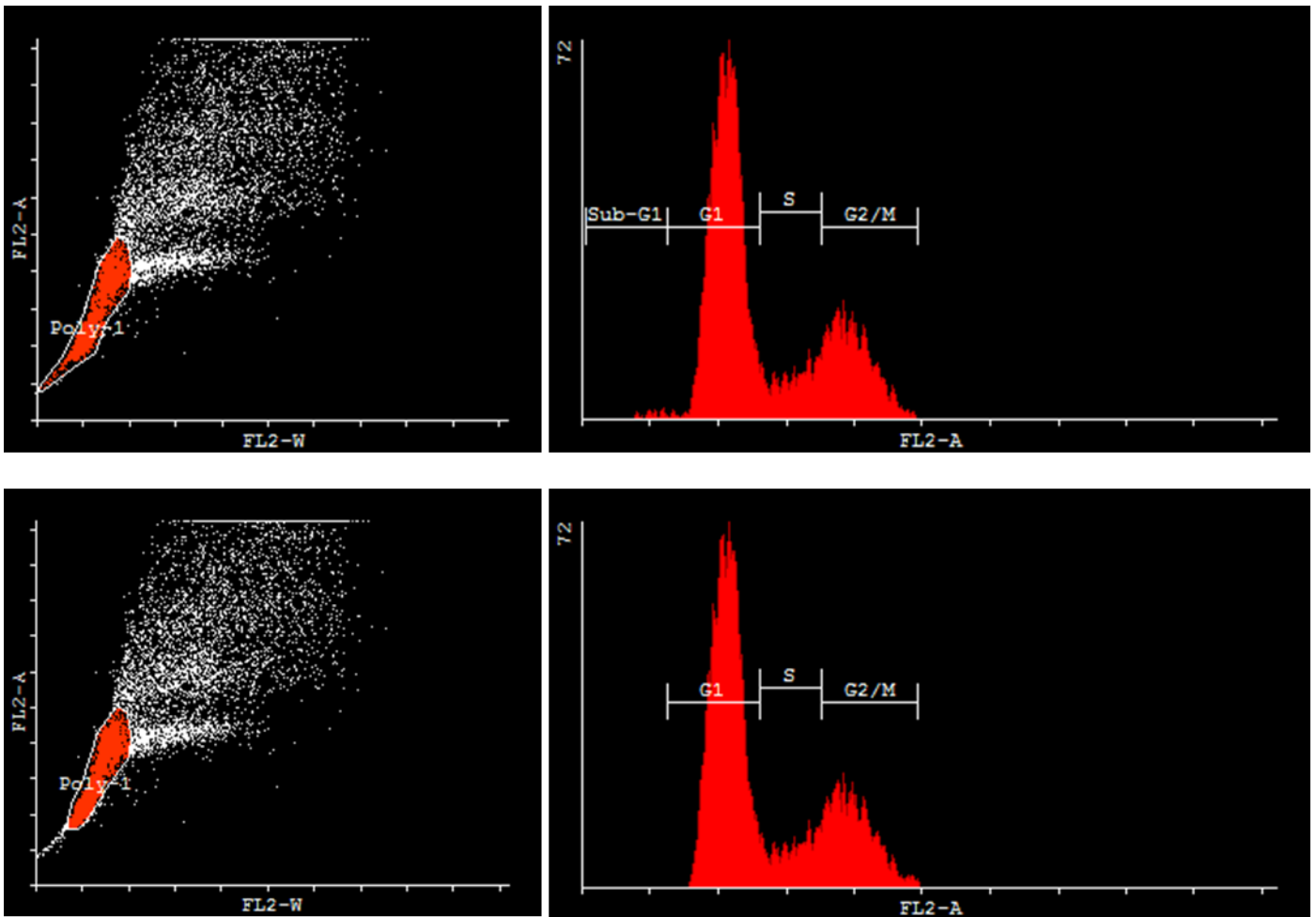
Figure 2.8. Example FL1-W versus FL2-A scatter plots and histograms showing the signal gating and regions of cell histograms selected for analysis of cell cycle stages, including and excluding sub-G1. (The example of plots shown are for the control DMSO treated MRK-nu-1 cells)

2.12 Immunofluorescence and confocal microscopy

MDMX Protein location was detected by immunofluorescence using a confocal microscope. The nucleus was visualised by staining with a nucleic acid fluorescent intercalating dye 4',6-Diamidino-2-Phenylindole, Dihydrochloride (DAPI).

2.12.1 Immunofluorescence protocol

Cells were seeded into a 6-well plate at 1×10^4 cells/well, with 22x22mm coverslips (Thermo Fisher Scientific, UK) inside the wells. The coverslips should be sterilized before culturing cells on them. After incubating for 24 hours, the medium was aspirated and the cells were washed in cold PBS twice. Cells on the coverslips were fixed by adding 2 ml ice cold methanol and placed in a -20°C freezer for 30 minutes. (The fixed cells on coverslips can be stored at -20°C for up to a week.) Methanol was removed and the coverslips were washed in PBS twice and transferred to a layer of parafilm in a 100mm petri dish. The blocking solution (table 2.13) was added onto the coverslips by pipetting, to cover the whole surface, and incubated at room temperature for 1 hour. The blocking solution was then removed and the anti-MDMX antibody diluted at 1 in 1000 in blocking buffer was added and incubated with the fixed cells at 4°C overnight. The primary antibody was removed gently from the coverslips by P1000 Gilson pipette. The coverslips were replaced into a 6-well plate and washed by PBS/Triton (2ml/well) for 3 repeats of 15 minutes on a platform shaker. The coverslips were replaced onto a fresh piece of parafilm. The fluorescent secondary antibodies (A11001, Thermo Fisher Scientific, UK) at 1 in 1000 dilution in the blocking buffer were added onto the coverslips and incubated for 1 hour at room temperature in the dark. After this step, the samples should be kept in the dark as much as possible. The secondary antibodies were removed and 50 µl of DAPI diluted 1/10 in PBS/T (H-1500, Vector Lab Inc., UK) was added and incubated for 15 minutes at room temperature in the dark. The coverslips were washed in PBS/T (table 2.13) for 15 minutes 4 times. Finally, the coverslips were placed face down on slides (Thermo Fisher Scientific, USA) using 5 µl mounting medium per coverslip. The samples were prepared for confocal microscopy.

	volume	concentration
Blocking buffer		
BSA (Sigma-Aldrich, UK)	0.2 g	2%
Triton-X-100 (Sigma-Aldrich, UK)	150 µl	1.5%
PBS (Gibco, Paisley, Scotland)	10 ml	
Washing buffer		
Triton-X-100 (Sigma-Aldrich, UK)	750 µl	1.5%
PBS (Gibco, Paisley, Scotland)	500 ml	

Table 2.13. Buffer for immunofluorescence

2.12.2 Confocal microscope

A Zeiss LSM 700 confocal microscopy system was used to capture 2D images and the z- stack for 3D image or video. The microscope was prepared for imaging using the Zen 2009 software. A drop of Immersol (Zeiss, #ISO 8036-1/2) oil was placed on the coverslip and the slide was placed into its allocated slot on the microscope platform. Z-stacking was used at 63× magnification, then a number of slices were taken for a different z-stack experiment ranged to present as a video.

2.13 Caspase 3/7 activity assay

The Caspase-Glo® 3/7 Assay (Promega, Southampton, UK) is a luminescent assay that measures caspase-3 and -7 activity in cell cultures. The assay provides a proluminescent caspase 3/7 substrate containing the tetrapeptide sequence DEVD. The substrate is cleaved by the caspase3/7 to release a substrate for luciferase. The light from the luciferase reaction can then be detected with a FLUOstar Omega plate reader (BMG Labtech, Germany).

Cells were seeded at 5000 cells/well in 96-well plates with a final volume of 100 µl/well medium. The Caspase 3/7 kit was defrosted and the buffer added to the tablet of caspase 3/7 substrate at room temperature. 75µl of medium was removed from each well, only 25µl of medium was left with the cells in each well before adding caspase 3/7 reagents. An equal volume of caspase reagent (25 µl) was added before

incubating for 1 hour at 37°C. After 1 hour, the resulting mixture was transferred to a white-welled 96-well plate and analysed using a FLUOstar Omega microplate Luminometer reader (BMG Labtech,Germany).

2.14 Statistical analyses

All statistical tests were performed using GraphPad Prism Version 6.0 software (GraphPad Software, Inc., USA). All t-tests were used two-tailed and paired or unpaired according to the experiments. A p-value of $p < 0.05$ was considered to be statistically significant.

Chapter 3 The effect of MDMX amplification and high expression on the response to MDM2-p53 antagonists and MDMX/2-p53 co-antagonist

3.1   Introduction

MDMX, which is an MDM2 structural homolog and p53 negative regulator, has been reported to be highly expressed in 40% of tumour cell lines (Ramos *et al.*, 2001). MDMX expression and amplification show a wide variety in different tumour types. Previous research has indicated that MDMX has 10% with gain and amplification in sarcoma (Ohnstad *et al.*, 2013). MDMX amplification was found in 4% of glioblastoma, 15% of breast, and over 10% of liver and lung adenocarcinomas (Burgess *et al.*, 2016). It is commonly detected with high expression in breast cancer (~18%), lung adenocarcinoma (~10%), liver tumours (~12%), glioblastoma multiform (~10%) (Riemenschneider *et al.*, 1999), retinoblastomas (~60%) (Laurie *et al.*, 2006) and cutaneous melanoma (~65%) (Gembarska *et al.*, 2012). Targeting both MDM2 and MDMX has been suggested to be highly desirable in cancer therapy, depending on the status of *TP53*, MDM2 and MDMX.

MDMX expression has been reported to confer resistance to MDM2-p53 binding inhibitors (Chandler *et al.*, 2006) and to play a significant role in the response to other therapeutic agents which are activated by a p53-dependent mechanism. Nutlin-3a specifically targets the MDM2-p53 interaction, but fails to disrupt the binding between MDMX-p53 and MDMX-S-p53 (Bozzi *et al.*, 2013). Furthermore, other MDM2 inhibitors were also found to be unable to inhibit the MDMX and p53 interaction (Koblish *et al.*, 2006; Patton *et al.*, 2006; Wade *et al.*, 2006; Shangary *et al.*, 2008). SJSA-1, which has *MDM2* amplification and *TP53* wild-type, has been used in many studies to test the growth inhibition and cytotoxicity of MDM2 inhibitors. A previous study reported that SJSA-1 transduced to overexpress MDMX were more resistant to MDM2 inhibitors (Hu *et al.*, 2006).

A small molecule dual MDM2/MDMX inhibitor, a co-antagonist, was developed by ROCHE to reactivate p53 function in the presence of high MDMX expression and to effectively treat cancer cells with high expression of MDMX (Graves *et al.*, 2012).

3.2   Hypotheses and aims

Hypothesis:

MDMX amplification and over-expression is associated with altered response to MDM2-p53 binding antagonists in a wide range of human cancer.

Aims:

To study the response of cell line models to small molecule MDM2-p53 binding antagonists Nutlin-3 & RG7388 and the MDM2/X- p53 co-antagonist RO5963.

To confirm the wild-type p53 status of the JEG3 and MRK-nu-1 by DNA sequence analysis.

To investigate the p53 functional response in JEG3, MRK-nu-1 cells exposed to Nutlin-3, RG7388 and RO5963 by the induction of p53 responsive genes, including p21, MDM2 and BAX.

3.3 Specific Materials and Methods

3.3.1 Cell lines

JEG-3 (placental choriocarcinoma) and MRK-nu-1 (breast carcinoma) were identified from chromosome 1 SNP array data on the Sanger database to have focal amplification of a genomic region encompassing the *MDMX* gene (figure 3.1). Neuroblastoma NGP, SKNSH and LAN-6 have been identified in our laboratory to have high expression of MDMX, also MDMX high expression was found in the breast carcinoma MCF-7 cell line (figure 3.2 and table 3.1).

3.3.2 MDMX location

JEG-3 cells were fixed on slides and probed with MDMX antibody by Immunofluorescence. DAPI was used to stain nuclei and a Zeiss LSM 700 confocal microscopy system was used to capture 2D images and z- stack images for 3D or video display. The microscope was prepared for imaging using the Zen 2009 software. The z-stacking was used at 63× magnification, then a number of slices were taken for different z-stack experiments ranging between 30-50.

3.3.3 Growth curve

Growth curves were used to decide the cell density and incubation time for growth inhibition studies. JEG-3 cells (adherent cells) were seeded in 96-well plates using 100 µl/well of $0.5x10^4$, $1.2x10^4$, $2.5x10^4$, $5x10^4$, $1x10^5$, $2x10^5$ cells/ml cell densities and then incubated at 37^0C, 5% CO_2 for 24, 48, 72, 96 and 120 hours. The cultures were fixed using 25µl/well of Carnoy's fixative (100ml of concentrated acetic acid to 300ml of methanol) and stored in a 4°C fridge for at least 1 hour before washing with tap water 5 times and drying the plates. The dried and fixed cells on the plates were stained with 0.4 % SRB in 1% acetic acid solution using 100 µl/well for 30 minutes, before washing with 1% acetic acid 5 times and drying the plates. Then the stain on the cells was dissolved by incubation with 10mM Tris pH10.5 for 20 minutes. After reading the absorbance at 570nm on a 96-well spectrophotometer, the relative cell growth could be quantified.

MRK-nu-1 cells were seeded in 96-well plates using 100 µl/well at $0.2x10^4$, $0.5x10^4$, $1.2x10^4$, $2.5x10^4$, $5x10^4$, $1x10^5$ cells/ml cell densities and incubated at 37^0C in a 5%

CO$_2$ incubator for 24, 48, 72, 96 and 120 hours. The data was collected each day. The XTT mixture (labelling reagent: electron-coupling reagent = 50:1) was added at 50 µl/well and incubated at 37°C for 6 hours. After reading the absorbance at 450nm on a 96-well spectrophotometer, the relative cell growth could be quantified.

3.3.4 TP53 DNA sequencing

The PCR products were analysed using a 2% agarose gel to check for a clean product of the expected size, which was then extracted using a PCR product purification kit (Invitrogen). The PCR products were sent to DBS Genomics (Durham, UK) for Sanger dideoxy sequencing. The p53 exon sequencing results were analysed by visual inspection of the chromatograms and alignment with a normal reference sequence using the SeqMan software package (DNAStar).

3.3.5 Clonogenic assay

JEG-3 cells were seeded into a 6-well plate with 100 cells/well density and left for 24 hours to ensure cells touched the bottom of the plate. The cells were treated with 0 – 30 µM of Nutlin-3 and 0 – 3 µM of RG7388 for 48 hours. After treatment for 48 hours, the drug was taken out of the cells and fresh media was added. The cells were then cultured and left to recover and form colonies. Once the individual colonies were big enough to see and count, cells were fixed with Carnoy's fixative and stained with crystal purple for 5 minutes. The plates were then washed with tap water and dried on the bench. The colonies were counted by visual inspection and the number of colonies recorded.

3.3.6 Protein response to drug treatment

JEG-3 and MRK-nu-1 cells were seeded into 60 mm dishes with 3×10^5 and 3×10^5 cells/well densities (table 2.5). After 48 hours, they were treated with 0 (DMSO only), 0.2, 1 and 5 µM Nutlin-3 for 4 hours and 24 hours and cell lysates collected. The same amount of lysate was loaded and probed by Western blotting for MDM2, MDMX, p53 and p21, with actin used as a loading control.

3.3.7   Growth inhibition

MRK-nu-1 cells were seeded into a 96-well plate with the cell densities shown in table 2.5. After 24 hours, cells were treated with different doses of Nutlin-3, RG7388 and RO5963 for 72 hours. XTT assay was used to measure the cell viability after drug treatment for the MRK-nu-1 suspension cell line.

JEG-3, SJSA-1, NGP and MCF-7 cells were seeded into 96-well plates with different cell densities (table 2.5) for 24 hours. A different dose of Nutlin-3, RG7388 and RO5963 was then added into each well for 72 hours. After the treatment, SRB assay was used to measure the cell proliferation for adherent cells.

Cell line	Type	*MDMX*	*MDM2*	p53
JEG-3	placental choriocarcinoma	amp	LE	WT
MRK-nu-1	breast carcinoma	amp	LE	WT
SJSA-1	osteosarcoma	LE	amp	WT
NGP	neuroblastoma	HE	amp	WT
MHM	osteosarcoma	LE	amp	WT
SaOS-2	osteosarcoma	LE	LE	del
SKNSH	neuroblastoma	HE	LE	WT
LAN-6	neuroblastoma	HE	LE	WT
NB1691	neuroblastoma	HE	amp	WT
MCF-7	breast carcinoma	HE	LE	WT

Table 3.1. Gene status or protein expression of p53, MDM2 and MDMX on cell lines. WT: wild-type; amp: amplified; del: deleted; HE: high expression; LE: low expression and basal level undetectable by Western blot
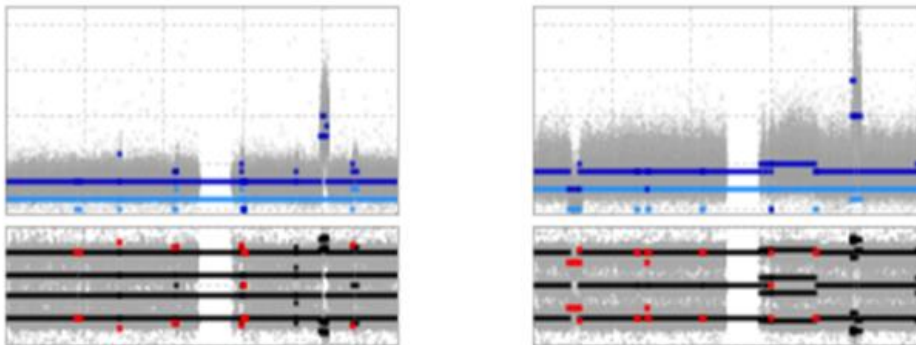
Figure 3.1. Chromosome 1 SNP array data for JEG-3 and MRK-nu-1 cell lines showing focal copy number amplification at the *MDMX* locus 1q32 (CONAN database, Sanger Institute).

3.4 Results

3.4.1 *MDMX protein expression in a panel of cell lines*

A panel of cell lines including the *MDMX* gene-amplified JEG-3 and MRK-nu-1 cells were probed for MDMX protein expression. As can be seen from figure 3.2, the MDMX amplified JEG-3 and MRK-nu-1 cells were confirmed to express MDMX protein. Interestingly, the cell lines NGP, MCF-7, SKNSH and LAN-6, which are not amplified for *MDMX*, also showed high levels of MDMX protein expression. However, *MDM2*-amplified SJSA-1 demonstrated a low expression level of MDMX. Table 3.1 summarizes the MDM2, MDMX and *TP53* status and protein expression levels based on figure 3.2.

The MDMX expression in MRK-nu-1 changes in a time-dependent manner in figure 3.2. MRK-nu-1 cells expressed the highest protein of MDMX on day 4. Figure 3.3 shows the location of MDMX protein in JEG-3 cells by confocal microscopy. Most of the MDMX protein (green stain) is located in the nuclei (DAPI blue stain) of the cells. As a p53 negative regulator, MDMX is located in the nucleus and inhibits p53 transcriptional activity by binding to p53 as an MDM2-MDMX heterodimer. The MDMX distribution within the nucleus was not uniform and appeared to show nucleolar exclusion (Li *et al.*, 2002a).
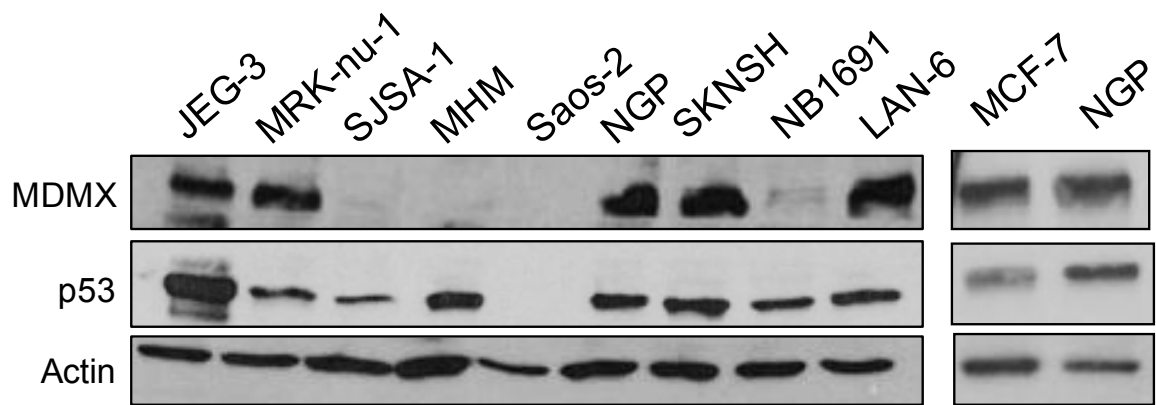
Figure 3.2. Basal levels of MDMX and p53 expression in the indicated cell lines. Actin is included as a loading control.
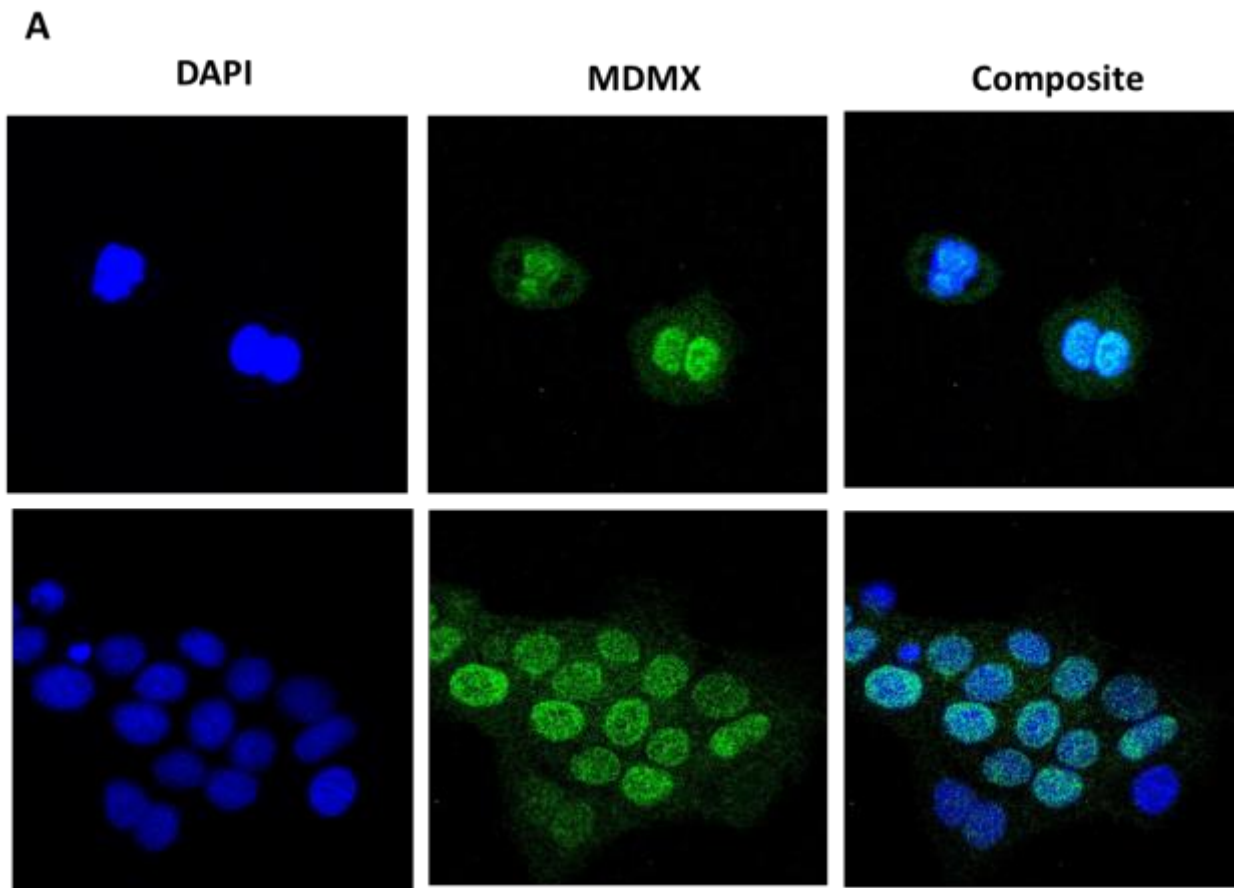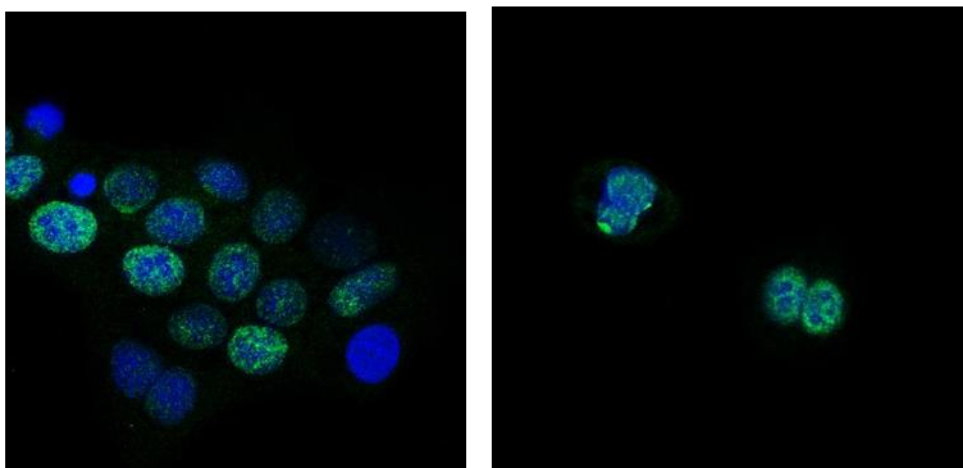
Figure 3.3. (A) MDMX protein location in JEG-3 cell line detected by confocal fluorescence microscopy with the anti-MDMX antibody (8C6, Millpore).Green stain shows MDMX protein. Blue shows DAPI stained nuclei (B) The image shows the normal cells (left) and mitotic cells (right).

3.4.2 The JEG-3 and MRK-nu-1 MDMX amplified cell lines have wild-type and functional p53

Chromosome 1 SNP array data from the CONAN database (figure 3.1) for JEG-3 (placental choriocarcinoma) and MRK-nu-1 (breast carcinoma) cells show focal *MDMX* amplification of these two cell lines. The Western blot result in figure 3.2 also shows high basal protein expression in JEG-3 and MRK-nu-1 cell lines.

The *TP53* status of these two *MDMX* amplified cell lines was confirmed by Sanger DNA sequencing. The PCR products of *TP53* exons were checked for their quantity and size, as well as absence of non-specific bands, by agarose gel electrophoresis (figure 3.5A). To illustrate the quality of the sequencing, the codon 72, exon 4, C/G (Arg/Pro) polymorphism in the JEG-3 cell line is shown (figure 3.5B). No point mutations or other sequence variants were detected in either cell line by PCR and Sanger sequencing of *TP53* exons 2-11, which encompasses the coding region. This was consistent with p53 in these two cell lines being wild-type in functional assays.

Figure 3.4 shows the growth curves for the *MDMX* amplified cell lines, JEG-3 (adherent cell line) and MRK-nu-1 (suspension cell line), from day 1 (24hr) to day 5 (120hr) after seeding cells at different densities. The SRB assay was used for the adherent cell line and XTT assay for the suspension cell line. Based on these growth curves, the seeding density and time course for assessing the growth inhibition by Nutlin-3 treatment was decided and the doubling time estimated (table 3.2). For seeding densities of $\leq 2.5 \times 10^4$ cells/ml both cell lines showed a significant growth delay for the first 72 hours after seeding. Initially, the cultures grew rapidly at the highest seeding densities, but the growth rate was then slowing down by 48 hours. For subsequent growth inhibition studies, an optimal seeding density of 5×10^4 cells per ml was chosen and the effect on optical density measured after 72 hours of drug treatment.
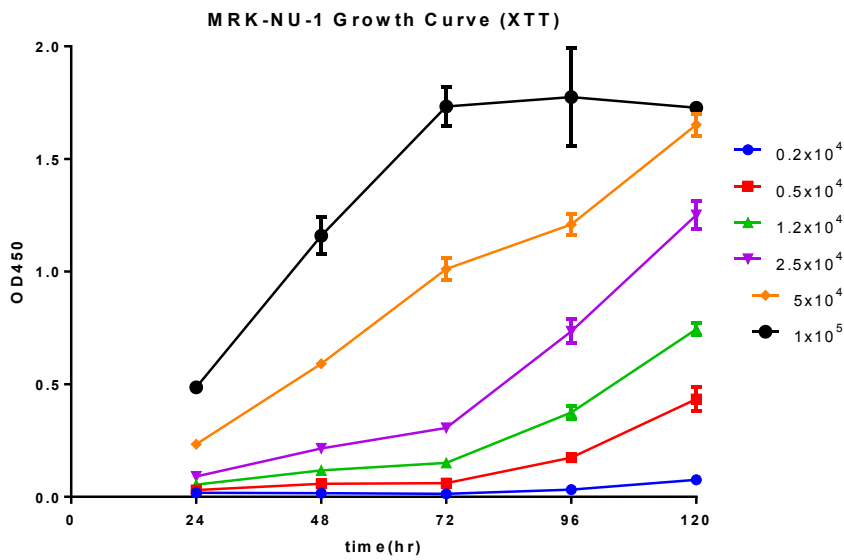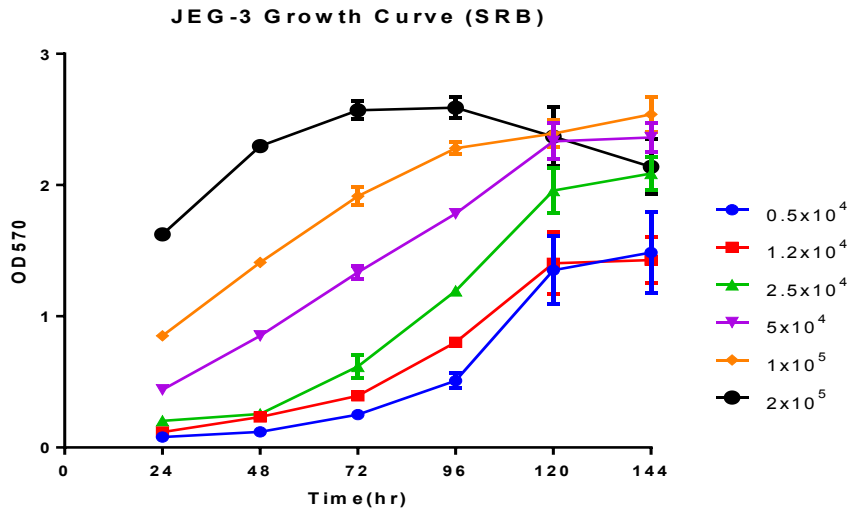
Figure 3.4. Growth curves of JEG-3 (adherent cell line) and MRK-nu-1 (suspension cell line).

JEG-3 (cells/ml)	0.5×10^4	1.2×10^4	2.5×10^4	5×10^4	1×10^5	2×10^5
Doubling Time (hr)	26.07	29.08	24.29	32.13	43.82	47.95
MRK-nu-1 (cells/ml)	0.2×10^4	0.5×10^4	1.2×10^4	2.5×10^4	5×10^4	1×10^5
Doubling Time (hr)	25.09	25.24	21.44	19.23	17.89	19.14

Table 3.2. The maximum doubling times of JEG-3 and MRK-nu-1 from the growth curves
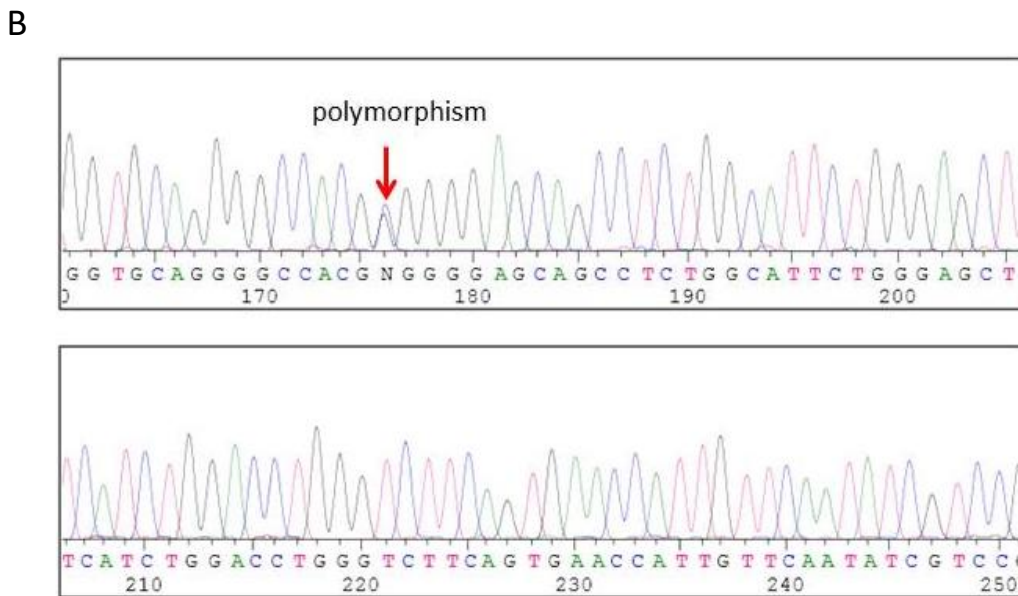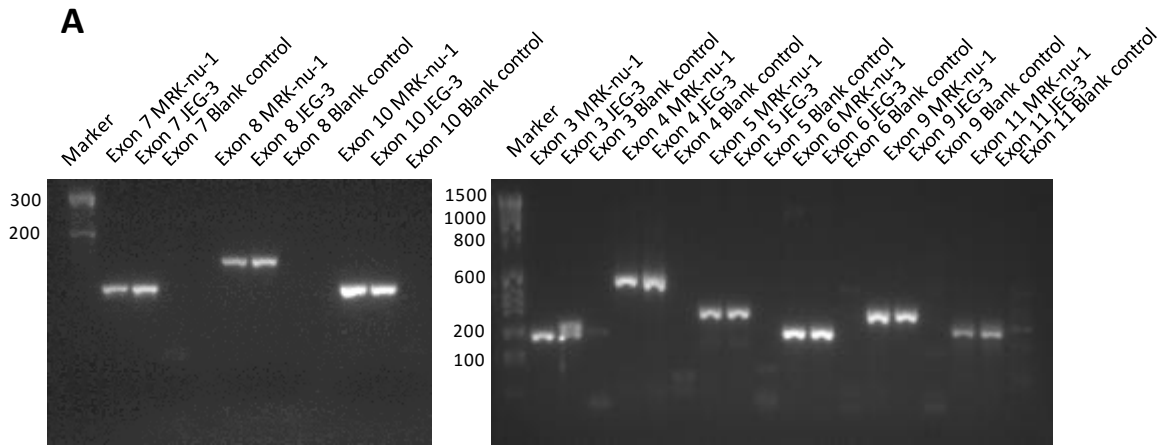
Figure 3.5. (A) 2% Agarose gel electrophoresis analysis of PCR products of exon 3 to exon 11 of *TP53* gene in JEG-3 and MRK-nu-1 cell lines. (B) Sequencing of JEG-3 *TP53* exon 4 antisense. The red arrow shows the position of the codon 72 C/G (Arg/Pro) polymorphism in the JEG-3 cell line.

The Western blot analysis in Figure 3.6 and Figure 3.7 shows the response of JEG-3 and MRK-nu-1 cells to different doses of Nutlin-3 treatment for 4 hours. MDMX was expressed at high levels in these two *MDMX* amplified cell lines, but the MDMX protein levels did not change after 4 and 24 hours of Nutlin-3 treatment at each dose. Dose-dependent stabilisation of p53 was observed in response to Nutlin-3 treatment in MRK-nu-1 cells and was accompanied by downstream activation of MDM2 and p21. A similar trend was seen in the JEG-3 cell line, although interestingly the basal p53 level was high prior to treatment and did not show any further increase in response to treatment, although increases in MDM2 and p21 indicated the p53 was functional. The inductions of MDM2 and p21 by Nutlin-3 were dose-dependent. BAX also increased in a dose-dependent manner after 24 hour drug exposure in both JEG-3 and MRK-nu-1 cells. The responses to Nutlin-3 were similar to those seen with MDM2 amplified and MDMX non-expressing cell lines such as SJSA-1 (Vassilev *et al.*, 2004). The reactivated response of p53 was also evidence that JEG-3 and MRk-nu-1 were carrying wild-type and functional p53.
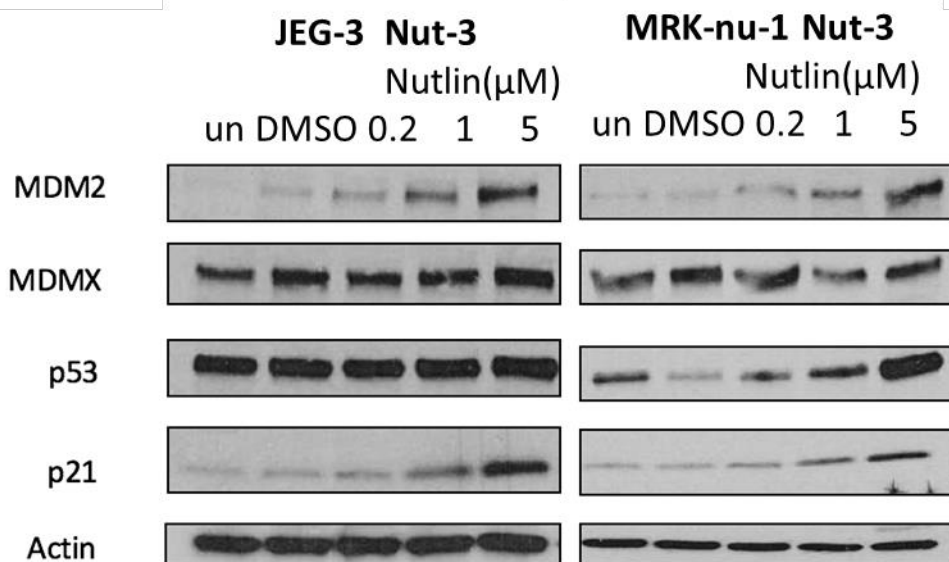
Figure 3.6. Nutlin-3 treatment (4 hours) responses of MDMX, MDM2, p53, p21, in JEG-3 and MRK-nu-1 cell lines. Actin used as a loading control.
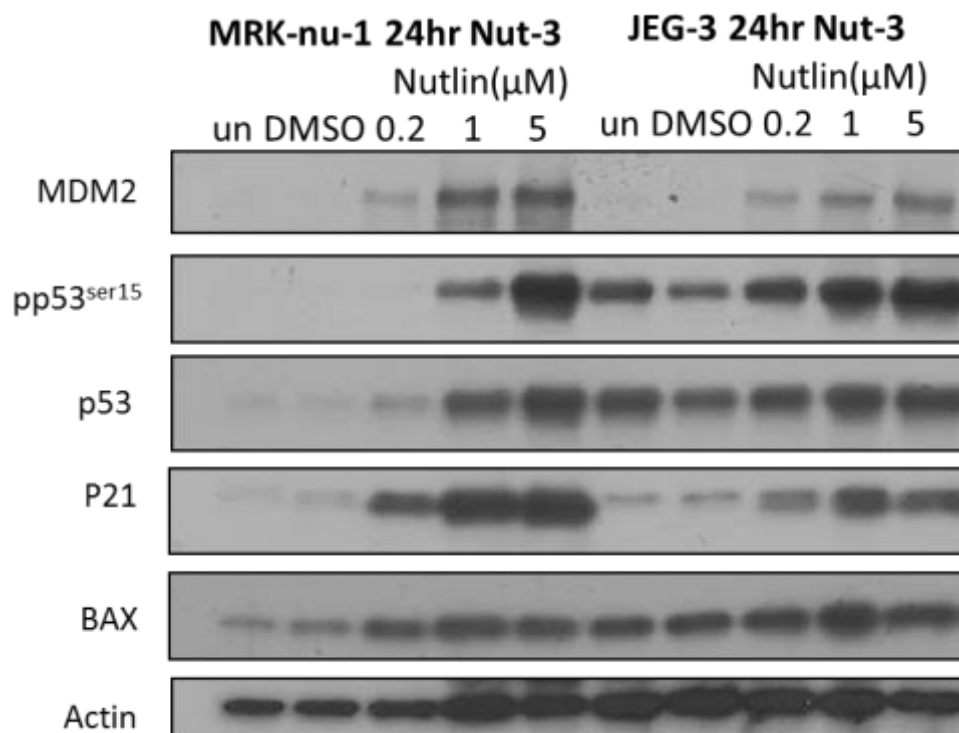
Figure 3.7. Nutlin-3 treatment responses of MDM2, p53, pp53^{ser15}, p21 and BAX in JEG-3 and MRK-nu-1 cell lines for 24 hours. Unfortunately, MDMX was not probed in this blot. Actin was used as a loading control.

Figure 3.8 shows DMSO sensitivity and growth inhibition by Nutlin-3 treatment for JEG-3 and MRK-nu-1 cell lines. JEG-3 and MRK-nu-1 cells showed around or over 80% cell survival in 1% DMSO for 72 hours. DMSO showed only slightly cytotoxic effects to these two cell lines. For growth inhibition by 72 hours Nutlin-3 treatments, the average (over 3 replicates) GI_{50} values were 11.7 ± 1.4 µM in JEG-3 and 3.0 ± 0.5 µM in MRK-nu-1 (table 3.3). These two MDMX amplified cell lines have similar sensitivity to Nutlin-3 compared with SJSA-1 with 2.8 ± 0.4 µM of Nutlin-3 GI_{50} value (table 3.3).

Clonogenic assay was used for testing tumour regrow and colony forming ability after removing drugs. JEG-3 cells were seeded into 6-well plates with 200 cells/well cell density. After 24 hour, the JEG-3 cells were treated by different doses of Nutlin-3 and RG7388 for 48 hours and then the drugs were removed. The cells regrew and formed colonies after incubating for 2 weeks. The clonogenic assay results of JEG-3 cells after 48 hour Nutlin-3 and RG7388 treatment are shown in figure 3.9. The JEG-3 clonogenic LC_{50} values for Nutlin-3 and RG7388 for 48 hour treatment were 18.3 ± 2.7 µM and 2.2 ± 0.215 µM respectively.
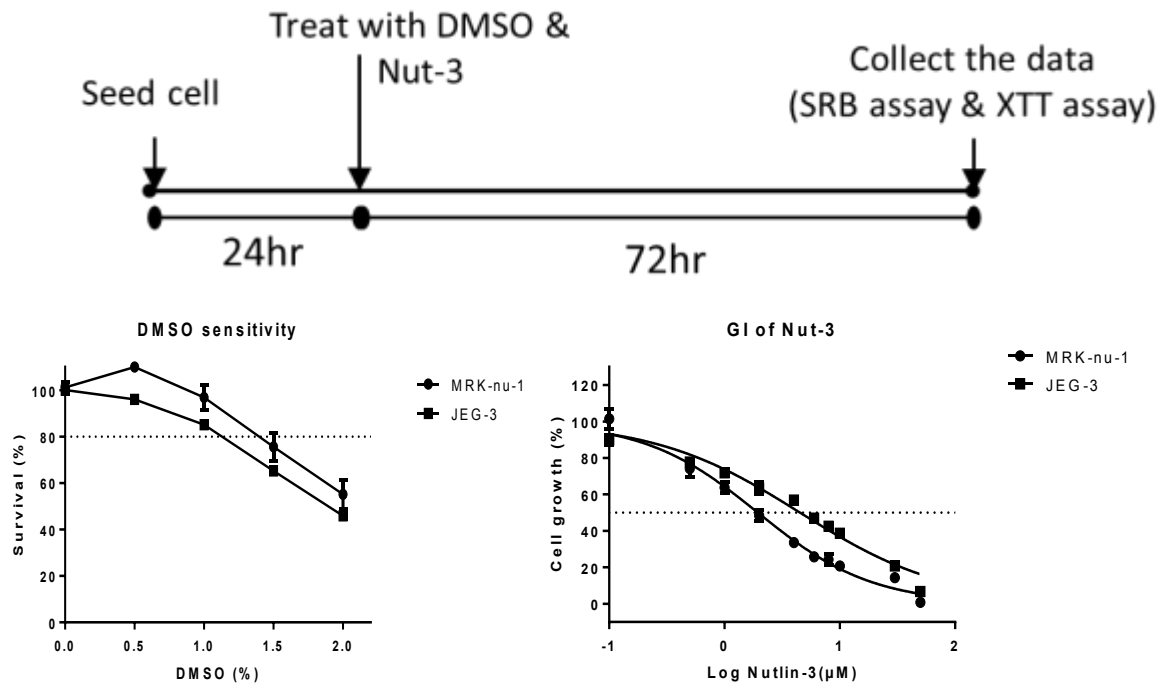
Figure 3.8. DMSO sensitivity and growth inhibition by Nutlin-3 in JEG-3 and MRK-nu-1 cells. JEG-3 and MRK-nu-1 cells were treated with Nutlin-3 dissolved in 1% DMSO from 0.1 μM to 30 μM for 72 hours.
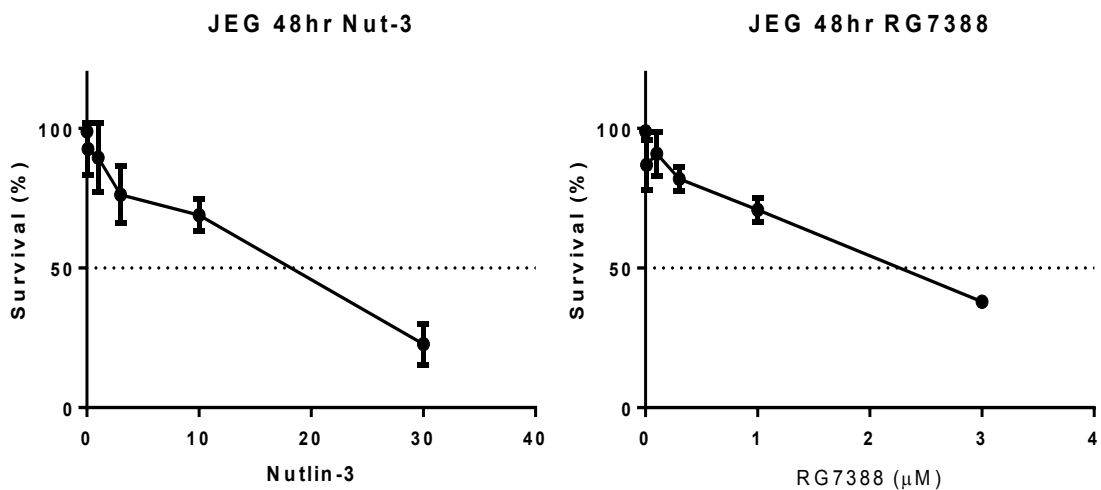
Figure 3.9. Clonogenic assay for 48 hours treatment with Nutlin-3 and RG7388 in JEG-3 cells. The average LC$_{50}$ values for Nutlin-3 and RG7388 were 18.3 ± 2.7 μM and 2.2 ± 0.2 μM respectively (n=3).

3.4.3 Cells with MDMX amplification and/or high expression are sensitive to MDM2-p53 binding antagonists

The cells with MDMX amplification (JEG-3 and MRK-nu-1) and high MDMX expression (NGP and MCF-7) were sensitive to 72 hour treatments with Nutlin-3 and RG7388 (figure 3.10A & B).

The Western blot results in figure 3.6 and figure 3.7 show MDMX was expressed at high levels in these two MDMX amplified cell lines but MDMX protein levels did not change after 4 hours of Nutlin-3 treatment. The p53 showed dose-dependent stabilization in MRK-nu-1 cells, followed by dose-dependent down-stream activation of MDM2 and p21 protein levels. Despite high basal levels of p53, a similar p53-dependent downsteam transcriptional response was seen in the JEG-3 cell line, including pp53^{ser15} phosphorylation. The overall pattern of response to Nutlin-3 was similar to that seen with MDM2 amplified and MDMX non-expressing cell lines such as SJSA-1 (Drummond *et al.*, 2016).

3.4.4 Mutant p53 cells are resistant to MDM2-p53 antagonists and the MDMX/2-p53 co-antagonist

S-M6R1 and S-N40R2 (SJSA-1 daughter cell lines resistant to MI63 and Nutlin-3) and N-20R1 (NGP daughter cell line resistant to Nutlin-3) were both selected for resistance to MDM2-p53 binding antagonists and mutant for *TP53* (Drummond *et al.*, 2016)*.* The *TP53* mutant daughter cells (dashed line) were resistant to Nutlin-3, RG7388 and RO5963 compared with their parental *TP53* wild-type cell lines (solid line) SJSA-1 and NGP (figure 3.10). RG7388 as the more potent MDM2 antagonist also has better selectivity for growth inhibition between mutant and wild-type p53.

This indicates that MDMX amplification does not make cells resistant to MDM2 antagonists in the same way as observed for mutation of *TP53*. Mutant *TP53* cell lines have much higher GI_{50} values for Nutlin-3 (> 40 µM), RG7388 (> 3 µM) and co-inhibitor RO5963 (>30 µM), compared with the *TP53* wild-type and MDMX amplified cell lines (Table 3.3). This suggests that *TP53* gene status is a more important factor in the efficacy of MDM2-p53 antagonists than MDMX status.

3.4.5 Comparison of co-antagonist GI_{50} values in MDMX amplified/high expressed cell lines and MDM2 amplified cell lines

The MDMX amplified cells and MDMX high-expressing cells have similar sensitivity to the RO5963 co-inhibitor. Interestingly, SJSA-1 cells had the highest GI_{50} value for RO5963 of 13.1 ± 1.0 µM among all the *TP53* wild-type cell lines. Thus low or undetectable expression of MDMX in SJSA-1 was associated with resistance to the RO5963 MDMX/MDM2 co-inhibitor and highest sensitivity to Nutlin-3 and RG7388 (figure 3.10 and table 3.3).

Cell line	MDM2	MDMX	Nutlin-3 (µM)	RG7388 (µM)	RO-5963 (µM)
JEG-3	LE	Amp	11.7 ± 1.4	1.76 ± 0.64	4.5 ± 0.7
MRK-nu-1	LE	Amp	3.0 ± 0.5	0.54 ± 0.13	2.4 ± 0.2
SJSA-1	Amp	LE	2.8 ± 0.4	0.007 ± 0.003	15.7 ± 0.7
S-N40R2	Amp	LE	49 ± 0.4	> 5	> 30
MCF-7	LE	HE	5.3 ± 1.3	0.14 ± 0.05	2.7 ± 0.1
NGP	Amp	HE	2.0 ± 0.7	0.12 ± 0.01	2.7 ± 1.1
N20R1	Amp	HE	41 ± 6	> 3	-

The cells were treated with the drugs for 72 hr and the cell viability tested by SRB and XTT (MRK-nu-1 only) assay. The average GI_{50} values were calculated from at least n=3 individual repeats (Means ± SEM). (Amp: amplification; HE: high expression; LE: low expression and basal level undetectable by Western blot.)

Table 3.3. The GI_{50} values for Nutlin-3, RG7388 and RO5963 in a panel of cell lines of differing MDM2, MDMX and TP53 status.
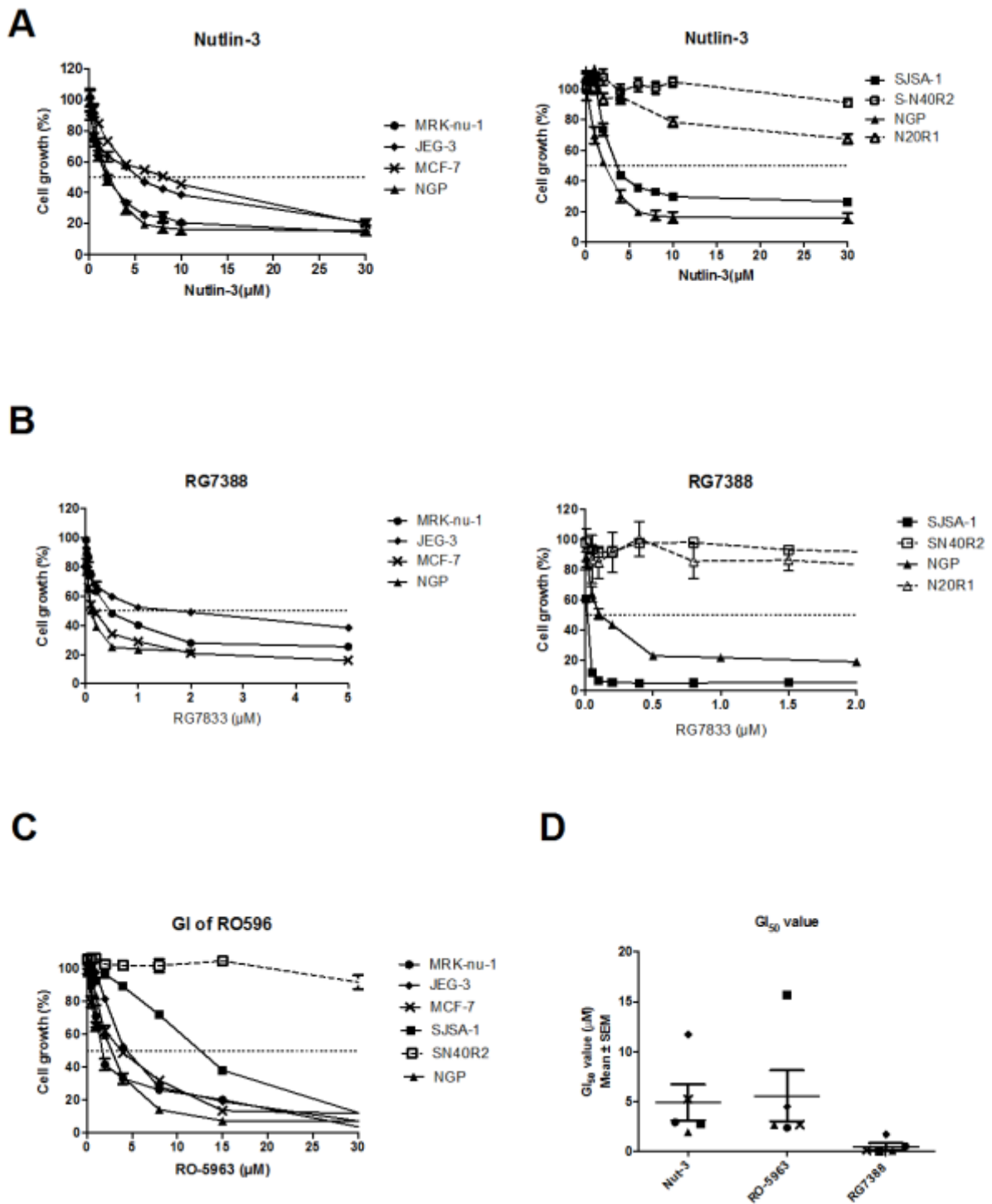
Figure 3.10. Dose-dependent growth inhibition response of cell lines of varying MDMX status to MDM2-p53 binding antagonists, Nutlin-3 (A) & RG7388 (B), and the MDMX/2-p53 co-inhibitor RO5963 (C). (D) Summary plot of the GI$_{50}$ values for Nutlin-3, RG7388 and RO5963 for wild-type *TP53* cell lines.

3.5   Discussion

TP53 status has a much greater impact on the response to MDM2-p53 binding antagonists compared with MDMX expression. The summary GI_{50} value bar chart in figure 3.11 indicates *MDMX* amplified cell lines and cell lines with high MDMX expression have similar Nutlin-3 GI_{50} values as MDM2 amplified and *TP53* wild-type cell lines. *MDMX* amplification does not make tumour cells as resistant to MDM2 antagonists as observed for mutation of *TP53*.

According to the results of Nutlin-3 treatment in the present study, MDMX protein levels did not show a significant change in either of the MDMX amplified cell lines after treatment with different concentrations of Nutlin-3. These results are consistent with previous studies (Hu *et al.*, 2006; Patton *et al.*, 2006; Wade *et al.*, 2006). It has reported that MDMX expression is associated with cell growth and proliferation. MDMX expression is induced at the transcriptional level by activation of K-Ras and IGF-1 (insulin-like growth factor 1) via the MAPK pathway; also, increased MDMX correlates with ERK phosphorylation. An increase of MDMX expression by mitogenic signals might contribute to the protection of tumour cell proliferation from p53 activation (Gilkes *et al.*, 2008).The p53, phosphorylated pp53[ser15], MDM2 and p21 protein levels increased in a dose-dependent manner after Nutlin-3 treatment. The *MDMX* amplified cells showed a similar response to other *TP53* wild-type cell lines. The p53 was stabilized and the transcriptional function was reactivated after treatment with MDM2 antagonists in the cells with *MDMX* amplification as typically seen for wild-type *TP53* cell lines (Vassilev *et al.*, 2004).

MDMX amplification and high expression showed some, but not strong, association with resistance to MDM2-p53 binding antagonists in wild-type p53 cells. These findings are consistent with a previous study in acute myeloid leukaemia that high levels of MDMX expression do not block function of MDM2 inhibitors in AML. Also AML cells with high MDMX remain sensitive to Nutlin-3 treatment (Tan *et al.*, 2014). By contrast, another study reported that cell lines with high MDMX expression presented more resistance to growth inhibition by Nutlin-3, which was different from our findings (Hu *et al.*, 2006). This might be due to the shorter treatment duration (48 hours) in the previous study compared with the current study (72 hours).

MDMX expression is associated with sensitivity to MDM2/X-p53 binding co-inhibitor (Graves *et al.*, 2012). High MDM2 and undetectable MDMX in SJSA-1 cells was associated with resistance to RO5963, although RO5963 has similar and strong binding ability to both MDM2 and MDMX. *TP53* status is the major factor in resistance to co-inhibitors. Selection for resistance to MDM2 inhibitors is not associated with increased MDMX expression, which might be expected if MDMX expression was an important mediator of resistance to MDM2 inhibitors (Drummond *et al.*, 2016).
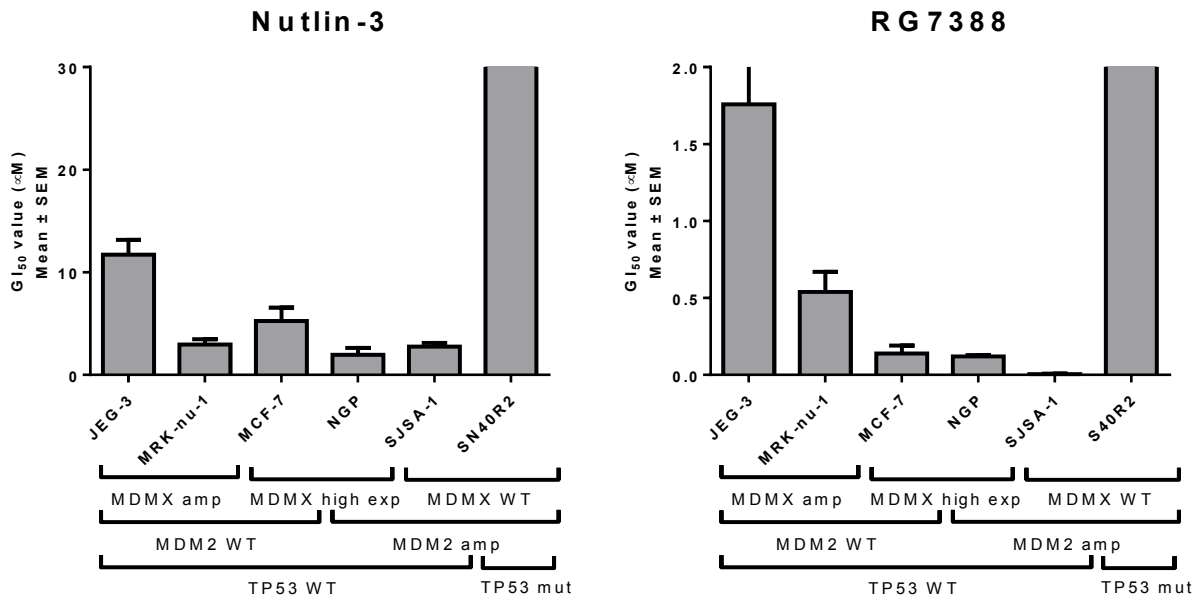
Figure 3.11. GI$_{50}$ values of Nutlin-3 and RG7388 in different cell lines with different *TP53, MDM2 and MDM4(MDMX)* status.JEG-3 and MRK-nu-1 cells have a GI$_{50}$ value for Nutlin-3 which is similar to other *TP53* wild-type cell lines, such as SJSA-1, and not resistant like the *TP53* mutant cell lines.

Chapter 4 The effect of knockdown of MDMX expression by lentiviral shRNA on the response to MDM2-p53 binding antagonists & MDMX/2 co-antagonist

4.1   Introduction

MDMX as a homolog of MDM2 is also a p53-binding negative regulator that can inhibit p53 function in tumour cells and in normal cells. Suppression of MDMX expression may lead to p53 reactivation, particularly in cells with MDMX amplification or high MDMX expression. In addition, some research has suggested that knockdown of MDMX improves response and cell sensitivity to Nutlin-3 and other MDM2 inhibitors (Hu *et al.*, 2006; Patton *et al.*, 2006; Wade *et al.*, 2006). A previous study indicated that U2OS cells transduced to overexpress MDMX were rendered resistant to growth inhibition and activation of p53 down-stream protein responses (Hu *et al.*, 2006). Knockdown of MDMX in MCF-7 cells infected with lentivirus shRNA has also been reported to enhance Nutlin-3 induced cytotoxicity (Wade *et al.*, 2006). Therefore, in chapter 4 and chapter 5 of this thesis, results are described for the effects of two different knockdown systems used to suppress MDMX protein expression on the subsequent response to treatment with MDM2-p53 binding antagonists Nutlin-3 & RG7388 and the MDM2/X-p53 binding co-antagonist RO5963. In this chapter, the establishment and testing of a lentiviral shRNA system as a long-term and stable method of decreasing MDMX protein expression in a panel of cell lines is described.

4.2   Hypotheses and aims

Hypotheses:

Cell lines amplified for and/or expressing high levels of the *MDMX* gene are nevertheless responsive to MDM2-p53 binding antagonists and response to these agents is altered by suppression of MDMX expression by lentiviral shRNA.

Suppression of MDMX expression by lentiviral shRNA is associated with increased sensitivity to MDM2-p53 binding antagonists for growth inhibition apoptosis and cell cycle arrest.

Suppression of MDMX expression by lentiviral shRNA is associated with decreased response and increased resistance to MDM2/X-p53 binding antagonist RO5963 for growth inhibition, apoptosis and cell cycle arrest.

Aim:

To test the ability of MDM2-p53 binding inhibitors Nutlin-3, RG7388 and RO5963 to activate p53 in the presence and relative reduction of MDMX expression achieved by a regulated lentiviral shRNA knockdown system
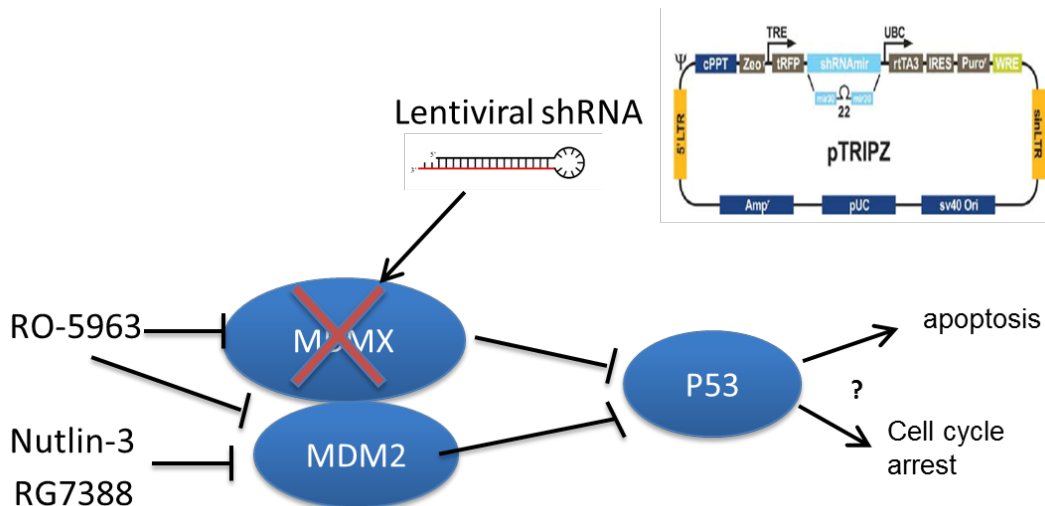
Figure 4.1 Knockdown of MDMX by lentiviral shRNA affects the response to MDM2 inhibitors and MDMX/MDM2 co-inhibitors via the p53 pathway

4.3   Specific Materials and Methods

4.3.1 Transduced cell lines

Two MDMX amplified cell lines, JEG-3 & MRK-nu-1, and high MDMX-expressing neuroblastoma cell lines NGP and SKNSH were transduced with the TRIPZ MDMX shRNA knockdown construct (chapter 2.8). They were selected for uptake and expression of the viral DNA by growth in puromycin based on previously established puromycin sensitivity assays (work of Claire Hutton). Optimal puromycin doses were established to provide sufficient cell killing of non-transduced cells to allow selection of those successfully transduced with the construct and expressing the puromycin-resistance gene. After being transduced successfully, for example, the MRK-nu-1 L1 cells were named for the MRK-nu-1 lentiviral transduced clone 1.

4.3.2 Red fluorescent protein (RFP) check

Fluorescence microscopy was used to confirm doxycycline-inducible expression of the red fluorescent protein (RFP) gene marker, to check successful uptake of the lentivirus and inducible gene expression from the DNA construct in the MRK-nu-1, JEG-3, NGP and SKNSH cells (figures 4.3-6). The red fluorescence signal was also checked by flow cytometry microscopy (figure 4.2).

4.3.3 Response of p53 pathway proteins to MDM2/MDMX inhibitor treatment after knockdown of MDMX

The lentivirus models were used to explore the effect of MDMX expression knockdown on cell growth and on the response to treatment with the MDM2 antagonists Nutlin-3 & RG7388 and the MDM2/MDMX co-inhibitor RO-50963. The treatment time for Nutlin-3, RG7388 and RO5963 was chosen to be after 72 hours of doxycycline induction in order to treat the cells at the optimal time for knockdown of MDMX protein expression. The time points of treatment and lysate collection for Western blots followed the time line shown in figure 4.8.

4.3.4 Growth inhibition of MDM2 antagonists after knockdown of MDMX

Nutlin-3, RG7388 and RO5963 treatments were performed after knocking down MDMX by doxycycline-induced lentiviral shRNA for 72 hours. The time points of

treatment and XTT assay for growth inhibition after MDMX knockdown followed the time line in figure 4.9.

4.3.5 FACS analysis in lentiviral transduced cells

FACS analysis was also used to confirm doxycycline inducible expression of the red fluorescent protein (RFP) gene marker from the DNA construct in the MRK-nu-1 cells (figure 4.2).

Nutlin-3, RG7388 and RO5963 treatment were performed after knocking down MDMX by doxycycline-induced lentiviral shRNA for 72 hours. The time points of treatment and FACS analysis for cell cycle distribution change after MDMX knockdown followed the time line in figure 4.8. The time points of collecting data was the same with lysate collecting.

Measurement of sub-G1 signals was not included with the cell cycle distribution changes in lentiviral transduced MRK-nu-1 cells. The sub-G1 data was affected by RFP signals on the setting for PI staining, because the doxycycline-inducible RFP signal peak overlapped with the sub-G1 peak, as shown in figure 4.2.
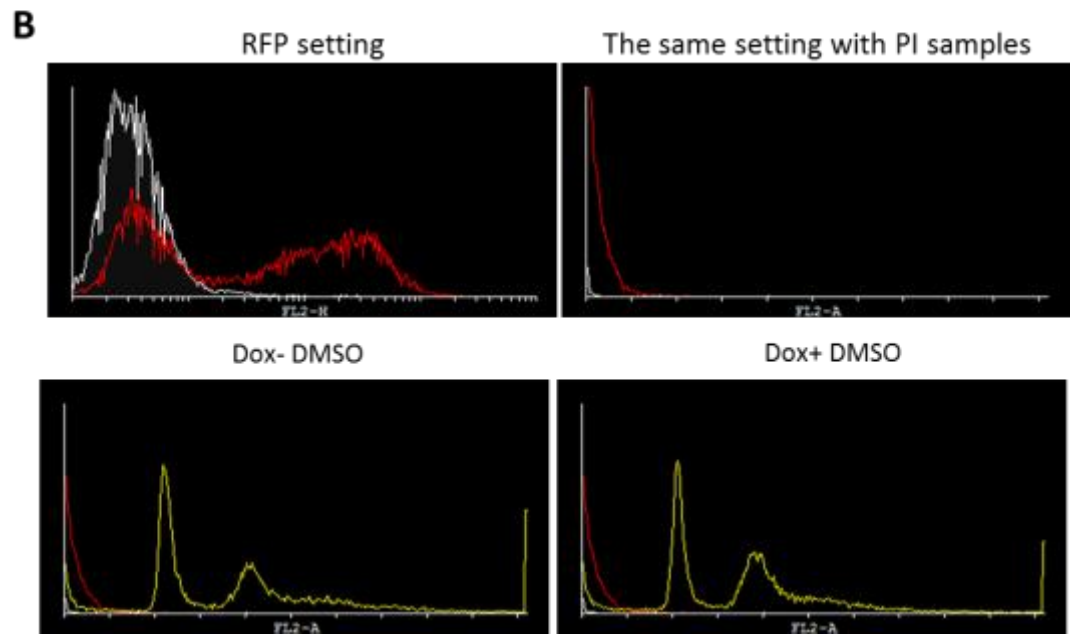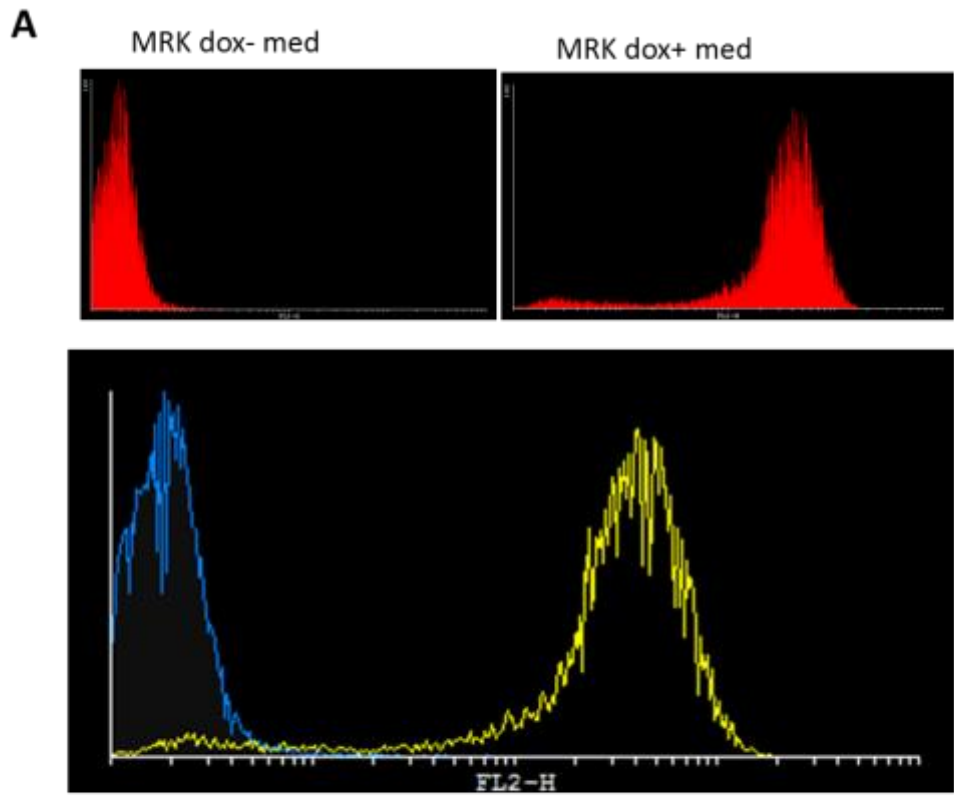
Figure 4.2. (A) Red fluorescence signal to check the doxycycline induction in MRK-nu-1 by FACS. (B) RFP signal check of dox- (white) & dox+ (red) in MRK L1 DMSO control. The same setting for the PI stained sample showed that the sub-G1 peak overlapped with the RFP signal.

4.4   Results

4.4.1. Knockdown of MDMX by lentiviral shRNA has low efficiency for suppressing MDMX protein levels in the cell lines except MRK-nu-1

MDMX protein level did not show significant decrease in JEG-3 and SKNSH cells after 48, 72 and 96 hour doxycycline-induced lentiviral shRNA knockdown of MDMX, although doxycycline-induced RFP was detected (figure 4.3, figure 4.4 & figure 4.5). JEG-3 cells had low level of RFP signal after doxycycline induction, and the MDMX level was not decreased by lentiviral shRNA (figure 4.4). JEG-3 cells with more copies of the lentivirus plasmid construct were selected by increasing the dose of puromycin up to 10 µg/ml, but the induction of RFP was still lower than in the other cells, consistent with MDMX knockdown not working as well as in the other cell lines. NGP cells showed a decrease of MDMX after 48-hour induction. However, the blots shown in figure 4.5 was the best example and there was only one case in which the lentiviral shRNA knockdown worked in NGP cells.

However, MRK-nu-1 cells had significant inducible RFP signal after 72 & 96 hour doxycycline induction (figure 4.6) and successful knockdown of MDMX expression by lentiviral shRNA was obtained. The MDMX protein level decreased more than 70% over the 72 hour induction (figure 4.7A).

4.4.2. Suppression of MDMX expression by lentiviral shRNA has no effect on cell growth

The cell growth curve shown in figure 4.7B indicates that doxycycline inducible lentiviral shRNA-mediated knockdown of MDMX did not affect the growth of JEG-3 and MRK-nu-1 cells. Absence and presence of puromycin might affect cell growth and keep the lentiviral shRNA sequence in the cells. The Western blot for daily MDMX expression of MRK-nu-1 cells showed highly significant knockdown of MDMX from 48 hour induction to 120 hours. The same level of p53 protein expression was maintained after knocking down MDMX expression.

MRK-nu-1 Puro+ (3µg/ml) dox+ (1µg/ml) for 48 hr
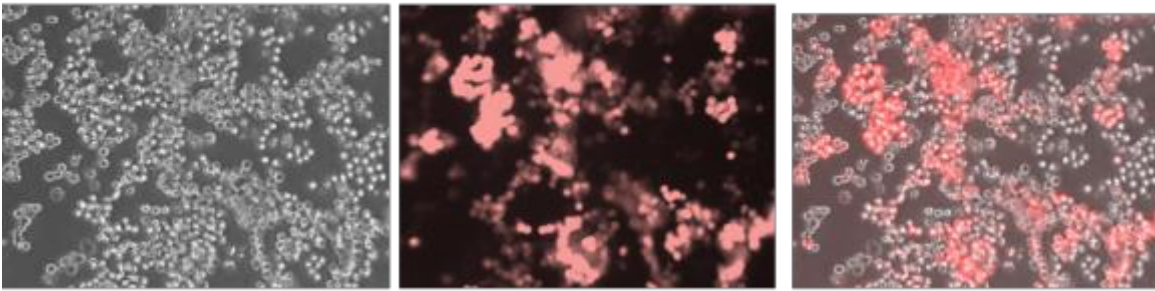
SKNSH Puro+ (1.5µg/ml) dox+ (1µg/ml) for 48 hr
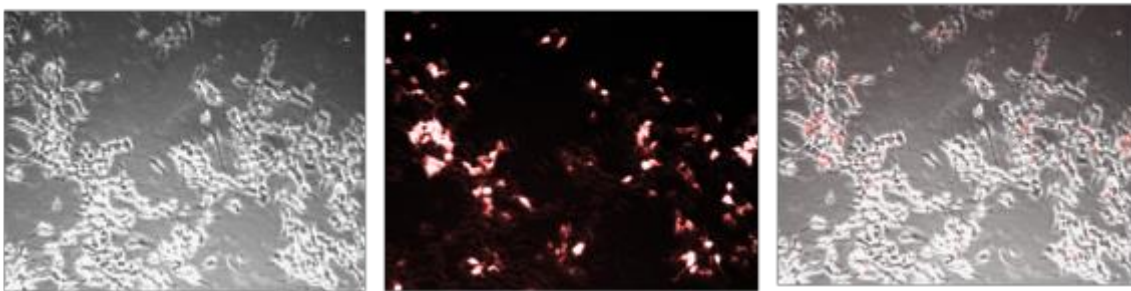
NGP Puro+ (3µg/ml) dox+ (1µg/ml) for 48 hr
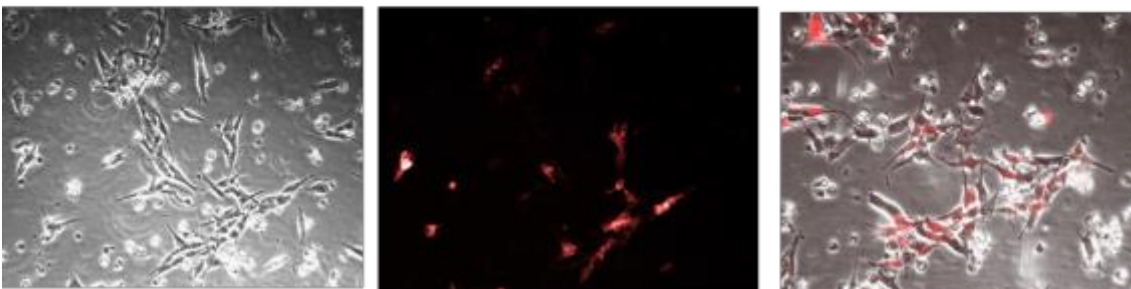
Figure 4.3. Red fluorescent protein (RFP) signal check following 1 µg/ml doxycycline induction for 48 hours in MRK-nu1, SKNSH and NGP cells. Left panel: white-light microscopy; middle panel: red fluorescence image; right hand panel: merged image.
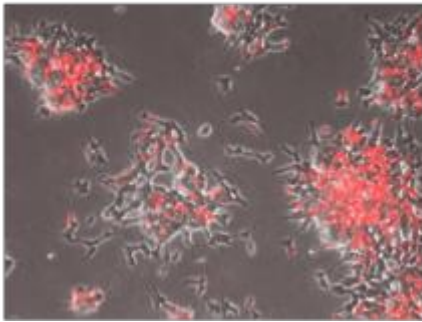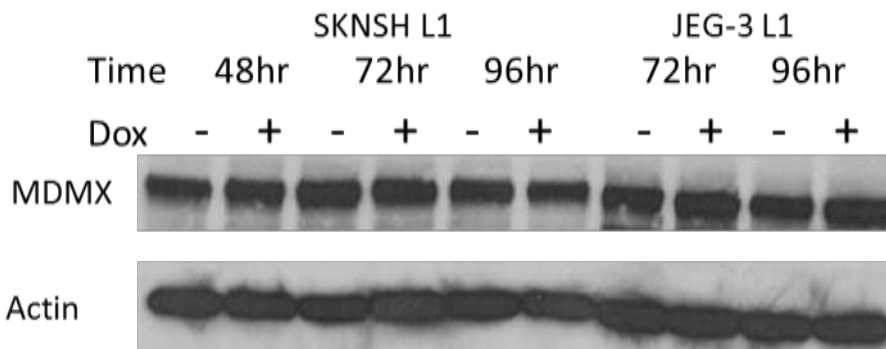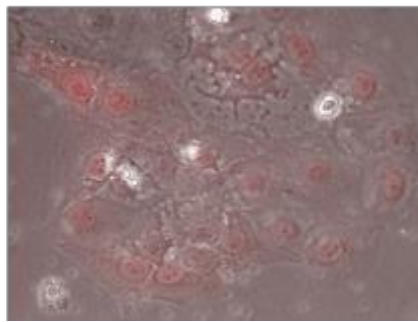
Figure 4.4 Red fluorescent protein (RFP) signal and MDMX protein level check following 1 µg/ml doxycycline induction for 72 hours in SKNSH & JEG-3 cells.
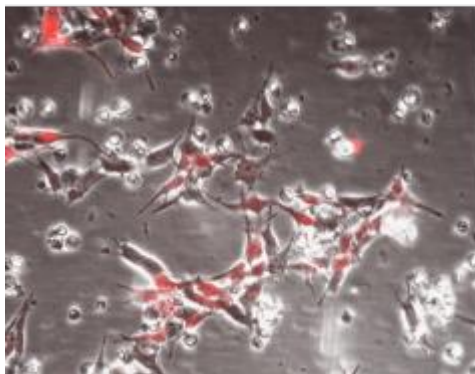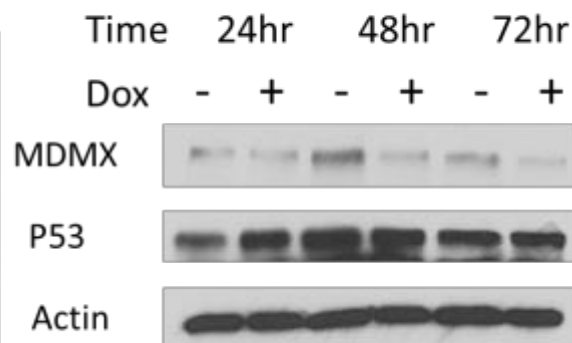
Figure 4.5. Red fluorescent protein (RFP) signal and protein expression check following 1.5 µg/ml doxycycline induction for 48 hour in NGP cells
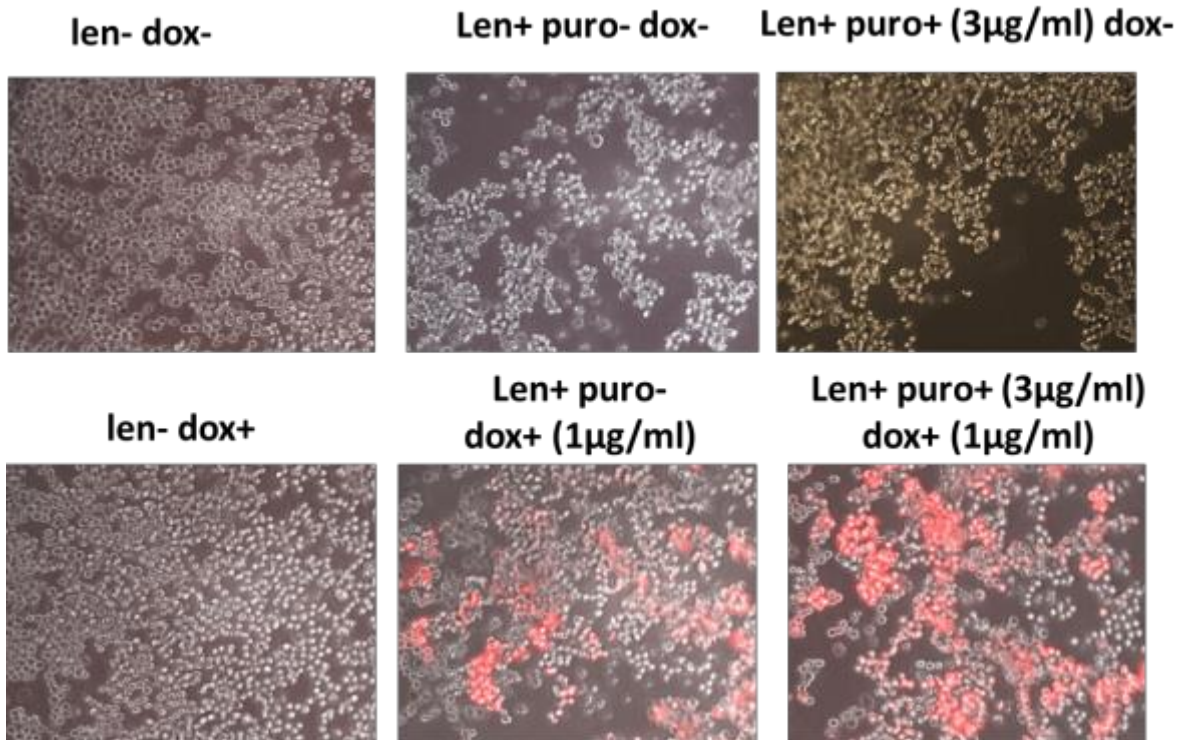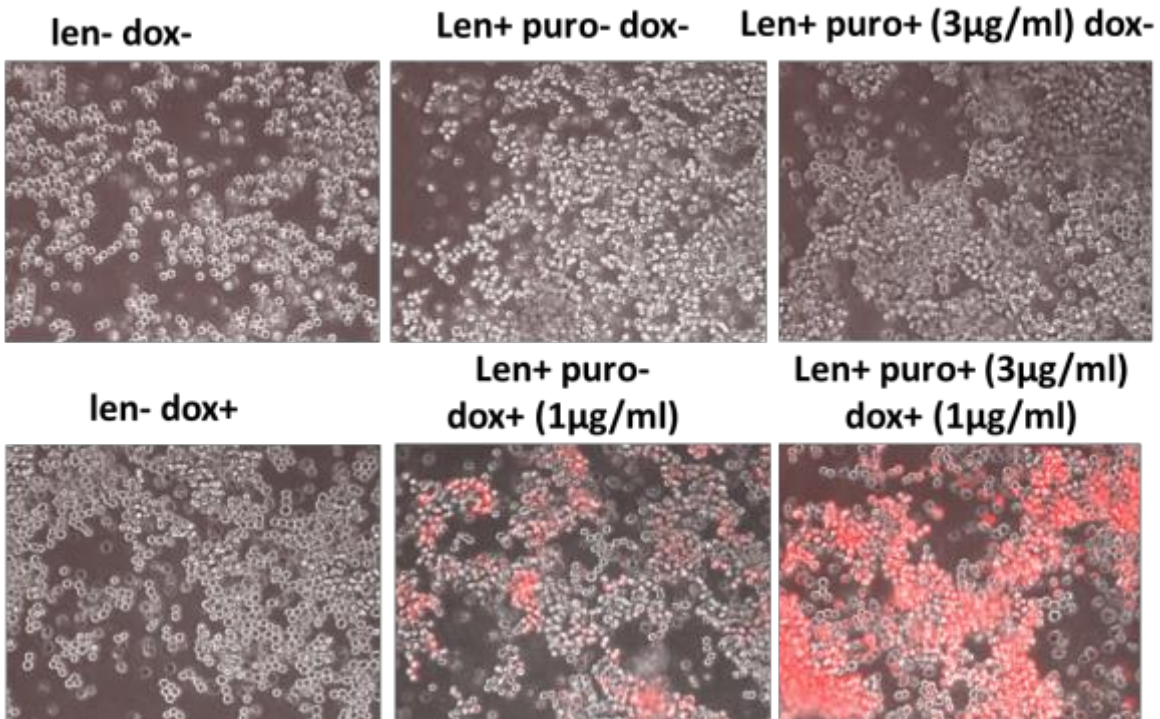
Figure 4.6. Doxycycline (1 μg/ml) induction of RFP signal for 72 & 96 hours in MRK-nu-1 cells.

A

Induction time (hr)	48	72	96	120
Knockdown MDMX	61%	70%	76%	73%
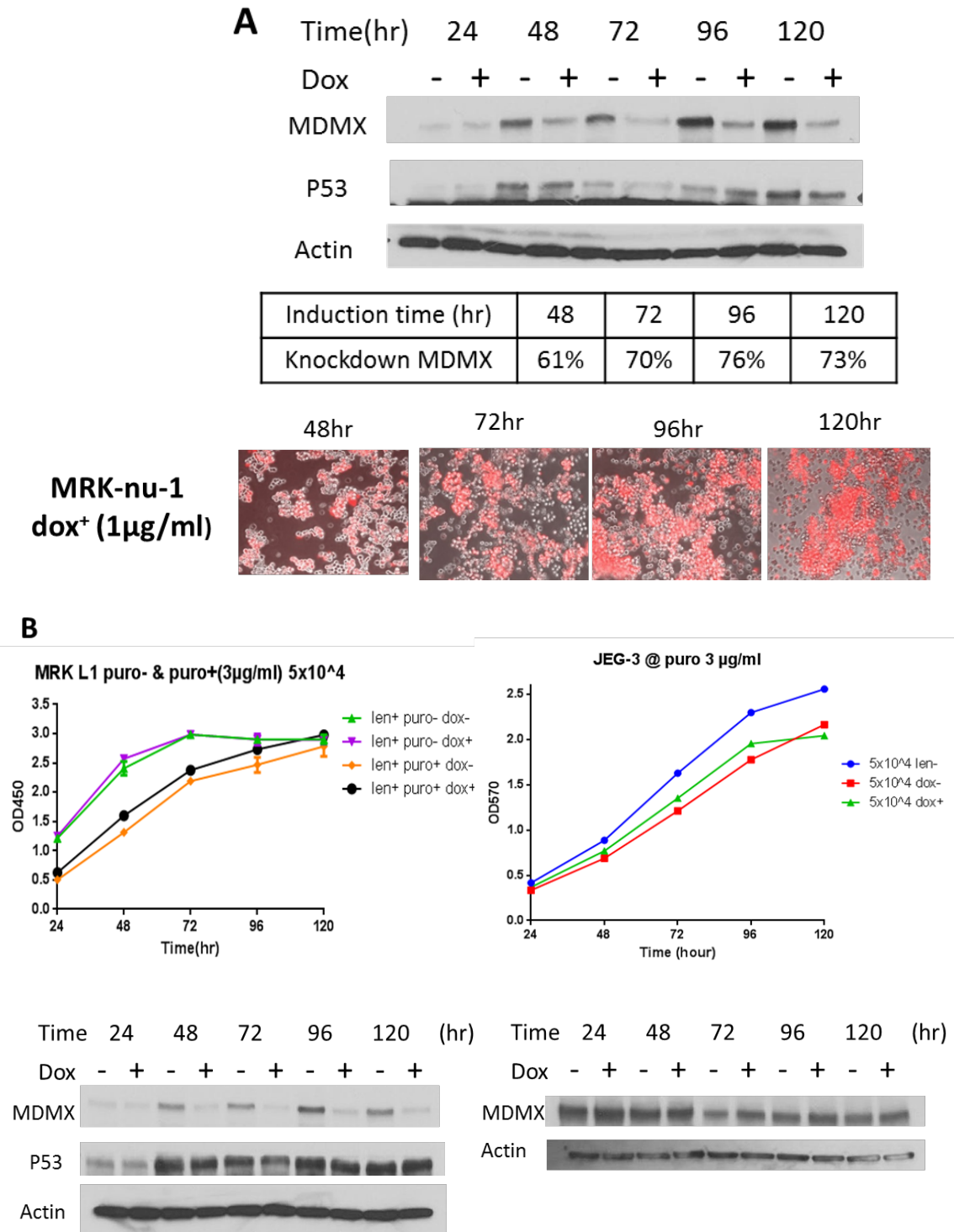
Figure 4.7. (A) The percentage of MDMX protein expression after lentiviral shRNA-mediated knockdown by doxycycline induction from 24 hours to 120 hours in MRK-nu-1 cells. (B) Growth curves and Western blots for MRK-nu-1 and JEG-3 with lentiviral shRNA knockdown of MDMX. MDMX expression is reduced by 24 hours (day 1) and maintained for 120 hours (day 5) of 1 µg/ml doxycycline induction. The RFP signal was used to provide a non-invasive quick check of induction by doxycycline.
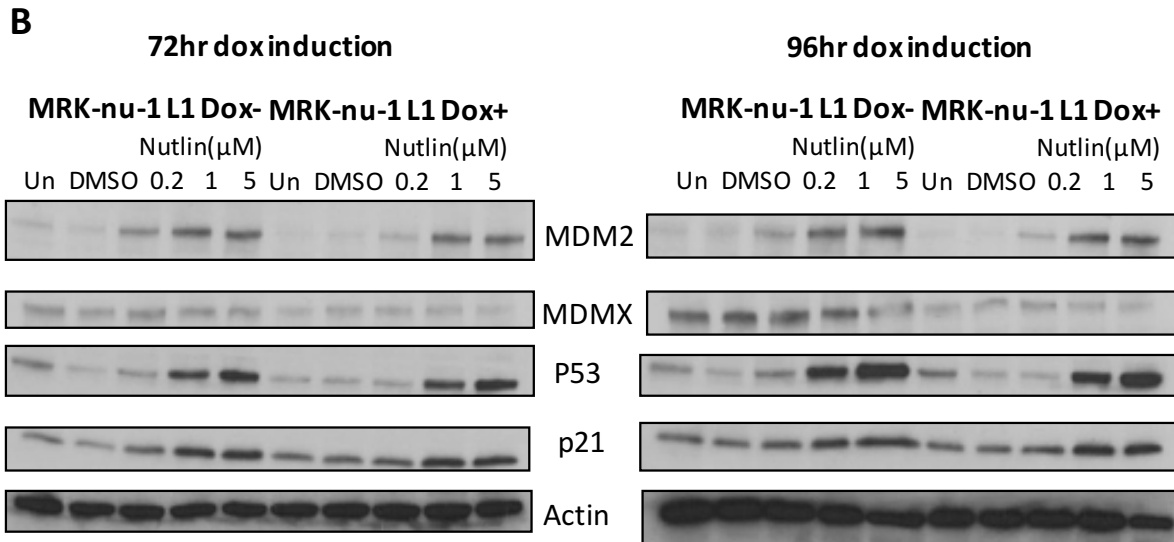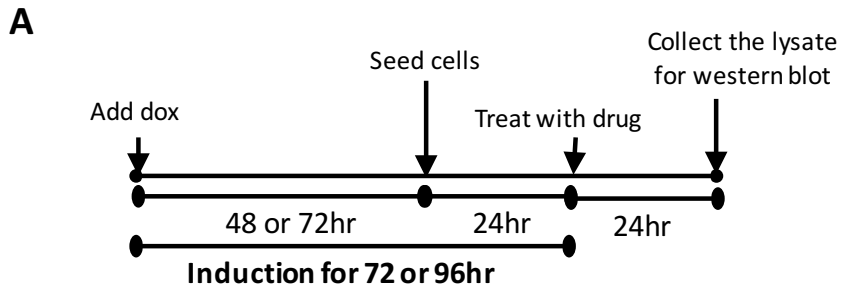
Figure 4.8. MDM2, p53 and p21 protein response to 4 hour Nutlin-3 after knockdown of MDMX. (A) Time line graph showed the experiment design. (B) The immunoblots showed the knockdown of MDMX did not affect the increasing p53, MDM2 and p21 by Nutlin-3 in 72 hour and longer 96 hour doxycycline induction.

4.4.3. MRK-nu-1 cells were slightly more resistant to Nutlin-3 & RO5963 but not RG7388 after knockdown of MDMX expression by lentiviral shRNA

The Western blot result in figure 4.7 & 4.8 shows MDMX expression in MRK-nu-1 cells was knocked down successfully after 72 & 96 hours of doxycycline induction. Figure 4.9 shows n=3 repeats for the effect on growth inhibition by Nutlin-3, RG7388 and RO5963 following lentiviral shRNA-mediated knockdown of MDMX in MRK-nu-1 cells. The mean GI_{50} value of Nutlin-3 had a statistically significant increase of approximately 2-fold after 72 hour drug exposure, while the mean GI_{50} value of the co-inhibitor RO5963 slightly increased as well after knockdown of MDMX, although the difference in GI_{50} value narrowly failed to reach statistical significance. However, no significant difference following MDMX knockdown was observed for the potent MDM2 inhibitor RG7388. In summary, MDMX lentiviral shRNA knockdown increased the Nutlin-3 and RO-5963 GI_{50} values for MRK-nu-1 cells, but had little or no effect on the GI_{50} value for RG7388.
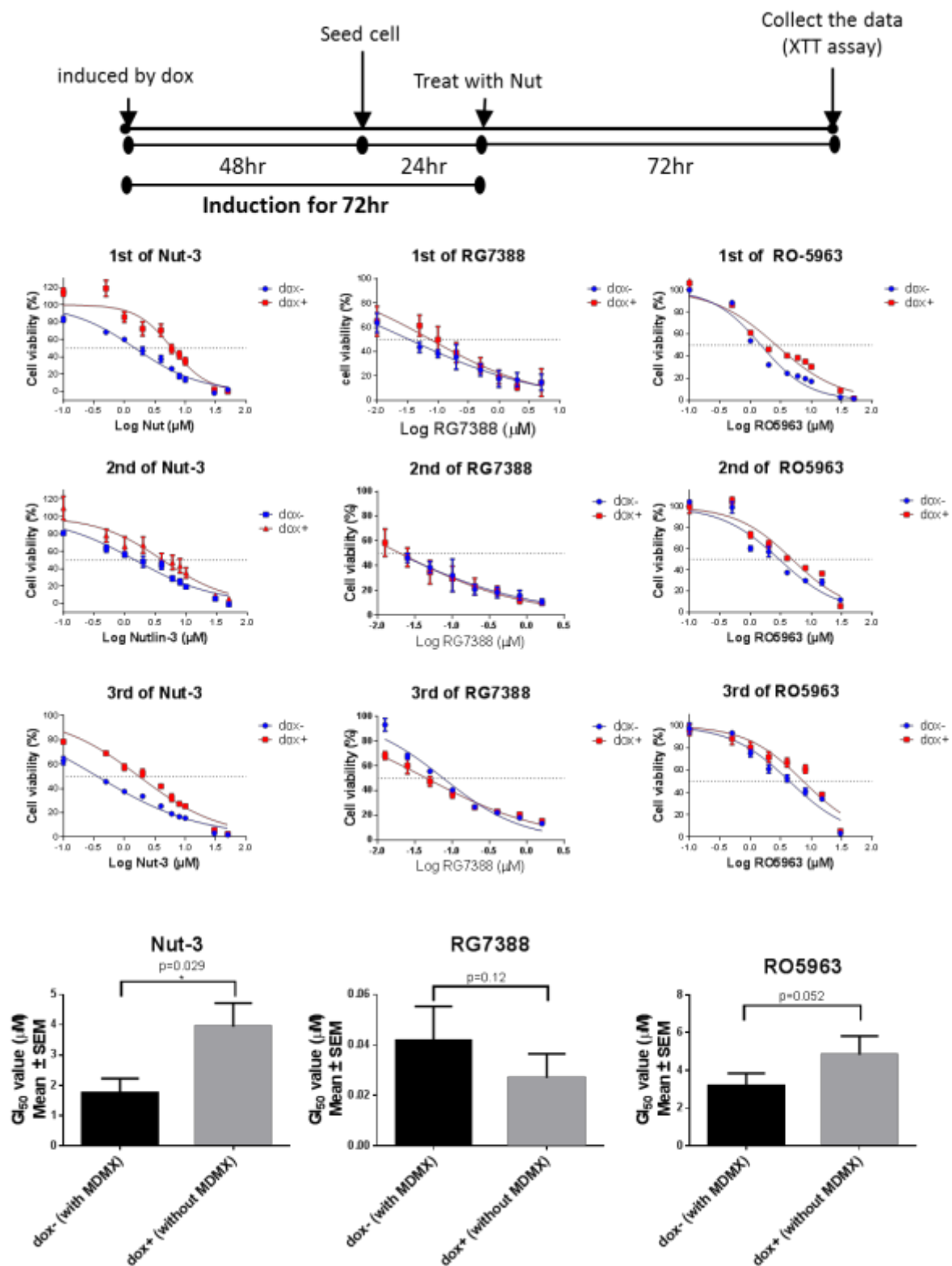
Figure 4.9. Growth inhibition by 72 hour drug treatment to Nutlin-3, RG7388 and RO5963 following lentiviral shRNA-mediated knockdown of MDMX in MRK-nu-1 cells. Two-tailed paired t test used.

4.4.4. MDM2, p53 and p21 protein levels did not change significantly after knockdown of MDMX by lentiviral shRNA

The images in A show that the doxycycline-induced RFP signal in MRK-nu-1 cells was not affected by Nutlin-3 treatment. The dose-dependent stabilization of p53 and induction of MDM2 and p21 by 4 hour Nutlin-3 exposure shown in figure 4.13B were maintained after knockdown of MDMX. BAX expression showed no change in the response to 4 hour Nutlin-3 treatment following knockdown of MDMX.

4.4.5. Lentiviral shRNA-mediated knockdown of MDMX suppressed p53 stabilization and expression of its downstream transcriptional targets by RO5963

The Western blots in figure 4.13 & figure 4.14 show the results for different treatment times with RO5963. The blot in figure 4.13C shows the comparison between Nutlin-3, RG7388 and RO5963 for 4 hour drug exposure following knockdown of MDMX. The p53 stabilization reached a peak at 4 hour treatment time with MDM2 inhibitors. BAX expression slightly increased after 24 hour RO5963 exposure (figure 4.14A). MDMX expression was stabilized in a dose-dependent manner by RO5963 (figure 4.14B). After knockdown of MDMX, the increase in p53 and MDM2 was modestly reduced for 6 and 24 hours RO5963 treatment.
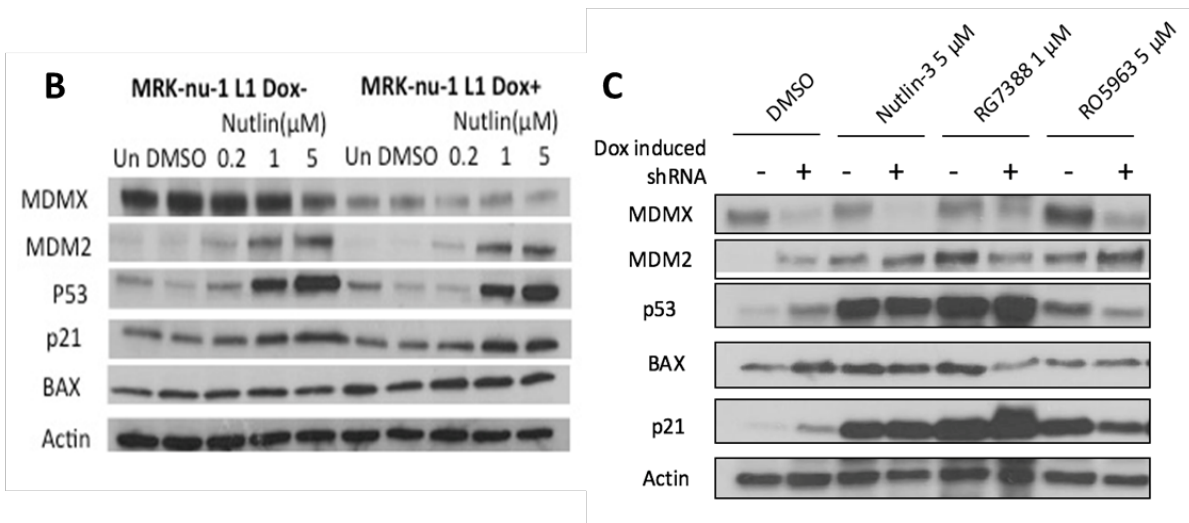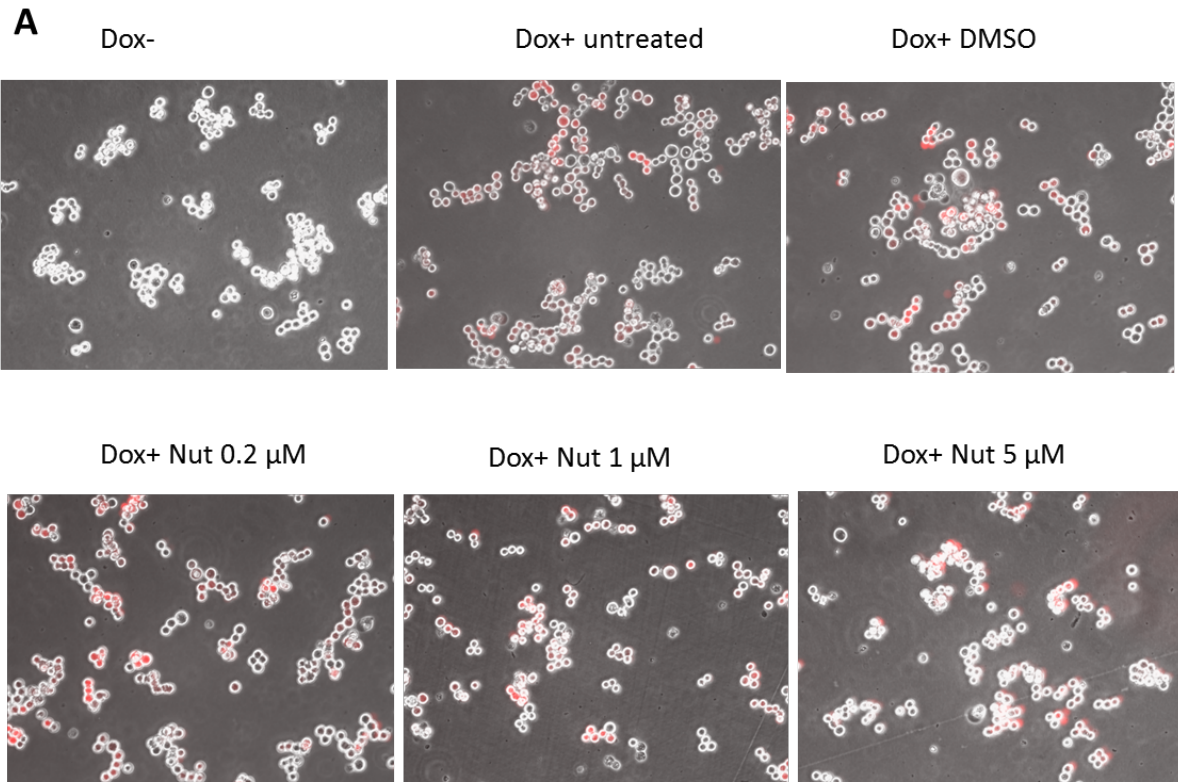
Figure 4.10 (A) A quick check of the induction system of RFP signal by doxycycline in MRK-nu-1 with Nutlin-3 treatment for 4 hours (B) 4 hour Nutlin-3 treatment following doxycycline-induced lentiviral shRNA knockdown of MDMX in MRK-nu-1 breast tumour cells. (C) The response to 4 hour drug treatment with Nutlin-3, RG7388 and RO5963 after 72 hours doxycycline-induced lentiviral shRNA knockdown of MDMX in MRK-nu-1 breast tumour cells.

5µM RO5963	-	-	+	+	+	+	+	+	+	+	+	+
Dox	-	+	-	+	-	+	-	+	-	+	-	+
Time (hr)	24		2		4		6		8		24	

MDMX

MDM2

p53

BAX

Actin
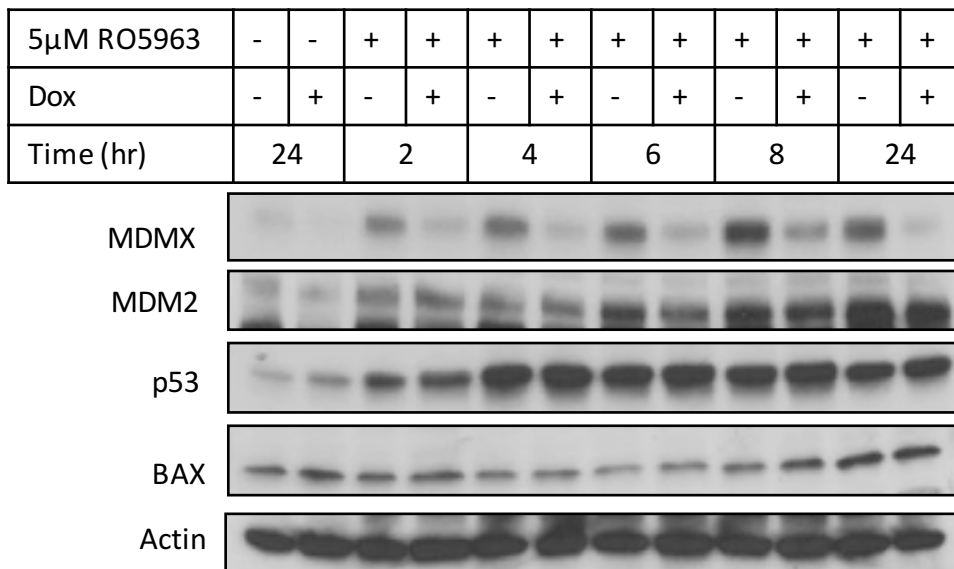
Figure 4.11. Time dependence of RO5963 response for MRK-nu-1 cells following MDMX knockdown by lentiviral shRNA. The response of p53, MDM2 and MDMX expression showed different time dependent increase by RO5963 treatment.

4.4.6. At lower doses Nutlin-3 and RO5963 treatment result in G1 arrest while high doses result in G2/M arrest

The propidium iodide FACS analysis histograms in figure 4.15 & figure 4.17 show the cell cycle distribution after 24 & 48 hours respectively of treatment with 5 µM & 10 µM of Nutlin-3 and RO5963 in MRK-nu-1 cells with lentiviral shRNA knockdown of MDMX. The G1 peak increased dramatically after Nutlin-3 and RO5963 treatment for 24 hours. This G1 arrest did not change statistically significantly after knockdown of MDMX (figure 4.17A). The Western blot in figure 4.16B was for the same cell set as used for the FACS analysis to confirm MDMX suppression and p53 activation. The sub-G1 peak was excluded from the bar charts of whole cell cycle distribution because the lentiviral transduced cells have background red fluorescence protein (RFP) signals which are strongly induced by doxycycline and overlap with the sub-G1 propidium iodide signal (chapter 4.3.5) The histograms in figure 4.17 show the strong background RFP signal even in the sub-G1 of untreated medium control.

Dose-dependent G1 and G2 accumulation was observed for both Nutlin-3 and RO50963 after 24 hour treatment (figure 4.16A). However, the MDMX knockdown by lentiviral shRNA did not affect the G1 & G2 arrest statistically significantly, although there was a trend for increased G1 and G2 arrest in the MDMX knocked-down samples, particularly for G2 arrest at high doses of Nutlin-3. The G1 and G2 arrest in the bar charts in figure 4.18 show no statistically significant difference due to the knockdown of MDMX after 48 hour drug exposure. Two-tailed paired t-tests were carried out for comparison of control (Dox -) and MDMX knockdown (Dox +) samples.
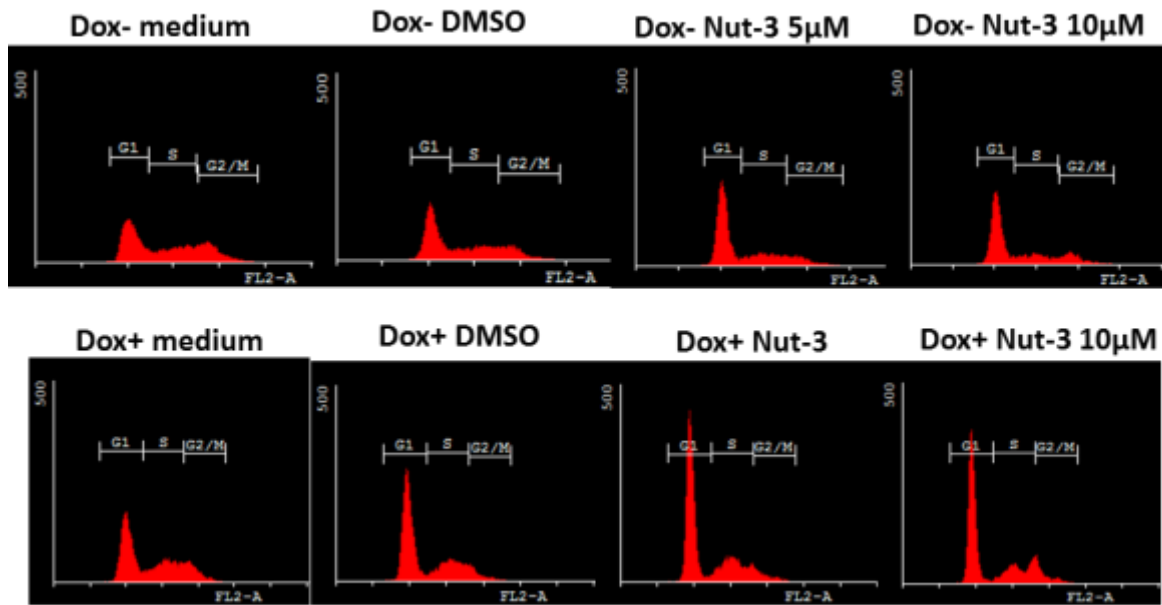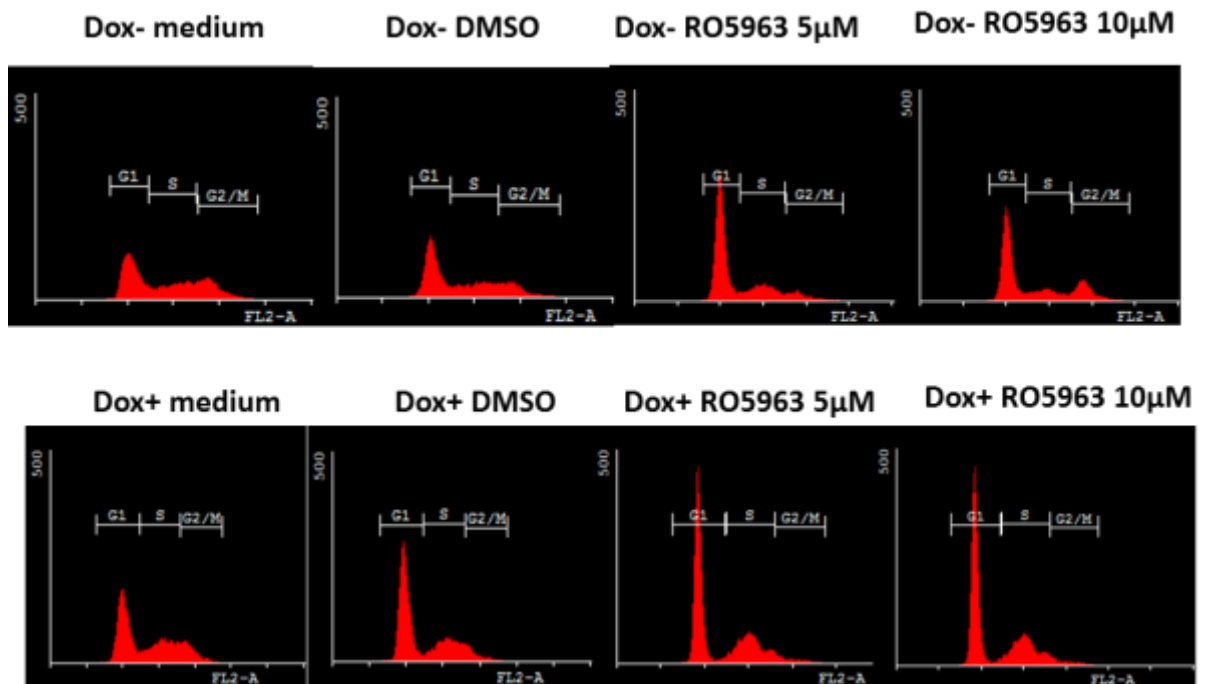
Figure 4.12. FACS analysis of cell cycle distribution after 24 hour Nutlin-3 & RO5963 treatments in MRK-nu-1 cells with lentiviral shRNA knockdown of MDMX.
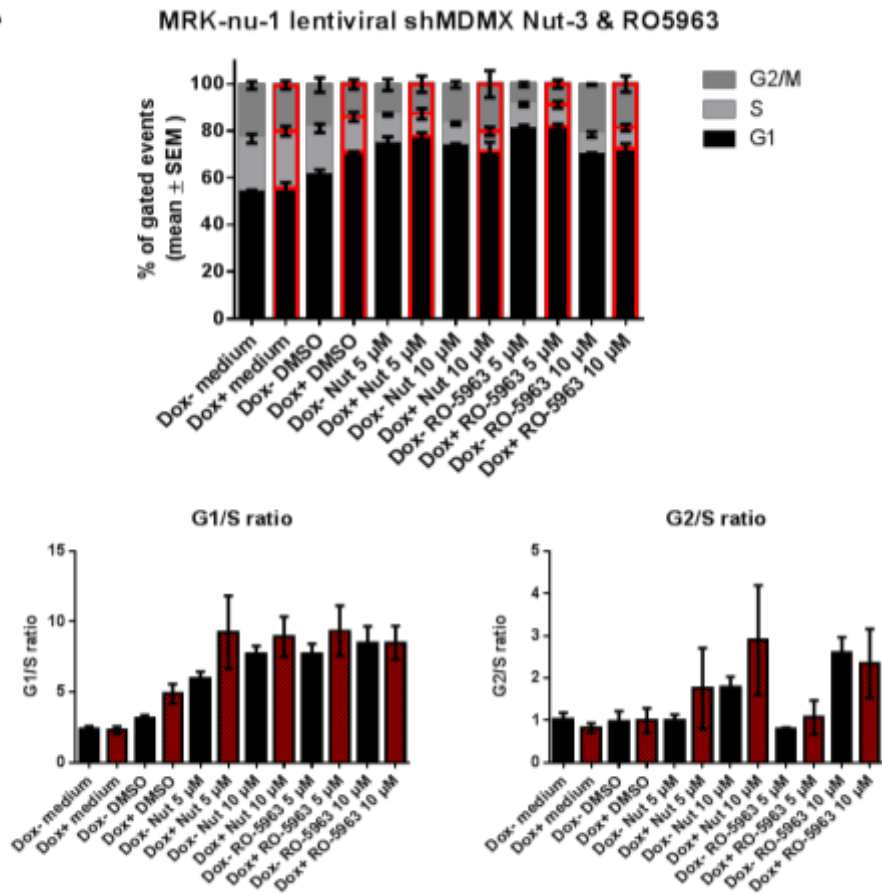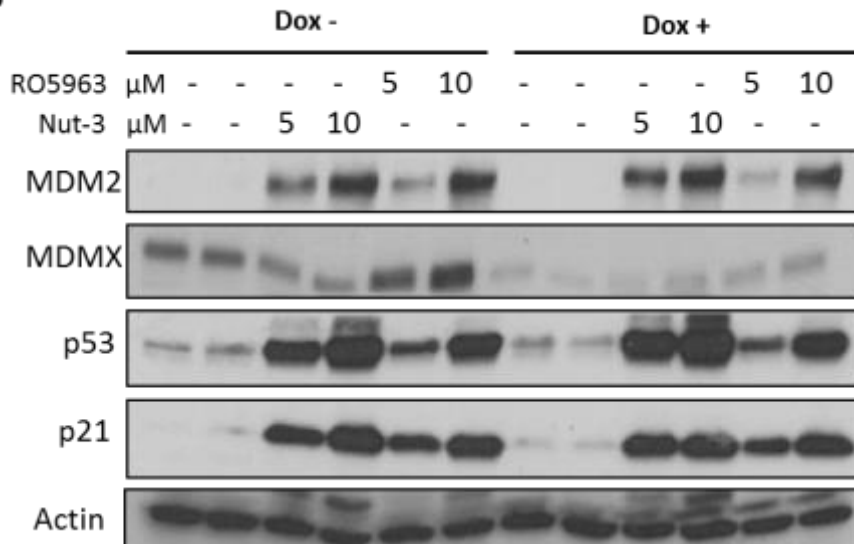
Figure 4.13. The effect of knockdown of MDMX by lentiviral shRNA on cell cycle distribution changes (A) and protein expression (B) in response to Nutlin-3 & RO5963 after 24 hour drug treatments in MRK-nu-1 cells. A two-tailed paired t-test used for comparison of knockdown of MDMX and there was no statistically significant difference after knockdown.
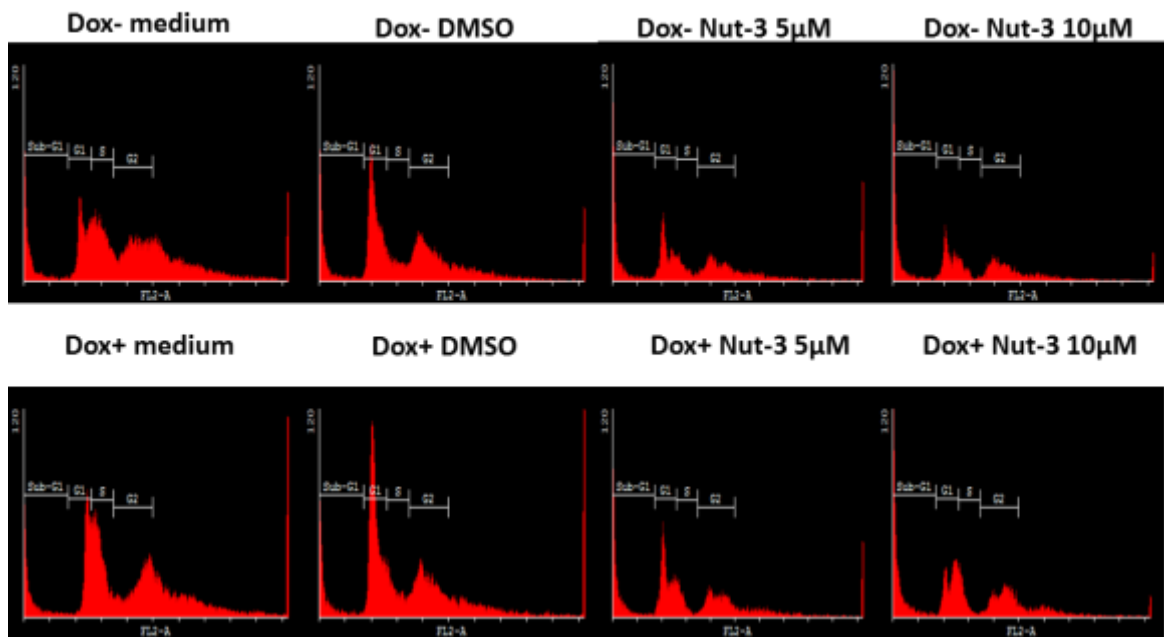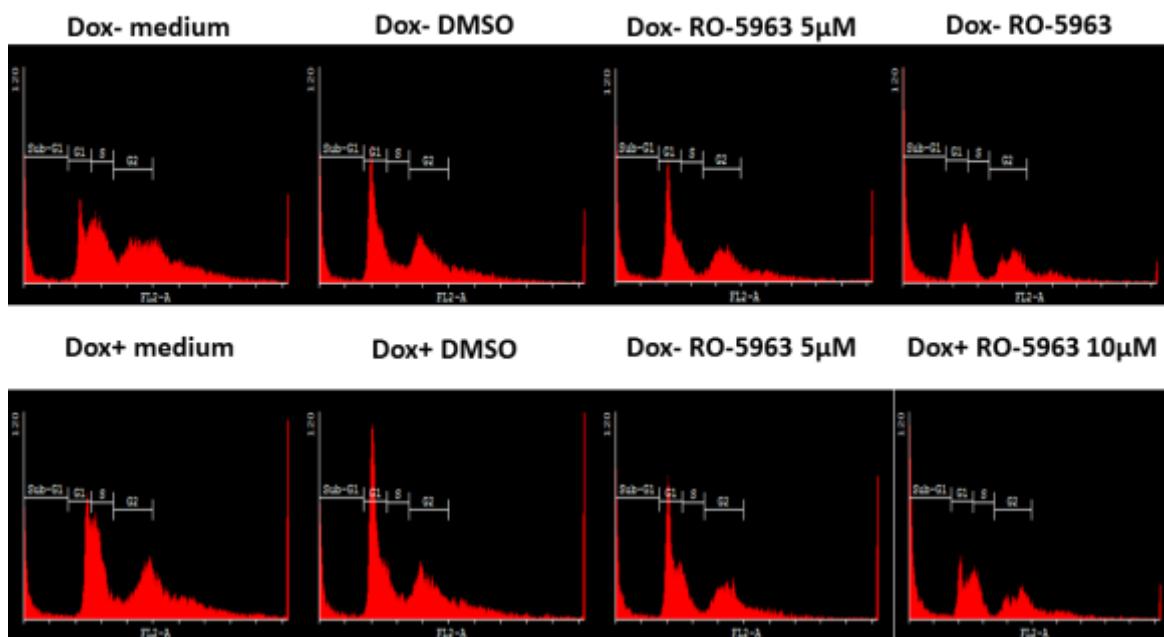
Figure 4.14. FACS analysis of cell cycle distribution after 48 hours Nut-3 & RO5963 treatments in MRK-nu-1 cells with lentiviral shRNA knockdown of MDMX.
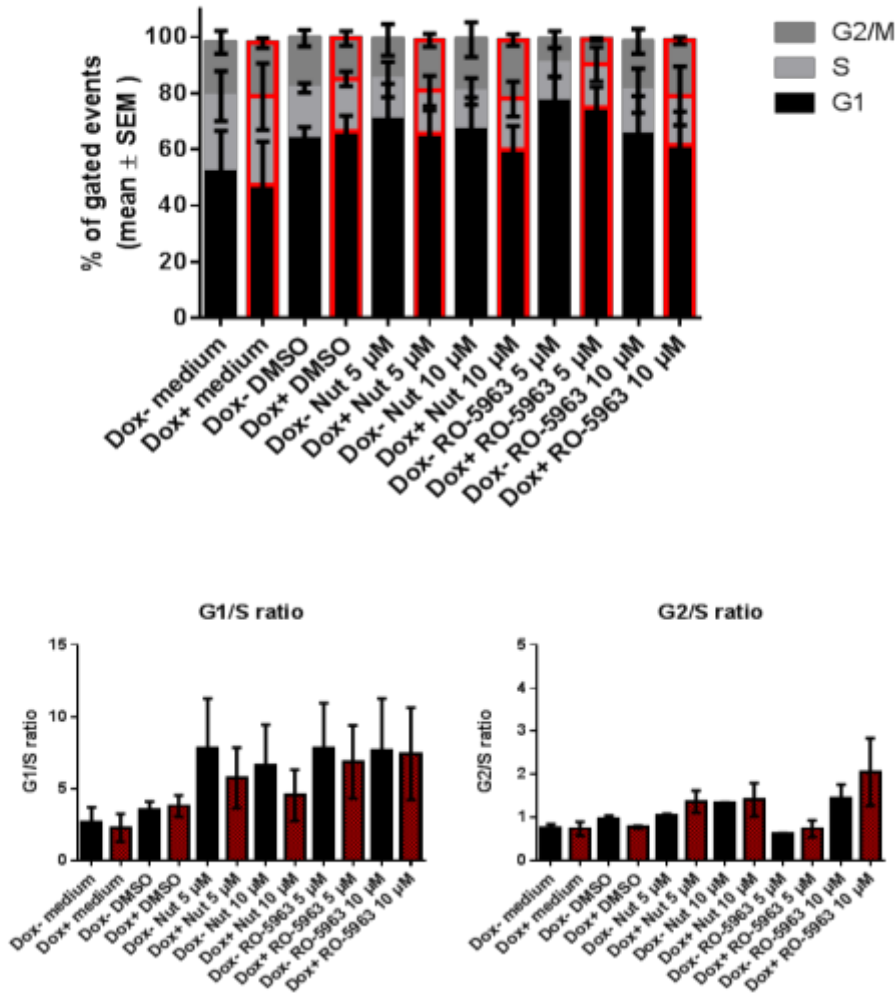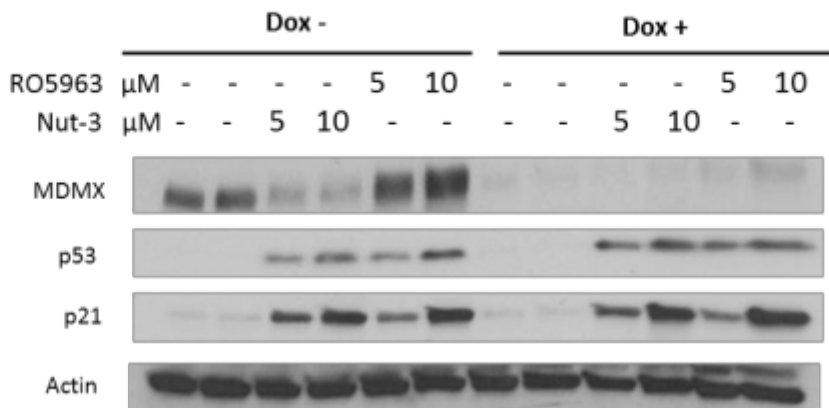
Figure 4.15. The effect of knockdown of MDMX by lentiviral shRNA on cell cycle distribution changes (A) and protein expression (B) in response to Nutlin-3 & RO5963 after 48 hour drug treatments in MRK-nu-1 cells. MDMX shRNA knockdown had no significant effect on the p53 functional response to Nutlin-3.

4.5   Discussion

4.5.1 The effect of suppression of MDMX by lentiviral shRNA on cell proliferation

The MDMX shRNA knockdown in the MRK-nu-1 cell line shows that MDMX expression can be inhibited successfully for approximately a week in MDMX amplified cells without inducing MDM2. However, so far attempts to transduce and knock down MDMX in the JEG-3, NGP and SKNSH cell lines have not been as successful. Both FACS analysis and fluorescence microscopy showed evidence of doxycycline induction of the RFP marker protein. But, there was a lack of MDMX knockdown in JEG-3 NGP and SKNSH cells when the cells were probed with an anti-MDMX antibody in Western blot analysis.

Despite the successful suppression of MDMX in MRK-nu-1 cells they maintained a similar growth rate, even though MDMX expression was reduced over 70% by lentiviral shRNA. Knockdown of MDMX expression by long-term lentiviral shRNA did not reduce cell growth. This result may be explained by the fact that long-term lentiviral shRNA did not completely suppress MDMX expression to the same extent as siRNA (Chapter 5). As mentioned in the literature, decreasing MDMX expression in tumour cells would be expected to result in p53 reactivation leading to cell death as reported for melanoma cells (Gembarska *et al.*, 2012). It is also reported that *MDM2*-null mice embryos die because of apoptosis initiated at 3.5 days postcoitum (dpc), which was shown to be p53-dependent by rescue with *Trp53* knockout. By contrast, Mdm4-null mice embryos died at 7.5–8.5 dpc because of cell proliferation lost and not induction of apoptosis (Chavez-Reyes *et al.*, 2003). The loss of *Trp53* completely rescued the *MDM4* –/– embryonic lethality show it was nevertheless a p53-dependent effect (Parant *et al.*, 2001). This demonstrates that MDMX and Mdm2 have non-redundant functions during embryonal development.

4.5.2 The effect of lentiviral shRNA-mediated knockdown of MDMX on response to MDM2-p53 binding antagonists

MRK-nu-1 cells were more resistant to Nutlin-3 (statistically significant) but more sensitive to RG7388 after suppression of MDMX expression by lentiviral shRNA. MDMX shRNA knockdown had no significant effect on the p53 functional response to

Nutlin-3 and RG7388. These results differ from some published studies (Wade *et al.*, 2006), which reported that shRNA-mediated decrease of MDMX in cancer cells enhanced Nutlin-induced cytotoxicity.

Nutlin-3 and RO5963-induced G1 and G2 arrest in the MDMX amplified cells after 24 hours of treatment. The higher dose of Nutlin-3 and RO5963 increased p53 and p21 expression and showed higher G1 and G2 arrest. This is consistent with previous findings that p21 is able to activate both G1 and G2 arrest in a p53-dependent manner (Hoeferlin *et al.*, 2011; Warfel and El-Deiry, 2013). The p53, MDM2 and p21 protein level responses to Nutln-3 and RG7388 showed no significant change after knockdown of MDMX. In addition, no differences were found in cell cycle distribution between the absence and presence of MDMX expression.

Longer induced lentiviral shRNA knockdown of MDMX in MRK-nu-1 cells caused some measurable resistance to Nutlin-3. A possible explanation for this might be that MDMX expression is variable and reaches a peak at 96 hours (figure 4.10B) & day 4 on (figure 3.2), so the knockdown made the biggest difference at that point.

4.5.3 The effect of lentiviral shRNA-mediated knockdown of MDMX on response to the RO5963 MDM2/X-p53 binding co-antagonist

MRK-nu-1 cells showed a trend to more resistance to the MDM2/X co-inhibitor RO5963 after suppression of MDMX expression by lentiviral shRNA although this narrowly failed to reach statistical significance (p=0.052, figure 4.12). The result further supported previous findings that MDMX expression is associated with sensitivity to RO5963 (Graves *et al.*, 2012). Similarly, reduction of MDMX expression also suppressed p53 stabilization and p53 functional response induction. Knockdown of MDMX increases resistance in MRK-nu-1, indicating that the co-inhibitor has selectivity according to the absence and presence of MDMX expression. This is also consistent with the relative resistance to RO5963 of the SJSA-1 cell line, which does not express MDMX, compared to cell lines which do express high levels of MDMX.

4.5.4 The limitation of shRNA-mediated knockdown

One of the major limitations of the study was that a negative control of lentiviral shRNA transduced cells with control shRNA should be used as a negative control.

Present and absent of doxycycline was unable to distinguish the effect of MDMX depletion. Moreover, the efficiency of knockdown by lentiviral shRNA was only effective with the MRK-nu-1 cell line. The shRNA sequence was designed by the company supplying the lentiviral construct. Ideally, multiple shRNA sequences should be tested to find the best knockdown and they need to be tested for absence of off-target effects. Lentiviral shRNA-mediated knockdown of MDMX was unstable and difficult to suppress MDMX expression in most of cell lines I tested. Therefore, the knockdown system used for subsequent experimentation was a lipofectamine-based siRNA knockdown strategy. Also time limitation was considered. More evidence for the contribution of MDMX is discussed in relation to the siRNA-mediated knockdown of MDMX in a panel of cell lines described in Chapter 5.

Chapter 5 The effect of knockdown of MDMX expression by siRNA on the response to MDM2-p53 binding antagonists & MDMX/2 co-antagonist

5.1 Introduction

Suppression of MDMX expression has been suggested to lead to p53 reactivation in cells, particularly those with *MDMX* amplification or high expression. A previous study reported that transduction of U2OS cells with an MDMX expression construct resulted in resistance to Nutlin-3 induced growth inhibition and p53 down-stream protein response (Hu *et al.*, 2006). Another study reported that siRNA-mediated decrease of MDMX enhanced apoptotic induction and cell cycle arrest by an MDM2 inhibitor in human prostate adenocarcinoma cells (Hu *et al.*, 2006; Wade *et al.*, 2006; Shangary and Wang, 2009). To validate MDMX as a potential drug development target, in chapter 4 and chapter 5, two different knockdown systems were used to suppress MDMX protein expression and the consequences for the response to treatment with MDM2-p53 binding antagonists Nutlin-3 & RG7388 and MDM2/X-p53 binding co-antagonist RO5963 examined. In this chapter, results are presented for siRNA knockdown, which was shown to be a highly efficient system for short-term decrease of MDMX protein expression in a panel of cell lines.

5.2 Hypotheses and aims

Hypotheses:

Suppression of MDMX expression by siRNA is associated with the sensitivity of cells and the response to MDM2-p53 an MDM2/X-p53 binding antagonists for growth inhibition, apoptosis and cell cycle arrest.

Aim:

To test the ability of MDM2-p53 binding inhibitors Nutlin-3, RG7388 and RO5963 to activate p53 in the presence of siRNA-mediated knockdown of MDMX expression.
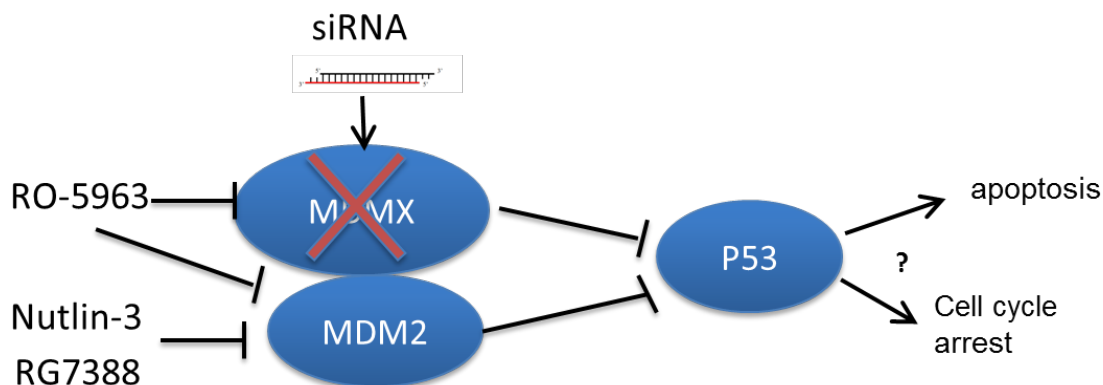
Figure 5.1. The effect of knockdown of MDMX by siRNA on response to MDM2 inhibitors and MDMX/MDM2 co-inhibitor via the p53 pathway

5.3 Specific Materials and Methods

5.3.1 Cell lines

Two *MDMX*-amplified cell lines JEG-3 & MRK-nu-1 and high MDMX-expressing MCF-7 & NGP were used with transfected siRNA to study the effect of knocking down MDMX in a panel of cell lines.

5.3.2 Time point of knockdown

Cells were seeded into 6-well plates with a suitable cell density (shown in table 2.8) in serum free Optimem medium. MDMX siRNA was transfected into target cells by lipofectamine reagent with 20nM final siRNA concentration for 48 hours (detail in chapter 2.9). The best knockdown condition was chosen from the Western blot comparison of different conditions shown in figure 2.5.

5.3.3 Growth curve after knockdown of MDMX by siRNA

Cells were seeded and treated with 20 nM siRNA to suppress MDMX (table 5.1). For adherent cell lines, after 24 hours of treatment, the cells were re-seeded into 96-well plates for SRB-based growth curve analysis and into 6-well plates for protein expression analysis by Western blot. For MRK-nu-1 suspension cells, the cells were counted each day after siRNA knockdown to plot the growth curve by cell numbers.

5.3.4 Growth inhibition by MDM2 antagonists after knockdown of MDMX

Nutlin-3 and RG7388 treatment took place after 48 hours siRNA-mediated knockdown of MDMX. The time points of treatment and XTT assay for growth inhibition of MRK-nu-1 suspension cells after MDMX knockdown followed the time line in figure 5.3A. For the adherent cell lines, the time line of treatment and SRB assay is shown in figure 5.4A.

5.3.5 Protein response to drug treatment after knockdown of MDMX

Treatment with Nutlin-3, RG7388 and RO5963 was carried out after siRNA treatment for 48 hours. The time points of treatment and lysate collection for Western blots followed the time line in figure 5.3B and figure 5.4B.

5.3.6 Clonogenic assay for response to MDMD2 inhibitors after knockdown of MDMX

JEG-3 cells were treated with siRNA for 48 hours to knock down MDMX. The cells were re-seeded into a 6-well plate with 100 cells/well cell density for clonogenic assay. Different doses of Nutlin-3 and RG7388 were added into each well for 48-hour exposure. After that, the medium was replaced with drug-free medium and the cells were incubated to wait for the surviving cells to form colonies for approximately 2 weeks.

5.3.7 FACS analysis of MDMX knocked down cells

MRK-nu-1, JEG-3, NGP and N20R1 cells were seeded and treated with 20nM siRNA to knock down MDMX for 48 hours. Nutlin-3 and RG7388 treatment took place after knocking down MDMX by siRNA for 48 hours. The time points of treatment and FACS analysis for cell cycle distribution change after MDMX knockdown are shown in figure 5.3C and figure 5.4C. The 2D overlapping histograms were analysed using Cyflogic v1.2.1 software.

5.3.8 Caspase 3/7 apoptotic activity in MDMX knocked down cells

MRK-nu-1, JEG-3 and MCF-7 cells were seeded and treated with 20nM siRNA to knock down MDMX for 48 hours. Treatment with Nutlin-3 and RG7388 for 24 hours was carried out after siRNA-mediated knockdown of MDMX. Following 24 hours of drug treatment, the Caspase-Glo® 3/7 Assay (Promega, Southampton, UK) was used to detected caspase 3/7 apoptotic activity in JEG-3 and MRK-nu-1 cells. Details of the protocol were presented in chapter 2.13.

	Sequence (5' -> 3')RNA(tt)DNA
MDM4 (MDMX)	
Sense	GCAGUUAGGUGUUGGAAUA
Antisense	UAUUCCAACACCUAACUGC
UCR	Universal negative control
Sense	GCGCGCUUUGUAGGAUUCG
Antisense	CGAAUCCUACAAAGCGCGC

Table 5.1. Sequence of siRNA and negative control.

Where does MDMX siRNA bind to ?
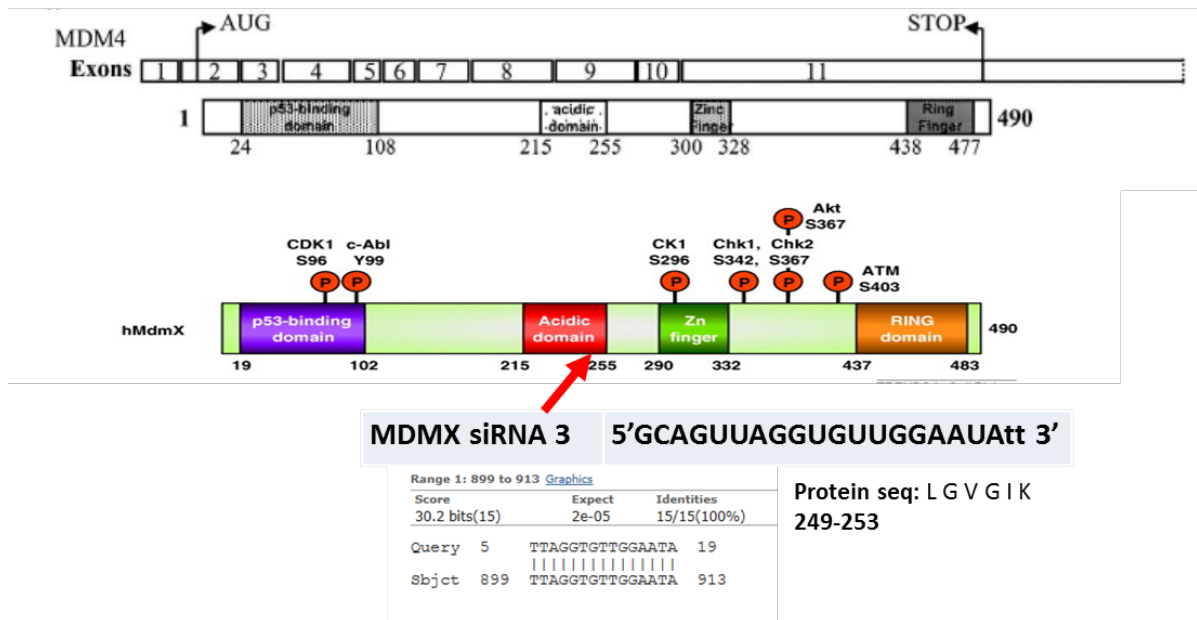
Figure 5.2. The siRNA mRNA target site in relation to the coding region for the MDMX protein (Mancini *et al.*, 2009; Wade *et al.*, 2010).
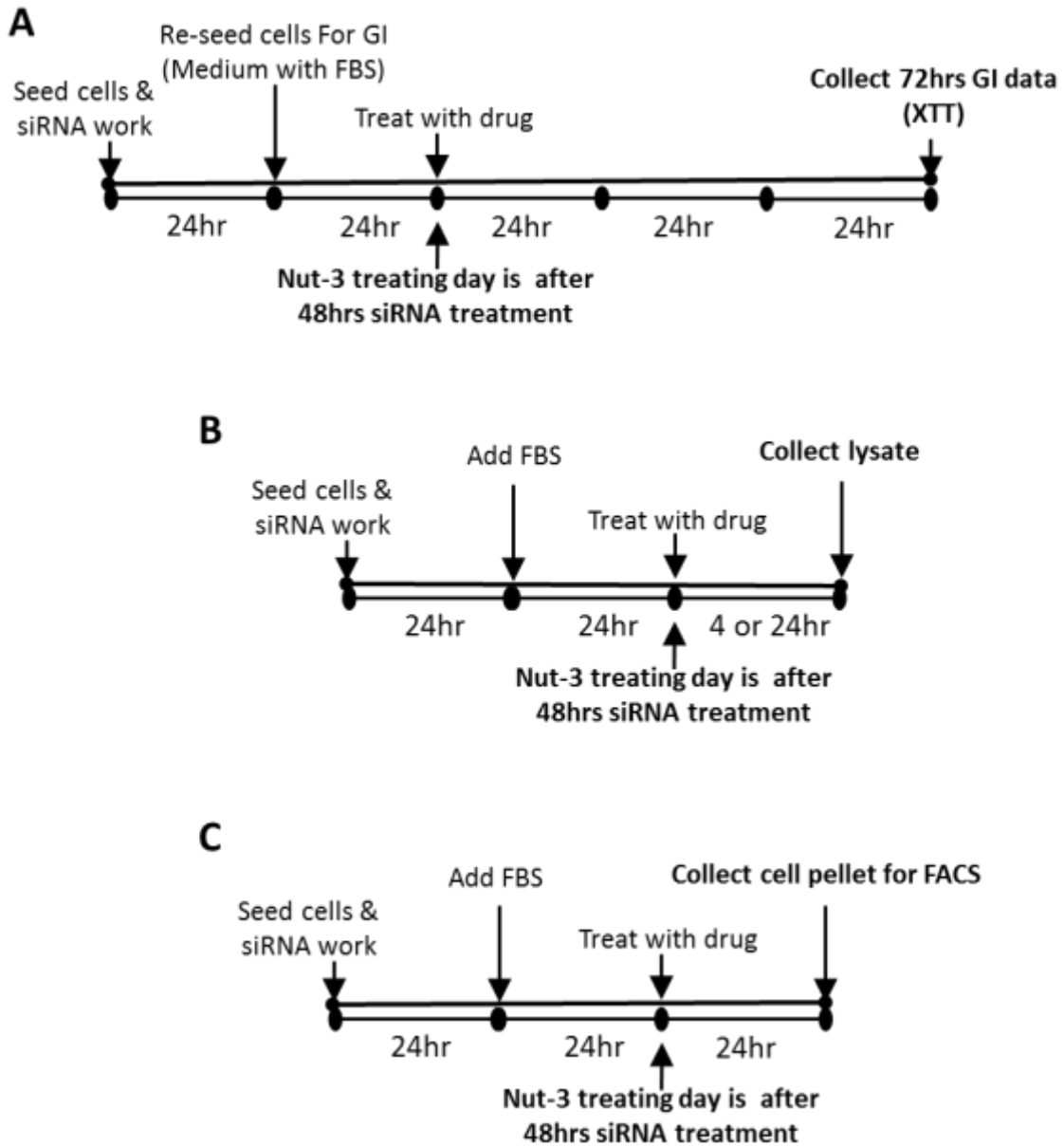
Figure 5.3. Time lines of siRNA-mediated knockdown of MDMX in MRK-nu-1 suspension cells following drug treatment for (A) growth inhibition, (B) protein response and (C) FACS analysis.
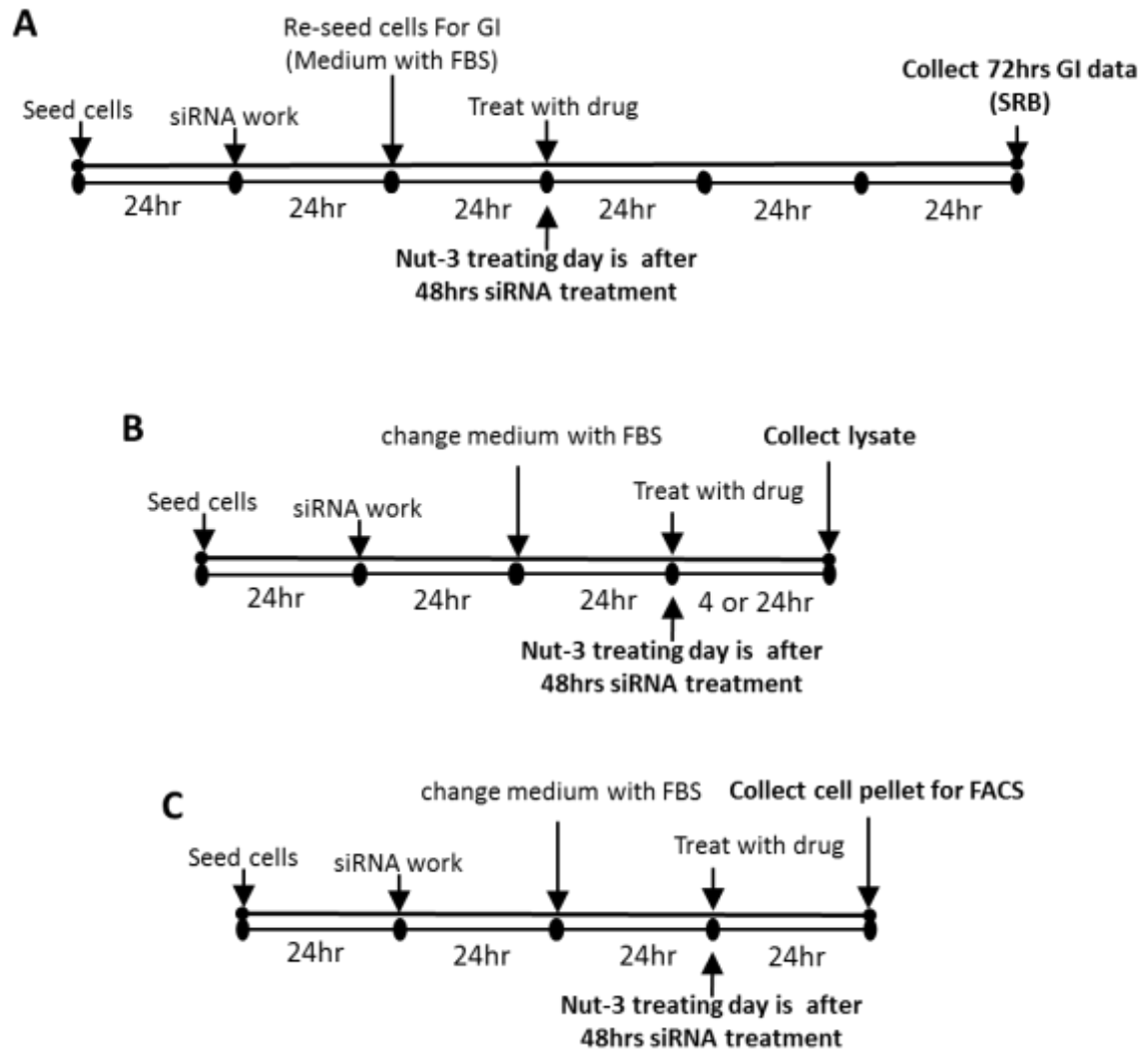
Figure 5.4. Time lines of siRNA-mediated knockdown of MDMX in adherent cells following drug treatment for (A) growth inhibition, (B) protein response and (C) FACS analysis

5.4 Results

5.4.1 *The siRNA-mediated knockdown of MDMX slowed the growth rate of cells*

The growth curves in figure 5.5 show that the siUCR and siMDMX treated cells grew more slowly compared to untreated cells. The knockdown of MDMX in JEG-3 cells slowed down their cell growth rate compared to siUCR (universal negative control siRNA; however, for the MRK-nu-1 cells there was no difference between the siUCR and siMDMX treated cells). The western blots showed that MDMX was efficiently knocked down by the MDMX siRNA in both cell lines and resulted in p53 stabilisation and the increase of p21 expression in both cell lines after knockdown of MDMX by siRNA. Since p21 was not induced by the siUCR, the growth inhibition seen with this negative control must have been via a p21-independent mechanism.

Figure 5.6 shows the growth curves after knockdown of MDMX in three cell lines with normal *MDMX* gene copy number and positive for MDMX expression. All three cell lines, NGP, N20R1 and MCF-7, grew more slowly after knockdown of MDMX expression by siRNA. Interestingly, the growth inhibition associated with MDMX knockdown in the NGP (*TP53* WT) and N20R1 (*TP53* Mut) otherwise isogenic cell line pair was independent of *TP53* status. This was the case despite the clear induction of p21 by MDMX knockdown in the NGP cell line and relative lack of p21 expression in the N20R1 cells, as typical for *TP53* mutant cell lines. This suggests that the growth suppression seen on MDMX knockdown in the N20R1 cells is through a p21-independent mechanism.
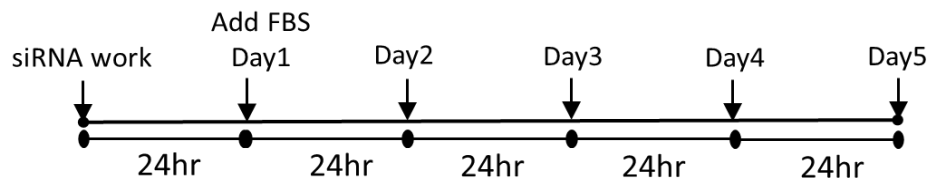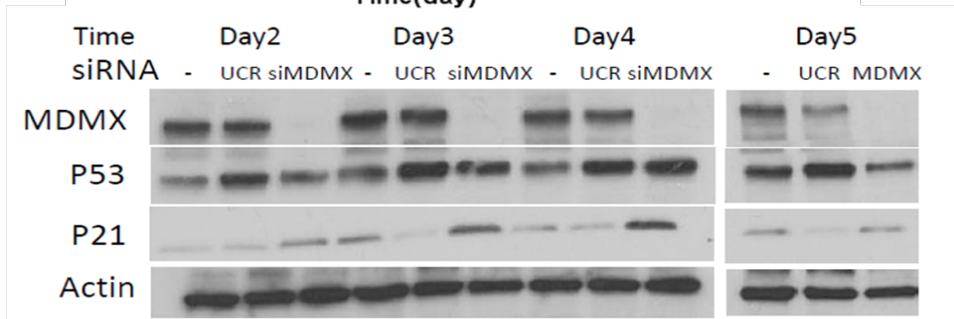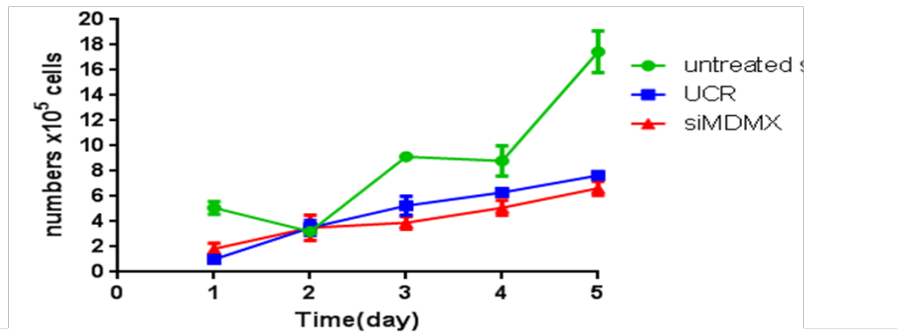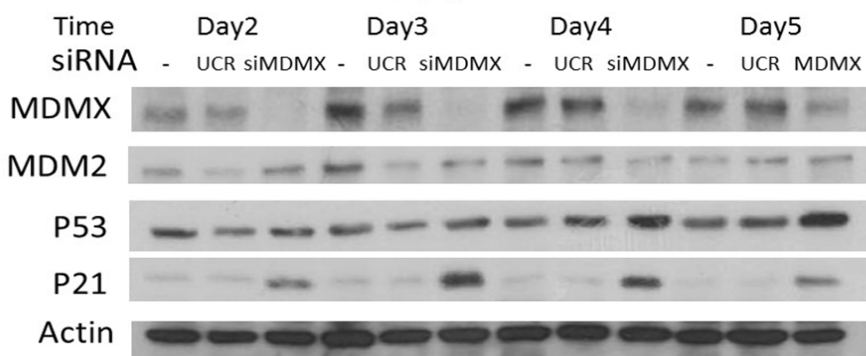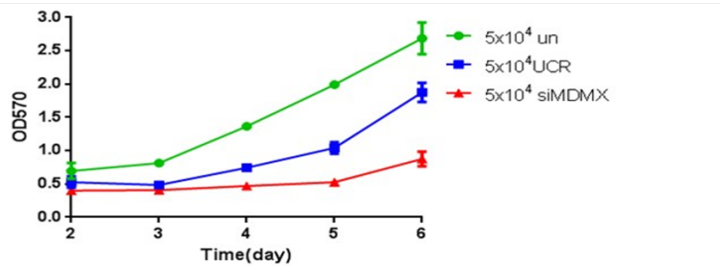
Figure 5.5. Growth curve and MDMX protein expression of MRK-nu-1(A) and JEG-3 (B) with siRNA knockdown of MDMX after 24 (Day 1)-120 hours (Day 5). UCR (universal control siRNA) was used as negative control.
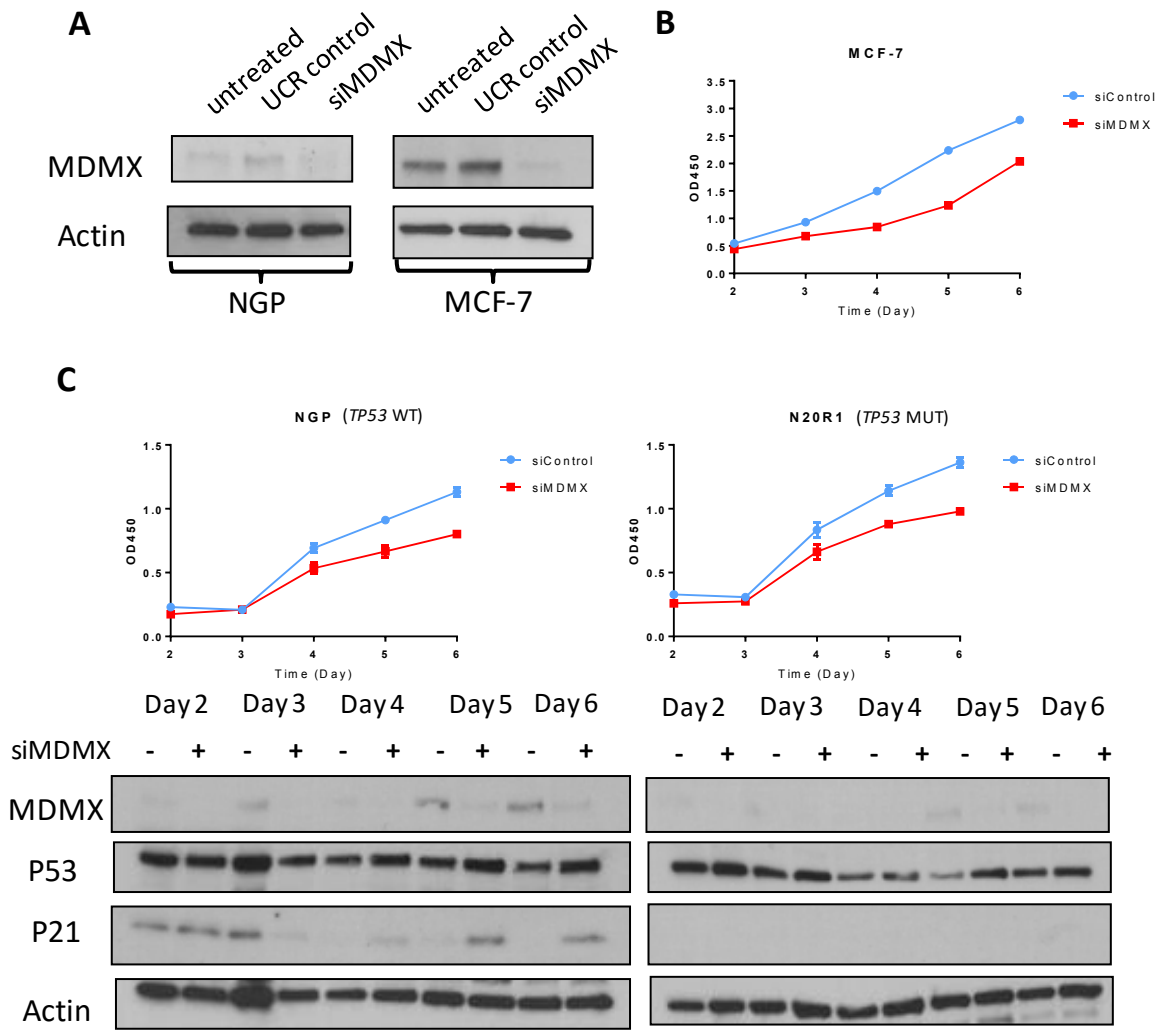
Figure 5.6. (A) MDMX protein expression in NGP and MCF-7 cells with 48-hour siRNA knockdown of MDMX. (B) Growth curve of MCF-7 after siRNA knockdown of MDMX from 48 hours (day 2) to 144 hours (day 6). (C) Growth curve of NGP (*TP53* WT) & N20R1 (*TP53* Mut) cell line pair after siRNA knockdown of MDMX from 48 hours (day 2) to 144 hours (day 6). UCR (universal scrambled control siRNA) was used as negative control.

5.4.2 The siRNA knockdown of MDMX did not affect the time-dependent response to Nutlin-3 in JEG-3 cells

JEG-3 cells were treated with 20 nM siRNA to supress MDMX expression for 48 hours. Then the cells were treated with 0.65 μM Nutlin-3 from 2 hours to 24 hours as shown in figure 5.7A. The Western blot result showed p53 expression increased rapidly by 2 and 4 hours treatment. The dose of Nultin-3 used was a dilution mistake; however, surprisingly the protein levels showed a better time-dependent increase in p53, MDM2 and p21. MDM2 reached a peak after approximately 8 hours of treatment. Levels of p21 protein increased by 4-6 hours of Nutlin-3 treatment. MDMX siRNA knockdown strongly enhanced the levels of p21 following induction by Nutlin-3, but had a relatively small effect on p53 stabilisation and MDM2 induction in the JEG-3 cells. This reflects the effect of MDMX siRNA knockdown alone on p21 expression seen in the minus Nutlin-3 control track in figure 5.7A and the time course following siRNA knockdown alone in figure 5.5B, indicating that MDMX has an important role in the regulation of p21 expression.

The Western blot results in figure 5.7B show the results of 4 hours of 5μM Nutlin-3 treatment in JEG-1 and MRk-nu-1 with siRNA-mediated knockdown of MDMX. The protein level of p21 increased after knockdown of MDMX in both JEG-3 and MRK-nu-1 cells. The p53 stabilization and MDM2 induction by Nutlin-3 modestly increased after knockdown of MDMX in MRK-nu-1 cells but not JEG-3 cells. However, in both cell lines the increase in p21 was enhanced by siRNA knockdown of MDMX.
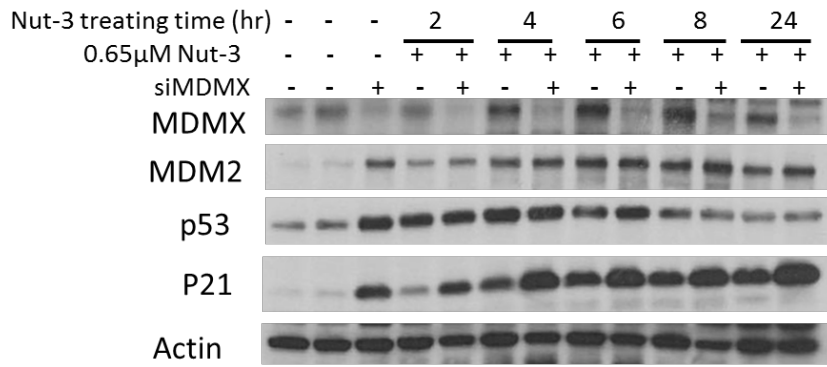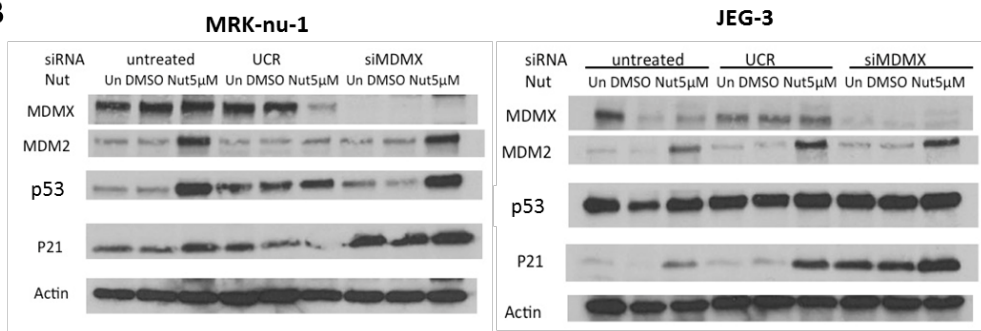
Figure 5.7. (A) Time dependence of Nutlin-3 response for JEG-3 cells with MDMX knockdown by siRNA (B) MDM2, p53 and p21 protein levels in MRK-nu-1 and JEG-3 cells after 4 hours Nutlin-3 treatment with siRNA MDMX knockdown

5.4.3 Day 0 subtraction of growth inhibition in MRK-nu-1 & JEG-3

Figure 5.8 shows the effect of siRNA-mediated knockdown of MDMX on growth inhibition by Nutlin-3 in MRK-nu-1 and JEG-3 cells in two different ways. One is the growth inhibition curve, normalized to DMSO control, which indicates cell growth inhibition by the drug. The other is a day 0 subtraction curve. The day 0 optical density values were subtracted from the values of the 72 hour treatment plates and the data was normalized to DMSO control. The day 0 subtraction growth inhibition curve shows whether the cell number is lower than at the start of treatment and if below 0 shows the drug is cytotoxic and not just growth inhibitory.

The GI_{50} values were affected by subtraction of day 0 optical densities. The GI_{50} values for Nutlin-3 in JEG-3 (28.9 µM) decreased by around half after day 0 subtraction (14.3 µM) while the GI_{50} values in MRK-nu-1 (16.2 µM) decreased more than 3-fold after day 0 subtraction (5.0 µM), dependent on cell growth. Knockdown of MDMX expression by siRNA decreased the GI_{50} values of Nutlin-3 for *MDMX*-amplified JEG-3 cells by half compared to the negative siRNA control on both with and without subtraction of day 0 optical densities. The GI_{50} values of Nutlin-3 without day 0 subtraction in the siRNA control and after knockdown of MDMX were 26.5 µM and 12.0 µM respectively. The GI_{50} values for Nutlin-3 in MRK-nu-1 also decreased from 16.4 µM to 10.7 µM after knockdown of MDMX by siRNA (figure 5.8).

GI$_{50}$ of Nut-3 (µM) (n=1)	MRK-nu-1	- Day0	JEG-3	- Day0
Optimem (medium)	16.2	5.0	28.9	14.3
UCR control (siControl)	16.4	3.7	26.5	12.3
siMDMX	10.7	2.3	12.0	5.7
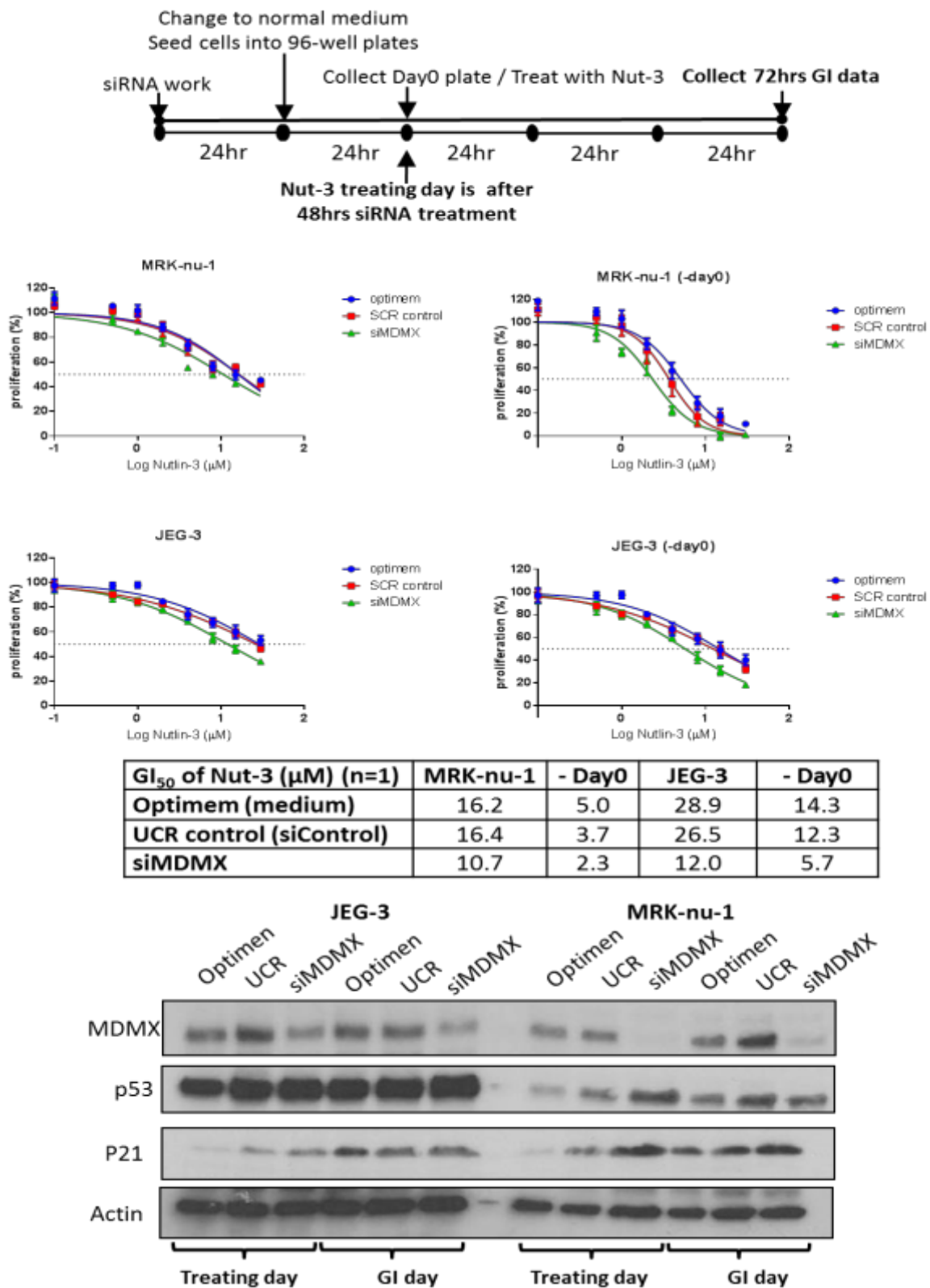
Figure 5.8. The relative growth inhibitory effect of Nutlin-3 on MRk-nu-1 and JEG-3 cells after siRNA knockdown of MDMX, plotted and GI$_{50}$ calculated with and without day 0 subtraction. Western blot results confirming siRNA knockdown of MDMX expression.

5.4.4 The siRNA-mediated knockdown of MDMX sensitized JEG-3 cell response to Nutlin-3 and RG7388

Knockdown of MDMX expression by siRNA decreased the GI_{50} values of Nutlin-3 and RG7388 for *MDMX*-amplified JEG-3 cells by half compared to the negative siRNA control. The GI_{50} values of Nutlin-3 in the siRNA control and after knockdown of MDMX were 12.7 ± 1.3 μM and 4.6 ± 0.8 μM respectively, and the difference was statistically significant (p=0.002). The GI_{50} values of RG7388 in siRNA control and after knockdown of MDMX were 2.03 ± 0.70 μM and 1.05 ± 0.79 μM respectively, showing a trend towards increased sensitivity on MDMX knockdown, although the difference was not statistically significant (p=0.10) (figure 5.9 and figure 5.10).

The effect of knockdown of MDMX with MRK-nu-1 cells on the growth inhibition response to Nutlin-3 and RG7388 varied. MRK-nu-1 cells showed a trend towards increased sensitivity to Nutlin-3, with the 3.6 ± 0.5 μM GI_{50} value after knockdown of MDMX compared to the negative siRNA control with 5.9 ± 1.0 μM GI_{50}, although the difference was not statistically significant (p=0.054). The GI_{50} values of RG7388 were not significantly different after siRNA-mediated knockdown of MDMX in MRK-nu-1 cells. The growth inhibitory effect of Nutlin-3 remained the same in MCF-7 cells after suppression of MDMX expression.

5.4.5 The siRNA-mediated knockdown of MDMX sensitized JEG-3 cells to Nutlin-3 and RG7388 treatment measured by clonogenic assay

The clonogenic cell survival results presented in figure 5.11 show that 48 hour siRNA-mediated knockdown of MDMX increased sensitivity to Nutlin-3 and RG7388 for 48 hour drug treatment. The LC_{50} values of Nutlin-3 and RG7388 of 23.6 ± 2.4 μM and > 3 μM respectively in the control siRNA group were reduced by half to 10.2 ± 5.2 μM and 1.2 ± 0.5 μM respectively in the MDMX knocked down group.
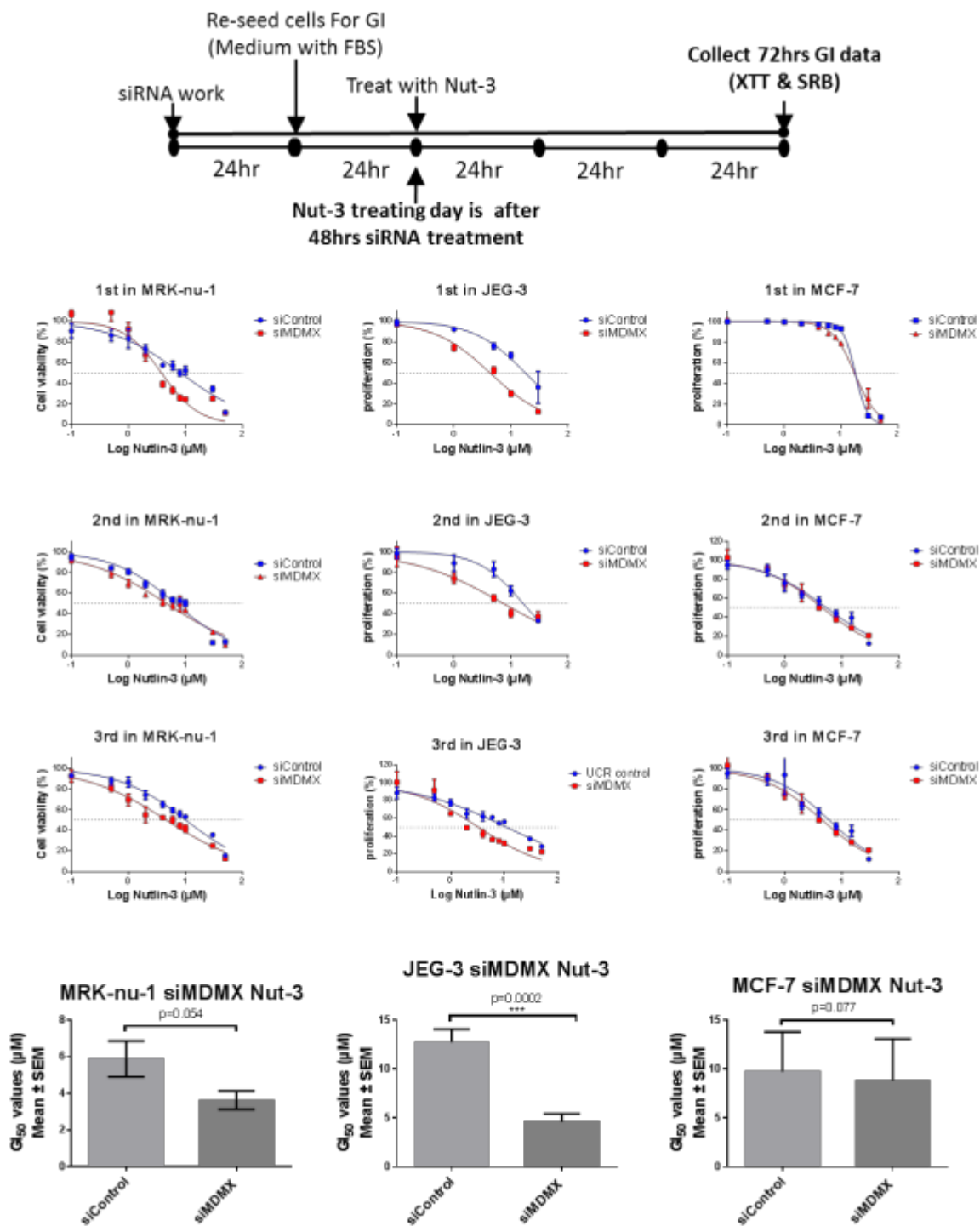
Figure 5.9. The effect of siRNA knockdown of MDMX on GI$_{50}$ values of Nutlin-3 in MRK-nu-1, JEG-3 and MCF-7 cells. The average of GI$_{50}$ values for 72 hour growth inhibition treatment after knockdown of MDMX by siRNA for 48hours. (Av.GI$_{50}$ values in MRK-nu-1: siControl 5.9 ± 1.0 µM & siMDMX 3.6 ± 0.5 µM, n=4; Av. GI$_{50}$ value JEG-3 siControl 12.7 ± 1.3 µM siMDMX 4.6 ± 0.8 µM, n=7; Av. GI$_{50}$ value MCF-7 siControl 9.7 ± 1.0 µM siMDMX 8.8 ± 4.2 µM, n=3). The p-values shown are for paired t-tests.
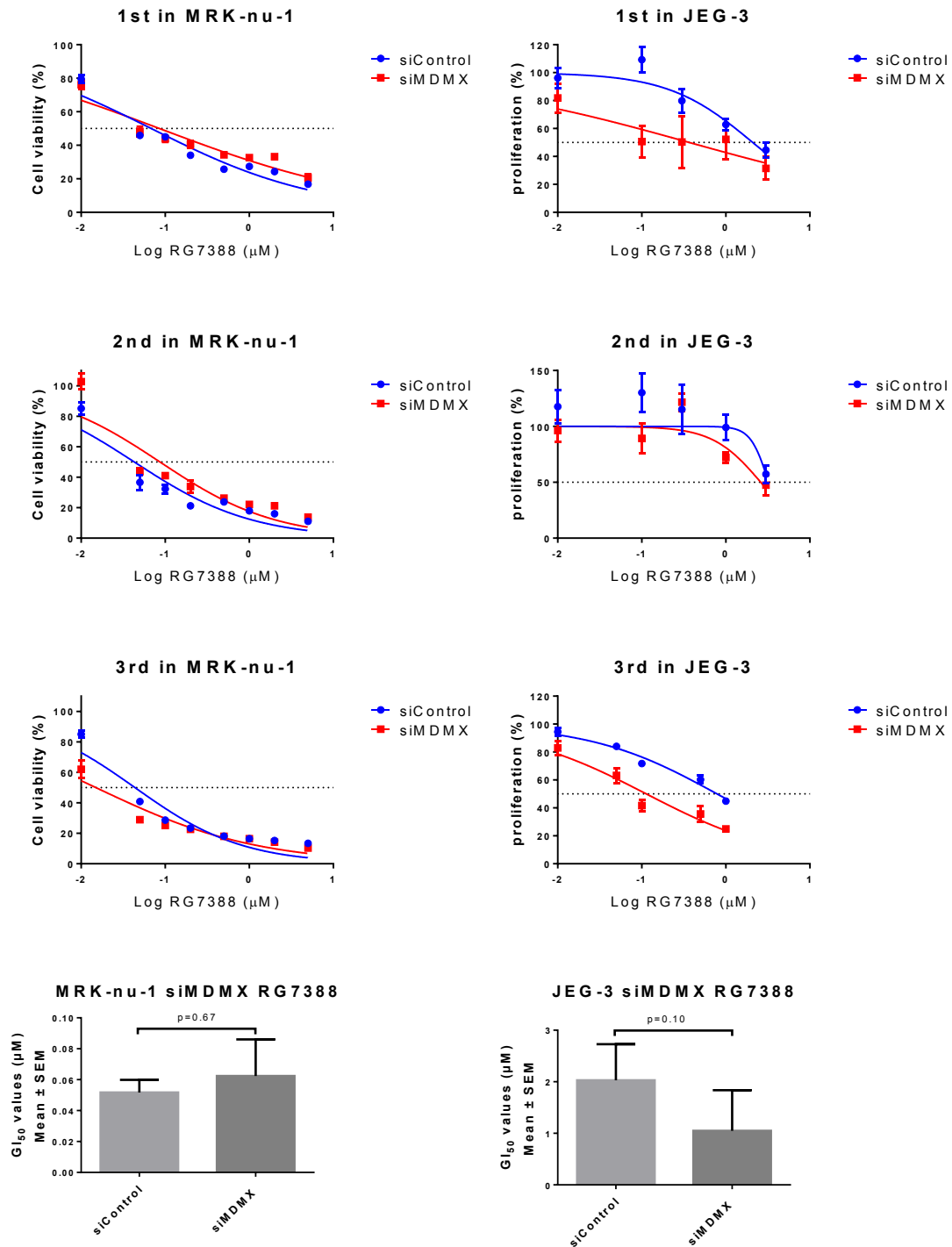
Figure 5.10. The effect of siRNA knockdown of MDMX on GI$_{50}$ values of RG7388 in MRK-nu-1 and JEG-3 cells. The average of GI$_{50}$ values from 72 hour growth inhibition treatment after knockdown of MDMX by siRNA for 48hours. (Av. GI$_{50}$ value MRK-nu-1 siControl 0.052± 0.008 µM siMDMX 0.062 ± 0.023 µM, n=3; Av. GI$_{50}$ value JEG-3 siControl 2.03 ± 0.70 µM siMDMX 1.05 ± 0.79 µM; n=3). The p-values shown are for paired t-tests.

151

LC$_{50}$ value (n=3)	siControl	siMDMX	2-way ANOVA paired t-test
Nut-3	23.6 ± 2.4 μM	10.2 ±5.2 μM	Not significant P=0.72
RG7388	> 3 μM	1.2 ± 0.5 μM	significant P=0.0002
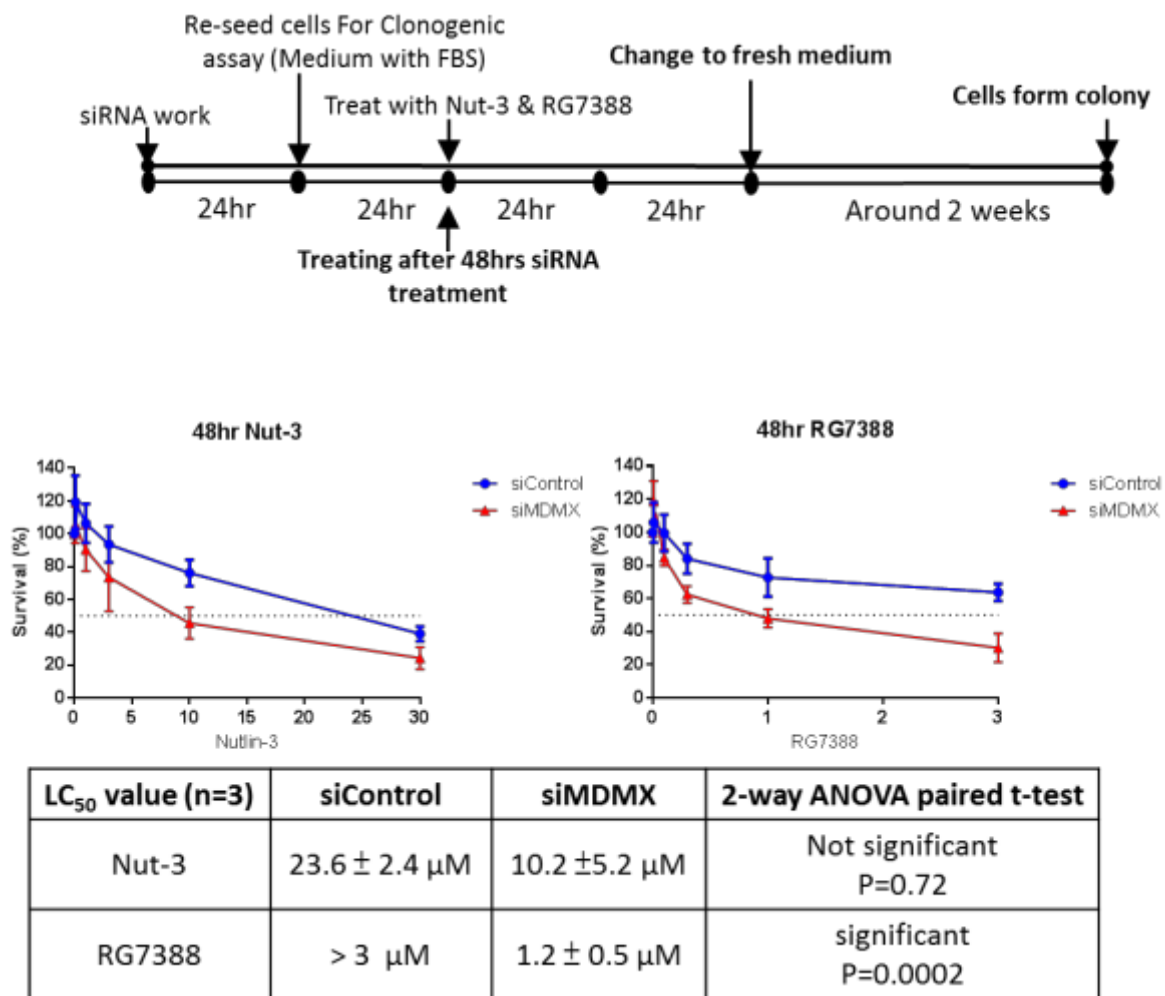
Figure 5.11. The effect of 48 hour siRNA knockdown of MDMX on the clonogenic cell survival of JEG-3 cells following treatment with Nutlin-3 and RG7388 for 48 hours. The average LC$_{50}$ values for clonogenic cell survival were measured for n=3 repeat experiments (Means ± SEM).

5.4.6 The siRNA-mediated knockdown of MDMX decreased the protein responses to RO5963 but not Nutlin-3 or RG7388

Figure 5.12A shows the immunoblots of the protein response to 5 µM Nutlin-3 and 1 µM RG7388 in JEG-3 and MRKn-1 cells for 4 and 24 hour drug exposure after siRNA-mediated knockdown of MDMX. The inductions of MDM2 and p21 by activated p53 were higher for 24 hour drug exposure. After knockdown of MDMX by siRNA, p53 stabilization and MDM2 induction increased to some extent in these two *MDMX*-amplified cell lines, depending on the time point, the drug and which cell line. The p21 protein expression showed the largest increases after knockdown of MDMX by siRNA, particularly in the JEG3 cells and enhanced the effect of MDM2 inhibitor treatment.

The Western blot in figure 5.12B shows the protein expression response to 4 hours treatment with Nutlin-3, RG7388 and RO5963 in MCF-7 cells in the presence and absence of MDMX expression knockdown. RO5963 stabilized p53 and then induced phosphorylated p53^{ser15}, MDM2, p21 and BAX expression. However, knockdown of MDMX reduced p53 stabilization and phosphorylated p53^{ser15} by the MDM2/X co-inhibitor RO5963, despite a small decrease in WIP1 expression after knockdown of MDMX, which would tend to increase p53^{ser15} phosphorylation.

Similarly to JEG-3 and MRK-nu-1 cells, knockdown of MDMX expression in MCF7 cells did not affect p53 stabilization by Nutlin-3 and RG7388, although MDM2 protein levels increased after MDMX knockdown. The protein level of p21 in control and MDM2 inhibitor treated cells increased markedly after knockdown of MDMX in JEG-3, MRK-nu-1 and MCF-7 cells. BAX also increased after knockdown of MDMX in MCF-7 cells. However, the inductions of phosphorylated p53^{ser15} by Nutlin-3, RG7388 and RO5963 were decreased after knockdown of MDMX in MCF-7 cells.
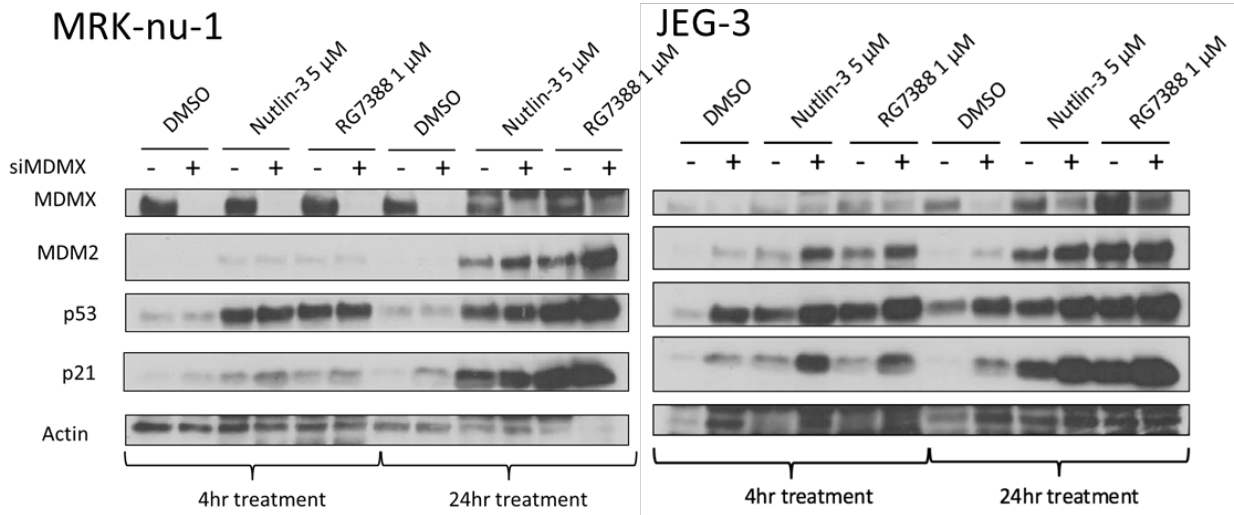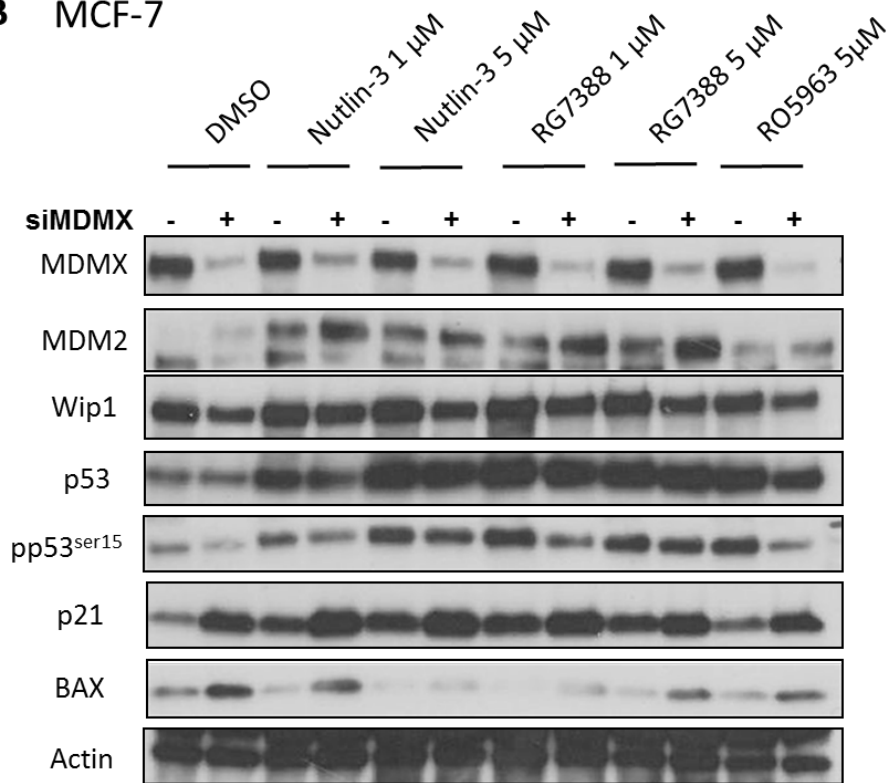
Figure 5.12. (A). The effect of MDMX knockdown on p53, MDM2 and p21 response to Nutlin-3 and RG7388 in MDMX amplified JEG-3 and MRK-nu-1 cells. (B) MCF-7 cell response to 4 hours Nutlin-3, RG7388 and RO5963 exposure after 48 hours siRNA-mediated MDMX knockdown.

5.4.7 The effect of MDMX siRNA knockdown on Nutlin-3 and RG7388-induced G1 & G2 arrest

The overlapping histograms in figure 5.13 show the effect of MDMX siRNA knockdown on the cell cycle distribution for DMSO control and Nut-3 or RG7388 after 24 hours treatment with the MDM2 inhibitors, for the *MDMX*-amplified JEG-3 and MDMX high expression MCF-7 cells. The siRNA knockdown of MDMX expression did not affect the cell cycle distribution in JEG-3 and MCF-7 cells in the DMSO treated control cells. However, knockdown of MDMX decreased the population of cells in S phase in JEG-3 and MCF-7 cells after 24 hours of Nutlin-3 treatment. The siRNA knockdown of MDMX had little effect on the cell cycle distribution of JEG-3 cells following treatment with 1µM RG7388. However, for the MCF-7 cells 1µM RG7388 treatment for 24 hours resulted in an accumulation of cells in S-phase, which appeared to be abrogated by the MDMX knockdown.

The bar chats of cell cycle distributions in figure 5.14 showed G1 & G2 arrest by 24 hour Nutlin-3 and RG7388 treatments in JEG-3, MRK-nu-1 and NGP cells. The G1 & G2 arrest by MDM2 inhibitors showed a slight increase trend in JEG-3 cells after knockdown of MDMX (figure 5.14B). The induction of G2/S ratio by Nutlin-3 and RG7388 showed a modest increase trend in MRK-nu-1 cells after knockdown of MDMX. JEG-3 cells showed a better response to MDM2 inhibitors after siRNA mediated knockdown of MDMX in growth inhibition, G1&G2 arrest and p53 downstream activated protein response.

5.4.8 Knockdown of MDMX in NGP cells decreased the response to Nutlin-3 and RG-7388 for cell cycle change and caspase 3/7 apoptotic activity

Knockdown of MDMX in NGP cells (with MDM2 amplification and high MDMX expression) increased the GI_{50} values of Nutlin-3 for 72 hour drug exposure (figure 5.15C). Figure 5.14C shows that G1 and G2 cell cycle arrest was induced by MDM2 antagonists in NGP cells. Knockdown of MDMX by siRNA in NGP cells reduced the induction of G1 and G2 arrest by both MDM2 inhibitors (figure 5.14C). The induction of G1 and G2 arrest by MDM2 inhibitors was not seen in *TP53* mutant N20R1 cells.

Figure 5.15 shows caspase 3/7 apoptotic activity after 24 hour Nutlin-3 and RG7388 in MRK-nu-1, JEG-3, NGP and N20R1 cells. A dose dependent increase in Caspase 3/7 activity after 24 hours Nutlin-3 and RG7388 treatments was seen in NGP cells, while N20R1 (with mutant p53) did not respond to Nutlin-3 and RG7388 (figure 5.15A & B). Following knockdown of MDMX, the increase of caspase activity was reduced for high doses of both Nutlin-3 and RG7388 in NGP cells. The results were consistent with the increase in resistance to Nutlin-3 and RG7388 after knockdown of MDMX for both growth inhibition and cell cycle arrest response to MDM2 inhibitors. The two MDMX amplified cell lines JEG-3 and MRK-nu-1 have no caspase 3/7 activity (figure 5A & B).

Caspase 3/7 apoptotic activity remained at a very low level after treatment with different doses of Nutlin-3 and RG7388 for 24 hours in JEG-3 and MRK-nu-1 cells with both siUCR and siMDMX. These two *MDMX(MDM4)*-amplified cells have very low detectable caspase apoptotic activity (figure 5.15A & B). In support of this, JEG-3 and MRK-nu-1 did not show cleaved caspase expression in immunoblots (data not shown). However, the findings of the current study do not support previously reported research. A previous study reported that MDMX enhances the p53-mediated intrinsic-apoptotic pathway when MDMX localizes at the mitochondria (Rallapalli *et al*., 2003). MDMX was suggested to bind BCL-2, facilitate phosphorylated p53[Ser46] and release cytochrome C for apoptosis (Rallapalli *et al*., 2003). In the current study, the results for growth inhibition by Nutlin-3 and RG7388 with JEG-3 and MRK-nu-1, the cytotoxic effect might not be caused by caspase3/7 dependent apoptosis and more likely reflects growth arrest and/or induction of senescence by Nutlin-3 and RG7388.
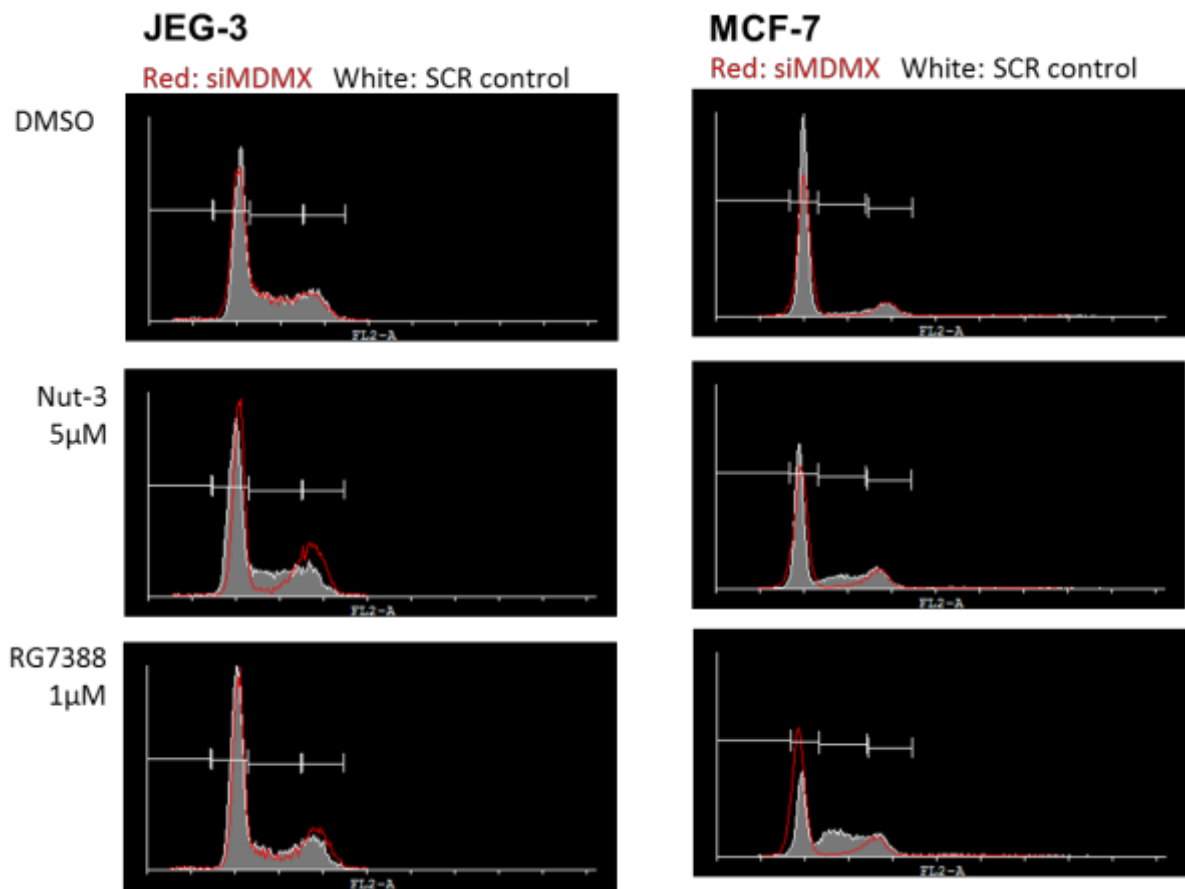
Figure 5.13. The effect of siRNA-mediated knockdown of MDMX on cell cycle distribution change with 24-hour 5µM Nutlin-3 and 1µM RG7388 treatment in JEG-3 and MCF-7 cells (n=1). Red: siMDMX; White: SCR control.
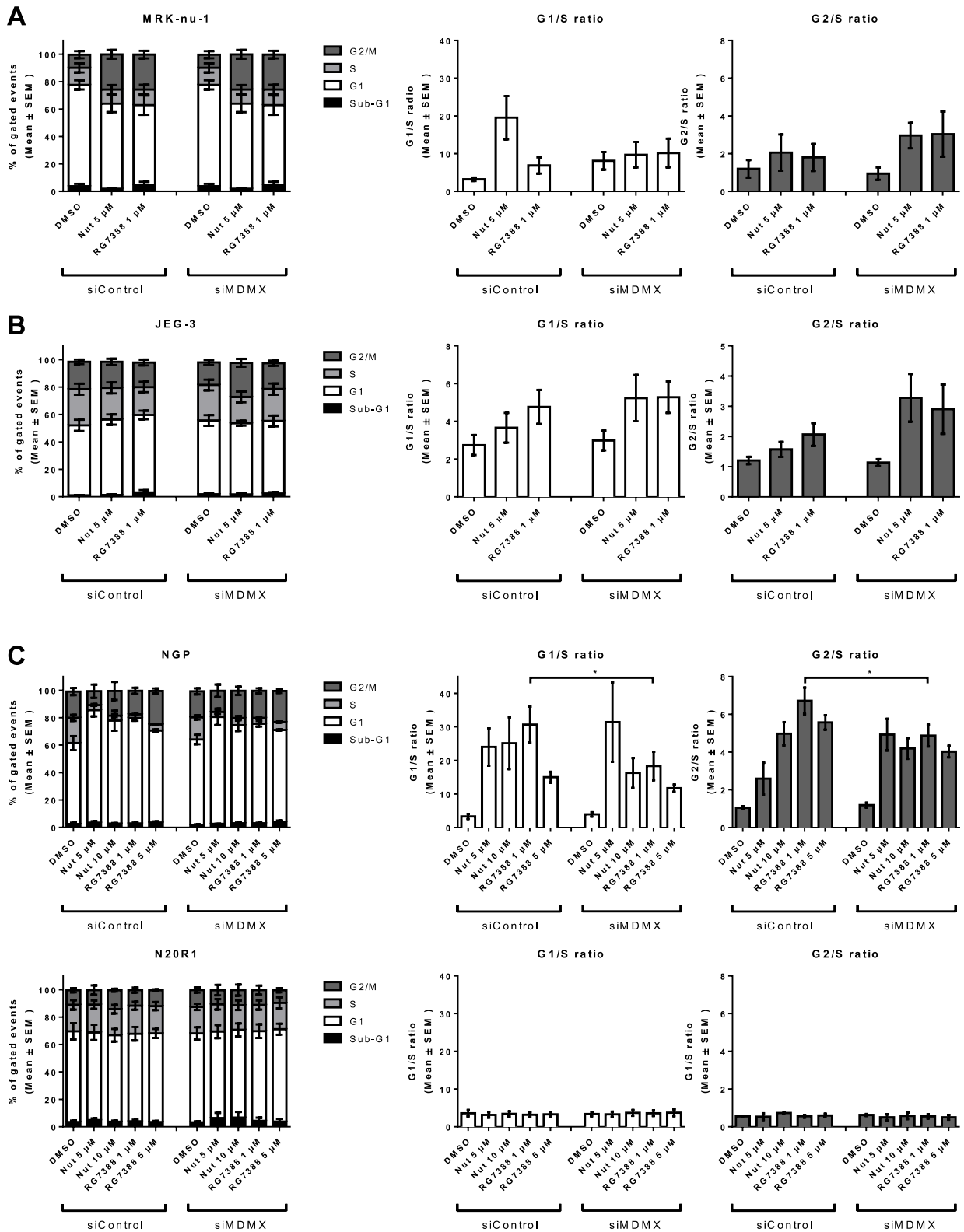
Figure 5.14. Knockdown of MDMX increased the Nutlin-3 and RG7388 induced G1 and G2 arrest in JEG-3 cells but decreased G1 and G2 arrest in NGP cells. The effect of MDMX knockdown on cell cycle distribution changes in response to Nutlin-3 & RG7388 after 24 hours drug treatments in MRK-nu-1(A), JEG-3(B), NGP and N20R1 (C) cells measured by flow cytometry. The cells were treated by siRNA for 48 hours and then treated with Nutlin-3 RG7388. Two-tail t test was used for comparison of MDMX knockdown effect.
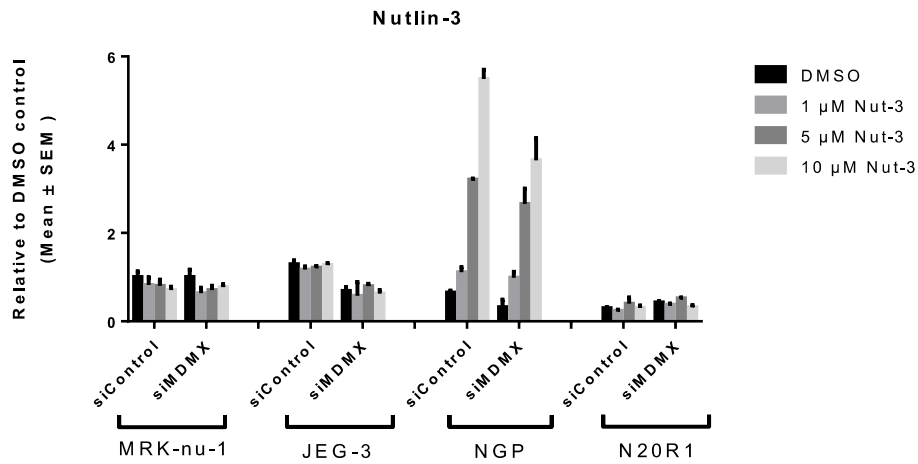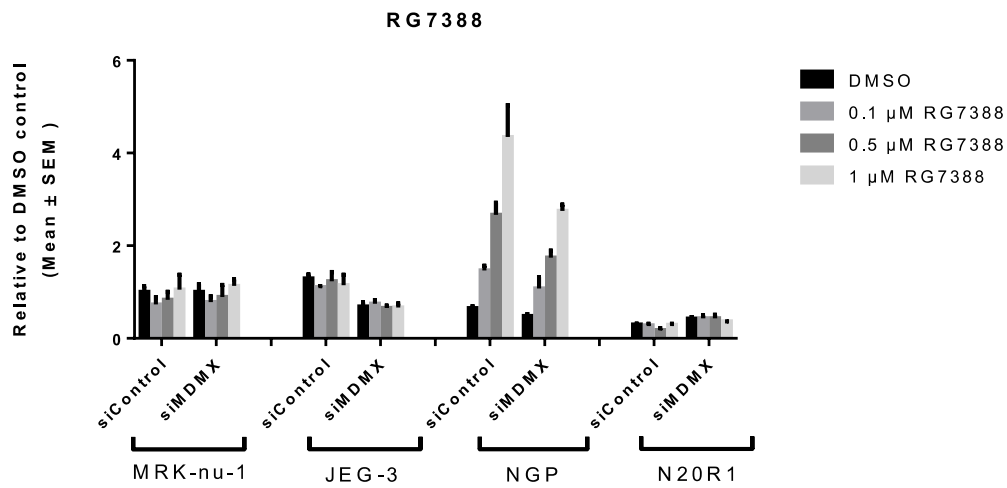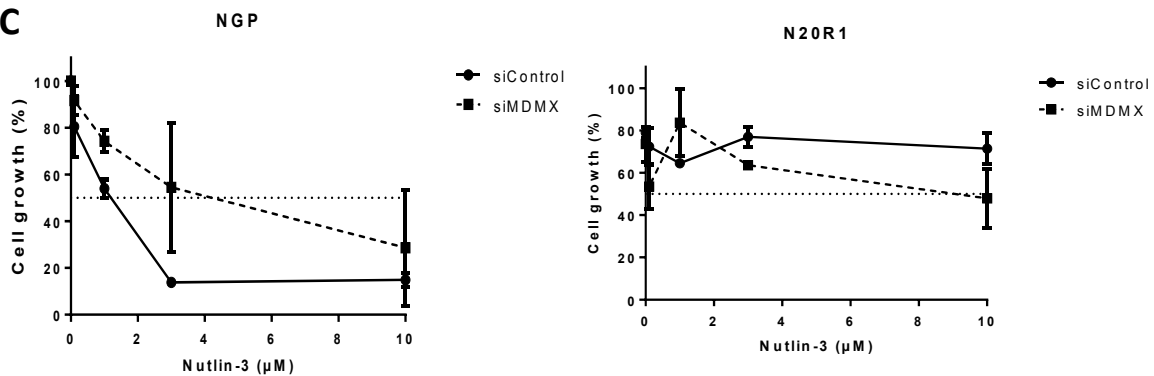
Figure 5.15. Caspase 3/7 apoptotic activity reduced by knockdown of MDMX in NGP. The effect of MDMX knockdown on caspase 3/7 apoptotic activity in response to Nutlin-3 (A) & RG7388 (B) after 24-hour drug treatment in MRK-nu-1, JEG-3, NGP and N20R1 cells. (C) The effect of siRNA knockdown of MDMX on growth inhibitions of Nutlin-3 in NGP (TP53 WT) and N20R1 (TP53 MUT) paired cell lines.

5.5 Discussion

5.5.1 High efficiency of knockdown of MDMX by siRNA

SiRNA-mediated knockdown of MDMX was successful and efficient in the cell lines, compared to lentiviral shRNA system. The Western blot in figure 5.15 shows that while MDMX expression was reduced significantly by lentiviral shRNA, the MDMX expression was nearly undetectable after siRNA-mediated knockdown in MRK-nu-1 cells. Moreover, lentiviral shRNA knockdown did not supress MDMX expression successfully in the other cell lines apart from MRK-nu-1 cells. This also shows the consistent strong increase in p21 seen on knockdown of MDMX by either method.
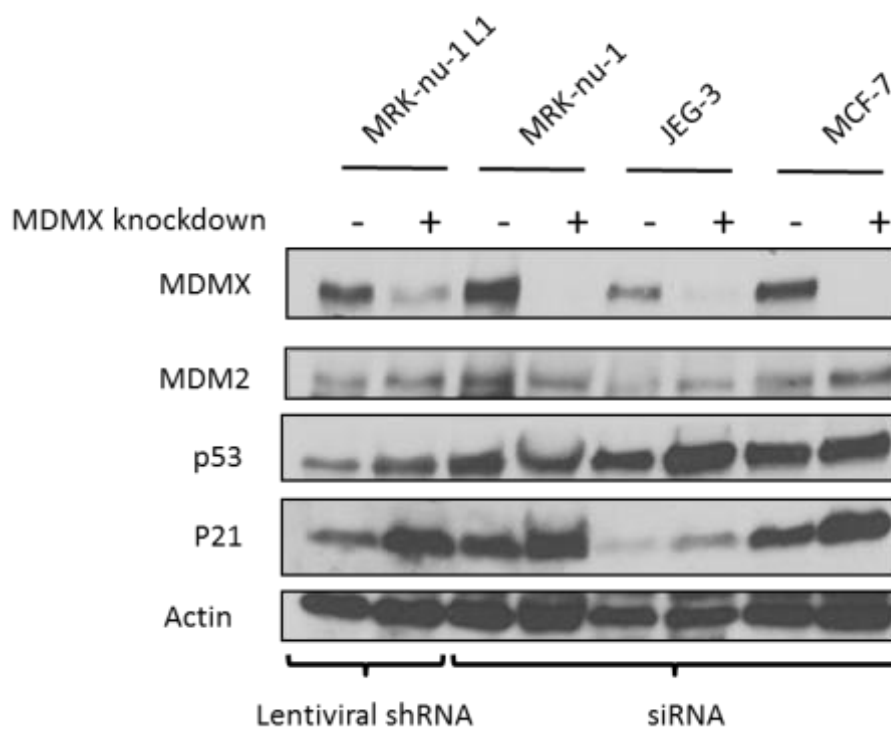
Figure 5.16. A comparison of 72 hour induced lentiviral shRNA & 48 hour siRNA knockdown of MDMX expression in MRK-nu-1, JEG-3 and MCF-7 cell lines.

5.5.2 *The effect of suppression of MDMX by siRNA on cell growth*

Knockdown of MDMX decreased cell proliferation in *MDMX*-amplified and MDMX high expression cell lines. These results are consistent with data obtained for a cutaneous melanoma cell line and metastatic melanoma cells. (Gembarska *et al.*, 2012). Previous research also reported that knockdown of MDMX suppressed the growth of cells with high expression of MDMX but not cells with low MDMX expression. All of the cells they used had wild-type p53 (Hirose *et al.*, 2014). In the current study, suppression of MDMX expression did not completely inhibit cell proliferation but slowed down the increase in cell number. MDMX as a co-operator of MDM2 is not as important as MDM2 in the p53-dependent pathway and knockdown of MDMX expression does not have as dramatic effect on cell proliferation. These differences are reflected in studies with the MDMX knockout mice, which die later than MDM2 knockout mice because of over-activation of p53 leading to cell apoptosis, but can also be rescued by *Trp53* (mouse *TP53*) knockout (Gannon and Jones, 2012).

Consistently the highest effects on siRNA-mediated knockdown of MDMX is an increase of p21 level in all *TP53* wild-type cell lines. Previous research reported that MDMX directly bound to p21 and mediated its proteasomal degradation (Jin *et al.*, 2008). Knockdown of MDMX induced the level of endogenous p21 proteins resulting in G1 arrest in p53-null cells. The level of p21 was low at early S phase but markedly induced by knocking down either MDMX or MDM2 in human cells. MDMX and MDM2 have been demonstrated to independently and cooperatively regulate the proteasome-mediated degradation of p21 at the G1 and early S phases (Jin *et al.*, 2008). The other previous research showed that siRNA-mediated knockdown of MDMX in MCF-7 cells causes a slight increase in p21 levels without other drug treatment (Hu *et al.*, 2006). Furthermore, a published study presented that 14-3-3gamma induced p21 via inhibition of MDMX-mediated proteasomal turnover independent of p53 after DNA damage induction. The level of 14-3-3gamma -MDMX complex increased in response to DNA damage whereas that of the MDMX-p21 complex declined leading to the induction of p21 in p53-null cells. (Lee and Lu, 2011).The mRNA expression level of *CDKN1A* (gene name of p21) will be tested by microarray and qRT-PCR in Chapter 6by absent and present MDMX expression.

5.5.3 The effect of siRNA-mediated knockdown of MDMX response on MDM2-p53 binding antagonists

Knockdown of MDMX by siRNA sensitized JEG-3 cells to growth inhibition by two MDM2 inhibitors, Nutlin-3 and RG7388. JEG-3, which is one of the cell lines with the highest MDMX expression, also expressed a shorter isoform of MDMX (data not shown). Several studies have indicated that short isoforms of MDMX have higher binding for and inhibitory ability against p53 than full-length MDMX (Rallapalli *et al.*, 2003; Bartel *et al.*, 2005; Jacob *et al.*, 2013; Jacob *et al.*, 2014; Tournillon *et al.*, 2015). It has been reported that MDMXp60 binds MDM2 with higher affinity by the C-terminal RING domain compared with full-length MDMX (Tournillon *et al.*, 2015). The other report identified that MDMX-S (skipped or deleted exon 6 form) is responsible for its high affinity interaction with p53 and high-level expression (Rallapalli *et al.*, 2003). The shorter isoform of MDMX might protect JEG-3 cells from MDM2 inhibitors, resulting in the higher GI_{50} values of Nutlin-3 and RG7388 (table 5.2).

MDMX amplification and high expression showed a minor association with resistance to MDM2-p53 binding antagonists in wild-type p53 cells. Our findings are consistent with a previous study in acute myeloid leukaemia that high levels of MDMX expression do not block function of MDM2 inhibitors in AML also AML cells with high MDMX remain sensitive to Nutlin-3 treatment (Tan *et al.*, 2014). This contrasted with a study that reported cell lines with high exogenous MDMX expression were more resistant to growth inhibition by Nutlin-3, which was very different to our findings (Hu *et al.*, 2006). That might resulted from the shorter treatment duration (48 hours) in previous study than current study (72 hours) and the supranormal non-physiological levels of MDMX in transfection studies.

The stabilization of p53 by MDMX suppression in JEG-3 cells showed increased transcriptional reactivation of p53. This results in sensitivity to MDM2 inhibitors after knockdown of MDMX. Previous research indicated that the proportion of cells in S-phase showed no change in JEG-3 with 8 hour 5µM Nutlin-3 treatment, but was decreased by 8 hour Nutlin-3 treatment in the JEG-3 cells with knockdown of MDMX (Hu *et al.*, 2006). By contrast, NGP cells (with MDM2 amplification and high MDMX expression) showed a reduction in sensitivity and apoptotic response to MDM2

inhibitors after suppression of MDMX expression. Overall, the effect of siRNA mediated knockdown of MDMX on the response to MDM2 inhibitors are varied and cell line dependent.

5.5.4 The effect of siRNA-mediated knockdown of MDMX on response to the MDM2/X-p53 binding co-antagonist

Knockdown of MDMX in the cells expressing high MDMX reduced the response to the RO5963 co-inhibitor. A previous study determined that response to the MDM2/X co-inhibitor is associated with MDMX expression (Graves *et al.*, 2012). In the current study, the high efficiency of MDMX suppression by siRNA was associated with a reduction of the response to the RO5963 co-inhibitor. Similarly, the results of lentiviral shRNA-mediated knockdown of MDMX on response to RO5963 treatment also indicated this trend (Chapter 4).

5.5.5 The limitations of siRNA-mediated knockdown

The three different siRNA sequences for targeting MDMX were tested by a previous PhD student, Dr Laura Gamble (Gamble, 2011). In this study, the best siRNA sequence used was based on Dr Gamble's results. However, multiple siRNA sequences still should be tested to make sure that they are not simply off-target effects. Knockdown of MDMX by siRNA in JEG-3 cells was unstable and inconsistent. It could be because of variation in the seeding density of JEG-3 cells. MDMX expression failed to be suppress by siRNA mediated knockdown when the cells were confluent.

The GI_{50} values for Nutlin-3 in the cells with siUCR were slightly higher than parental in some cell lines (table 5.2). The effect of MDMX knockdown appeared to increase sensitivity compared to siUCR control for growth inhibition. However, the change of sensitivity to Nutlin-3 was minor compared to parental cell lines.

Nutlin-3	Parental	Control	Knockdown
MRK-nu-1 (lenti shRNA)	3.0 ± 0.5	1.7± 0.5	3.9 ± 0.8
MRK-nu-1 (siRNA)	3.0 ± 0.5	5.9 ± 1.0	3.6 ± 0.5
JEG-3 (siRNA)	11.7 ± 1.4	12.7 ± 1.3	4.6 ± 0.8
MCF-7 (siRNA)	5.3 ± 1.3	9.7 ± 1.0	8.8 ± 4.2
NGP (siRNA)	2.0 ± 0.7	0.9 ± 0.3	2.8 ± 0.1

RG7388	Parental	Control	Knockdown
MRK-nu-1 (lenti shRNA)	0.54 ± 0.13	0.04 ± 0.01	0.03 ± 0.01
MRK-nu-1 (siRNA)	0.54 ± 0.13	0.052± 0.008	0.062 ± 0.023
JEG-3 (siRNA)	1.76 ± 0.64	2.03 ± 0.70	1.05 ± 0.79

Table 5.2. GI$_{50}$ values of Nutlin-3 & RG7388 with and without suppression of MDMX

Chapter 6 The effect of MDMX knockdown on cellular gene expression profiles

6.1 Introduction

Cells maintain a constant level of MDMX in healthy tissue. *MDM4* gene expression remains constitutive during cell proliferation and differentiation or following DNA damage. Unlike MDM2, DNA damage does not regulate MDMX mRNA levels, or posttranslational modifications (Jackson and Berberich, 1999). Previous studies reported that mutant knockout mice could be generated that lacked p53 together with either *MDM2* or *MDM4* (Iwakuma and Lozano, 2007; Barboza *et al.*, 2008). *MDM4* null mice are embryonic lethal, but can be rescued by crossing with p53 null mice (Parant *et al.*, 2001; Migliorini *et al.*, 2002). Absence of *MDM2* or *MDM4* had different effects. Loss of *MDM2* promoted p53-dependent activation of apoptosis related genes, while loss of *MDM4* promoted p53-dependent activation of cell cycle arrest genes (Migliorini *et al.*, 2002; Minsky and Oren, 2004; Ohkubo *et al.*, 2006).

In the relationship between MDMX and MDM2 antagonists, previous studies have indicated that *MDM4* amplification and/or increased protein expression may be associated with resistance to MDM2-p53 binding antagonists (Hu *et al.*, 2006; Patton *et al.*, 2006; Wade *et al.*, 2006). However, specific inhibitors for MDMX have yet to be developed and an MDM2/MDMX-p53 co-inhibitor (RO-5963) does not particularly show better efficacy against high MDMX-expressing cells than single target MDM2 inhibitors (chapter 3-5). The question goes back to what MDMX affects, other than inhibitors of p53 binding.

In this chapter, results are presented for the use of Affymetrix Human Transcriptome Array 2.0 to scan the gene expression profile of both MDMX knockdown and expression in MRK-nu-1 cells. The results of differential gene expression can reveal possible genes and their related pathways that could be regulated by MDMX.

6.2 Hypotheses and aims

Hypothesis:

Suppression of MDMX expression increases the *TP53*-dependent and/or *TP53*-independent downstream transcriptional activity and pathways regulated by MDMX.

Aim:

To better understand the cellular function and therapeutic potential of targeting MDMX by investigating the downstream transcriptomic consequences of knocking down MDMX expression.

6.3 Materials and methods

6.3.1 Knockdown of MDMX in MRK-nu-1 cells

MRK-nu-1 cells were seeded and induced by 1µg/ml doxycycline for 72 hours. The conditions for knockdown of MDMX were according to the results described in chapter 4.

MRK-nu-1 cells were also seeded and treated with 20 nM siRNA to knock down MDMX. RNA samples were collected after siRNA treatment for 48 hours. This time point showed the highest efficiency of suppression of MDMX expression by siRNA (chapter 5).

6.3.2 RNA extraction

Total RNA samples from MRK-nu-1 cells were extracted using an RNeasy mini kit (QIAGEN, Germany). The MRK-nu-1 total RNA samples were quantified and the quality checked using a Nano Drop (ND-1000) spectrophotometer to measure light absorbance at 260 & 280 nm wavelengths. A 260:280 ratio of ~2.0 was considered as pure RNA.

6.3.3 RNA quality analysis

The quality and concentration of mRNA were determined using an Agilent RNA 6000 nano kit (Agilent Technologies, CA, USA) on an Agilent 2100 Bioanalyser (Agilent Technologies, CA, USA) to determine an RNA integrity number (RIN) (Schroeder *et al.*, 2006). The RIN values of 16 RNA samples, which included 4 replicated samples of each lentiviral shRNA and siRNA knockdown and control pair, were measured with an Agilent 2100 Bioanalyser.

A fluorescent intercalating nucleotide dye and a sieving polymer were loaded into a 16-well chip, which was interconnected with microcapillaries. Finally, the samples and an RNA 6000 ladder (as size reference) were loaded in separate wells. Electric current was applied throughout the polymer-filled capillaries interconnecting the wells, to separate charged molecules migrating at a rate proportional to their size. The smaller molecules migrate faster through the path of the laser, which excites the

dye molecules intercalated with the RNA molecules resulting in their fluorescence. An electropherogram is then digitally generated by the 2100 Expert software (Agilent Technologies, CA, USA) (figure 6.1). Fluorescence units are proportional to the amount of dye intercalated into the RNA molecules. A smaller marker is also run with each sample to use as a control for potential shifts between the different samples run on each chip.

RNA has stable 28S and 18S ribosomal RNA (rRNA) components that are normally detected as two distinct peaks with a ~2:1 ratio in FU (fluorescence unit) peak intensity. Human 28S and 18S rRNA produce a theoretical ratio of 2.6:1. RNA integrity was traditionally calculated based on the 28S:18S ratio with optical densities obtained by running samples on a denaturing agarose gel (alkaline conditions) followed by densitometry. Aligent expert software calculates the RIN value of RNA samples based on the whole electropherogram trace (Schroeder *et al*., 2006). RIN values range from 1-10, with values above 8 considered acceptable for microarray applications (Schroeder *et al*., 2006).

Figure 6.1. Aligent Bioanalyzer electropherogram trace and gel electrophoresis image (on the right). RNA concentration and RIN value are calculated and presented. The ratio of 28S:18S rRNA molecules is calculated based on the area under each curve. Peaks associated with other rRNA or tRNA molecules have been arrowed in addition to the control molecule. (y-axis: fluorescent units (FU) v x-axis: size relative to ladder fragments.)

6.3.4 Microarray analysis of gene expression

The 3 replicates of both lentiviral shRNA and siRNA were chosen based on their RIN values and quality of RNA. The 3 repeats of total RNA extraction samples in each lentiviral shRNA pair and siRNA pair from MRK-nu-1 cells with MDMX knockdown treatment were sent to AROS Applied Biotechnology (A/S, Demark). The Affymetrix Human Transcriptome Array 2.0 (HTA 2.0) was used to detect differences in the expression of full genes and alternatively spliced forms between negative control and MDMX knockdown groups. A total of 67539 genes including 44710 coding and 22829 non-coding genes were scanned for analysis of the expression of alternatively spliced genes. Full gene differential expression analysis included a total 67528 genes including 44699 coding genes and 22829 non-coding genes.

6.3.5 Data analysis

Transcriptome Analysis Console 3.0 software (TAC, Affymetrix Thermo Fisher Scientific, CA, USA) was used to analyse the microarray data to identify significant changes in gene expression, alternative splicing and associated functional pathways. One-Way paired ANOVA was used for the statistical t-test. The data for full gene level differential expression was filtered to remove non-statistically significant changes and showed the data with over 2-fold increase or decrease and ANOVA p-value <0.05.

The data for alternative splicing expression was filtered to show the data with over 2-fold change in splicing index (SI) and ANOVA p-value <0.05. The Splicing Index algorithm is a way to measure how much exon specific expression differs between two conditions after excluding gene level influences (figure 6.2). The algorithm first normalizes the exon and junction expression values by the level of gene expression and creates a ratio of normalized signal estimates from one condition relative to another (Srinivasan *et al.*, 2005; Gardina *et al.*, 2006; Clark *et al.*, 2007; Kwan *et al.*, 2007). Furthermore, there are some other conditions. A gene is expressed in both conditions of groups, that means, for example, the gene is expressed in both the knockdown of MDMX group and the negative control group in this study. A probe selection region (PSR) or junction must be expressed in at least one condition of

group. A gene must contain at least one PSR. PSR is the smallest unit on the exon array for expression profiling and each PSR is represented by an individual probe set (Clark *et al.*, 2007; Kwan *et al.*, 2007).

Scatter plots, volcano plots and Hierarchical clustering of full gene level differential expression between knockdown and MDMX expression were analysed by TAC 3.0 software. Scatter plots of alternative splicing expression was also analysed by TAC 3.0 software. Pathways related to the full gene changes and alternative splicing expression changes were generated by using TAC 3.0 software to link to the Wikipathway database (Pico *et al.*, 2008; Kelder *et al.*, 2012) (http://www.wikipathways.org/). The WebGestalt analysis website (Zhang *et al.*, 2005; Wang *et al.*, 2013) was also used to find related pathways based on a profile panel of differentially expressed genes linked to KEGG pathway analysis (Kanehisa and Goto, 2000; Kanehisa *et al.*, 2016) and wikipathway databases (Pico *et al.*, 2008; Kelder *et al.*, 2012).

6.3.6 qRT-PCR Confirmation of array results

The same RNA samples used to generate the microarray data were used for qRT-PCR analysis. Alterations in mRNA expression for a selected panel of genes was investigated by qRT-PCR. The details of the qRT-PCR protocol can be found in chapter 2.3. The genes chosen for qRT-PCR were based on the array differential expression results for the alternative splicing dataset with siRNA-mediated knockdown of MDMX. The sequences of primers used are shown in table 2.4. For example, for the *VGLL1* gene, the $\Delta\Delta$Ct Algorithm was $\Delta\Delta$Ct = ΔCt (VGLL1$_{siMDMX}$ - GAPDH$_{siMDMX}$) - Δct (VGLL1siControl - GAPDHsiControl$^)$ The fold change = $2^{\Delta\Delta Ct}$.

Alternative Splicing Analysis

(1) Use an eligible PSR to determine gene expression if it is present in greater than or equal to `50` % of all the transcript isoforms

(2) A gene is expressed in a sample if greater than or equal to `50` % of its eligible PSRs have DABG p-value less than `0.05`

(3) A condition has this gene expressed if greater than or equal to `50` % of its samples have this gene expressed.

(4) A PSR/Junction is expressed in a condition if greater than or equal to `50` % of the samples have DABG p-value less than `0.05`

(5) False Discovery Rate < `0.05`

$$\text{Splicing index} = \frac{\left\{ \dfrac{\text{Exon 1 Condition 1 Intensity}}{\text{Gene 1 Condition 1 Intensity}} \right\}}{\left\{ \dfrac{\text{Exon 1 Condition 2 Intensity}}{\text{Gene 1 Condition 2 Intensity}} \right\}}$$

Figure 6.2. Splicing Index (SI) Algorithm and Configurable Parameters for alternative splicing data (Affymetrix TCA 3.0 user guide)

6.4 Results

6.4.1 Quality control of the RNA samples

The 4 replicates of RNA samples in both lentiviral shRNA and siRNA-mediated MDMX knockdown groups were tested for their RNA quality before selection for microarray analysis. The gel representation results are shown in figure 6.3. The first replicate of the lentiviral shRNA-mediated knockdown samples showed some evidence of degradation and had an RIN value of 8.3. This pair of lentiviral shRNA samples were taken out and were not included for the following transcriptome microarray analysis. Some of the samples did not present their RIN values. This might be because the concentrations of RNA samples were too high and over the range which the machines can measure and calculate for an RIN value. Although the RIN values for these samples are shown as N/A in figure 6.4, the electropherogram curve showed high quality for these samples equal to those with RIN values of 10. The 12 samples which showed RIN values >9 were chosen for the Human Transcriptome microarray. Aligent Bioanalyzer electropherogram traces and MDMX protein knockdown confirmation checks for the 12 samples chosen for microarray analysis are shown in figure 6.4.
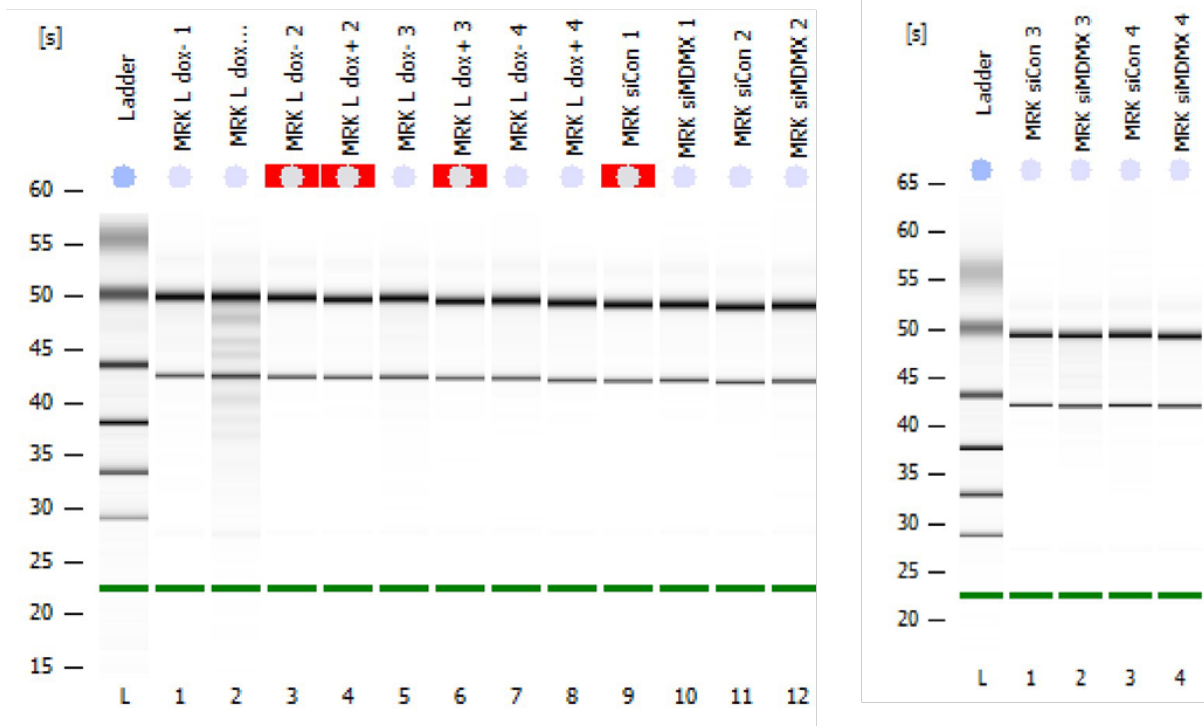
Figure 6.3 Aligent Bioanalyzer electropherogram images of the 16 RNA samples. An RNA 6000 ladder was loaded in the first column for size reference.
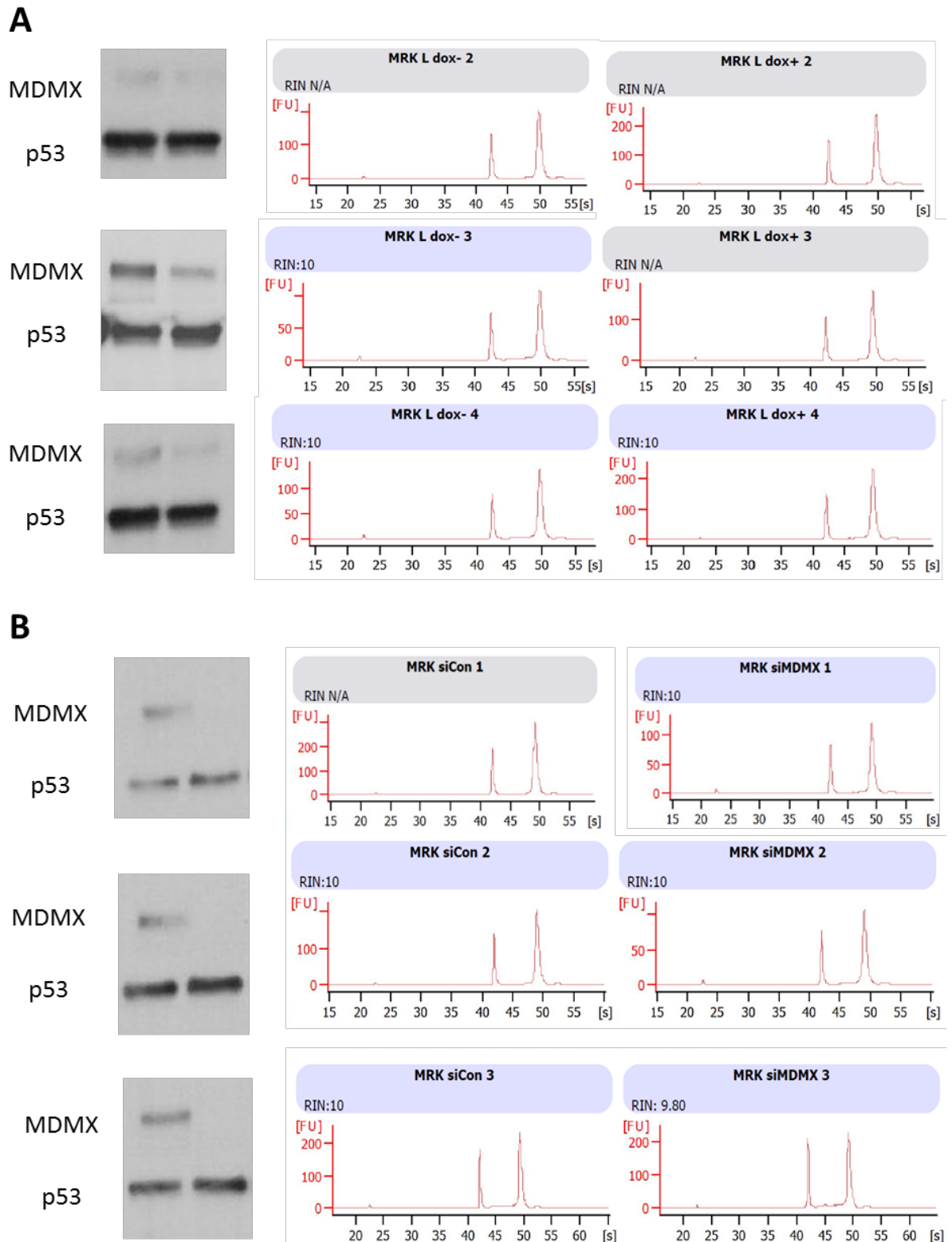
Figure 6.4. Protein level checks for confirmation of the suppression of MDMX and Agilent Bioanalyzer electropherogram traces for 3 repeated MDMX knockdown experiments with MRK-nu-1 cells. (A) Lentiviral shRNA and (B) siRNA knockdown.

6.4.2 Close relationship between each group of samples based on 33832 genes

The PCA (Principal Component Analysis) cluster results for the microarray-based gene expression results (Data kindly provided by Dr Sirintra Nakjang) in figure 6.6 show the array datasets clustered together more closely according to the knockdown method. The lentiviral shRNA knockdown repeats clustered together and the siRNA repeats clustered together.

6.4.3 Full gene differential expression in relation to lentiviral shRNA-mediated knockdown of MDMX

Full level of gene expression analysis scanned total 67528 genes. Only two genes were shown to be differentially expressed over 2-fold between lentiviral shRNA-mediated knockdown of MDMX and control. One of them was *OR2J2* (olfactory receptor, family 2, subfamily J, member 2) with 2.41-fold increase after knockdown of MDMX by lentiviral RNA. The other one was a noncoding gene (TC07000215hg.1). A 2-fold cut-off for change in gene expression was shown. The data was re-gated to show over 1.5-fold change (figure 6.6 and figure 6.7) to see if there were additional smaller changes in gene expression which might be interesting. After 1.5-fold cut-off, *MDM4* gene expression showed up as a 1.57-fold significant decrease after lentiviral-mediated knockdown treatment. In the PCA, the lentiviral shRNA pairs did not group together like siRNA pairs. Lentiviral shRNA pairs showed smaller set of genes change then siRNA pairs. The minor change of genes might affect and be difficult to group the same pair of repeats together in the PCA results.
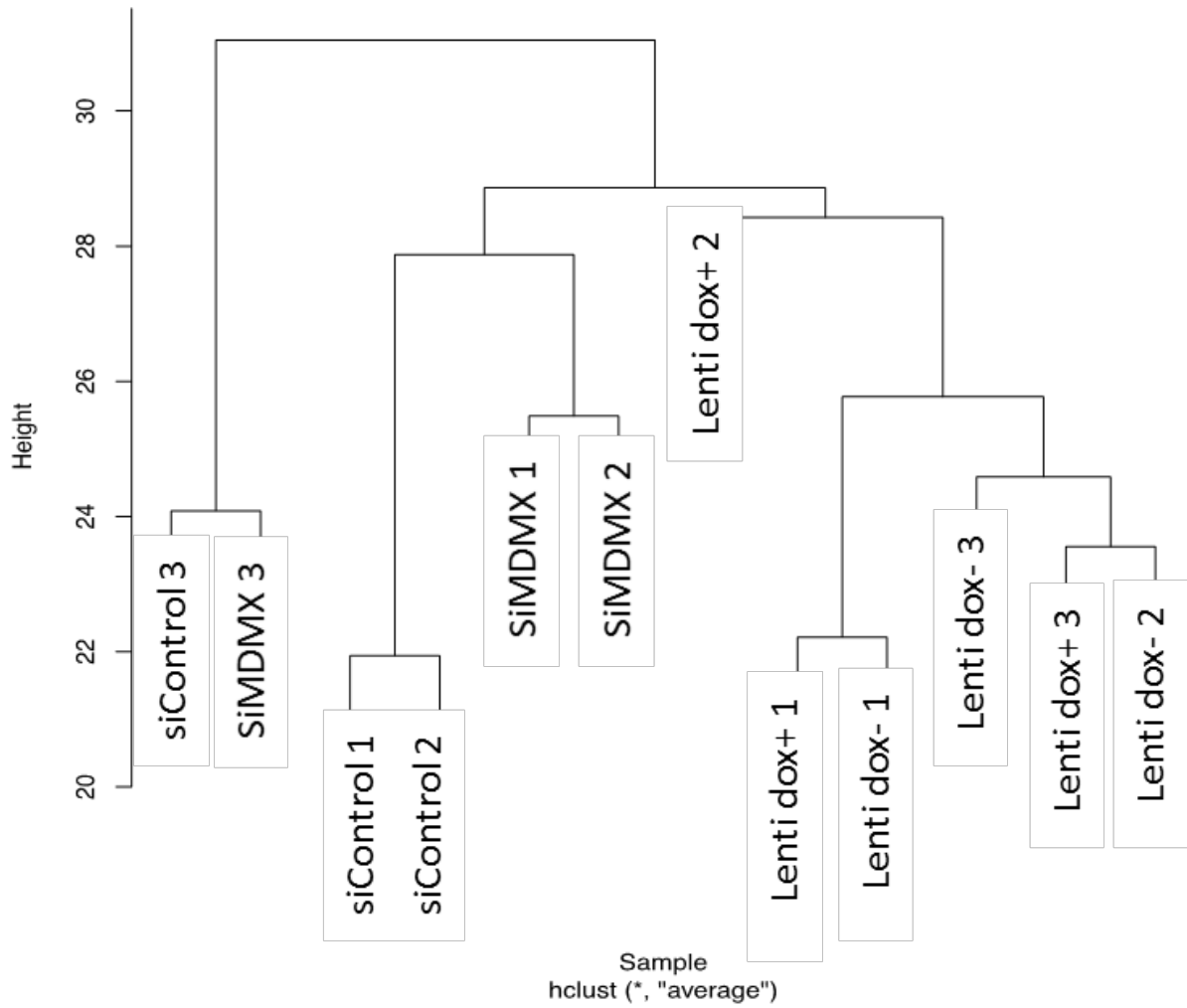
Figure 6.5. Relationship of the samples by PCA cluster analysis (Data kindly provided by Dr. Sirintra Nakjang) based on gene expression profiles from the HTA 2.0 microarray results. SiMDMX knockdown and shRNA knockdown gene expression datasets clustered separately.
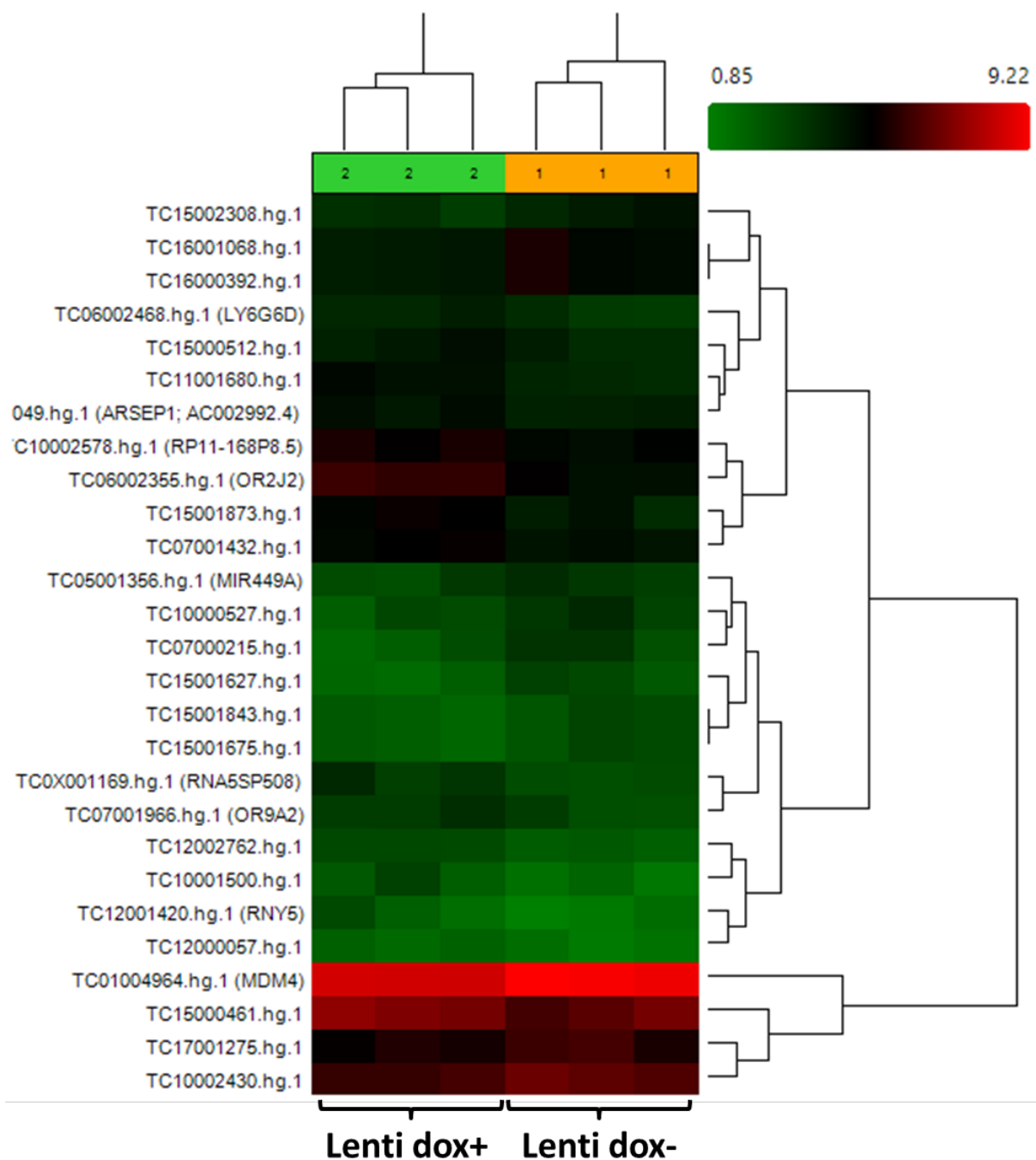
Figure 6.6. Hierarchical clustering of MRK-nu-1 full gene level >1.5-fold differential expression analysis between lenti dox- (MDMX expression) and lenti dox+ (knockdown of MDMX). The corresponding volcano plot and scatter plot is shown in Figure 6.7.
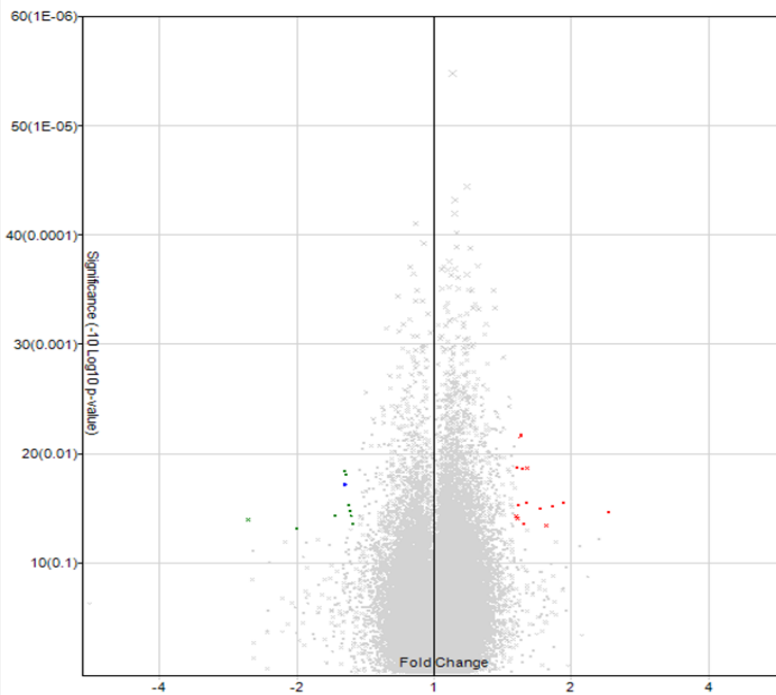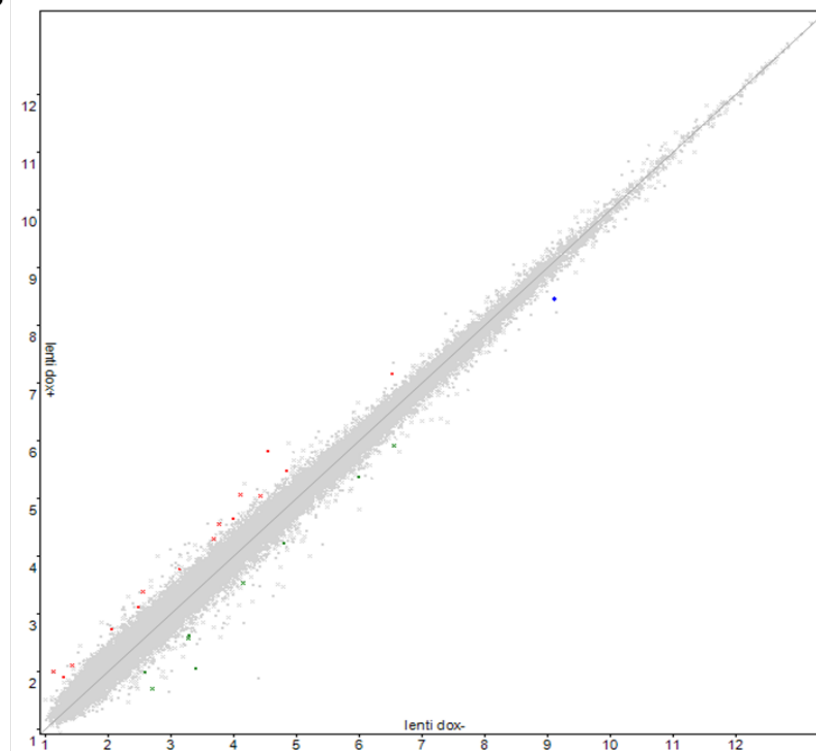
Figure 6.7. (A) Volcano plot of full gene differential expression in MRK-nu-1 cells. (B) Scatter plot of full gene differential expression in MRK-nu-1 cells between lenti dox- (X-axis, MDMX expression) and lenti dox+ (y-axis, knockdown of MDMX). (Red spot: significantly higher expression in knockdown group; green spot: significantly higher expression in control group; grey spots: less than 1.5-fold difference; blue spot: *MDM4*)

6.4.4 Full gene differential expression in relation to siRNA-mediated knockdown of MDMX

A set of 18 gene transcripts of the total 67528 genes increased while 24 genes decreased after siRNA-mediated knockdown of MDMX. The Hierarchical clustering in figure 6.8 shows all significantly up-relegated and down-regulated genes after MDMX knockdown. Figure 6.9 presents the volcano plot and scatter plot of MRK-nu-1 full gene differential expression. *MDM4* gene expression was reduced significantly (2.48-fold) after siRNA-mediated knockdown. *VGLL1* (vestigial-like 1 in Drosophila) was the gene with the highest increase (3.9-fold change) after knockdown of MDMX by siRNA in MRK-nu-1 cells. *CCNG2* and *TNFS10,* which are involved in the p53 pathway, increased 1.92 and 2.05-fold after knockdown of MDMX by siRNA.
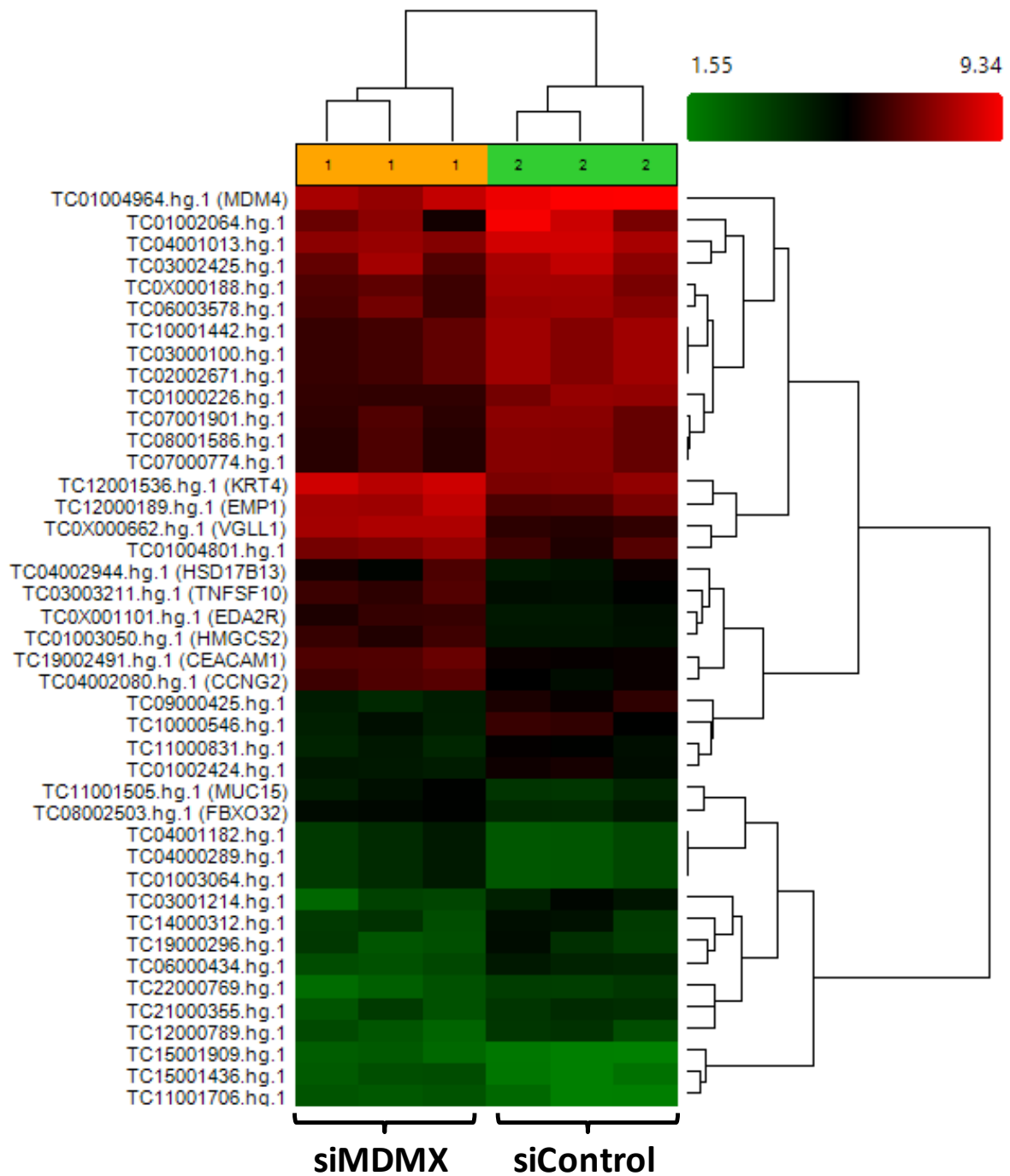
Figure 6.8. Hierarchical clustering of MRK-nu-1 full gene level >2-fold differential expression analysis between siControl and siMDMX. (Group 1: siMDMX, Group 2: siControl).The corresponding volcano plot and scatter plot is shown in Figure 7.9.
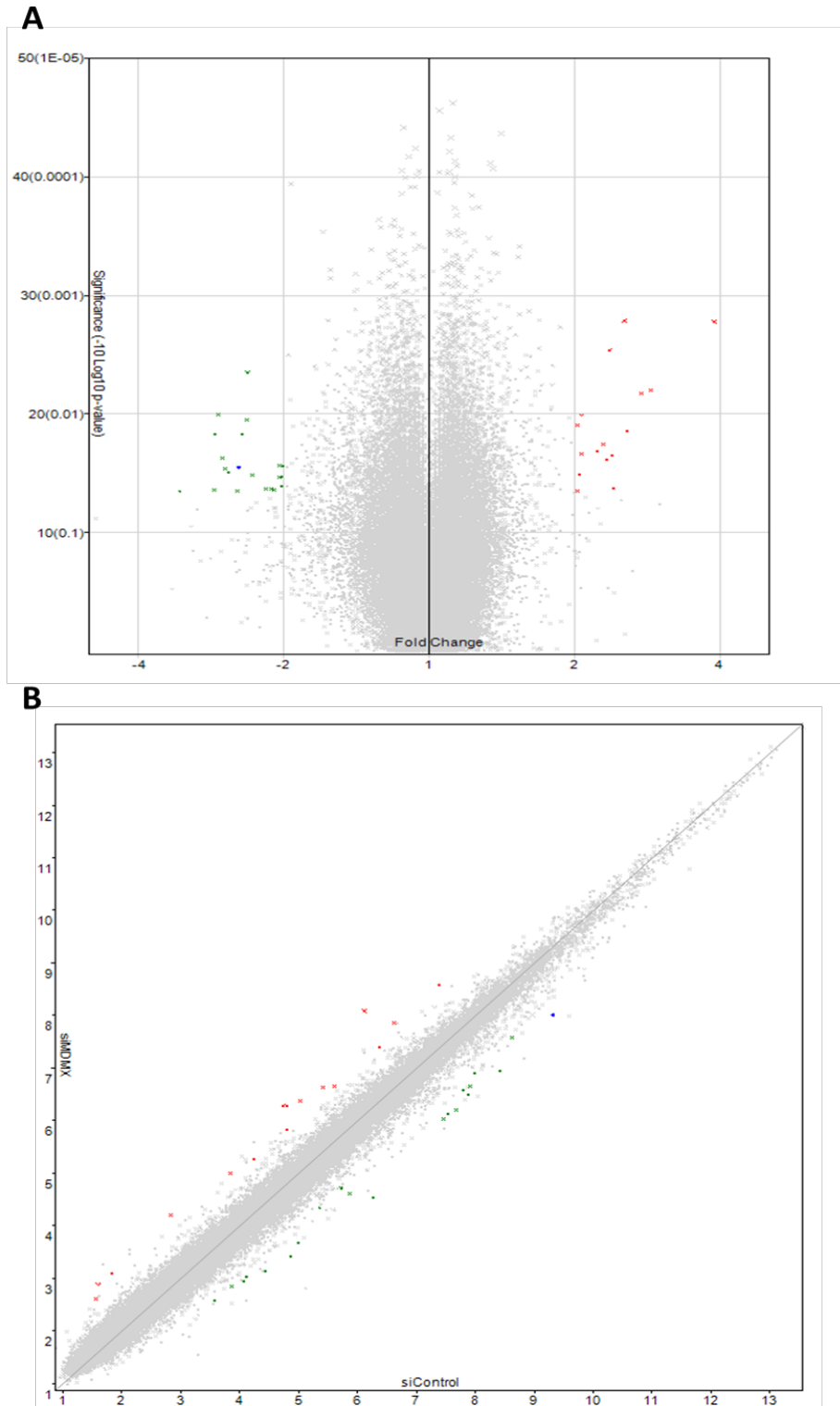
Figure 6.9. (A) Volcano plot of full gene differential expression in MRK-nu-1 cells. (B) Scatter plot of full gene differential expression in MRK-nu-1 cells between siControl (X-axis, MDMX expression) and siMDMX(y-axis, knockdown of MDMX). bRed spot: significantly higher expression in knockdown group; green spot: significantly higher expression in control group; grey spots: less than 2-fold difference; blue spot: *MDM4*)

6.4.5 The differential alternative splicing expression in relation to the presence and knockdown of MDMX expression by lentiviral shRNA

33072 coding and 14685 non-coding gene transcripts were detected both in cells expressing MDMX and those with MDMX expression knocked down by lentiviral shRNA cells, and 7810 coding and 5433 non-coding genes were not expressed in either condition. The MDMX-expressing (dox-) group showed expression of 2742 coding genes and 1899 non-coding which were not expressed in the MDMX knockdown (dox+) group. On the other hand, there were 1086 coding and 812 non-coding genes which were expressed in lentiviral shRNA knockdown (dox+) group but not in lentiviral control (dox-) group. Although MDMX expression did not reduce (1.6-fold) statistically significantly, *CLCA2* (chloride channel accessory 2) increased statistically significantly (4.82-fold) after knockdown of MDMX by lentiviral shRNA. *ATM* and *MDM2* also increased after knocking down MDMX (1.35-fold and 1.33-fold change respectively).

6.4.6 The differential alternative splicing expression in relation to the presence and knockdown of MDMX expression by siRNA

33010 coding and 14630 non-coding transcripts were detected both in cells expressing MDMX and those with MDMX expression knocked down by siRNA, and 6810 coding and 4767 non-coding genes were not expressed in either condition. The MDMX-expressing group showed expression of 4292 coding genes and 2908 non-coding transcripts that were not expressed in the MDMX knockdown group. On the other hand, there were 598 coding genes and 524 non-coding genes that were expressed in the siMDMX group but not in the siControl group.

The splicing *MDM4(MDMX)* expression was reduced significantly (2.4-fold) after siRNA-mediated knockdown. *VGLL1* (vestigial-like 1 in Drosophila) was the gene with the highest increase (4.51-fold change) after knockdown of MDMX by siRNA in MRK-nu-1 cells. The expression of a number of p53 transcriptional target genes (table 6.1) was found to be altered, including *CDKN1A, CCNG2, RRM2B, BTG2, ZMAT3, TNFRSF10C* and *FAS* with over 1.5-fold increase, consistent with a role for MDMX in suppression of p53 function in these *MDM4*-amplified MRK-nu-1 cells.

Gene Symbol	Description	Gene Fold Change (linear) (siMDMX vs. siControl)	ANOVA p-value (siMDMX vs. siControl)
VGLL1	vestigial-like family member 1; vestigial like 1 (Drosophila)	4.51	0.013644
BTG2	BTG family, member 2	2.19	0.042507
RRM2B (p53R2)	ribonucleotide reductase M2 B (TP53 inducible)	2.06	0.007845
CDKN1A	cyclin-dependent kinase inhibitor 1A (p21, Cip1)	2.05	0.029863
CCNG2 (Cyclin G)	cyclin G2	1.95	0.018056
FAS	Fas cell surface death receptor; Fas (TNF receptor superfamily, member 6)	1.92	0.026146
ZMAT3 (PAG608)	zinc finger, matrin-type 3; zinc finger, matrin type 3	1.98	0.004174
GHR	growth hormone receptor	1.71	0.003162
TNFRSF10C	tumor necrosis factor receptor superfamily, member 10c, decoy without an intracellular domain; uncharacterized LOC254896	1.84	0.021207
MDM4	MDMX, p53 regulator; Mdm4 p53 binding protein homolog (mouse); putative novel transcript	-2.4	0.036038

Table 6.1. Splicing gene expression change between siControl and siMDMX from HTA 2.0 results.
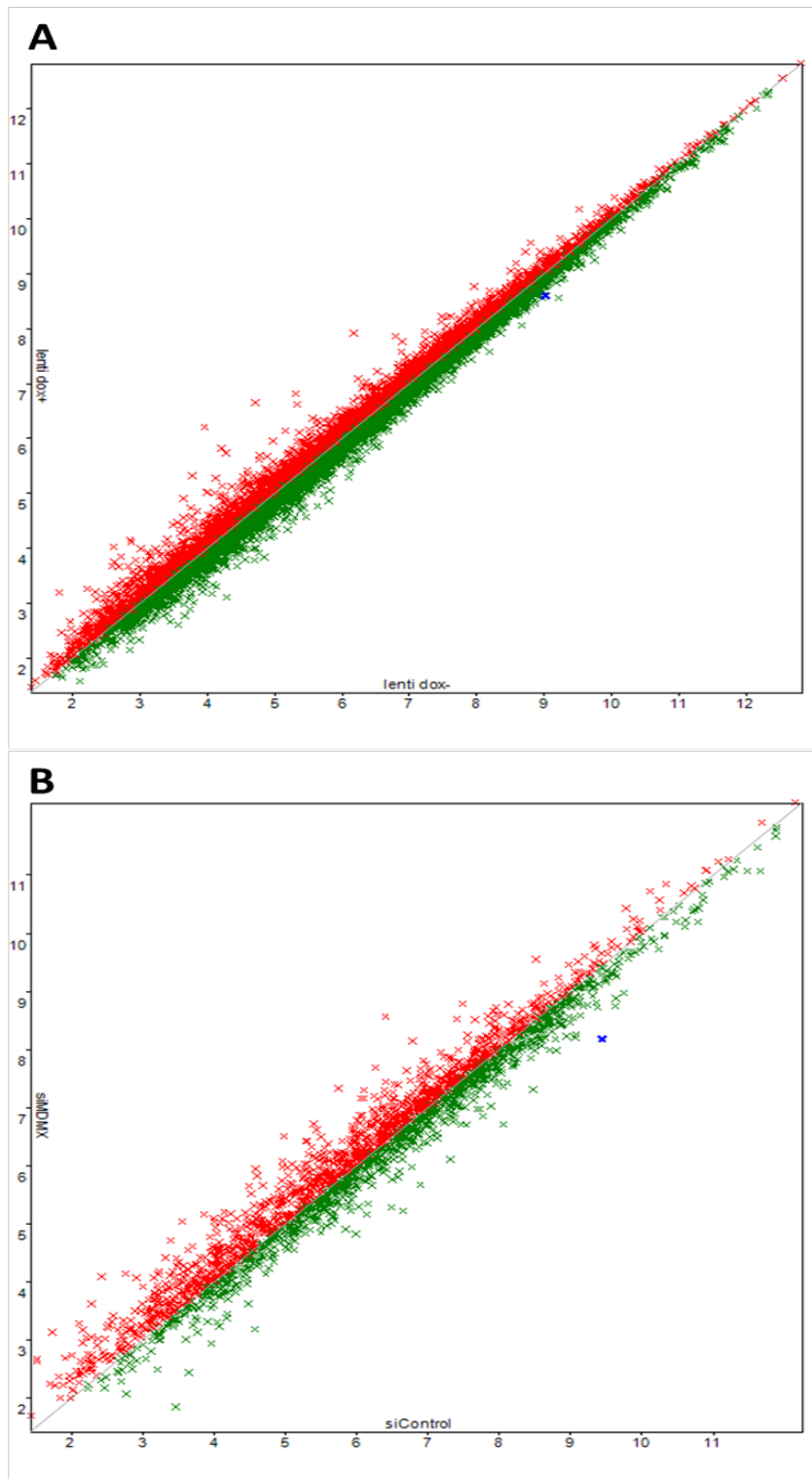
Figure 6.10. Scatter plot of alternative splicing differential gene expression in relation to lentiviral shRNA (A) and siRNA (B)-mediated knockdown of MDMX. X-axis is negative control with normal MDMX expression; y-axis is knockdown of MDMX. Green spots show higher level of gene expression in MDMX-expressing control; red spots show higher level of gene expression in MDMX knockdown. The one blue spot in each plot is *MDM4(MDMX)*.

6.4.7 *Microarray results confirmation by qRT-PCR*

Figure 6.10 shows the bar charts of ΔCt and $\Delta\Delta$Ct values for increased genes after siRNA-mediated knockdown of MDMX. The *MDM4* transcript levels decreased, as shown in figure 6.11A and B, after lentiviral and siRNA-mediated knockdown of MDMX. The bar chart shows that VGLL1 had the highest increase of around 4-fold gene change. Because the genes were chosen based on the siRNA HTA 2.0 results, as expected some genes were not detected as significantly increased after knockdown of MDMX by lentiviral shRNA.

Figure 6.11C shows *VGLL1* and *CDKN1A* expression also increased over 4-fold in MRK-nu-1, JEG-3 and MCF-7 cells after siRNA mediated knockdown of MDMX for 48 hours. By contract, the *VGLL1* expression decreased after siRNA mediated knockdown of MDMX in NGP cells. The *TP53* and *CDKN1A* expression showed more increase by MDMX suppression in JEG-3 than MRK-nu-1 cells. These results were consistent with the protein level results in chapter 5.
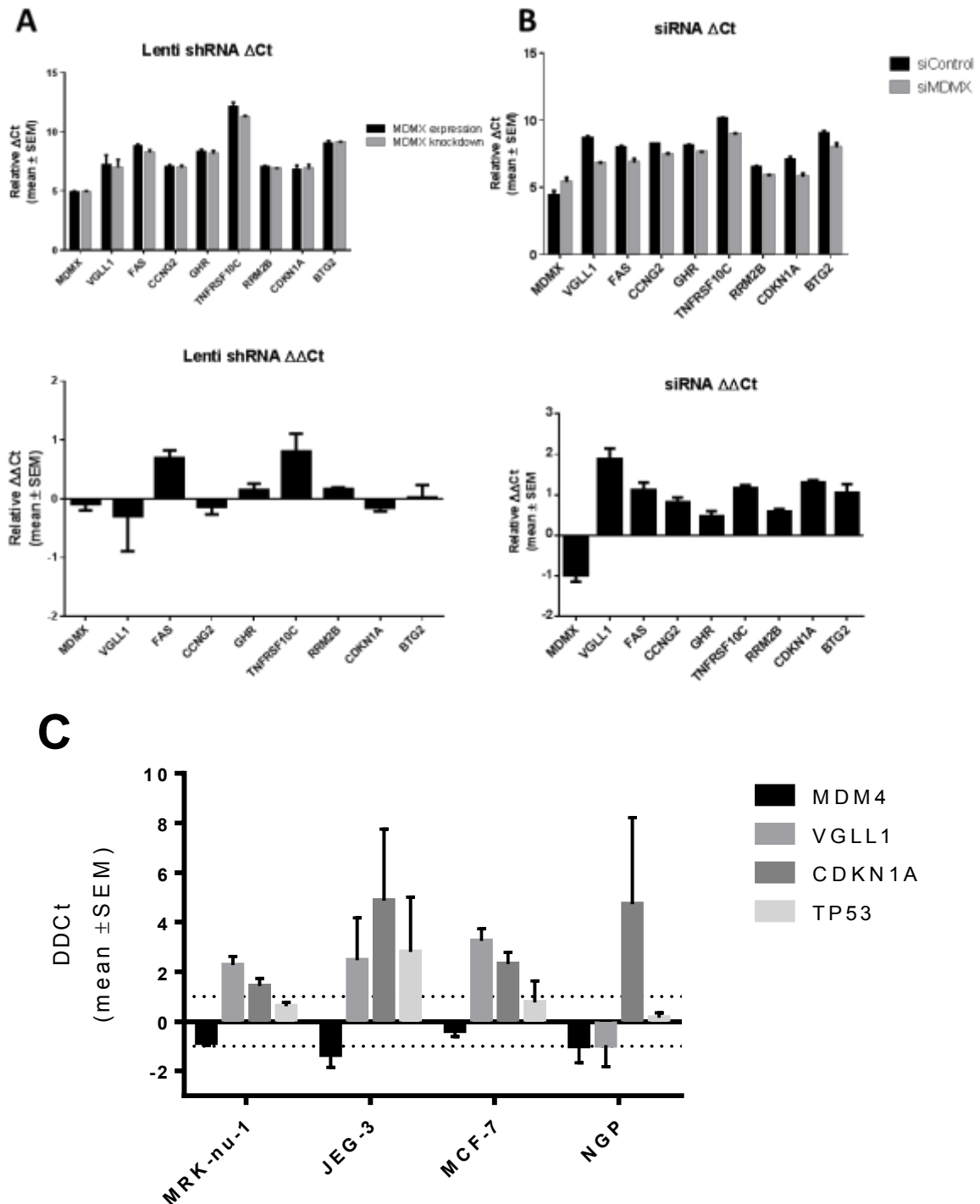
Figure 6.11. The qRT-PCR results show the ΔCt and $\Delta\Delta$Ct values of increased genes after MDMX knockdown by lentiviral shRNA (A) and siRNA (B), confirming the results of HTA 2.0 data. (C) The qRT-PCR results show the $\Delta\Delta$Ct values of increased genes after MDMX knockdown by siRNA in MRK-nu-1, JEG-3, MCF-7 and NGP cells. (y-axis shows log_2 fold gene change) $\Delta\Delta$Ct = ΔCt (VGLL1$_{siMDMX}$ - GAPDH$_{siMDMX}$) - Δct (VGLL1siControl - GAPDHsiControl$^)$ The fold change = $2^{\Delta\Delta Ct}$

6.5 Discussion

6.5.1 The gene expression changes of p53-dependent pathways

A greater degree of MDMX expression knockdown was achieved with the siRNA (>95%) than the lentiviral shRNA (>50%) This was reflected by increased suppression of growth and larger changes in gene expression patterns with the siRNA knockdown.

The 48-hour MDMX knockdown time point of was chosen as the best time point for suppressing MDMX protein expression based on Western blot. The reason for choosing the most efficient knockdown of MDMX protein is that the aim was to see what the MDMX protein affects.

ATM and *MDM2* showed a slight increase after lentiviral shRNA-mediated knockdown of MDMX. Compared to siRNA-mediated knockdown of MDMX, *CDKN1A, FAS, CCNG2, RRM2B* and *ZMAT3* were increased over 1.5-fold by siRNA-mediated knockdown of MDMX. They are down-regulated by p53 (figure 6.12).
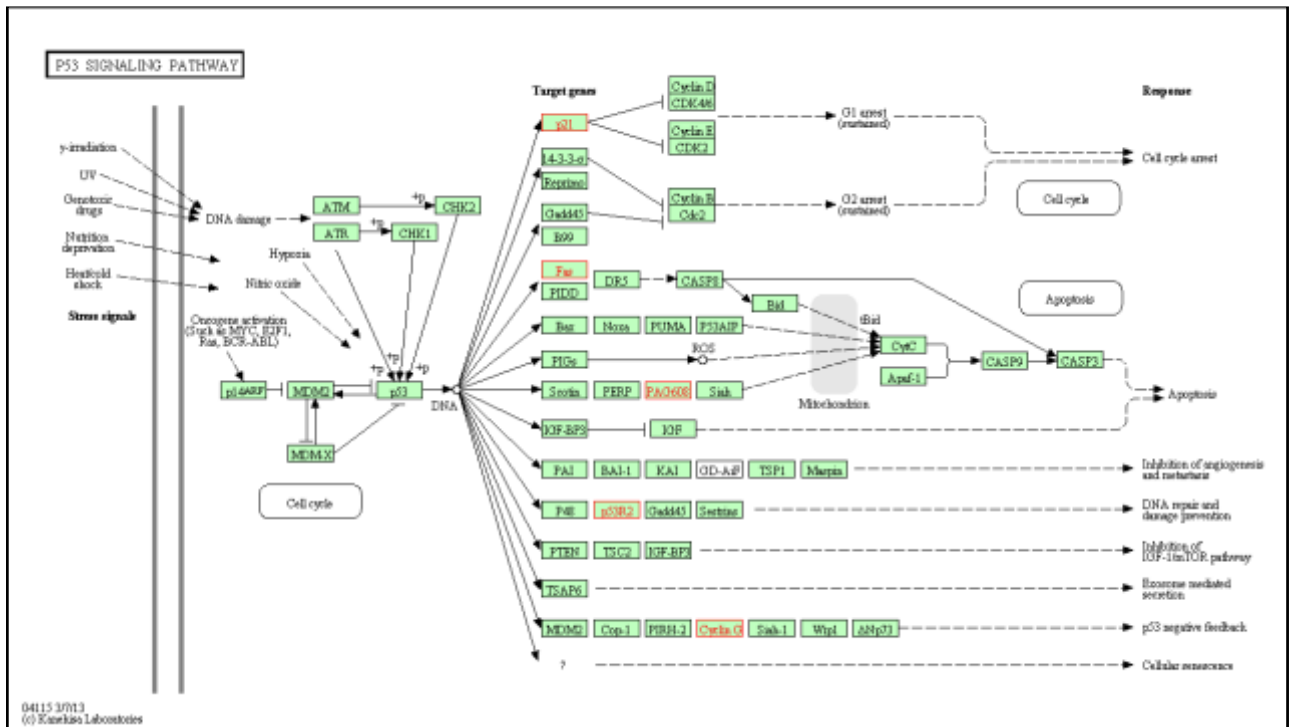
Figure 6.12. The p53 signal pathway from HTA 2.0 alternative splicing form of differential gene expression between siControl and siMDMX. Taking HTA 2.0 data of siMDMX and siControl with over 1.5-fold change, the gene set was found to be enriched for genes from the p53 pathway, using pathway enrichment analysis from the WebGestalt website linked to the KEGG pathway database (Kanehisa and Goto, 2000; Zhang *et al.*, 2005; Wang *et al.*, 2013; Kanehisa *et al.*, 2016). (Red: genes with increased expression) (PAG608=ZMAT3, p53R2=RRM2B, Cyclin G=CCNG2) http://www.webgestalt.org/

6.5.2 Knockdown of MDMX increased both gene and protein expression of p21(CDKN1A)

SiRNA-mediated knockdown of MDMX increased *CDKN1A* (p21) expression, these results are consistent with the western blots results shown in chapter 5. The p21 protein level was increased significantly in JEG-3, MRK-nu-1, MCF-7 (figure 5.12) and NGP (figure 5.6) cells by siRNA knockdown MDMX. MDMX not only promotes proteasomal degradation of p21 but it also regulates transcriptional of CDKN1A expression via p53 activation (Kruse and Gu, 2009). Knockdown of MDMX protein expression reactivates p53 activity and leads to increased down-stream target gene expression. The effect was minor but still show detectable transcriptional activation of p21. Similarly, MDMX and MDM2 is also reported to regulate p21 proteasomal degradation (Jin *et al.*, 2003; Jin *et al.*, 2008). A published study presented that 14-3-3gamma induced p21 via inhibition of MDMX-mediated proteasomal turnover independent of p53 after DNA damage induction (Lee and Lu, 2011). The level of 14-3-3gamma -MDMX complex increased in response to DNA damage whereas that of the MDMX-p21 complex declined leading to the induction of p21 in p53-null cells (Lee and Lu, 2011). MDMX might regulate *CDKN1A* expression via p53 dependent pathway but p21 protein degradation via a p53 independent pathway.

6.5.3 VGLL1 was the gene showing the highest increase in expression induced by MDMX knockdown

VGLL1 was the gene that increased the most, with over 4-fold change in gene expression after knockdown of MDMX by siRNA in MRK-nu-1 breast cancer cells. A search of the Sanger COSMIC database revealed *VGLL1* to be mutant in the MRK-nu-1 cell line. MRK-nu-1 cells have a coding missense mutation (p.R47K; c.140G>A) resulting in an arginine to lysine substitute in the *VGLL1* gene which is likely to have functional consequences. The position of the mutation is near the VGLL1-TEAD binding sites which are V41, H44, I45 (Pobbati *et al.*, 2012; Pobbati and Hong, 2013). The mutation and high expression of VGLL1 might result in the activation of cell proliferation via VGLL1. It might be an explanation for no net cell growth change in MRK-nu-1 cells after siRNA-mediated knockdown of MDMX in figure 5.5.

VGLL1 (Vestigial Like Family Member 1, Vestigial-like 1 in Drosophila) is a gene encoding a transcriptional co-activator structurally homologous to TAZ and YAP that modulates the Hippo pathway in Drosophila. VGLL1 is recognized as an oncogene, which has similar structure and function to TAZ and YAP in the Hippo signalling pathway (Pobbati *et al*., 2012; Mesrouze *et al*., 2014). *VGLL1* is located on Xq26.3. The protein encoded by this gene binds proteins of the TEA transcription factors (TEAD) through the Vg (vestigial) homology region found in its N-terminus. It may thus function as a specific coactivator for the mammalian Thyrotroph embryonic transcription factor family (TEFs). The TEAD transcription factors, the most downstream elements in the Hippo signaling pathway, are regulated by different cofactors, such as the VGLL proteins. Investigation of the interaction between VGLL1-derived peptides and human TEAD4 shows that, although it lacks a key secondary structure element required for tight binding by two other TEAD co-factors (YAP and TAZ), VGLL1-derived peptides bind to TEAD with nanomolar affinity (Pobbati *et al*., 2012; Mesrouze *et al*., 2014).

The Hippo signalling pathway controls organ size in animals through the regulation of cell proliferation and promoting apoptosis. Over-activation of the Hippo signalling pathway is linked to tumour development. The Hippo signalling pathway will be discussed further in chapter 7.2. The siRNA-mediated knockdown of MDMX showed higher efficacy in MRK-nu-1 cells, which may have been required to trigger increased *VGLL1* expression. Thus, when one oncogene, *MDM4(MDMX)*, was knocked down, the expression of another oncogene, *VGLL1*, was increased. This might indicate that tumour cells are able to survive p53-dependent growth inhibition and apoptosis by increasing the expression of an alternative oncogene that regulates a growth-promoting pathway. The *VGLL1* oncogene may play an important role in regulating and linking the Hippo signalling pathway and the p53-dependent pathway through MDMX.

Chapter 7 General Discussion

7.1 Does MDMX affect sensitivity to MDM2-p53 binding antagonists?

7.1.1 TP53 status and response to MDM2-p53 binding antagonists

Pre-clinical studies of MDM2 inhibitors as single agents or combination treatments have been reported in a wide range of cancers, such as neuroblastoma (Chen *et al.*, 2015), ovarian cancer (Mir *et al.*, 2013; Zanjirband *et al.*, 2016), renal carcinoma (Polanski *et al.*, 2014), breast cancer (Pechackova *et al.*, 2016). Clinical trials studies have also reported response to MDM2 inhibitors in acute myeloid leukemia (Reis *et al.*, 2016) and relapsed/refractory chronic lymphocytic leukemia and small cell lymphocytic leukemia (Andreeff *et al.*, 2016). MDM2 inhibitors have also been investigated across a wide range of tumours in pre-clinical and clinical trial research (figure 1.17) as signal agents and combinations with other drugs (chapter 1.7) According to the results of the present study, amplification and high expression of MDMX do not markedly reduce the efficacy of MDM2 antagonists and cells with amplification and high expression of MDMX are still responsive to MDM2 antagonists. This would suggest that MDMX status is not the main factor which needs to be a concern before treatment with MDM2 inhibitors in human cancer therapy.

The findings of this project for Nutlin-3 and RG7388 treatments show response and growth inhibition in the two *TP53* wild-type *MDMX* amplified cell lines (JEG-3 and MRK-nu-1) and MDMX high-expressing cell lines (NGP and MCF-7). These results are in agreement with those available for Nutlin-3a on the Sanger Cancer Genome Project website (figure 7.1), in which *TP53* status has by far the most influence on sensitivity to Nutlin-3a, while *MYCN* and *BRAF* alterations are also associated with sensitivity to Nutlin-3a (figure 7.1). The growth inhibition effect of Nutlin-3 from a previously published study (figure 7.2A) and GI_{50} values distribution in a wild panel of cell lines (figure 7.2B) show that cells carrying a *TP53* mutation, on average are more resistant to Nutlin-3 than cells with wild-type *TP53*. However, it is interesting to note that the alleged wild-type *TP53* cell lines have a much broader range of sensitivity, the distribution for which is bimodal, with a high proportion of the wild-type *TP53* cell lines having GI_{50} values for Nutlin-3a which overlap with those for the mutant *TP53* cell lines.

In reviewing the literature for other potential determinants of response to MDM2-p53 binding antagonists, it was noted that *MYCN*-amplified cell lines are sensitive to these inhibitors. It was reported that MYCN knockdown in neuroblastoma cell lines with wild-type p53 made them more resistant to the MDM2-p53 binding inhibitors, Nutlin-3 and MI-63 (Gamble *et al.*, 2012). This result shows that other cellular regulating proteins, like MYCN, could affect the response to MDM2-p53 binding antagonists. These observations for MYCN status are supported by data for response to Nutlin-3 on the Sanger Cancer Genome Project website (figure 7.1).

MDMX expression has been reported to be associated with sensitivity to MDM2/X-p53 binding co-inhibitor (Ray-Coquard *et al.*, 2012). High MDM2 expression and undetectable MDMX in the SJSA-1 cells were associated with resistance to RO5963, although RO5963 has similar and strong binding ability to both MDM2 and MDMX. *TP53* status is also the major factor in resistance to the co-inhibitors. However, selection for resistance to MDM2 inhibitors was found not to be associated with increased MDMX expression, which might be expected if MDMX expression was an important mediator of resistance to MDM2 inhibitors (Drummond *et al.*, 2016).
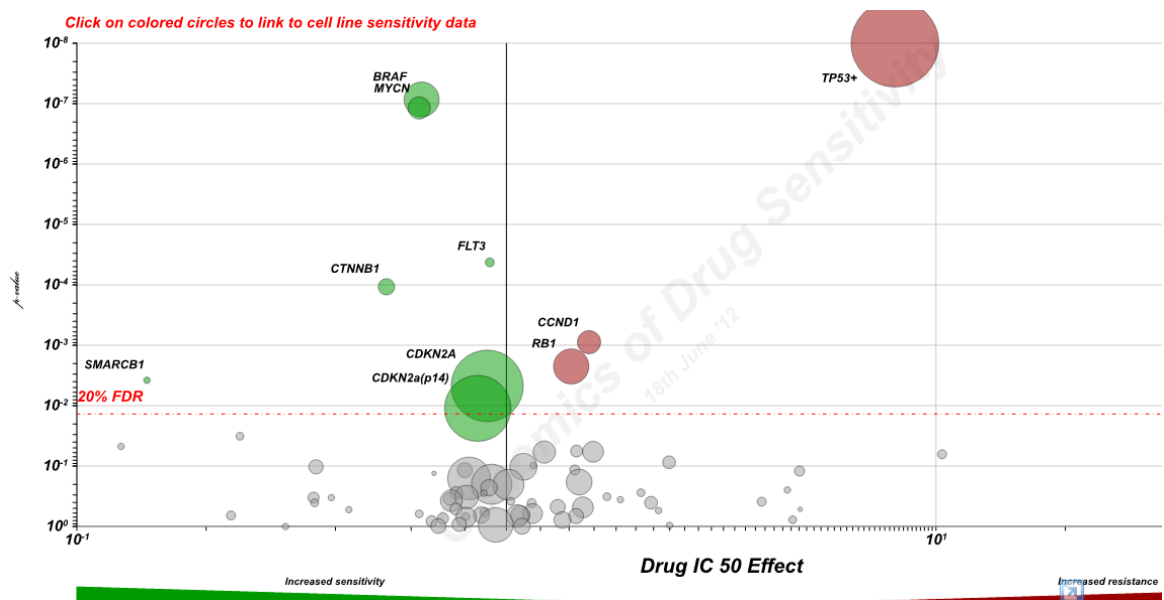
Figure 7.1. Volcano plot of the relationship of Nutlin-3a sensitivity to genetic alterations in cells (Sanger Cancer Genome Project website). Note the dominant association of *TP53* mutation to Nutlin-3a resistance. http://www.sanger.ac.uk/genetics/CGP/).
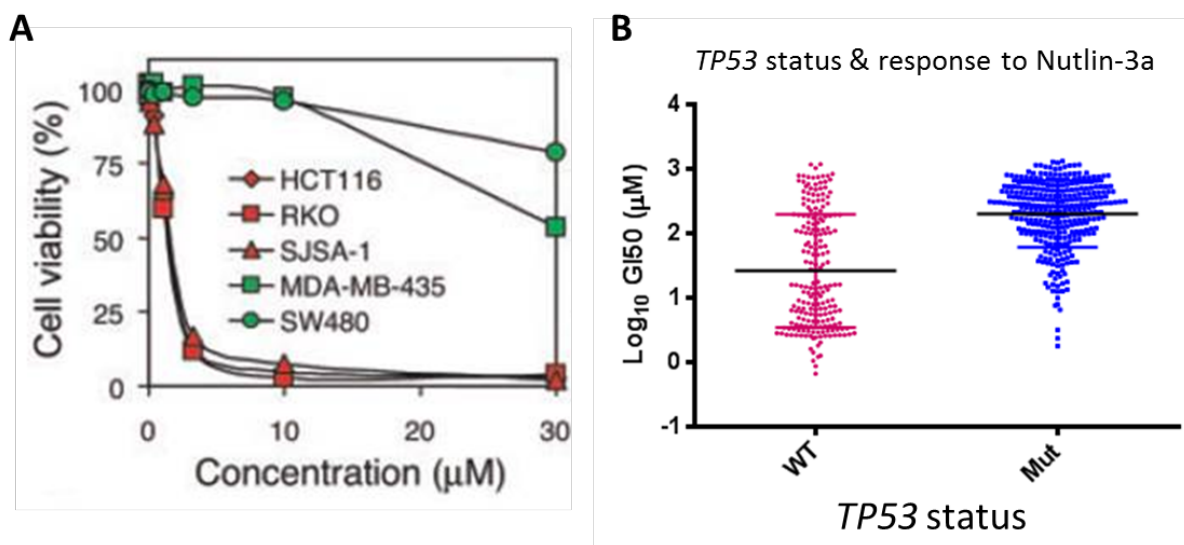
Figure 7.2. (A) Growth inhibition by Nutlin-3 treatment for wild-type p53 cell lines (HCT116, RKO and SJSA-1) and mutant p53 cell lines (MDA-MB-435 and SW480) (Vassilev *et al.*, 2004). (B) The GI$_{50}$ distributions of Nutlin-3 and *TP53* status for 527 cell lines on the Sanger data base. http://cancer.sanger.ac.uk/cosmic.

7.1.2 MDMX expression and response to MDM2-p53 binding antagonists

The results of this project have shown that *MDMX* amplification and high expression was not associated with resistance to MDM2-p53 binding antagonists. Suppression of MDMX expression showed a significant increase in sensitivity to the two MDM2 inhibitors in just one cell line, MRK-nu-1. In this case, the results did seem to be consistent with other research which suggests that MDMX is resistant to MDM2 inhibitors and that its inactivation is necessary to achieve full activation of p53 in tumour cells (Hu *et al.*, 2006; Patton *et al.*, 2006; Wade *et al.*, 2006; Hirose *et al.*, 2014). However, in the cases of other cell lines, the overall results indicated that suppression of MDMX expression did not significantly affect sensitivity or response to MDM2 inhibitors in either MDMX amplified or MDMX high-expressing cell lines. One neuroblastoma cell line, NGP, showed a decrease in sensitivity and apoptotic response to MDM2 inhibitors after suppression of MDMX expression.

Furthermore, the data mined from the Sanger database, shown in figure 7.3, supports the findings of this project, which is that MDMX expression is not associated with altered response to MDM2-p53 binding antagonists in a wide range of human cancer cell lines. The plot in figure 7.3A shows the increasing trend for increased expression of both MDM2 and MDMX to be associated with increased sensitivity to Nultin-3. A stronger trend is seen for MDM2 mRNA expression than for MDMX, and there is no evidence of an overall increase in resistance to be associated with MDMX expression. The GI_{50} values for the subset of mutant *TP53* cell lines were not associated with MDM2 and MDMX mRNA expression (figure 7.3B). The overall GI_{50} values of Nutlin-3 including wild-type and mutant p53 in Figure 7.3C also showed a more strongly dependent trend for MDM2 mRNA but a weaker similar trend for MDMX mRNA. For the *TP53* wild-type subset of cell lines, higher MDM2/MDMX mRNA is associated with increased sensitivity to Nutlin-3, as shown in Figure 7.3D. However, this ratio is driven by MDM2 expression changes and MDMX expression shows relatively little change across cell lines. Therefore, *TP53* status and MDM2 expression are the dominant factors associated with increased sensitivity to MDM2-p53 binding antagonists.
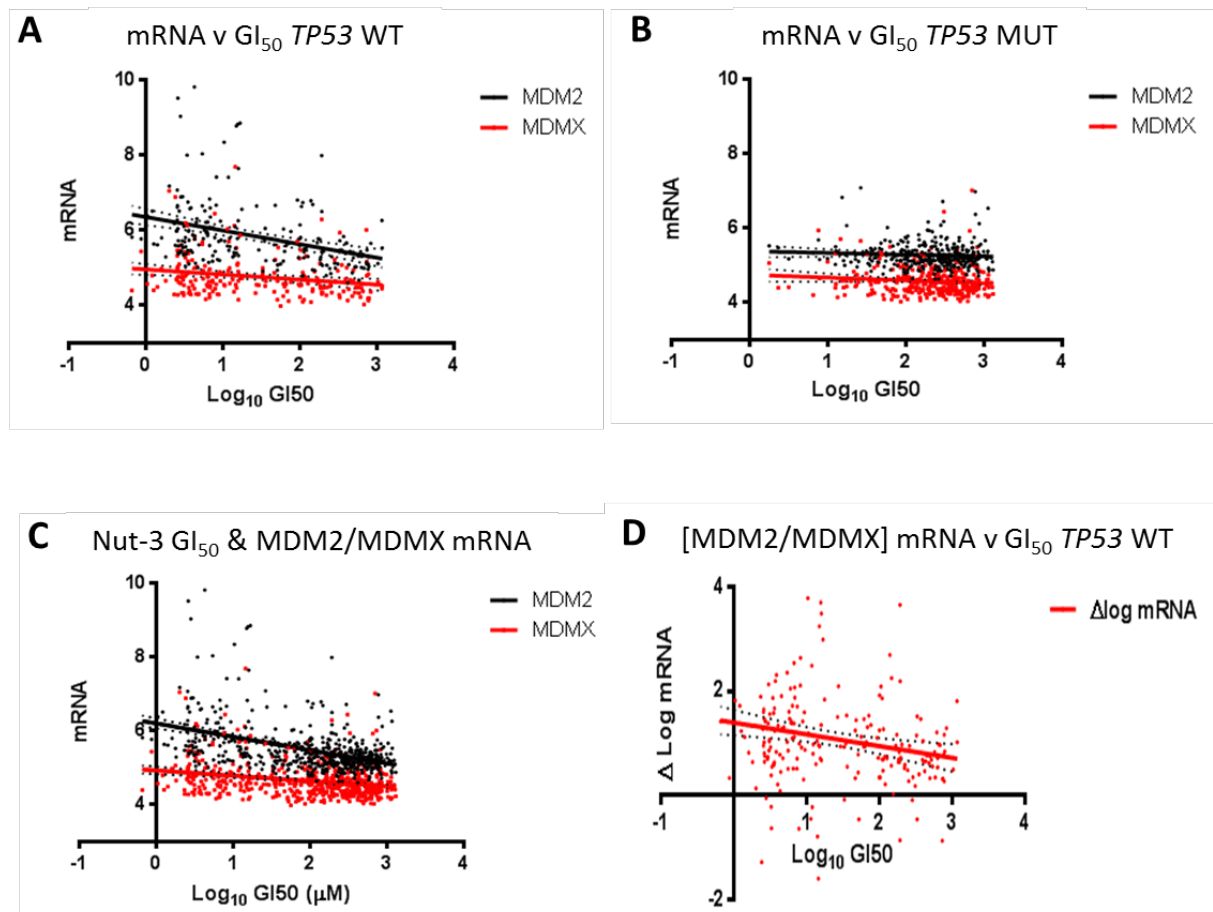
Figure 7.3. The dependence of Nutlin-3 GI$_{50}$ values on MDM2 and MDMX mRNA levels across a wide range of cell lines including wild-type *TP53* (A), mutant *TP53* (B), and both *TP53* wild-type and mutant (C) from Sanger database mining. (D) MDM2 and MDMX ratio of mRNA relative to Nutlin-3 GI$_{50}$ values. http://cancer.sanger.ac.uk/cosmic

7.1.3 Lentiviral shRNA and siRNA-mediated knockdown of MDMX expression

Cell lines amplified for and/or expressing high levels of the MDMX gene are nevertheless responsive to MDM2-p53 binding antagonists, and the response to these agents was not altered significantly by suppression of MDMX expression by lentiviral shRNA. Significant sensitisation to Nutlin-3 by siRNA knockdown was only seen for JEG-3 cells, although similar, but not statistically significant, trends were observed for MRK-nu-1 and MCF-7 (see figure 5.10 and table 5.2). Suppression of MDMX expression by lentiviral shRNA and siRNA was associated with increased sensitivity to MDM2-p53 binding antagonists for growth inhibition apoptosis and cell cycle arrest in the case of JEG-3 cells. It shows the effect of suppressing MDMX expression on the response to MDM2 inhibitors was cell line-dependent also dependent on the extent to which MDMX expression could be suppressed. Suppression of MDMX expression by lentiviral shRNA and siRNA was also associated with decreased response and increased resistance to the RO5963 MDM2/X-p53 binding dual antagonist, which was converse to the effect on MDM2-p53 binding antagonists.

Lentiviral shRNA knockdown showed more difficulties in suppressing MDMX expression successfully in all of the cell lines which have been tested. Although it might be a long-term and switchable knockdown system with less damage to cells, it was hard to achieve a high efficiency of suppression of MDMX expression in the cell lines apart from MRK-nu-1. The short-term siRNA-mediated knockdown of MDMX gave successful and efficient knockdown in the cell lines compared to the lentiviral shRNA system. The less efficient shRNA-mediated MDMX knockdown might be an explanation for why there was no cell growth effect after knockdown of MDMX expression by lentiviral shRNA. Similarly, the gene expression profiles for lentiviral shRNA-mediated knockdown of MDMX showed few and smaller significant changes in gene expression compared to the effect of siRNA knockdown. The MDMX suppression effect achieved by either shRNA or siRNA might not be big enough to produce biologically significant cellular changes. In further studies, it would be interesting to use CRISPR methods to investigate the consequences of completely deleting *MDMX*.

7.2   The role of MDMX and VGLL1 in the Hippo pathway

The Hippo signalling pathway is a growth and organ size control pathway that regulates cell proliferation and stem cell function as illustrated in figure 7.4 (Pan, 2010; Johnson and Halder, 2014). The name of the pathway comes from one of the protein kinases, Hippo (Hpo), in Drosophila development, because of the hippopotamus-like phenotype of the mutated body parts (Harvey *et al.*, 2003; Pantalacci *et al.*, 2003; Udan *et al.*, 2003; Wu *et al.*, 2003). Over-activation of its downstream YAP (Yes-associated protein) and TAZ (PDZ-binding motif) contribute to cancer development and drug resistance. Activated YAP/TAZ binds to TEADs (TEA domain transcription factor 1-4) as a complex to promote the expression of target genes involved in cell proliferation and anti-apoptosis. YAP/TAZ are regulated and phosphorylated in the cytoplasm by kinase Lats1/2 (Large tumour suppressor 1/2) and then degraded by 14-3-3 protein (figure 7.4) (Chan *et al.*, 2011; Johnson and Halder, 2014). YAP overexpression derived from the potent growth-regulatory activity of the Hippo signalling pathway leads to a dramatic increase in organ size shown in figure 7.4B&C (Pan, 2010).

Previous study established that LATS2 binds and inhibits MDM2 E3 ligase activity resulting in activation of p53. It shows a positive feedback loop between p53 and LATS2 by inhibition of MDM2 (Aylon *et al.*, 2006). It has been reported that silencing of LATS1 and LATS2 in non-transformed mammary epithelial cells reduces p53 phosphorylation (Furth *et al.*, 2015). Moreover, LATS down-regulation promotes p53-dependent cell migration (Furth *et al.*, 2015). LATS2 was shown to stabilize p53 by binding and inhibiting MDM2 in G1 tetraploidy checkpoint (Aylon *et al.*, 2006; Visser and Yang, 2010). Recent research demonstrated that the Hippo kinases, LATS1 and LATS2, control human breast cell fate YAP/TAZ independently though intrinsic and paracrine mechanisms via ERα (Britschgi *et al.*, 2017).

VGLL1 (vestigial-like family member 1), which is a structural and functional homolog of YAP/TAZ, also binds to transcriptional enhancer TEAD as a complex by protein-protein interaction to promote anchorage-independent cell growth in cancer progression (Figure 7.5) (Pobbati *et al.*, 2012; Pobbati and Hong, 2013). Previous studies have showed that a subset of YAP/TAZ-responsive genes are not activated

by VGLL1. This finding suggests that VGLL1 and YAP/TAZ have different transcriptional specificity targeting different genes, which also has been observed in *Drosophila* (Pobbati *et al*., 2012). The Hippo signalling pathway is the main up regulating pathway to control YAP/TAZ-TEAD interaction and TEAD dependent transcriptional activity.

Several publications have reported that over expression of oncogene *VGLL1* has the potential to promote cancer progression, and it has also been reported that nuclear *VGLL1* expression was observed in over 40% of triple-negative (TN) breast cancer and over 50% in BRCA1-assciated positive TN breast carcinomas in primary human tumours (Castilla *et al*., 2014). The data from this published research showed MDMX high expression in triple-negative primary breast tumour (Castilla *et al*., 2014). Moreover, *VGLL1* expression is associated with reduced overall survival (Castilla *et al*., 2014). It also has been reported that the Hippo pathway plays an important contributory role in the cell fate of human breast cells and tumour progression. The results from the current study showed that a significant increase of VGLL1 expression occurs after knockdown of MDMX. MDMX might contribute to a negative regulation of VGLL1 and affect VGLL1-TEAD downstream transcriptional activation in cell proliferation especially in tumours with VGLL1 overexpression (Figure 7.5). However, there is a lack of knowledge about the interaction between the p53-dependent and Hippo pathways.
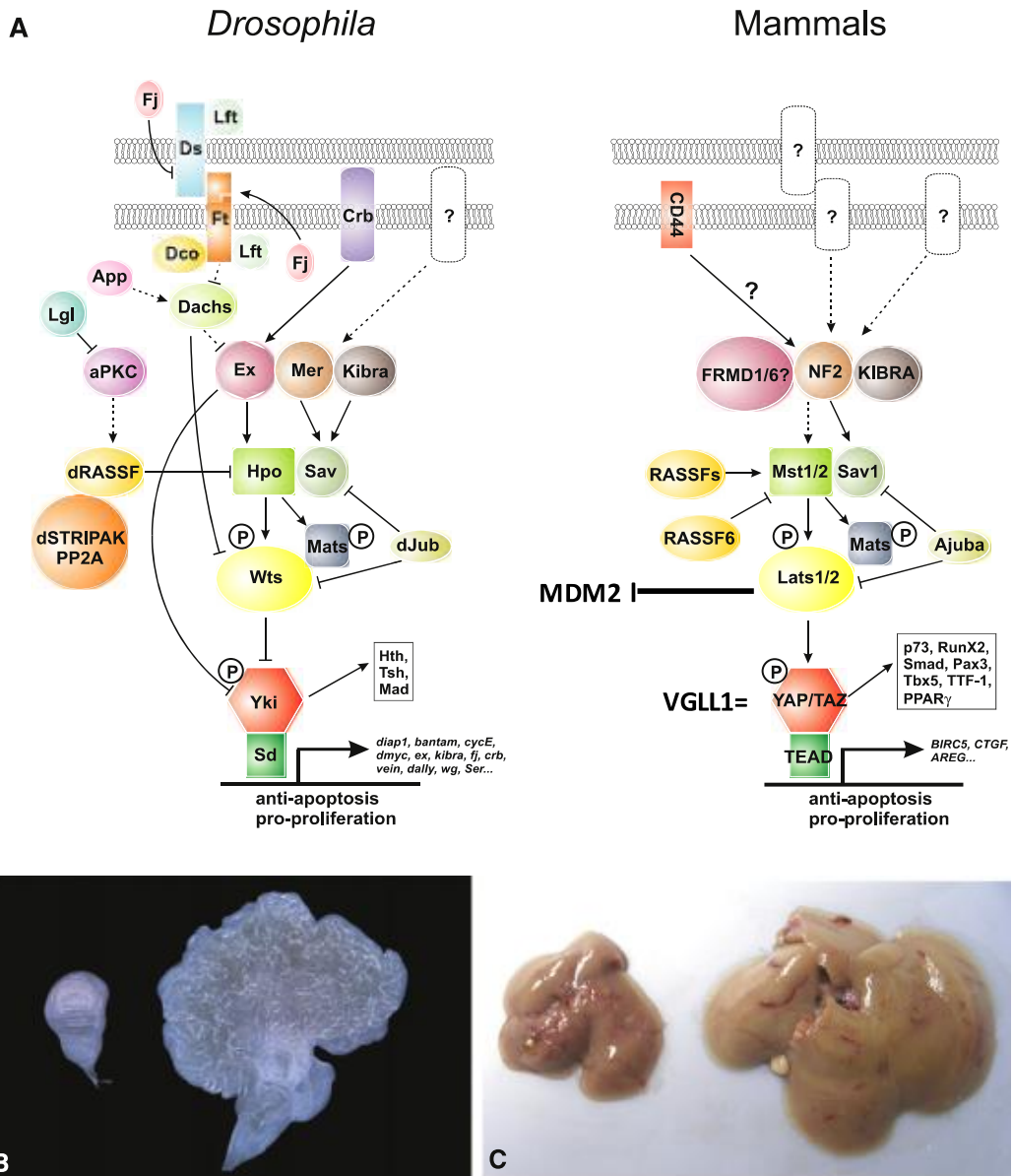
Figure 7.4. (A) The Hippo Signalling Network in Drosophila and Mammals. (B) A normal (left) and a *yki*-overexpressing (right) *Drosophila* wing imaginal disc (Huang *et al.*, 2005). (C) A normal (left) and a YAP-overexpressing (right) mouse liver (Dong *et al.*, 2007). The dramatic increase in organ size induced by Yki/YAP overexpression illustrates the potent growth-regulatory activity of Hippo signalling in *Drosophila* and mammals (Pan, 2010)**.**
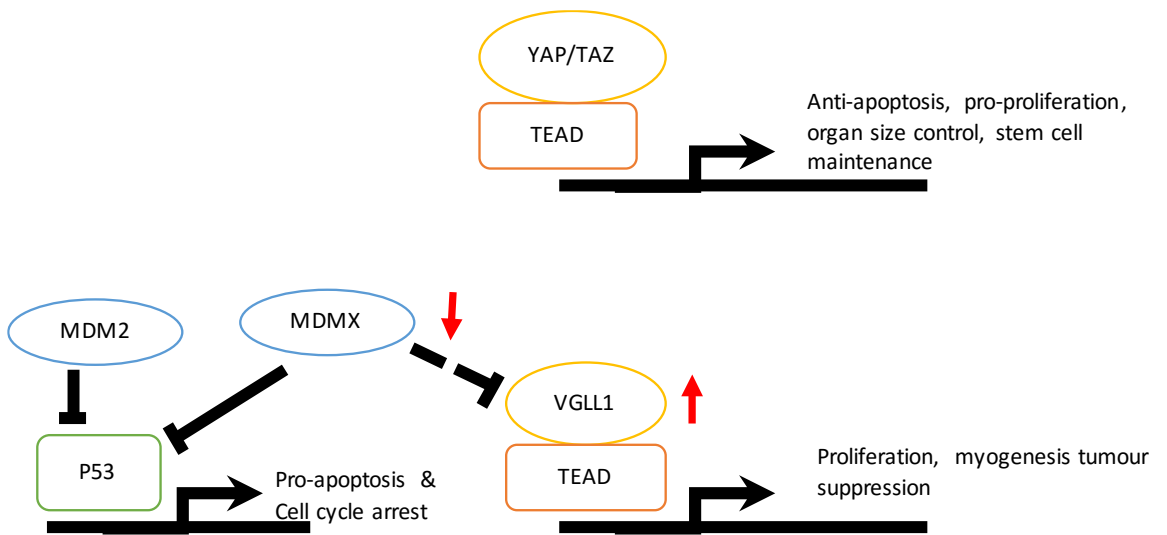
Figure 7.5. Proposed model for the regulation of p53-MDMX and VGLL1-TEAD dependent transcriptional activity. Activated YAP/TAZ binds to TEADs to promote target genes involved in cell proliferation and anti-apoptosis. VGLL1 also binds to transcriptional enhancer TEAD to promote anchorage-independent cell growth in cancer progression. Suppression of MDMX increases VGLL1 expression leading to transcriptional activation of VGLL1-TEAD counteracting p53-dependent apoptosis and cell cycle arrest.

7.3   Overall conclusion

In summary, *TP53* status is the major factor influencing response to MDM2-p53 binding antagonists and the MDM2/X-p53 binding co-inhibitor. Cell lines amplified for and/or expressing high levels of the *MDMX* gene are nevertheless responsive to MDM2-p53 binding antagonists. The effect of MDMX knockdown varied according to cell line and which MDM2-p53 binding antagonist was being tested, but overall, suppression of MDMX had minimal effect on the response to MDM2-p53 binding antagonists. The MDM2/MDMX-p53 co-inhibitor showed better efficacy with high MDMX-expressing cells and was more effective for growth inhibition than MDMX knockdown. Highly efficient suppression of MDMX expression increased *TP53*-dependent downstream activity. MDMX might play an important role in regulating the link between Hippo signalling pathway and p53-dependent pathway via the VGLL1 oncoprotein.

7.4 Future work

In further studies, CRISPR could be used to completely delete *MDMX* in order to investigate the contribution of MDMX function relative to P53-dependent and independent regulation as a therapeutic target in human cancer. A stapled peptide MDM2/X co-inhibitor has been developed and tested in a Phase I clinical study. It would be interesting to test the stapled peptide co-inhibitor or more potent MDM2/X co-inhibitors and moreover test the drug combination with WIP1 inhibitors to see if the potentiating effect on MDM2 inhibitors is also seen with MDM1/X co-inhibitors.

This study has found and validated that the mRNA expression of VGLL1 is increased by siRNA-mediated knockdown of MDMX in MRK-nu-1. More research is needed to better understand the importance of VGLL1 in relation to MDMX and its connection effect on the p53 pathway. More evidence of VGLL1 induction after siRNA-mediated MDMX knockdown needs to be investigated in other cell lines. The protein level expression of VGLL1 and the Hippo pathway down-stream activity need to be tested and investigated on a wider panel of cell lines. The other VGLL family members are also worth studying, as well as the relationship between the MDMX-p53 and the Hippo signalling pathways.

References

Abida, W.M., Nikolaev, A., Zhao, W., Zhang, W. and Gu, W. (2007) 'FBXO11 promotes the Neddylation of p53 and inhibits its transcriptional activity', *J Biol Chem*, 282(3), pp. 1797-804.

Andreeff, M., Kelly, K.R., Yee, K., Assouline, S., Strair, R., Popplewell, L., Bowen, D., Martinelli, G., Drummond, M.W., Vyas, P., Kirschbaum, M., Iyer, S.P., Ruvolo, V., Gonzalez, G.M., Huang, X., Chen, G., Graves, B., Blotner, S., Bridge, P., Jukofsky, L., Middleton, S., Reckner, M., Rueger, R., Zhi, J., Nichols, G. and Kojima, K. (2016) 'Results of the Phase I Trial of RG7112, a Small-Molecule MDM2 Antagonist in Leukemia', *Clin Cancer Res*, 22(4), pp. 868-76.

Arya, A.K., El-Fert, A., Devling, T., Eccles, R.M., Aslam, M.A., Rubbi, C.P., Vlatkovic, N., Fenwick, J., Lloyd, B.H., Sibson, D.R., Jones, T.M. and Boyd, M.T. (2010) 'Nutlin-3, the small-molecule inhibitor of MDM2, promotes senescence and radiosensitises laryngeal carcinoma cells harbouring wild-type p53', *Br J Cancer*, 103(2), pp. 186-95.

Aylon, Y., Michael, D., Shmueli, A., Yabuta, N., Nojima, H. and Oren, M. (2006) 'A positive feedback loop between the p53 and Lats2 tumor suppressors prevents tetraploidization', *Genes Dev*, 20(19), pp. 2687-700.

Banin, S., Moyal, L., Shieh, S., Taya, Y., Anderson, C.W., Chessa, L., Smorodinsky, N.I., Prives, C., Reiss, Y., Shiloh, Y. and Ziv, Y. (1998) 'Enhanced phosphorylation of p53 by ATM in response to DNA damage', *Science*, 281(5383), pp. 1674-7.

Barboza, J.A., Iwakuma, T., Terzian, T., El-Naggar, A.K. and Lozano, G. (2008) 'Mdm2 and Mdm4 loss regulates distinct p53 activities', *Mol Cancer Res*, 6(6), pp. 947-54.

Bardot, B., Bouarich-Bourimi, R., Leemput, J., Lejour, V., Hamon, A., Plancke, L., Jochemsen, A.G., Simeonova, I., Fang, M. and Toledo, F. (2015) 'Mice engineered for an obligatory Mdm4 exon skipping express higher levels of the Mdm4-S isoform but exhibit increased p53 activity', *Oncogene*, 34(22), pp. 2943-8.

Bartel, F., Schulz, J., Bohnke, A., Blumke, K., Kappler, M., Bache, M., Schmidt, H., Wurl, P., Taubert, H. and Hauptmann, S. (2005) 'Significance of HDMX-S (or MDM4) mRNA splice variant overexpression and HDMX gene amplification on primary soft tissue sarcoma prognosis', *Int J Cancer*, 117(3), pp. 469-75.

Baylin, S.B. (2005) 'DNA methylation and gene silencing in cancer', *Nat Clin Pract Oncol*, 2 Suppl 1, pp. S4-11.

Bernal, F., Wade, M., Godes, M., Davis, T.N., Whitehead, D.G., Kung, A.L., Wahl, G.M. and Walensky, L.D. (2010) 'A stapled p53 helix overcomes HDMX-mediated suppression of p53', *Cancer Cell*, 18(5), pp. 411-22.

Bista, M., Petrovich, M. and Fersht, A.R. (2013) 'MDMX contains an autoinhibitory sequence element', *Proc Natl Acad Sci U S A*, 110(44), pp. 17814-9.

Bossi, G., Lapi, E., Strano, S., Rinaldo, C., Blandino, G. and Sacchi, A. (2006) 'Mutant p53 gain of function: reduction of tumor malignancy of human cancer cell lines through abrogation of mutant p53 expression', *Oncogene*, 25(2), pp. 304-9.

Bottger, A., Bottger, V., Garcia-Echeverria, C., Chene, P., Hochkeppel, H.K., Sampson, W., Ang, K., Howard, S.F., Picksley, S.M. and Lane, D.P. (1997) 'Molecular characterization of the hdm2-p53 interaction', *J Mol Biol*, 269(5), pp. 744-56.

Boyd, M.T., Vlatkovic, N. and Haines, D.S. (2000a) 'A novel cellular protein (MTBP) binds to MDM2 and induces a G1 arrest that is suppressed by MDM2', *J Biol Chem*, 275(41), pp. 31883-90.

Boyd, M.T., Vlatkovic, N. and Rubbi, C.P. (2011) 'The nucleolus directly regulates p53 export and degradation', *J Cell Biol*, 194(5), pp. 689-703.

Boyd, M.T., Zimonjic, D.B., Popescu, N.C., Athwal, R. and Haines, D.S. (2000b) 'Assignment of the MDM2 binding protein gene (MTBP) to human chromosome band 8q24 by in situ hybridization', *Cytogenet Cell Genet*, 90(1-2), pp. 64-5.

Boyd, S.D., Tsai, K.Y. and Jacks, T. (2000c) 'An intact HDM2 RING-finger domain is required for nuclear exclusion of p53', *Nat Cell Biol*, 2(9), pp. 563-8.

Bozzi, F., Conca, E., Laurini, E., Posocco, P., Lo Sardo, A., Jocolle, G., Sanfilippo, R., Gronchi, A., Perrone, F., Tamborini, E., Pelosi, G., Pierotti, M.A., Maestro, R., Pricl, S. and Pilotti, S. (2013) 'In vitro and in silico studies of MDM2/MDMX isoforms predict Nutlin-3A sensitivity in well/de-differentiated liposarcomas', *Lab Invest*, 93(11), pp. 1232-40.

Brady, M., Vlatkovic, N. and Boyd, M.T. (2005) 'Regulation of p53 and MDM2 activity by MTBP', *Mol Cell Biol*, 25(2), pp. 545-53.

Britschgi, A., Duss, S., Kim, S., Couto, J.P., Brinkhaus, H., Koren, S., De Silva, D., Mertz, K.D., Kaup, D., Varga, Z., Voshol, H., Vissieres, A., Leroy, C., Roloff, T., Stadler, M.B., Scheel, C.H., Miraglia, L.J., Orth, A.P., Bonamy, G.M., Reddy, V.A. and Bentires-Alj, M. (2017) 'The Hippo kinases LATS1 and 2 control human breast cell fate via crosstalk with ERalpha', *Nature*, 541(7638), pp. 541-545.

Brooks, C.L. and Gu, W. (2003) 'Ubiquitination, phosphorylation and acetylation: the molecular basis for p53 regulation', *Curr Opin Cell Biol*, 15(2), pp. 164-71.

Brooks, C.L. and Gu, W. (2011) 'p53 regulation by ubiquitin', *FEBS Lett*, 585(18), pp. 2803-9.

Burgess, A., Chia, K.M., Haupt, S., Thomas, D., Haupt, Y. and Lim, E. (2016) 'Clinical Overview of MDM2/X-Targeted Therapies', *Front Oncol*, 6, p. 7.

Canner, J.A., Sobo, M., Ball, S., Hutzen, B., DeAngelis, S., Willis, W., Studebaker, A.W., Ding, K., Wang, S., Yang, D. and Lin, J. (2009) 'MI-63: a novel small-molecule inhibitor targets MDM2 and induces apoptosis in embryonal and alveolar rhabdomyosarcoma cells with wild-type p53', *Br J Cancer*, 101(5), pp. 774-81.

Cao, C., Shinohara, E.T., Subhawong, T.K., Geng, L., Kim, K.W., Albert, J.M., Hallahan, D.E. and Lu, B. (2006) 'Radiosensitization of lung cancer by nutlin, an inhibitor of murine double minute 2', *Mol Cancer Ther*, 5(2), pp. 411-7.

Carter, B.Z., Mak, D.H., Schober, W.D., Koller, E., Pinilla, C., Vassilev, L.T., Reed, J.C. and Andreeff, M. (2010) 'Simultaneous activation of p53 and inhibition of XIAP enhance the activation of apoptosis signaling pathways in AML', *Blood*, 115(2), pp. 306-14.

Carter, S., Bischof, O., Dejean, A. and Vousden, K.H. (2007) 'C-terminal modifications regulate MDM2 dissociation and nuclear export of p53', *Nat Cell Biol*, 9(4), pp. 428-35.

Castilla, M.A., Lopez-Garcia, M.A., Atienza, M.R., Rosa-Rosa, J.M., Diaz-Martin, J., Pecero, M.L., Vieites, B., Romero-Perez, L., Benitez, J., Calcabrini, A. and Palacios, J. (2014) 'VGLL1 expression is associated with a triple-negative basal-like phenotype in breast cancer', *Endocr Relat Cancer*, 21(4), pp. 587-99.

Cerami, E., Gao, J., Dogrusoz, U., Gross, B.E., Sumer, S.O., Aksoy, B.A., Jacobsen, A., Byrne, C.J., Heuer, M.L., Larsson, E., Antipin, Y., Reva, B., Goldberg, A.P., Sander, C. and Schultz, N. (2012) 'The cBio cancer genomics portal: an open platform for exploring multidimensional cancer genomics data', *Cancer Discov*, 2(5), pp. 401-4.

Chan, S.W., Lim, C.J., Chen, L., Chong, Y.F., Huang, C., Song, H. and Hong, W. (2011) 'The hippo pathway in biological control and cancer development', *Journal of Cellular Physiology*, 226, pp. 928-939.

Chandler, D.S., Singh, R.K., Caldwell, L.C., Bitler, J.L. and Lozano, G. (2006) 'Genotoxic stress induces coordinately regulated alternative splicing of the p53 modulators MDM2 and MDM4', *Cancer Res*, 66(19), pp. 9502-8.

Chang, Y.S., Graves, B., Guerlavais, V., Tovar, C., Packman, K., To, K.H., Olson, K.A., Kesavan, K., Gangurde, P., Mukherjee, A., Baker, T., Darlak, K., Elkin, C., Filipovic, Z., Qureshi, F.Z., Cai, H., Berry, P., Feyfant, E., Shi, X.E., Horstick, J., Annis, D.A., Manning, A.M., Fotouhi, N., Nash, H., Vassilev, L.T. and Sawyer, T.K. (2013) 'Stapled alpha-helical peptide drug development: a potent dual inhibitor of MDM2 and MDMX for p53-dependent cancer therapy', *Proc Natl Acad Sci U S A*, 110(36), pp. E3445-54.

Chavez-Reyes, A., Parant, J.M., Amelse, L.L., de Oca Luna, R.M., Korsmeyer, S.J. and Lozano, G. (2003) 'Switching mechanisms of cell death in mdm2- and mdm4-null mice by deletion of p53 downstream targets', *Cancer Res*, 63(24), pp. 8664-9.

Chehab, N.H., Malikzay, A., Appel, M. and Halazonetis, T.D. (2000) 'Chk2/hCds1 functions as a DNA damage checkpoint in G(1) by stabilizing p53', *Genes Dev*, 14(3), pp. 278-88.

Chen, H., Liao, S.B., Cheung, M.P., Chow, P.H., Cheung, A.L. and O, W.S. (2012) 'Effects of sperm DNA damage on the levels of RAD51 and p53 proteins in zygotes and 2-cell embryos sired by golden hamsters without the major accessory sex glands', *Free Radic Biol Med*, 53(4), pp. 885-92.

Chen, L., Gilkes, D.M., Pan, Y., Lane, W.S. and Chen, J. (2005a) 'ATM and Chk2-dependent phosphorylation of MDMX contribute to p53 activation after DNA damage', *EMBO J*, 24(19), pp. 3411-22.

Chen, L., Li, C., Pan, Y. and Chen, J. (2005b) 'Regulation of p53-MDMX interaction by casein kinase 1 alpha', *Mol Cell Biol*, 25(15), pp. 6509-20.

Chen, L., Rousseau, R.F., Middleton, S.A., Nichols, G.L., Newell, D.R., Lunec, J. and Tweddle, D.A. (2015) 'Pre-clinical evaluation of the MDM2-p53 antagonist RG7388 alone and in combination with chemotherapy in neuroblastoma', *Oncotarget*, 6(12), pp. 10207-21.

Chen, L., Yin, H., Farooqi, B., Sebti, S., Hamilton, A.D. and Chen, J. (2005c) 'p53 alpha-Helix mimetics antagonize p53/MDM2 interaction and activate p53', *Mol Cancer Ther*, 4(6), pp. 1019-25.

Chipuk, J.E., Bouchier-Hayes, L., Kuwana, T., Newmeyer, D.D. and Green, D.R. (2005) 'PUMA couples the nuclear and cytoplasmic proapoptotic function of p53', *Science*, 309(5741), pp. 1732-5.

Chuikov, S., Kurash, J.K., Wilson, J.R., Xiao, B., Justin, N., Ivanov, G.S., McKinney, K., Tempst, P., Prives, C., Gamblin, S.J., Barlev, N.A. and Reinberg, D. (2004) 'Regulation of p53 activity through lysine methylation', *Nature*, 432(7015), pp. 353-60.

Chun, H.H. and Gatti, R.A. (2004) 'Ataxia-telangiectasia, an evolving phenotype', *DNA Repair (Amst)*, 3(8-9), pp. 1187-96.

Clark, S.J. and Melki, J. (2002) 'DNA methylation and gene silencing in cancer: which is the guilty party?', *Oncogene*, 21(35), pp. 5380-7.

Clark, T.A., Schweitzer, A.C., Chen, T.X., Staples, M.K., Lu, G., Wang, H., Williams, A. and Blume, J.E. (2007) 'Discovery of tissue-specific exons using comprehensive human exon microarrays', *Genome Biol*, 8(4), p. R64.

Croce, C.M. (2008) 'Oncogenes and cancer', *N Engl J Med*, 358(5), pp. 502-11.

Dagnell, M., Frijhoff, J., Pader, I., Augsten, M., Boivin, B., Xu, J., Mandal, P.K., Tonks, N.K., Hellberg, C., Conrad, M., Arner, E.S. and Ostman, A. (2013) 'Selective activation of oxidized PTP1B by the thioredoxin system modulates PDGF-beta receptor tyrosine kinase signaling', *Proc Natl Acad Sci U S A*, 110(33), pp. 13398-403.

Danovi, D., Meulmeester, E., Pasini, D., Migliorini, D., Capra, M., Frenk, R., de Graaf, P., Francoz, S., Gasparini, P., Gobbi, A., Helin, K., Pelicci, P.G., Jochemsen, A.G. and Marine, J.C. (2004) 'Amplification of Mdmx (or Mdm4) directly contributes to tumor formation by inhibiting p53 tumor suppressor activity', *Mol Cell Biol*, 24(13), pp. 5835-43.

Ding, Q., Zhang, Z., Liu, J.J., Jiang, N., Zhang, J., Ross, T.M., Chu, X.J., Bartkovitz, D., Podlaski, F., Janson, C., Tovar, C., Filipovic, Z.M., Higgins, B., Glenn, K., Packman, K., Vassilev, L.T. and Graves, B. (2013) 'Discovery of RG7388, a potent and selective p53-MDM2 inhibitor in clinical development', *J Med Chem*, 56(14), pp. 5979-83.

Dong, J., Feldmann, G., Huang, J., Wu, S., Zhang, N., Comerford, S.A., Gayyed, M.F., Anders, R.A., Maitra, A. and Pan, D. (2007) 'Elucidation of a universal size-control mechanism in Drosophila and mammals', *Cell*, 130(6), pp. 1120-33.

Drummond, C.J., Esfandiari, A., Liu, J., Lu, X., Hutton, C., Jackson, J., Bennaceur, K., Xu, Q., Makimanejavali, A.R., Del Bello, F., Piergentili, A., Newell, D.R., Hardcastle, I.R., Griffin, R.J. and Lunec, J. (2016) 'TP53 mutant MDM2-amplified cell lines selected for resistance to MDM2-p53 binding antagonists retain sensitivity to ionizing radiation', *Oncotarget*.

Esfandiari, A., Hawthorne, T.A., Nakjang, S. and Lunec, J. (2016) 'Chemical Inhibition of Wild-Type p53-Induced Phosphatase 1 (WIP1/PPM1D) by GSK2830371 Potentiates the Sensitivity to MDM2 Inhibitors in a p53-Dependent Manner', *Mol Cancer Ther*, 15(3), pp. 379-91.

Fecher, L.A., Amaravadi, R.K. and Flaherty, K.T. (2008) 'The MAPK pathway in melanoma', *Curr Opin Oncol*, 20(2), pp. 183-9.

Fiszer-Kierzkowska, A., Vydra, N., Wysocka-Wycisk, A., Kronekova, Z., Jarzab, M., Lisowska, K.M. and Krawczyk, Z. (2011) 'Liposome-based DNA carriers may induce cellular stress response and change gene expression pattern in transfected cells', *BMC Mol Biol*, 12, p. 27.

Francoz, S., Froment, P., Bogaerts, S., De Clercq, S., Maetens, M., Doumont, G., Bellefroid, E. and Marine, J.C. (2006) 'Mdm4 and Mdm2 cooperate to inhibit p53 activity in proliferating and quiescent cells in vivo', *Proc Natl Acad Sci U S A*, 103(9), pp. 3232-7.

Furet, P., Masuya, K., Kallen, J., Stachyra-Valat, T., Ruetz, S., Guagnano, V., Holzer, P., Mah, R., Stutz, S., Vaupel, A., Chene, P., Jeay, S. and Schlapbach, A. (2016) 'Discovery of a novel class of highly potent inhibitors of the p53-MDM2 interaction by structure-based design starting from a conformational argument', *Bioorg Med Chem Lett*, 26(19), pp. 4837-41.

Furth, N., Ben-Moshe, N.B., Pozniak, Y., Porat, Z., Geiger, T., Domany, E., Aylon, Y. and Oren, M. (2015) 'Down-regulation of LATS kinases alters p53 to promote cell migration', *Genes and Development*, 29, pp. 2325-2330.

Gamble, L. (2011) *MYCN and the p53-MDM2/MDMX-p14ARF network in neuroblastoma and response to MDM2-p53 antagonists*. Newcastle University.

Gamble, L.D., Kees, U.R., Tweddle, D.A. and Lunec, J. (2012) 'MYCN sensitizes neuroblastoma to the MDM2-p53 antagonists Nutlin-3 and MI-63', *Oncogene*, 31(6), pp. 752-63.

Ganguli, G. and Wasylyk, B. (2003) 'p53-independent functions of MDM2', *Mol Cancer Res*, 1(14), pp. 1027-35.

Gannon, H.S. and Jones, S.N. (2012) 'Using Mouse Models to Explore MDM-p53 Signaling in Development, Cell Growth, and Tumorigenesis', *Genes Cancer*, 3(3-4), pp. 209-18.

Gao, J., Aksoy, B.A., Dogrusoz, U., Dresdner, G., Gross, B., Sumer, S.O., Sun, Y., Jacobsen, A., Sinha, R., Larsson, E., Cerami, E., Sander, C. and Schultz, N. (2013) 'Integrative analysis of complex cancer genomics and clinical profiles using the cBioPortal', *Sci Signal*, 6(269), p. pl1.

Gardina, P.J., Clark, T.A., Shimada, B., Staples, M.K., Yang, Q., Veitch, J., Schweitzer, A., Awad, T., Sugnet, C., Dee, S., Davies, C., Williams, A. and Turpaz, Y. (2006) 'Alternative splicing and differential gene expression in colon cancer detected by a whole genome exon array', *BMC Genomics*, 7, p. 325.

Gembarska, A., Luciani, F., Fedele, C., Russell, E.A., Dewaele, M., Villar, S., Zwolinska, A., Haupt, S., de Lange, J., Yip, D., Goydos, J., Haigh, J.J., Haupt, Y., Larue, L., Jochemsen, A., Shi, H., Moriceau, G., Lo, R.S., Ghanem, G., Shackleton, M., Bernal, F. and Marine, J.C. (2012) 'MDM4 is a key therapeutic target in cutaneous melanoma', *Nat Med*, 18(8), pp. 1239-47.

Geyer, R.K., Yu, Z.K. and Maki, C.G. (2000) 'The MDM2 RING-finger domain is required to promote p53 nuclear export', *Nat Cell Biol*, 2(9), pp. 569-73.

Giacinti, C. and Giordano, A. (2006) 'RB and cell cycle progression', *Oncogene*, 25(38), pp. 5220-7.

Gilkes, D.M. and Chen, J. (2007) 'Distinct roles of MDMX in the regulation of p53 response to ribosomal stress', *Cell Cycle*, 6(2), pp. 151-5.

Gilkes, D.M., Chen, L. and Chen, J. (2006) 'MDMX regulation of p53 response to ribosomal stress', *EMBO J*, 25(23), pp. 5614-25.

Gilkes, D.M., Pan, Y., Coppola, D., Yeatman, T., Reuther, G.W. and Chen, J. (2008) 'Regulation of MDMX expression by mitogenic signaling', *Mol Cell Biol*, 28(6), pp. 1999-2010.

Goh, A.M., Coffill, C.R. and Lane, D.P. (2011) 'The role of mutant p53 in human cancer', *J Pathol*, 223(2), pp. 116-26.

Goldberg, Z., Vogt Sionov, R., Berger, M., Zwang, Y., Perets, R., Van Etten, R.A., Oren, M., Taya, Y. and Haupt, Y. (2002) 'Tyrosine phosphorylation of Mdm2 by c-Abl: implications for p53 regulation', *EMBO J*, 21(14), pp. 3715-27.

Goodman, R.H. and Smolik, S. (2000) 'CBP/p300 in cell growth, transformation, and development', *Genes Dev*, 14(13), pp. 1553-77.

Graves, B., Thompson, T., Xia, M., Janson, C., Lukacs, C., Deo, D., Di Lello, P., Fry, D., Garvie, C., Huang, K.S., Gao, L., Tovar, C., Lovey, A., Wanner, J. and Vassilev, L.T. (2012) 'Activation of the p53 pathway by small-molecule-induced MDM2 and MDMX dimerization', *Proc Natl Acad Sci U S A*, 109(29), pp. 11788-93.

Han, X., Garcia-Manero, G., McDonnell, T.J., Lozano, G., Medeiros, L.J., Xiao, L., Rosner, G., Nguyen, M., Fernandez, M., Valentin-Vega, Y.A., Barboza, J., Jones, D.M., Rassidakis, G.Z., Kantarjian, H.M. and Bueso-Ramos, C.E. (2007) 'HDM4 (HDMX) is widely expressed in adult pre-B acute lymphoblastic leukemia and is a potential therapeutic target', *Mod Pathol*, 20(1), pp. 54-62.

Hanahan, D. and Weinberg, R.A. (2011) 'Hallmarks of cancer: the next generation', *Cell*, 144(5), pp. 646-74.

Hardcastle, I.R., Ahmed, S.U., Atkins, H., Farnie, G., Golding, B.T., Griffin, R.J., Guyenne, S., Hutton, C., Kallblad, P., Kemp, S.J., Kitching, M.S., Newell, D.R., Norbedo, S., Northen, J.S., Reid, R.J., Saravanan, K., Willems, H.M. and Lunec, J. (2006) 'Small-molecule inhibitors of the MDM2-p53 protein-protein interaction based on an isoindolinone scaffold', *J Med Chem*, 49(21), pp. 6209-21.

Harris, S.L. and Levine, A.J. (2005) 'The p53 pathway: positive and negative feedback loops', *Oncogene*, 24(17), pp. 2899-908.

Harvey, K.F., Pfleger, C.M. and Hariharan, I.K. (2003) 'The Drosophila Mst ortholog, hippo, restricts growth and cell proliferation and promotes apoptosis', *Cell*, 114(4), pp. 457-67.

Haupt, S., Buckley, D., Pang, J.M., Panimaya, J., Paul, P.J., Gamell, C., Takano, E.A., Lee, Y.Y., Hiddingh, S., Rogers, T.M., Teunisse, A.F., Herold, M.J., Marine, J.C., Fox, S.B., Jochemsen, A. and Haupt, Y. (2015) 'Targeting Mdmx to treat breast cancers with wild-type p53', *Cell Death Dis*, 6, p. e1821.

Haupt, Y., Maya, R., Kazaz, A. and Oren, M. (1997) 'Mdm2 promotes the rapid degradation of p53', *Nature*, 387(6630), pp. 296-9.

Hirose, M., Yamato, K., Endo, S., Saito, R., Ueno, T., Hirai, S., Suzuki, H., Abei, M., Natori, Y. and Hyodo, I. (2014) 'MDM4 expression as an indicator of TP53 reactivation by combined targeting of MDM2 and MDM4 in cancer cells without TP53 mutation', *Oncoscience*, 1(12), pp. 830-43.

Hoeferlin, L.A., Oleinik, N.V., Krupenko, N.I. and Krupenko, S.A. (2011) 'Activation of p21-Dependent G1/G2 Arrest in the Absence of DNA Damage as an Antiapoptotic Response to Metabolic Stress', *Genes Cancer*, 2(9), pp. 889-99.

Hollstein, M., Sidransky, D., Vogelstein, B. and Harris, C.C. (1991) 'p53 mutations in human cancers', *Science*, 253(5015), pp. 49-53.

Honda, R., Tanaka, H. and Yasuda, H. (1997) 'Oncoprotein MDM2 is a ubiquitin ligase E3 for tumor suppressor p53', *FEBS Lett*, 420(1), pp. 25-7.

Hu, B., Gilkes, D.M. and Chen, J. (2007) 'Efficient p53 activation and apoptosis by simultaneous disruption of binding to MDM2 and MDMX', *Cancer Res*, 67(18), pp. 8810-7.

Hu, B., Gilkes, D.M., Farooqi, B., Sebti, S.M. and Chen, J. (2006) 'MDMX overexpression prevents p53 activation by the MDM2 inhibitor Nutlin', *J Biol Chem*, 281(44), pp. 33030-5.

Hu, L., Zhang, H., Bergholz, J., Sun, S. and Xiao, Z.X. (2016) 'MDM2/MDMX: Master negative regulators for p53 and RB', *Mol Cell Oncol*, 3(2), p. e1106635.

Huang, J., Perez-Burgos, L., Placek, B.J., Sengupta, R., Richter, M., Dorsey, J.A., Kubicek, S., Opravil, S., Jenuwein, T. and Berger, S.L. (2006) 'Repression of p53 activity by Smyd2-mediated methylation', *Nature*, 444(7119), pp. 629-32.

Huang, J., Wu, S., Barrera, J., Matthews, K. and Pan, D. (2005) 'The Hippo signaling pathway coordinately regulates cell proliferation and apoptosis by inactivating Yorkie, the Drosophila Homolog of YAP', *Cell*, 122(3), pp. 421-34.

Iancu-Rubin, C., Mosoyan, G., Glenn, K., Gordon, R.E., Nichols, G.L. and Hoffman, R. (2014) 'Activation of p53 by the MDM2 inhibitor RG7112 impairs thrombopoiesis', *Exp Hematol*, 42(2), pp. 137-45 e5.

Iwakuma, T. and Lozano, G. (2007) 'Crippling p53 activities via knock-in mutations in mouse models', *Oncogene*, 26(15), pp. 2177-84.

Iyer, N.G., Ozdag, H. and Caldas, C. (2004) 'p300/CBP and cancer', *Oncogene*, 23(24), pp. 4225-31.

Jackson, M.W. and Berberich, S.J. (1999) 'Constitutive mdmx expression during cell growth, differentiation, and DNA damage', *DNA Cell Biol*, 18(9), pp. 693-700.

Jackson, M.W., Lindstrom, M.S. and Berberich, S.J. (2001) 'MdmX binding to ARF affects Mdm2 protein stability and p53 transactivation', *J Biol Chem*, 276(27), pp. 25336-41.

Jacob, A.G., O'Brien, D., Singh, R.K., Comiskey, D.F., Jr., Littleton, R.M., Mohammad, F., Gladman, J.T., Widmann, M.C., Jeyaraj, S.C., Bolinger, C., Anderson, J.R., Barkauskas, D.A., Boris-Lawrie, K. and Chandler, D.S. (2013) 'Stress-induced isoforms of MDM2 and MDM4 correlate with high-grade disease and an altered splicing network in pediatric rhabdomyosarcoma', *Neoplasia*, 15(9), pp. 1049-63.

Jacob, A.G., Singh, R.K., Comiskey, D.F., Jr., Rouhier, M.F., Mohammad, F., Bebee, T.W. and Chandler, D.S. (2014) 'Stress-induced alternative splice forms of MDM2 and MDMX modulate the p53-pathway in distinct ways', *PLoS One*, 9(8), p. e104444.

Janz, M., Stuhmer, T., Vassilev, L.T. and Bargou, R.C. (2007) 'Pharmacologic activation of p53-dependent and p53-independent apoptotic pathways in Hodgkin/Reed-Sternberg cells', *Leukemia*, 21(4), pp. 772-9.

Jin, B. and Robertson, K.D. (2013) 'DNA methyltransferases, DNA damage repair, and cancer', *Adv Exp Med Biol*, 754, pp. 3-29.

Jin, Y., Lee, H., Zeng, S.X., Dai, M.S. and Lu, H. (2003) 'MDM2 promotes p21waf1/cip1 proteasomal turnover independently of ubiquitylation', *EMBO J*, 22(23), pp. 6365-77.

Jin, Y., Zeng, S.X., Sun, X.X., Lee, H., Blattner, C., Xiao, Z. and Lu, H. (2008) 'MDMX promotes proteasomal turnover of p21 at G1 and early S phases independently of, but in cooperation with, MDM2', *Mol Cell Biol*, 28(4), pp. 1218-29.

Johnson, R. and Halder, G. (2014) 'The two faces of Hippo: targeting the Hippo pathway for regenerative medicine and cancer treatment', *Nat Rev Drug Discov*, 13(1), pp. 63-79.

Joseph, T.L., Madhumalar, A., Brown, C.J., Lane, D.P. and Verma, C.S. (2010) 'Differential binding of p53 and nutlin to MDM2 and MDMX: computational studies', *Cell Cycle*, 9(6), pp. 1167-81.

Kanehisa, M. and Goto, S. (2000) 'KEGG: kyoto encyclopedia of genes and genomes', *Nucleic Acids Res*, 28(1), pp. 27-30.

Kanehisa, M., Sato, Y., Kawashima, M., Furumichi, M. and Tanabe, M. (2016) 'KEGG as a reference resource for gene and protein annotation', *Nucleic Acids Res*, 44(D1), pp. D457-62.

Kawai, H., Wiederschain, D., Kitao, H., Stuart, J., Tsai, K.K. and Yuan, Z.M. (2003) 'DNA damage-induced MDMX degradation is mediated by MDM2', *J Biol Chem*, 278(46), pp. 45946-53.

Kelder, T., van Iersel, M.P., Hanspers, K., Kutmon, M., Conklin, B.R., Evelo, C.T. and Pico, A.R. (2012) 'WikiPathways: building research communities on biological pathways', *Nucleic Acids Res*, 40(Database issue), pp. D1301-7.

Khoo, K.H., Verma, C.S. and Lane, D.P. (2014) 'Drugging the p53 pathway: understanding the route to clinical efficacy', *Nat Rev Drug Discov*, 13(3), pp. 217-36.

Kim, S. and An, S.S. (2016) 'Role of p53 isoforms and aggregations in cancer', *Medicine (Baltimore)*, 95(26), p. e3993.

Kim, S.S., Garg, H., Joshi, A. and Manjunath, N. (2009) 'Strategies for targeted nonviral delivery of siRNAs in vivo', *Trends Mol Med*, 15(11), pp. 491-500.

Koblish, H.K., Zhao, S., Franks, C.F., Donatelli, R.R., Tominovich, R.M., LaFrance, L.V., Leonard, K.A., Gushue, J.M., Parks, D.J., Calvo, R.R., Milkiewicz, K.L., Marugan, J.J., Raboisson, P., Cummings, M.D., Grasberger, B.L., Johnson, D.L., Lu, T., Molloy, C.J. and Maroney, A.C. (2006) 'Benzodiazepinedione inhibitors of the Hdm2:p53 complex suppress human tumor cell proliferation in vitro and sensitize tumors to doxorubicin in vivo', *Mol Cancer Ther*, 5(1), pp. 160-9.

Kojima, K., Konopleva, M., Tsao, T., Nakakuma, H. and Andreeff, M. (2008) 'Concomitant inhibition of Mdm2-p53 interaction and Aurora kinases activates the p53-dependent postmitotic checkpoints and synergistically induces p53-mediated mitochondrial apoptosis along with reduced endoreduplication in acute myelogenous leukemia', *Blood*, 112(7), pp. 2886-95.

Kojima, K., Kornblau, S.M., Ruvolo, V., Dilip, A., Duvvuri, S., Davis, R.E., Zhang, M., Wang, Z., Coombes, K.R., Zhang, N., Qiu, Y.H., Burks, J.K., Kantarjian, H., Shacham, S., Kauffman, M. and Andreeff, M. (2013) 'Prognostic impact and targeting of CRM1 in acute myeloid leukemia', *Blood*, 121(20), pp. 4166-74.

Kondo, T., Tatematsu, A., Sato, Y. and Ishikawa, M. (1991) '[A tumor sensitivity test, SDI test using XTT]', *Gan To Kagaku Ryoho*, 18(1), pp. 123-6.

Kruse, J.P. and Gu, W. (2009) 'Modes of p53 Regulation', *Cell*, 137, pp. 609-622.

Kubbutat, M.H., Jones, S.N. and Vousden, K.H. (1997) 'Regulation of p53 stability by Mdm2', *Nature*, 387(6630), pp. 299-303.

Kulis, M. and Esteller, M. (2010) 'DNA methylation and cancer', *Adv Genet*, 70, pp. 27-56.

Kussie, P.H., Gorina, S., Marechal, V., Elenbaas, B., Moreau, J., Levine, A.J. and Pavletich, N.P. (1996) 'Structure of the MDM2 oncoprotein bound to the p53 tumor suppressor transactivation domain', *Science*, 274(5289), pp. 948-53.

Kwan, T., Benovoy, D., Dias, C., Gurd, S., Serre, D., Zuzan, H., Clark, T.A., Schweitzer, A., Staples, M.K., Wang, H., Blume, J.E., Hudson, T.J., Sladek, R. and Majewski, J. (2007) 'Heritability of alternative splicing in the human genome', *Genome Res*, 17(8), pp. 1210-8.

Landre, V., Rotblat, B., Melino, S., Bernassola, F. and Melino, G. (2014) 'Screening for E3-ubiquitin ligase inhibitors: challenges and opportunities', *Oncotarget*, 5(18), pp. 7988-8013.

Laurie, N.A., Donovan, S.L., Shih, C.S., Zhang, J., Mills, N., Fuller, C., Teunisse, A., Lam, S., Ramos, Y., Mohan, A., Johnson, D., Wilson, M., Rodriguez-Galindo, C., Quarto, M., Francoz, S., Mendrysa, S.M., Guy, R.K., Marine, J.C., Jochemsen, A.G. and Dyer, M.A. (2006) 'Inactivation of the p53 pathway in retinoblastoma', *Nature*, 444(7115), pp. 61-6.

LeBron, C., Chen, L., Gilkes, D.M. and Chen, J. (2006) 'Regulation of MDMX nuclear import and degradation by Chk2 and 14-3-3', *EMBO J*, 25(6), pp. 1196-206.

Lee, J.H. and Lu, H. (2011) '14-3-3Gamma inhibition of MDMX-mediated p21 turnover independent of p53', *J Biol Chem*, 286(7), pp. 5136-42.

Lenos, K. and Jochemsen, A.G. (2011) 'Functions of MDMX in the modulation of the p53-response', *J Biomed Biotechnol*, 2011, p. 876173.

Li, C., Chen, L. and Chen, J. (2002a) 'DNA damage induces MDMX nuclear translocation by p53-dependent and -independent mechanisms', *Mol Cell Biol*, 22(21), pp. 7562-71.

Li, M., Chen, D., Shiloh, A., Luo, J., Nikolaev, A.Y., Qin, J. and Gu, W. (2002b) 'Deubiquitination of p53 by HAUSP is an important pathway for p53 stabilization', *Nature*, 416(6881), pp. 648-53.

Li, M. and Gu, W. (2011) 'A critical role for noncoding 5S rRNA in regulating Mdmx stability', *Mol Cell*, 43(6), pp. 1023-32.

Long, J., Parkin, B., Ouillette, P., Bixby, D., Shedden, K., Erba, H., Wang, S. and Malek, S.N. (2010) 'Multiple distinct molecular mechanisms influence sensitivity and resistance to MDM2 inhibitors in adult acute myelogenous leukemia', *Blood*, 116(1), pp. 71-80.

Lopez-Pajares, V., Kim, M.M. and Yuan, Z.M. (2008) 'Phosphorylation of MDMX mediated by Akt leads to stabilization and induces 14-3-3 binding', *J Biol Chem*, 283(20), pp. 13707-13.

Lu, M., Breyssens, H., Salter, V., Zhong, S., Hu, Y., Baer, C., Ratnayaka, I., Sullivan, A., Brown, N.R., Endicott, J., Knapp, S., Kessler, B.M., Middleton, M.R., Siebold, C., Jones, E.Y., Sviderskaya, E.V., Cebon, J., John, T., Caballero, O.L., Goding, C.R. and Lu, X. (2013) 'Restoring p53 function in human melanoma cells by inhibiting MDM2 and cyclin B1/CDK1-phosphorylated nuclear iASPP', *Cancer Cell*, 23(5), pp. 618-33.

Macaluso, M., Montanari, M., Cinti, C. and Giordano, A. (2005) 'Modulation of cell cycle components by epigenetic and genetic events', *Semin Oncol*, 32(5), pp. 452-7.

Madden, M.M., Muppidi, A., Li, Z., Li, X., Chen, J. and Lin, Q. (2011) 'Synthesis of cell-permeable stapled peptide dual inhibitors of the p53-Mdm2/Mdmx interactions via photoinduced cycloaddition', *Bioorg Med Chem Lett*, 21(5), pp. 1472-5.

Mancini, F., Di Conza, G. and Moretti, F. (2009) 'MDM4 (MDMX) and its Transcript Variants', *Curr Genomics*, 10(1), pp. 42-50.

Manjunath, N., Wu, H., Subramanya, S. and Shankar, P. (2009) 'Lentiviral delivery of short hairpin RNAs', *Adv Drug Deliv Rev*, 61(9), pp. 732-45.

Marchenko, N.D., Wolff, S., Erster, S., Becker, K. and Moll, U.M. (2007) 'Monoubiquitylation promotes mitochondrial p53 translocation', *EMBO J*, 26(4), pp. 923-34.

Marine, J.C., Dyer, M.A. and Jochemsen, A.G. (2007) 'MDMX: from bench to bedside', *J Cell Sci*, 120(Pt 3), pp. 371-8.

Marine, J.C. and Jochemsen, A.G. (2005) 'Mdmx as an essential regulator of p53 activity', *Biochem Biophys Res Commun*, 331(3), pp. 750-60.

Markey, M. and Berberich, S.J. (2008) 'Full-length hdmX transcripts decrease following genotoxic stress', *Oncogene*, 27(52), pp. 6657-66.

Mayo, L.D. and Donner, D.B. (2001) 'A phosphatidylinositol 3-kinase/Akt pathway promotes translocation of Mdm2 from the cytoplasm to the nucleus', *Proc Natl Acad Sci U S A*, 98(20), pp. 11598-603.

Mayo, L.D., Turchi, J.J. and Berberich, S.J. (1997) 'Mdm-2 phosphorylation by DNA-dependent protein kinase prevents interaction with p53', *Cancer Res*, 57(22), pp. 5013-6.

McCormack, E., Haaland, I., Venas, G., Forthun, R.B., Huseby, S., Gausdal, G., Knappskog, S., Micklem, D.R., Lorens, J.B., Bruserud, O. and Gjertsen, B.T. (2012) 'Synergistic induction of p53 mediated apoptosis by valproic acid and nutlin-3 in acute myeloid leukemia', *Leukemia*, 26(5), pp. 910-7.

Melchior, F. and Hengst, L. (2002) 'SUMO-1 and p53', *Cell Cycle*, 1(4), pp. 245-9.

Mesrouze, Y., Hau, J.C., Erdmann, D., Zimmermann, C., Fontana, P., Schmelzle, T. and Ch??ne, P. (2014) 'The surprising features of the TEAD4-Vgll1 protein-protein interaction', *ChemBioChem*, 15, pp. 537-542.

Meulmeester, E., Pereg, Y., Shiloh, Y. and Jochemsen, A.G. (2005) 'ATM-mediated phosphorylations inhibit Mdmx/Mdm2 stabilization by HAUSP in favor of p53 activation', *Cell Cycle*, 4(9), pp. 1166-70.

Michaelis, M., Rothweiler, F., Klassert, D., von Deimling, A., Weber, K., Fehse, B., Kammerer, B., Doerr, H.W. and Cinatl, J., Jr. (2009) 'Reversal of P-glycoprotein-mediated multidrug resistance by the murine double minute 2 antagonist nutlin-3', *Cancer Res*, 69(2), pp. 416-21.

Migliorini, D., Lazzerini Denchi, E., Danovi, D., Jochemsen, A., Capillo, M., Gobbi, A., Helin, K., Pelicci, P.G. and Marine, J.C. (2002) 'Mdm4 (Mdmx) regulates p53-induced growth arrest and neuronal cell death during early embryonic mouse development', *Mol Cell Biol*, 22(15), pp. 5527-38.

Minsky, N. and Oren, M. (2004) 'The RING domain of Mdm2 mediates histone ubiquitylation and transcriptional repression', *Mol Cell*, 16(4), pp. 631-9.

Mir, R., Tortosa, A., Martinez-Soler, F., Vidal, A., Condom, E., Perez-Perarnau, A., Ruiz-Larroya, T., Gil, J. and Gimenez-Bonafe, P. (2013) 'Mdm2 antagonists induce apoptosis and synergize with cisplatin overcoming chemoresistance in TP53 wild-type ovarian cancer cells', *Int J Cancer*, 132(7), pp. 1525-36.

Ohkubo, S., Tanaka, T., Taya, Y., Kitazato, K. and Prives, C. (2006) 'Excess HDM2 impacts cell cycle and apoptosis and has a selective effect on p53-dependent transcription', *J Biol Chem*, 281(25), pp. 16943-50.

Ohnstad, H.O., Castro, R., Sun, J., Heintz, K.M., Vassilev, L.T., Bjerkehagen, B., Kresse, S.H., Meza-Zepeda, L.A. and Myklebost, O. (2013) 'Correlation of TP53 and MDM2 genotypes with response to therapy in sarcoma', *Cancer*, 119(5), pp. 1013-22.

Okamoto, K., Kashima, K., Pereg, Y., Ishida, M., Yamazaki, S., Nota, A., Teunisse, A., Migliorini, D., Kitabayashi, I., Marine, J.C., Prives, C., Shiloh, Y., Jochemsen, A.G. and Taya, Y. (2005) 'DNA damage-induced phosphorylation of MdmX at serine 367 activates p53 by targeting MdmX for Mdm2-dependent degradation', *Mol Cell Biol*, 25(21), pp. 9608-20.

Olivier, M., Eeles, R., Hollstein, M., Khan, M.A., Harris, C.C. and Hainaut, P. (2002) 'The IARC TP53 database: new online mutation analysis and recommendations to users', *Hum Mutat*, 19(6), pp. 607-14.

Pan, D. (2010) 'The hippo signaling pathway in development and cancer', *Dev Cell*, 19(4), pp. 491-505.

Pan, Y. and Chen, J. (2003) 'MDM2 promotes ubiquitination and degradation of MDMX', *Mol Cell Biol*, 23(15), pp. 5113-21.

Pantalacci, S., Tapon, N. and Leopold, P. (2003) 'The Salvador partner Hippo promotes apoptosis and cell-cycle exit in Drosophila', *Nat Cell Biol*, 5(10), pp. 921-7.

Papazisis, K.T., Geromichalos, G.D., Dimitriadis, K.A. and Kortsaris, A.H. (1997) 'Optimization of the sulforhodamine B colorimetric assay', *J Immunol Methods*, 208(2), pp. 151-8.

Parant, J., Chavez-Reyes, A., Little, N.A., Yan, W., Reinke, V., Jochemsen, A.G. and Lozano, G. (2001) 'Rescue of embryonic lethality in Mdm4-null mice by loss of Trp53 suggests a nonoverlapping pathway with MDM2 to regulate p53', *Nat Genet*, 29(1), pp. 92-5.

Patton, J.T., Mayo, L.D., Singhi, A.D., Gudkov, A.V., Stark, G.R. and Jackson, M.W. (2006) 'Levels of HdmX expression dictate the sensitivity of normal and transformed cells to Nutlin-3', *Cancer Res*, 66(6), pp. 3169-76.

Pazgier, M., Liu, M., Zou, G., Yuan, W., Li, C., Li, C., Li, J., Monbo, J., Zella, D., Tarasov, S.G. and Lu, W. (2009) 'Structural basis for high-affinity peptide inhibition of p53 interactions with MDM2 and MDMX', *Proc Natl Acad Sci U S A*, 106(12), pp. 4665-70.

Pechackova, S., Burdova, K., Benada, J., Kleiblova, P., Jenikova, G. and Macurek, L. (2016) 'Inhibition of WIP1 phosphatase sensitizes breast cancer cells to genotoxic stress and to MDM2 antagonist nutlin-3', *Oncotarget*, 7(12), pp. 14458-75.

Pei, D., Zhang, Y. and Zheng, J. (2012) 'Regulation of p53: a collaboration between Mdm2 and Mdmx', *Oncotarget*, 3(3), pp. 228-35.

Pelengaris, S. and Khan, M. (2013) *The Molecular biology of cancer : a bridge from bench to bedside*. Second edition. edn. Hoboken, NJ: Wiley-Blackwell.

Petitjean, A., Achatz, M.I., Borresen-Dale, A.L., Hainaut, P. and Olivier, M. (2007) 'TP53 mutations in human cancers: functional selection and impact on cancer prognosis and outcomes', *Oncogene*, 26(15), pp. 2157-65.

Pico, A.R., Kelder, T., van Iersel, M.P., Hanspers, K., Conklin, B.R. and Evelo, C. (2008) 'WikiPathways: pathway editing for the people', *PLoS Biol*, 6(7), p. e184.

Pobbati, A.V., Chan, S.W., Lee, I., Song, H. and Hong, W. (2012) 'Structural and functional similarity between the Vgll1-TEAD and the YAP-TEAD complexes', *Structure*, 20, pp. 1135-1140.

Pobbati, A.V. and Hong, W. (2013) 'Emerging roles of TEAD transcription factors and its coactivators in cancers', *Cancer Biol Ther*, 14(5), pp. 390-8.

Polanski, R., Noon, A.P., Blaydes, J., Phillips, A., Rubbi, C.P., Parsons, K., Vlatkovic, N. and Boyd, M.T. (2014) 'Senescence induction in renal carcinoma cells by Nutlin-3: a potential therapeutic strategy based on MDM2 antagonism', *Cancer Lett*, 353(2), pp. 211-9.

Popowicz, G.M., Czarna, A. and Holak, T.A. (2008) 'Structure of the human Mdmx protein bound to the p53 tumor suppressor transactivation domain', *Cell Cycle*, 7(15), pp. 2441-3.

Popowicz, G.M., Czarna, A., Rothweiler, U., Szwagierczak, A., Krajewski, M., Weber, L. and Holak, T.A. (2007) 'Molecular basis for the inhibition of p53 by Mdmx', *Cell Cycle*, 6(19), pp. 2386-92.

Popowicz, G.M., Czarna, A., Wolf, S., Wang, K., Wang, W., Domling, A. and Holak, T.A. (2010) 'Structures of low molecular weight inhibitors bound to MDMX and MDM2 reveal new approaches for p53-MDMX/MDM2 antagonist drug discovery', *Cell Cycle*, 9(6), pp. 1104-11.

Rallapalli, R., Strachan, G., Tuan, R.S. and Hall, D.J. (2003) 'Identification of a domain within MDMX-S that is responsible for its high affinity interaction with p53 and high-level expression in mammalian cells', *J Cell Biochem*, 89(3), pp. 563-75.

Ramos, Y.F., Stad, R., Attema, J., Peltenburg, L.T., van der Eb, A.J. and Jochemsen, A.G. (2001) 'Aberrant expression of HDMX proteins in tumor cells correlates with wild-type p53', *Cancer Res*, 61(5), pp. 1839-42.

Ray-Coquard, I., Blay, J.Y., Italiano, A., Le Cesne, A., Penel, N., Zhi, J., Heil, F., Rueger, R., Graves, B., Ding, M., Geho, D., Middleton, S.A., Vassilev, L.T., Nichols, G.L. and Bui, B.N. (2012) 'Effect of the MDM2 antagonist RG7112 on the P53 pathway in patients with MDM2-amplified, well-differentiated or dedifferentiated liposarcoma: an exploratory proof-of-mechanism study', *Lancet Oncol*.

Reid, Y., Storts, D., Riss, T. and Minor, L. (2004) 'Authentication of Human Cell Lines by STR DNA Profiling Analysis', in Sittampalam, G.S., Coussens, N.P., Nelson, H., Arkin, M., Auld, D., Austin, C., Bejcek, B., Glicksman, M., Inglese, J., Iversen, P.W., Li, Z., McGee, J., McManus, O., Minor, L., Napper, A., Peltier, J.M., Riss, T., Trask, O.J., Jr. and Weidner, J. (eds.) *Assay Guidance Manual*. Bethesda (MD).

Reis, B., Jukofsky, L., Chen, G., Martinelli, G., Zhong, H., So, W.V., Dickinson, M.J., Drummond, M., Assouline, S., Hashemyan, M., Theron, M., Blotner, S., Lee, J.H., Kasner, M., Yoon, S.S., Rueger, R., Seiter, K., Middleton, S.A., Kelly, K.R., Vey, N., Yee, K., Nichols, G., Chen, L.C. and Pierceall, W.E. (2016) 'Acute myeloid leukemia patients' clinical response to idasanutlin (RG7388) is associated with pre-treatment MDM2 protein expression in leukemic blasts', *Haematologica*, 101(5), pp. e185-8.

Ribas, J., Boix, J. and Meijer, L. (2006) '(R)-roscovitine (CYC202, Seliciclib) sensitizes SH-SY5Y neuroblastoma cells to nutlin-3-induced apoptosis', *Exp Cell Res*, 312(12), pp. 2394-400.

Riedinger, C. and McDonnell, J.M. (2009) 'Inhibitors of MDM2 and MDMX: a structural perspective', *Future Med Chem*, 1(6), pp. 1075-94.

Rieke, D.T., Ochsenreither, S., Klinghammer, K., Seiwert, T.Y., Klauschen, F., Tinhofer, I. and Keilholz, U. (2016) 'Methylation of RAD51B, XRCC3 and other homologous recombination genes is associated with expression of immune checkpoints and an

inflammatory signature in squamous cell carcinoma of the head and neck, lung and cervix', *Oncotarget*, 7(46), pp. 75379-75393.

Riemenschneider, M.J., Buschges, R., Wolter, M., Reifenberger, J., Bostrom, J., Kraus, J.A., Schlegel, U. and Reifenberger, G. (1999) 'Amplification and overexpression of the MDM4 (MDMX) gene from 1q32 in a subset of malignant gliomas without TP53 mutation or MDM2 amplification', *Cancer Res*, 59(24), pp. 6091-6.

Roehm, N.W., Rodgers, G.H., Hatfield, S.M. and Glasebrook, A.L. (1991) 'An improved colorimetric assay for cell proliferation and viability utilizing the tetrazolium salt XTT', *J Immunol Methods*, 142(2), pp. 257-65.

Rufini, A., Tucci, P., Celardo, I. and Melino, G. (2013) 'Senescence and aging: the critical roles of p53', *Oncogene*, 32(43), pp. 5129-43.

Saha, M.N., Jiang, H. and Chang, H. (2010) 'Molecular mechanisms of nutlin-induced apoptosis in multiple myeloma: evidence for p53-transcription-dependent and -independent pathways', *Cancer Biol Ther*, 10(6), pp. 567-78.

Schnekenburger, M. and Diederich, M. (2012) 'Epigenetics Offer New Horizons for Colorectal Cancer Prevention', *Curr Colorectal Cancer Rep*, 8(1), pp. 66-81.

Schroeder, A., Mueller, O., Stocker, S., Salowsky, R., Leiber, M., Gassmann, M., Lightfoot, S., Menzel, W., Granzow, M. and Ragg, T. (2006) 'The RIN: an RNA integrity number for assigning integrity values to RNA measurements', *BMC Mol Biol*, 7, p. 3.

Secchiero, P., Barbarotto, E., Tiribelli, M., Zerbinati, C., di Iasio, M.G., Gonelli, A., Cavazzini, F., Campioni, D., Fanin, R., Cuneo, A. and Zauli, G. (2006) 'Functional integrity of the p53-mediated apoptotic pathway induced by the nongenotoxic agent nutlin-3 in B-cell chronic lymphocytic leukemia (B-CLL)', *Blood*, 107(10), pp. 4122-9.

Secchiero, P., Vaccarezza, M., Gonelli, A. and Zauli, G. (2004) 'TNF-related apoptosis-inducing ligand (TRAIL): a potential candidate for combined treatment of hematological malignancies', *Curr Pharm Des*, 10(29), pp. 3673-81.

Shadfan, M., Lopez-Pajares, V. and Yuan, Z.M. (2012) 'MDM2 and MDMX: Alone and together in regulation of p53', *Transl Cancer Res*, 1(2), pp. 88-89.

Shangary, S., Qin, D., McEachern, D., Liu, M., Miller, R.S., Qiu, S., Nikolovska-Coleska, Z., Ding, K., Wang, G., Chen, J., Bernard, D., Zhang, J., Lu, Y., Gu, Q., Shah, R.B., Pienta, K.J., Ling, X., Kang, S., Guo, M., Sun, Y., Yang, D. and Wang, S. (2008) 'Temporal activation of p53 by a specific MDM2 inhibitor is selectively toxic to tumors and leads to complete tumor growth inhibition', *Proc Natl Acad Sci U S A*, 105(10), pp. 3933-8.

Shangary, S. and Wang, S. (2009) 'Small-molecule inhibitors of the MDM2-p53 protein-protein interaction to reactivate p53 function: a novel approach for cancer therapy', *Annu Rev Pharmacol Toxicol*, 49, pp. 223-41.

Sharp, D.A., Kratowicz, S.A., Sank, M.J. and George, D.L. (1999) 'Stabilization of the MDM2 oncoprotein by interaction with the structurally related MDMX protein', *J Biol Chem*, 274(53), pp. 38189-96.

Sherr, C.J. and McCormick, F. (2002) 'The RB and p53 pathways in cancer', *Cancer Cell*, 2(2), pp. 103-12.

Shi, X., Kachirskaia, I., Yamaguchi, H., West, L.E., Wen, H., Wang, E.W., Dutta, S., Appella, E. and Gozani, O. (2007) 'Modulation of p53 function by SET8-mediated methylation at lysine 382', *Mol Cell*, 27(4), pp. 636-46.

Shieh, S.Y., Ahn, J., Tamai, K., Taya, Y. and Prives, C. (2000) 'The human homologs of checkpoint kinases Chk1 and Cds1 (Chk2) phosphorylate p53 at multiple DNA damage-inducible sites', *Genes Dev*, 14(3), pp. 289-300.

Shieh, S.Y., Ikeda, M., Taya, Y. and Prives, C. (1997) 'DNA damage-induced phosphorylation of p53 alleviates inhibition by MDM2', *Cell*, 91(3), pp. 325-34.

Shvarts, A., Bazuine, M., Dekker, P., Ramos, Y.F., Steegenga, W.T., Merckx, G., van Ham, R.C., van der Houven van Oordt, W., van der Eb, A.J. and Jochemsen, A.G. (1997) 'Isolation and identification of the human homolog of a new p53-binding protein, Mdmx', *Genomics*, 43(1), pp. 34-42.

Sionov, R.V., Coen, S., Goldberg, Z., Berger, M., Bercovich, B., Ben-Neriah, Y., Ciechanover, A. and Haupt, Y. (2001) 'c-Abl regulates p53 levels under normal and stress conditions by preventing its nuclear export and ubiquitination', *Mol Cell Biol*, 21(17), pp. 5869-78.

Srinivasan, K., Shiue, L., Hayes, J.D., Centers, R., Fitzwater, S., Loewen, R., Edmondson, L.R., Bryant, J., Smith, M., Rommelfanger, C., Welch, V., Clark, T.A., Sugnet, C.W., Howe, K.J., Mandel-Gutfreund, Y. and Ares, M., Jr. (2005) 'Detection and measurement of alternative splicing using splicing-sensitive microarrays', *Methods*, 37(4), pp. 345-59.

Sriraman, A., Radovanovic, M., Wienken, M., Najafova, Z., Li, Y. and Dobbelstein, M. (2016) 'Cooperation of Nutlin-3a and a Wip1 inhibitor to induce p53 activity', *Oncotarget*.

Stommel, J.M. and Wahl, G.M. (2004) 'Accelerated MDM2 auto-degradation induced by DNA-damage kinases is required for p53 activation', *EMBO J*, 23(7), pp. 1547-56.

Tabe, Y., Sebasigari, D., Jin, L., Rudelius, M., Davies-Hill, T., Miyake, K., Miida, T., Pittaluga, S. and Raffeld, M. (2009) 'MDM2 antagonist nutlin-3 displays antiproliferative and proapoptotic activity in mantle cell lymphoma', *Clin Cancer Res*, 15(3), pp. 933-42.

Tan, B.X., Khoo, K.H., Lim, T.M. and Lane, D.P. (2014) 'High Mdm4 levels suppress p53 activity and enhance its half-life in acute myeloid leukaemia', *Oncotarget*, 5(4), pp. 933-43.

Tang, Y., Luo, J., Zhang, W. and Gu, W. (2006) 'Tip60-dependent acetylation of p53 modulates the decision between cell-cycle arrest and apoptosis', *Mol Cell*, 24(6), pp. 827-39.

Tanimura, S., Ohtsuka, S., Mitsui, K., Shirouzu, K., Yoshimura, A. and Ohtsubo, M. (1999) 'MDM2 interacts with MDMX through their RING finger domains', *Febs Letters*, 447(1), pp. 5-9.

Tao, W. and Levine, A.J. (1999) 'Nucleocytoplasmic shuttling of oncoprotein Hdm2 is required for Hdm2-mediated degradation of p53', *Proc Natl Acad Sci U S A*, 96(6), pp. 3077-80.

Tasdemir, E., Maiuri, M.C., Galluzzi, L., Vitale, I., Djavaheri-Mergny, M., D'Amelio, M., Criollo, A., Morselli, E., Zhu, C., Harper, F., Nannmark, U., Samara, C., Pinton, P., Vicencio, J.M., Carnuccio, R., Moll, U.M., Madeo, F., Paterlini-Brechot, P., Rizzuto, R., Szabadkai, G., Pierron, G., Blomgren, K., Tavernarakis, N., Codogno, P., Cecconi, F. and Kroemer, G. (2008) 'Regulation of autophagy by cytoplasmic p53', *Nat Cell Biol*, 10(6), pp. 676-87.

Thompson, T., Andreeff, M., Studzinski, G.P. and Vassilev, L.T. (2010) '1,25-dihydroxyvitamin D3 enhances the apoptotic activity of MDM2 antagonist nutlin-3a in acute myeloid leukemia cells expressing wild-type p53', *Mol Cancer Ther*, 9(5), pp. 1158-68.

Toledo, F. and Wahl, G.M. (2007) 'MDM2 and MDM4: p53 regulators as targets in anticancer therapy', *Int J Biochem Cell Biol*, 39(7-8), pp. 1476-82.

Tournillon, A.S., Lopez, I., Malbert-Colas, L., Naski, N., Olivares-Illana, V. and Fahraeus, R. (2015) 'The alternative translated MDMX(p60) isoform regulates MDM2 activity', *Cell Cycle*, 14(3), pp. 449-58.

Tovar, C., Higgins, B., Kolinsky, K., Xia, M., Packman, K., Heimbrook, D.C. and Vassilev, L.T. (2011) 'MDM2 antagonists boost antitumor effect of androgen withdrawal: implications for therapy of prostate cancer', *Mol Cancer*, 10, p. 49.

Udan, R.S., Kango-Singh, M., Nolo, R., Tao, C. and Halder, G. (2003) 'Hippo promotes proliferation arrest and apoptosis in the Salvador/Warts pathway', *Nat Cell Biol*, 5(10), pp. 914-20.

Valentin-Vega, Y.A., Barboza, J.A., Chau, G.P., El-Naggar, A.K. and Lozano, G. (2007) 'High levels of the p53 inhibitor MDM4 in head and neck squamous carcinomas', *Hum Pathol*, 38(10), pp. 1553-62.

van Kooten, T.G., Klein, C.L. and Kirkpatrick, C.J. (2001) 'Western blotting as a method for studying cell-biomaterial interactions: the role of protein collection', *J Biomed Mater Res*, 54(3), pp. 385-9.

Van Maerken, T., Ferdinande, L., Taildeman, J., Lambertz, I., Yigit, N., Vercruysse, L., Rihani, A., Michaelis, M., Cinatl, J., Jr., Cuvelier, C.A., Marine, J.C., De Paepe, A., Bracke, M., Speleman, F. and Vandesompele, J. (2009) 'Antitumor activity of the selective MDM2 antagonist nutlin-3 against chemoresistant neuroblastoma with wild-type p53', *J Natl Cancer Inst*, 101(22), pp. 1562-74.

Vassilev, L.T. (2004) 'Small-molecule antagonists of p53-MDM2 binding: research tools and potential therapeutics', *Cell Cycle*, 3(4), pp. 419-21.

Vassilev, L.T., Vu, B.T., Graves, B., Carvajal, D., Podlaski, F., Filipovic, Z., Kong, N., Kammlott, U., Lukacs, C., Klein, C., Fotouhi, N. and Liu, E.A. (2004) 'In vivo activation of the p53 pathway by small-molecule antagonists of MDM2', *Science*, 303(5659), pp. 844-8.

Vatsyayan, R., Singhal, J., Nagaprashantha, L.D., Awasthi, S. and Singhal, S.S. (2013) 'Nutlin-3 enhances sorafenib efficacy in renal cell carcinoma', *Mol Carcinog*, 52(1), pp. 39-48.

Verdine, G.L. and Hilinski, G.J. (2012) 'Stapled peptides for intracellular drug targets', *Methods Enzymol*, 503, pp. 3-33.

Visser, S. and Yang, X. (2010) 'LATS tumor suppressor: a new governor of cellular homeostasis', *Cell Cycle*, 9(19), pp. 3892-903.

Vousden, K.H. and Lu, X. (2002) 'Live or let die: the cell's response to p53', *Nat Rev Cancer*, 2(8), pp. 594-604.

Wade, M., Li, Y.C. and Wahl, G.M. (2013) 'MDM2, MDMX and p53 in oncogenesis and cancer therapy', in *Nat Rev Cancer*. England, pp. 83-96.

Wade, M., Rodewald, L.W., Espinosa, J.M. and Wahl, G.M. (2008) 'BH3 activation blocks Hdmx suppression of apoptosis and cooperates with Nutlin to induce cell death', *Cell Cycle*, 7(13), pp. 1973-82.

Wade, M., Wang, Y.V. and Wahl, G.M. (2010) 'The p53 orchestra: Mdm2 and Mdmx set the tone', *Trends Cell Biol*, 20(5), pp. 299-309.

Wade, M., Wong, E.T., Tang, M., Stommel, J.M. and Wahl, G.M. (2006) 'Hdmx modulates the outcome of p53 activation in human tumor cells', *J Biol Chem*, 281(44), pp. 33036-44.

Wang, F., Li, Y., Ma, Z., Wang, X. and Wang, Y. (2012) 'Structural determinants of benzodiazepinedione/peptide-based p53-HDM2 inhibitors using 3D-QSAR, docking and molecular dynamics', *J Mol Model*, 18(1), pp. 295-306.

Wang, J., Duncan, D., Shi, Z. and Zhang, B. (2013) 'WEB-based GEne SeT AnaLysis Toolkit (WebGestalt): update 2013', *Nucleic Acids Res*, 41(Web Server issue), pp. W77-83.

Warfel, N.A. and El-Deiry, W.S. (2013) 'p21WAF1 and tumourigenesis: 20 years after', *Curr Opin Oncol*, 25(1), pp. 52-8.

Weinberg, R.A. (1995) 'The retinoblastoma protein and cell cycle control', *Cell*, 81(3), pp. 323-30.

Wu, S., Huang, J., Dong, J. and Pan, D. (2003) 'hippo encodes a Ste-20 family protein kinase that restricts cell proliferation and promotes apoptosis in conjunction with salvador and warts', *Cell*, 114(4), pp. 445-56.

Xiong, S., Van Pelt, C.S., Elizondo-Fraire, A.C., Liu, G. and Lozano, G. (2006) 'Synergistic roles of Mdm2 and Mdm4 for p53 inhibition in central nervous system development', *Proc Natl Acad Sci U S A*, 103(9), pp. 3226-31.

Xirodimas, D.P., Saville, M.K., Bourdon, J.C., Hay, R.T. and Lane, D.P. (2004) 'Mdm2-mediated NEDD8 conjugation of p53 inhibits its transcriptional activity', *Cell*, 118(1), pp. 83-97.

Yu, Q., Li, Y., Mu, K., Li, Z., Meng, Q., Wu, X., Wang, Y. and Li, L. (2014) 'Amplification of Mdmx and overexpression of MDM2 contribute to mammary carcinogenesis by substituting for p53 mutations', *Diagn Pathol*, 9, p. 71.

Yu, S., Qin, D., Shangary, S., Chen, J., Wang, G., Ding, K., McEachern, D., Qiu, S., Nikolovska-Coleska, Z., Miller, R., Kang, S., Yang, D. and Wang, S. (2009) 'Potent and orally active small-molecule inhibitors of the MDM2-p53 interaction', *J Med Chem*, 52(24), pp. 7970-3.

Zanjirband, M., Edmondson, R.J. and Lunec, J. (2016) 'Pre-clinical efficacy and synergistic potential of the MDM2-p53 antagonists, Nutlin-3 and RG7388, as single agents and in combined treatment with cisplatin in ovarian cancer', *Oncotarget*.

Zauli, G., Celeghini, C., Melloni, E., Voltan, R., Ongari, M., Tiribelli, M., di Iasio, M.G., Lanza, F. and Secchiero, P. (2012) 'The sorafenib plus nutlin-3 combination promotes synergistic cytotoxicity in acute myeloid leukemic cells irrespectively of FLT3 and p53 status', *Haematologica*, 97(11), pp. 1722-30.

Zauli, G., Voltan, R., Bosco, R., Melloni, E., Marmiroli, S., Rigolin, G.M., Cuneo, A. and Secchiero, P. (2011) 'Dasatinib plus Nutlin-3 shows synergistic antileukemic activity in both p53 wild-type and p53 mutated B chronic lymphocytic leukemias by inhibiting the Akt pathway', *Clin Cancer Res*, 17(4), pp. 762-70.

Zhang, B., Kirov, S. and Snoddy, J. (2005) 'WebGestalt: an integrated system for exploring gene sets in various biological contexts', *Nucleic Acids Res*, 33(Web Server issue), pp. W741-8.

Zhang, H., Hu, L., Qiu, W., Deng, T., Zhang, Y., Bergholz, J. and Xiao, Z.X. (2015) 'MDMX exerts its oncogenic activity via suppression of retinoblastoma protein', *Oncogene*, 34(44), pp. 5560-9.

Zhang, W., Konopleva, M., Burks, J.K., Dywer, K.C., Schober, W.D., Yang, J.Y., McQueen, T.J., Hung, M.C. and Andreeff, M. (2010) 'Blockade of mitogen-activated protein kinase/extracellular signal-regulated kinase kinase and murine double minute synergistically induces Apoptosis in acute myeloid leukemia via BH3-only proteins Puma and Bim', *Cancer Res*, 70(6), pp. 2424-34.

Zhang, X., Lin, L., Guo, H., Yang, J., Jones, S.N., Jochemsen, A. and Lu, X. (2009) 'Phosphorylation and degradation of MdmX is inhibited by Wip1 phosphatase in the DNA damage response', *Cancer Res*, 69(20), pp. 7960-8.

Zhang, Y. and Xiong, Y. (2001) 'Control of p53 ubiquitination and nuclear export by MDM2 and ARF', *Cell Growth Differ*, 12(4), pp. 175-86.

Zhu, Y., Poyurovsky, M.V., Li, Y., Biderman, L., Stahl, J., Jacq, X. and Prives, C. (2009) 'Ribosomal protein S7 is both a regulator and a substrate of MDM2', *Mol Cell*, 35(3), pp. 316-26.

Zuckerman, V., Lenos, K., Popowicz, G.M., Silberman, I., Grossman, T., Marine, J.C., Holak, T.A., Jochemsen, A.G. and Haupt, Y. (2009) 'c-Abl phosphorylates Hdmx and regulates its interaction with p53', *J Biol Chem*, 284(6), pp. 4031-9.